TISSUE-SPECIFIC BIOSCAFFOLDS FOR ADIPOSE-DERIVED STEM/STROMAL CELL EXPANSION AND DELIVERY

by

Claire Yu

A thesis submitted to the Department of Chemical Engineering

in conformity with the requirements

for the degree of Doctor of Philosophy

Queen's University

Kingston, Ontario, Canada

July, 2016.

Abstract

Decellularized adipose tissue (DAT) is a promising biomaterial for soft tissue regeneration, and it provides a highly conducive microenvironment for human adipose-derived stem/stromal cell (ASC) attachment, proliferation, and adipogenesis. This thesis focused on developing techniques to fabricate 3-D bioscaffolds from enzymatically-digested DAT as platforms for ASC culture and delivery in adipose tissue engineering and large-scale ASC expansion.

Initial work investigated chemically crosslinked microcarriers fabricated from pepsin-digested DAT as injectable adipo-inductive substrates for ASCs. DAT microcarriers highly supported ASC adipogenesis compared to gelatin microcarriers in a CELLSPIN system, as confirmed by glycerol-3-phosphate dehydrogenase (GPDH) enzyme activity, lipid accumulation, and endpoint RT-PCR. ASCs cultured on DAT microcarriers in proliferation medium also had elevated *PPARγ, C/EBPα*, and *LPL* expression which suggested adipo-inductive properties. *In vivo* testing of the DAT microcarriers exhibited stable volume retention and enhanced cellular infiltration, tissue remodeling, and angiogenesis.

Building from this work, non-chemically crosslinked porous foams and bead foams were fabricated from α-amylase-digested DAT for soft tissue regeneration. Foams were stable and strongly supported ASC adipogenesis based on GPDH activity and endpoint RT-PCR. *PPARγ*, *C/EBPα*, and *LPL* expression in ASCs cultured on the foams in proliferation media indicated adipo-inductive properties. Foams with Young's moduli similar to human fat also influenced ASC adipogenesis by enhanced GPDH activity. *In vivo* adipogenesis accompanied by a potent angiogenic response and rapid resorption showed their potential use in wound healing applications.

Finally, non-chemically crosslinked porous microcarriers synthesized from α-amylase-digested DAT were investigated for ASC expansion. DAT microcarriers remained stable in culture and supported significantly higher ASC proliferation compared to Cultispher-S microcarriers in a

CELLSPIN system. ASC immunophenotype was preserved for all expanded groups, with reduced adhesion marker expression under dynamic conditions. DAT microcarrier expansion upregulated ASC expression of early adipogenic (*PPARγ, LPL*) and chondrogenic (*COMP*) markers without inducing a mature phenotype. DAT microcarrier expanded ASCs also showed similar levels of adipogenesis and osteogenesis compared to Cultispher-S despite a significantly higher population fold-change, and had the highest level of chondrogenesis among all groups. This study demonstrates the promising use of DAT microcarriers as a clinically relevant strategy for ASC expansion while maintaining multilineage differentiation capacity.

Co-Authorship Statement

Chapter 3 was published in Biomaterials in 2012: *"Turner A.E.B.*, Yu C.*, Bianco J., Watkins J.F., Flynn L.E. (2012). The performance of decellularized adipose tissue microcarriers as an inductive substrate for human adipose-derived stem cells. Biomaterials, 33(18), 4490-4499. (* equal first authors)."* Ms. Allison E. Turner, a previous Master's candidate in the group, was involved in the initial conceptualization and experimental design for the study in collaboration with Dr. Lauren Flynn. However, I repeated all of the experiments and expanded on her previous work, such that I was personally responsible for the *in vitro* studies and data analysis presented in the paper. Dr. Juares Bianco provided technical assistance with the *in vivo* studies.

Chapter 4 was published in Biomaterials in 2013: "*Yu C, Bianco J., Brown C., Fuetterer L., Watkins J.F., Samani A., Flynn L.E. (2013). Porous decellularized adipose tissue foams for soft tissue regeneration. Biomaterials, 34(13), 3290-3302."* I conceptualized this study in collaboration with Dr. Lauren Flynn and personally designed and conducted all of the *in vitro* experiments, assisted with the *in vivo* analyses, and wrote the manuscript. Dr. Juares Bianco, Mr. Cody Brown and Ms. Lydia Fuetterer provided technical support with sample preparation and the *in vivo* studies. Dr. Abbas Samani (Western University) performed the mechanical testing.

The work presented in Chapter 5 forms the basis of a manuscript that I have written, which we intend to submit to Biomaterials. I personally designed and performed all of the experimental studies described in the Chapter, with technical support as follows: Mr. Cody Brown and Ms. Anna Kornmuller assisted with the mechanical testing and Dr. Valerio Russo performed the immunohistochemical staining of the extracellular matrix components in the DAT microcarriers.

Acknowledgements

I would like to personally express my sincere gratitude to my supervisor Dr. Lauren Flynn for her incredible mentorship, support, and guidance throughout my PhD program. I am extremely honored to have worked in such an outstanding lab and given the unique opportunity to pursue my passion in tissue engineering. Thank you for giving me the confidence as well as wealth of skills, knowledge, advice, and encouragement over the years that have helped me establish a strong foundation as a researcher.

I would also like to thank Dr. Brian Amsden for his support and exceptional teaching as well as serving on my committee. Furthermore, I would like to thank my committee members Dr. Christopher Nicol and Dr. Craig Simmons for their insight and guidance on my research. To the surgeons at Kingston General Hospital and Hotel Dieu Hospital at Queen's University and University Hospital at Western University, thank you for your clinical collaboration and assistance in tissue acquisition which made this work possible. I would also like to thank Dr. Abbas Samani and Dr. J.F. Watkins for their collaboration on my publications as well as NSERC for my scholarship funding.

To all my wonderful Flynn lab colleagues both at Queen's and Western University, thank you for making this journey such an enriching experience both inside and outside the lab. Special thanks to Cody Brown, Valerio Russo, Lydia Fuetterer, Stuart Young, Andrew Carroll, Bryen Turco, Ming Gong, Hoi Ki Cheung, Allison Turner, and Anna Kornmuller who each helped me in different ways and for the fond memories we shared together during my time here.

Finally, I would like to thank my parents and grandparents for their love, support, and encouragement throughout my life and my studies. My thanks also to my brother, uncle, extended relatives here and abroad, and good friend Jess who have been there to listen and provided me with much needed humour, and my cat, Mao, for being my little furry companion.

Table of Contents

List of Tables

List of Figures

List of Abbreviations

ADIPOQ	Adiponectin
ALP	Alkaline phosphatase
ASC	Adipose-derived stem/stromal cell
ATP	Adenosine triphosphate
BAT	Brown adipose tissue
bFGF	Basic fibroblast growth factor
BMI	Body mass index
BMP	Bone morphogenetic protein
BMSC	Bone marrow-derived stem/stromal cell
BSA	Bovine serum album
BSP	Bone sialoprotein
C/EBPα	CCAAT/enhancer binding protein-alpha
C/EBPβ	CCAAT/enhancer binding protein-beta
C/EBPδ	CCAAT/enhancer binding protein-delta
CAMs	Cellular adhesion molecules
CCAC	Canadian Council on Animal Care
CHO	Chinese hamster ovary
CHOP-10	C/EBP homologous protein-10
COLL 1	Collagen 1
COLL 2	Collagen 2
COMP	Cartilage oligomerix matrix protein
CS	Chondroitin sulphate
DAPI	4',6-diamino-2-phenylindole
DAT	Decellularized adipose tissue
DEX	Dexamethasone
DNA	Deoxyribonucleic acid
D-PBS	Dulbecco's phosphate buffered saline
DS	Dermatan sulphate
ECM	Extracellular matrix
EDC	1-ethyl-3-(-3-dimethylaminopropyl) carbodiimide hydrochloride
EDTA	Ethylenediaminetetraacetic acid
ERK	Extracellular signal-regulated kinase
ESC	Embryonic stem cell
EWC	Equilibrium water content
FABP4/aP2	Fatty acid binding protein-4
FACIT	Fibril associated collagen with interrupted triple helices
FAS	Fatty acid synthase
FGF	Fibroblast growth factor
GAG	Glycosaminoglycan
Gal	Galactose
GalNAc	N-acetylgalactosamine
GAPDH	Glyceraldehyde-3-phosphate dehydrogenase
GATA2/3	GATA binding protein 2/3
GlcA	Glucuronate
GlcNAc	N-acetylglucosamine
GlcNS	N-sulphoglucosamine
GLUT4	Glucose transporter type 4

GMP	Good Manufacturing Practices
GPDH	Glycerol-3-phosphate dehydrogenase
GVHD	Graft-versus-host disease
HA	Hyaluronic acid
HDMS	Hexamethyldisilazane
HGF	Hepatocyte growth factor
HIF-1α	Hypoxia inducible factor-1 alpha
HLA-DR	Human leukocyte antigen-antigen D related
HMEC	Human microvascular endothelial cells
HS	Heparan sulphate
IBMX	3-isobutyl-1-methylxanthine
Id proteins	Inhibitor DNA binding proteins
IdoA	Iduronate
IFATS	International Federation for Adipose Therapeutics and Sciences
IgE	Immunoglobulin E
IGF-IR	Insulin-like growth factor-I receptor
IHC	Immunohistochemistry
IHH	Indian hedgehog
IL-1β	Interleukin-1 beta
IL-6	Interleukin-6
IL-10	Interleukin-10
IL-13	Interleukin-13
IPO8	Importin 8
ISCT	International Society for Cellular Therapy
KS	Keratin sulphate
LPL	Lipoprotein lipase
MCS	Methacrylated chondroitin sulphate
MCSF	Macrophage colony-stimulating factor
MGC	Methacrylated glycol chitosan
MHC-1	Major histocompatibility complex antigen class I
MSC	Mesenchymal stem/stromal cells
NF-kB	Nuclear factor kappa-light-chain-enhancer of activated B cells
OCN	Osteocalcin
ON	Osteonectin
OPN	Osteopontin
OSX	Osterix
p16	Cyclin-dependent kinase inhibitor 2A, multiple tumour suppressor 1
p21	Cyclin-dependent kinase inhibitor 1
PAI-1	Plasminogen inhibitor activator-1
PBP	PPAR binding protein
PBS	Phosphate buffered saline
PDGF	Platelet-derived growth factor
PEG	Poly(ethylene glycol)
PGA	Polyglycolic acid
PGE2	Prostaglandin E2
PGF2α	Prostaglandin F2 alpha
PGK1	Phosphoglycerate kinase 1
PKA	Protein kinase A
PLA	Polylactic acid
PLGA	Poly(lactic-co-glycolic acid)

PODXL	Podocalyxin-like
PPARγ	Peroxisome proliferator-activated receptor-gamma
PPRE	Peroxisome proliferator response elements
PTHrP-R	Parathyroid hormone related protein-receptor
RGD	Arginine-glycine-aspartic acid
RPL13A	Ribosomal protein L13a
RT-PCR	Reverse transcriptase-polymerase chain reaction
RUNX2	Runt-related transcription factor 2
RXRα	Retinoid X receptor alpha
SA-β-gal	Senescence-associated beta-galactosidase
SD	Standard deviation
SDS	Sodium dodecyl sulphate
SEM	Scanning electron microscopy
SFF	Solid free form
SIS	Small intestine submucosa
SLRP	Small leucine-rich proteoglycan
SMAD	Signaling mothers against decapentaplegic
SMC	Smooth muscle cell
SOX5	Sex-determining region Y-related high motility group box 5 transcription factor
SOX6	Sex-determining region Y-related high motility group box 6 transcription factor
SOX9	Sex-determining region Y-related high motility group box 9 transcription factor
SREBP1/ADD1	Sterol regulatory element binding protein-1/adipocyte determination and differentiation factor-1
SVF	Stromal vascular fraction
TAZ	Transcriptional co-activator with PDZ-binding motif
TCPS	Tissue culture polystyrene
TGF-β	Transforming growth factor-beta
TNF-α	Tumour necrosis factor-alpha
TUNEL	Terminal deoxynucleotidyl transferase (TdT) dUTP nick-end labeling
TZD	Thiazolidinedione
UACC	University Animal Care Committee
UBC	Ubiquitin C
UBM	Urinary bladder matrix
UCP-1	Uncoupling protein-1
VEGF	Vascular endothelial growth factor
WAT	White adipose tissue
Wnt	Wingless-related integration site

Chapter 1

Introduction

1.1 Clinical significance

With increasing interest in the clinical application of mesenchymal stem cells (MSCs), limitations concerning the scalability, reproducibility, and standardization of current cell culture methods are some of the major constraints for the widespread commercialization of cell-based therapies. Among these challenges, there is a need to develop new approaches to generate large populations of high-quality cells with predictable regenerative potential. It has been estimated that many future cell-based therapies will require multiple infusions delivering on the order of 1-5 million cells/kg body weight per session [1], [2]. However, conventional culturing systems involving expansion on rigid two-dimensional (2-D) tissue culture polystyrene (TCPS) lack the complexities of cell-cell and cell-extracellular matrix (ECM) interactions present in native tissues and have been associated with altered cell behaviour and differentiation capacity [3]–[5]. As such, there is a need to develop new strategies that yield clinically-relevant cell populations from small tissue biopsies, while maintaining the regenerative capacity of the cells. Furthermore, for many cell-therapy applications there is also strong evidence to support the design of improved cell delivery systems using instructive 3-D biomaterials to enhance cell retention and viability, as well as to direct cellular activities including lineage-specific differentiation [6]–[8].

Over the years, many tissue engineering strategies have been explored for culturing stem cells, as well as stimulating *in situ* tissue formation. The foundation of these approaches follows the well established concept that stem cell fate is regulated *in vivo* by physical and chemical interactions with the ECM and other local cell populations via cytokines, growth factors, surface chemistry, and mechanical stimuli [1], [2]. To design novel scaffolds to support cell expansion and improve the survival of transplanted cells, researchers have focused on the 'tissue-specific' niche, which describes the distinct biomechanical, biochemical, and biophysical cues present within

various tissue systems in the body [3]. Currently, studies examining the ECM, which makes up the physical structure of the niche, have been of significant interest in the design of novel cell delivery systems since the ECM provides structural and biological support and can serve as a local reservoir for growth factors and cytokines [9], [10].

In the context of biomaterials development, a range of synthetic and natural scaffolds have been used to recapitulate the ECM microenvironment to drive desired cellular responses [11]–[13]. Notably, an emerging field exploiting the natural heterogeneous ECM composition from diverse tissue structures involves the use of biodegradable decellularized tissues [4]. Decellularization processes aim to extract immunogenic components from tissue samples while preserving the innately complex ECM constituents as much as possible, which may be difficult to fully mimic through synthetic techniques. Ideally, ECM components such as collagens, laminin, fibronectin, proteoglycans, and growth factors, as well as the physical properties of the original ultrastructure will be at least partially retained [5]. As a result, naturally-derived ECM scaffolds have been shown to mediate subsequent cellular signaling and wound healing processes to help restore tissue function [6].

Among the available tissue sources for decellularization, human adipose tissue provides an abundant and readily available supply of ECM [14]–[16]. Adipose tissue is typically harvested from discarded fat following breast or abdominal reduction procedures or through minimally invasive techniques such as lipoaspiration. In addition, adipose tissue contains a rich source of adipose-derived stem/stromal cells (ASCs), which possess plasticity towards the mesenchymal lineages [17], [18]. ASCs can be induced in culture to differentiate into fat, bone, and cartilage, as well as to display markers of the myogenic, hematopoietic, neuronal, and endothelial lineages [7]. The growing popularity of ASC-based therapies has resulted in advancements in the fields of vasculogenesis and angiogenesis in ischemia, bone and cartilage tissue regeneration, soft tissue augmentation in plastic and cosmetic reconstruction, and in the treatment of diabetic skin

ulcerations [8]–[12]. Recently, decellularized adipose tissue (DAT) constructs combined with ASCs have emerged as potential tissue-specific autologous or allogenic cell-based treatments to promote soft tissue regeneration [14], [19]–[22].

At the initiation of this project, intact DAT had demonstrated potential as an adipogenic cell culture platform but few studies had looked into processing the DAT into more physically defined 3-D constructs to broaden its utility in tissue engineering applications [23]. While some investigators had processed DAT into injectable hydrogels as a minimally invasive cell delivery method for soft tissue reconstruction [22], [24], structurally defined 3-D DAT microcarriers and foams were not previously developed or studied as cell delivery and expansion platforms. In this regard, the work presented in this thesis aimed to examine the potential use of 3-D bioscaffolds fabricated from enzyme-digested DAT as substrates for adipose tissue engineering, as well as for the development of an ASC expansion system. More specifically, initial studies focused on fabricating novel crosslinked DAT microcarriers and porous non-chemically crosslinked DAT foams, and assessing the capacity of these bioscaffolds to support ASC adipogenesis [19], [20]. In the final work, a new approach was established for synthesizing non-chemically crosslinked DAT microcarriers and their application as a substrate for large-scale ASC expansion in dynamic culture was explored. Overall, this body of work provided useful insight into the influence of the tissue-specific ECM on directing stem cell responses and introduced novel bioscaffold fabrication techniques and dynamic cultivation strategies for ASCs.

1.2 Hypotheses

In the context of adipose tissue regeneration, several studies in the literature have supported the use of adipose-derived ECM bioscaffolds to regenerate fat [15]–[17]. Previous work in the Flynn lab helped to pioneer this field and demonstrated the natural *in vitro* adipo-inductive properties of intact DAT in the absence of inducing factors [18]. Given this promising evidence, in this doctoral thesis it was hypothesized that bioscaffolds derived from enzyme-digested DAT would also provide an adipo-inductive substrate for ASC adipogenesis. In addition, recent studies have suggested that utilizing tissue-specific ECM may be a promising approach to naturally modulate the stem cell response in the development of cell-based therapies [25]. With this guiding principle, it was further hypothesized that a cell expansion system incorporating DAT microcarriers in dynamic culture could be used to promote the large-scale expansion of human ASCs while maintaining their immunophenotype and multilineage differentiation capacity.

1.3 Research objectives

To address these hypotheses, three specific objectives were formulated:

1. To investigate ASC adipogenic differentiation under dynamic culture conditions on chemically crosslinked microcarriers derived from pepsin-digested DAT relative to gelatin microcarrier controls.
2. To develop methods to fabricate non-chemically crosslinked 3-D porous foams derived from α-amylase-digested DAT and investigate their use as a platform for ASC adipogenesis.
3. To develop methods to fabricate non-chemically crosslinked 3-D porous microcarriers derived from α-amylase-digested DAT and investigate their use as a platform for ASC expansion under dynamic culture conditions relative to Cultispher-S microcarriers and static TCPS controls.

1.4 Project overview

Based on previous studies in the Flynn lab, crosslinked microcarriers prepared from pepsin-solubilized DAT demonstrated enhanced human ASC attachment and proliferation within a dynamically stirred culture system in comparison to gelatin microcarriers and TCPS controls [26]. Expanding on these observations, the first objective involved further probing the potential use of the DAT microcarriers for applications in adipose tissue regeneration. More specifically, detailed *in vitro* adipogenic studies were conducted by dynamically culturing human ASCs on the DAT microcarriers in comparison to gelatin microcarrier controls. A one-month *in vivo* study was also performed using a subcutaneous rat model to assess the injectability and biocompatibility of the DAT microcarriers relative to the gelatin controls. This work, described in Chapter 3, was published in Biomaterials (2012) [19].

While the crosslinked DAT microcarriers served as a promising adipo-inductive substrate, it was recognized that improvements could be made in the fabrication process to circumvent the need for chemical crosslinking to ensure stability. As a result, methods were established to use α-amylase digestion to generate DAT bioscaffolds that were stable in culture without the need for chemical crosslinking. To assess the bioactivity of scaffolds synthesized with α-amylase-digested DAT, the second objective involved the *in vitro* and *in vivo* characterization of a range of novel DAT foams and bead foams (US and Canadian patents filed), with a focus on ASC adipogenesis and soft tissue regeneration. This study, described in Chapter 4, was published in Biomaterials (2013) [20].

Following the positive results from the second objective, the final aim involved applying this new fabrication method to overcome challenges associated with low porosity and large microcarrier size (i.e. 900-950 μm) during the initial study. In this case, an electrospraying technique was used to create porous non-chemically crosslinked DAT microcarriers within a size range of 350-500 μm to serve as an injectable ASC expansion system. Upon synthesizing the DAT microcarriers, the ultrastructural properties, stability, and ECM composition were assessed across a

range of formulations. Subsequently, ASC proliferation was evaluated on the DAT microcarriers compared to commercially available Cultispher-S microcarriers (crosslinked porcine gelatin) within a spinner flask culture system. Finally, the ASCs expanded on the DAT microcarriers, Cultispher-S microcarriers, and TCPS controls were characterized in terms of immunophenotype analysis, upregulation of lineage-specific genes (i.e. fat, bone, and cartilage) prior to differentiation, and multilineage differentiation capacity towards the adipogenic, osteogenic, and chondrogenic lineages. Details of this work are found in Chapter 5.

Chapter 2

Literature Review

2.1 Adipose tissue

In mammals, adipose tissue exists in two forms as white adipose tissue (WAT) or brown adipose tissue (BAT), with each functioning in distinct physiological roles [27]. WAT primarily functions in insulation and lipid storage, releasing fatty acids via lipolysis in response to energy demands. However, WAT also serves as an endocrine organ to help maintain homeostasis through the secretion of adipose tissue cytokines called adipokines [28], [29]. In particular, a large range of adipokines have been identified and are involved in a myriad of cellular functions such as glucose regulation, immune response, vascular homeostasis, the alternative complement system, blood clotting, blood pressure, and angiogenesis [28], [29]. For example, WAT is capable of the synthesis and secretion of adiponectin, which acts to control glucose levels and the breakdown of fatty acids [29]. Leptin is another secreted adipokine that mediates energy balance and metabolism by regulating appetite [29]. Other identified secreted factors include tumour necrosis factor-alpha (TNF-α) and interleukin-6 (IL-6), which are related to immune response, as well as angiotensinogen, plasminogen inhibitor activator-1 (PAI-1), and vascular endothelial growth factor (VEGF) [30]. In the design of tissue regeneration strategies, WAT has been of predominant interest since it makes up the major component of subcutaneous tissues in adult humans and offers a convenient source for both cells and scaffolding material [14]–[16], [18].

On the other hand, in humans BAT is found most abundantly in newborns and is responsible for regulating body temperature through the production of heat via adaptive thermogenesis [31]. BAT is a highly vascularized tissue that is innervated though the sympathetic nervous system, which allows for direct response to cold temperature-induced signaling [27]. Thermogenesis is achieved by the presence of a large number of mitochondria possessing a unique protein called

uncoupling protein-1 (UCP-1), which drives cellular adenosine triphosphate (ATP) production [32]. Interestingly, animal and human studies have suggested that BAT may play a metabolic role in obesity through the correlation of lowered BAT activity with high BMI and fat accumulation [27], [33]. These findings suggest that further investigation into the physiological role of BAT could be a potential direction for combating the onset of obesity.

2.2 Adipose-derived stem/stromal cells

In the late 1960s, Friedenstein *et al.* first reported evidence of a population of plastic-adherent bone marrow-derived stem/stromal cells (BMSCs) capable of clonal expansion and osteogenic differentiation [34], [35]. This pioneering work on the existence of mesenchymal stem/stromal cells (MSCs) within adult tissues revolutionized the field of regenerative stem cell therapy and initiated the exploration of alternative MSC sources. As a result, research on MSCs have rapidly expanded and the isolation of these cells have extended to other tissues including adipose, peripheral blood, dermis, heart, and lung [36]–[40]. In the context of clinical translation, MSCs should ideally be available in high cell numbers and be accessible with minimal impact to the patient. Furthermore, it would be advantageous if the cells could be expanded in culture while maintaining their multilineage differentiation capacity. Although BMSCs have been extensively studied for the development of MSC therapies, there are limitations regarding their low yields (with an estimated frequency of 1 BMSC in every 3.4×10^4 bone marrow nucleated cell population), as well as pain during collection [41], [42]. As such, MSCs from the adipose tissue stroma are now gaining significant interest within the research community since their initial identification in 2001 from processed lipoaspirate by Zuk *et al.* [17], [18], [43]. To clarify the inconsistencies in nomenclature describing these cells, the International Federation of Adipose Therapeutics and Sciences (IFATS) established the term "adipose-derived stem/stromal cells" (ASCs) to refer to the plastic adherent multipotent cell population following isolation [44]. To date, the introduction of

ASCs has spearheaded a new branch of research and development into the broad utility of these cells in tissue engineering and regenerative medicine.

ASCs are obtained from subcutaneous fat stores in the body and their ease of collection, as well as relative abundance, make them a highly attractive regenerative cell source for researchers and clinicians. ASCs are typically harvested using minimally invasive techniques such as lipoaspiration or en bloc following breast or abdominal reduction surgeries. By nature, ASCs are a readily available autologous stromal cell source for patients, with reported yields of 40 times more ASCs in a single aspiration than the number of BMSCs in a bone marrow aspiration [45]. Common protocols for ASC isolation involve enzymatic digestion and separation steps via centrifugation to yield a heterogeneous stromal vascular fraction (SVF) rich in pre-adipocytes, endothelial progenitor cells, macrophages, circulating blood cells, fibroblasts, pericytes, smooth muscle cells (SMCs), and MSCs [46], [47]. The SVF can then be further purified by selecting for the adherent ASC population via expansion on tissue culture plastic.

It is important to note that the diverse tissue-harvesting sites, isolation procedures, and growth conditions used among different laboratories can affect the cells in terms of yield, expansion rates, and differentiation capacity [48], [49]. The plastic-adherent population is inherently heterogeneous, possessing different morphologies (i.e. small rapidly self-renewing cells, spindle-like cells, and large flattened cells) and varying ratios of uni-, bi-, and tri-potent stem cells, progenitor cells, and more differentiated subpopulations [50]–[53]. As a consequence, attempts to standardize protocols and guidelines are now underway in order to achieve consistency and reproducibility necessary for commercialization and clinical translation.

2.2.1 Donor and depot effects on ASCs

Interestingly, recent studies have found differences in the function and quality of ASCs associated with donor variability. Increasing donor age has been shown to negatively impact the

frequency and proliferation rate of ASCs, which parallels the increased expression of senescence markers like SA-β-gal, p16, and p21 in older patients [54]. Studies examining ASCs from lipoaspirates collected from females ranging between 20-58 years old demonstrated no significant differences in adipogenic potential [55], [56]. However, osteogenic capacity was distinctly reduced in donors 37-46 years old and was postulated to be linked to decreased estrogen levels in perimenopausal and menopausal women [55], [56]. Donor health status is also a significant factor and several investigators have correlated increased body mass index (BMI) to reduced proliferation rates, colony forming unit frequency, and differentiation capacity [57], [58], while others have noted no significant differences [59], [60]. These discrepancies underline the need for larger studies to draw more concrete conclusions relating age and BMI, as well as recognizing the difficulties in dissecting the multitude of unknown patient parameters such as diabetes, smoking, and hormonal status that could potentially affect ASC functionality.

Increasing evidence has also shown that the selection of subcutaneous and visceral fat depots has a direct influence on ASC characteristics and are an important consideration for tailoring cell-based therapies. ASCs harvested from the upper arm and medial thigh via lipoaspiration consistently have higher proliferative and differentiation capacity, which is independent of age, as opposed to fat from the trochanteric and superficial or deep abdominal regions [61]. Russo *et al.* found that adipogenesis was enhanced in ASCs isolated from adipose tissue sourced from the subcutaneous, pericardial, and thymic remnant depots, while osteogenic differentiation levels were highest in ASCs isolated from the omentum [62]. In addition, differences in osteogenic properties from the superficial and deep adipose tissue layers of the abdomen have been correlated to gender, such that osteogenesis was highest in ASCs obtained from the superficial region in males, while no significant differences in osteogenic capacity were observed in females [63]. Taken together, these studies support the view that not all adipose tissue is equal and the source depot may be a factor that could be exploited to isolate specific subpopulations predisposed towards a desired cell fate.

2.2.2 ASC origin and immunophenotype

The current view is that ASCs *in vivo* are situated within a perivascular niche in co-existence with resident endothelial and pericyte cells [64]. This perivascular origin was visually identified through immunohistochemical staining; however, the exact localization of multipotent ASCs within the native tissues remains controversial due to the lack of a unique stem cell marker [65], [66]. As a result, several studies looking to characterize cultured ASCs rely on a panel of immunophenotypic markers following cell isolation for their identification.

With the intention of standardizing the characterization of ASCs, IFATS and the International Society for Cellular Therapy (ISCT) have jointly defined a set of standard parameters. In general, ASCs should adhere to the following minimum criteria: (1) plastic-adherent, (2) express the standard immunophenotypic profile (Table 2.1), and (3) maintain multipotency towards the adipogenic, osteogenic, and chondrogenic lineages [67]. In the undifferentiated state, the ASC immunophenotype exhibits very similar markers to BMSCs (e.g. CD29, CD44, CD73, and CD90) with the exception of abundant CD34 expression in ASCs at early passages and positive expression of CD36 (fatty acid translocase) [17], [68]–[72].

Table 2.1: ASC immunophenotype [67], [72].

	Antigen
Primary positive markers (>80%)	CD90 (Thy-1) CD105 (endoglin) CD73 (ecto-5'-nucleotidase) CD44 (hyaluronic acid receptor) CD29 (β1-integrin) CD13 (aminopeptidase-N) CD34 (progenitor associated marker)* CD146 (melanoma cell adhesion molecule, MCAM)*
Secondary positive markers	CD10 (neprilysin) CD26 (dipeptidyl peptidase-4) CD49d (α4-integrin)* CD49e (α5-integrin) CD36 (fatty acid translocase)
Primary negative markers (<2%)	CD31 (platelet endothelial cell adhesion molecule, PECAM) CD45 (leukocyte-common antigen, L-CA) CD235a (glycophorin A) HLA-DR (human leukocyte antigen-antigen D related)
Secondary negative markers	CD3 (T-cell co-receptor) CD11b (αM-integrin) CD49f (α6-integrin) CD106 (vascular cell adhesion protein 1, VCAM-1) PODXL (podocalyxin-like)

**Present at variable levels of expression*

It is recommended that immunophenotype analysis includes at least two positive and two negative markers in addition to the detection of secondary positive and negative markers to solidify the characterization of ASCs [67]. Furthermore, the viability of ASCs should be greater than 90%, while primary positive marker expression should be greater than 80% and less than 2% for primary negative markers, such as those for haematopoietic (CD45) and endothelial cells (CD31) [67].

From the aforementioned immunophenotype guidelines, slight discrepancies in the level of expression of some markers have been reported in literature. These differences have been attributed to the diverse culture conditions employed and/or time in culture [52], [73]. For instance, at early passages, CD34 and CD146 are highly expressed, but there is a significant decrease in levels during culture [74], [75]. In contrast, the inverse phenomenon has been reported for stromal markers such

as CD105, CD90, CD29, CD166, and CD73 [75]. While the niche serves to direct cell fate and function *in vivo*, the local microenvironment *in vitro* such as on 2-D plastic or 3-D substrates may also influence the immunophenotype of ASCs [52].

2.2.3 Paracrine mechanisms of regeneration with ASCs

An attractive characteristic of ASCs for cell-based regeneration is their capacity to secrete beneficial paracrine factors that can modulate the rate and extent of healing [76], [77]. At sites of injury, ASCs can secrete a wide range of growth factors such as platelet-derived growth factor (PDGF), basic fibroblast growth factor (bFGF), hepatocyte growth factor (HGF), and vascular endothelial growth factor (VEGF), as well as anti-inflammatory cytokines of the interleukin family (e.g. IL-10, IL-13) and prostaglandin E2 (PGE2) [78]–[80]. These secreted paracrine factors function to recruit nearby cells that promote constructive tissue remodeling [44].

Interestingly, several studies have linked the reduced oxygen levels in damaged tissues as an environmental stimulant for ASCs to undergo a regenerative cascade [76], [81], [82]. Under hypoxic stress, *in vitro* experiments have demonstrated enhanced ASC proliferation, collagen synthesis, and increased expression of VEGF and bFGF [83]–[85]. For instance, Kim *et al.* showed that human dermal fibroblasts (HDFs) cultured in hypoxic human ASC-conditioned media exhibited significantly enhanced *in vitro* migration [83]. ASC paracrine activity was also supported by Hsiao *et al.* who showed that human microvascular endothelial cells (HMECs) cultured in human ASC-conditioned media promoted angiogenic activity as a result of ASC-secreted VEGF-A and VEGF-D [86].

There is also growing evidence that ASCs are capable of modulating macrophage behaviour by promoting an anti-inflammatory M2 phenotype [87], [88]. This phenomenon was observed *in vitro* wherein mouse ASCs co-cultured with non-polarized M0 macrophages exhibited increased expression of the M2 phenotype, and mouse ASCs co-cultured with M1 macrophages significantly

lowered the secretion of pro-inflammatory cytokines: TNF-α and IL-1β [87]. In a study conducted by the Flynn lab, immunohistochemical analysis of *in vivo* explants of rat ASC-seeded decellularized adipose tissue (DAT) scaffolds showed that ASCs promoted host cell recruitment and a more pro-regenerative M2 phenotype, resulting in enhanced *in situ* angiogenesis and adipogenesis [88]. The immunosuppressive properties of ASCs were also observed in an allergic rhinitis mouse model. In this case, mouse ASCs reduced immunoglobulin E (IgE) antibodies and eosinophilic inflammation by decreasing IL-4 and IL-5 production, which are characteristically overproduced in response to allergens [89]. The ability for ASCs to modulate the immune response profile shows promise for extending the utility of these cells to improve the outcomes of wound healing, as well as the management of allogenic transplantation and graft-versus-host disease (GVHD).

2.2.4 Transcriptional control of ASC differentiation

It has been demonstrated that ASCs are capable of differentiating along the adipogenic, osteogenic, and chondrogenic lineages *in vitro* [90]. Understanding the transcriptional factors and signaling pathways involved in ASC differentiation is critical for the design of culture conditions and medium formulations.

2.2.4.1 *Adipogenesis*

The induction of ASCs towards the adipogenic cascade begins with the presence of hormonal inducers such as glucocorticoid agonists (e.g. hydrocortisone and dexamethasone (DEX)), as well as supra-physiological concentrations of insulin [91]. These in turn activate the early transcription factors CCAAT/enhancer binding protein-β (*C/EBPβ*) and CCAAT/enhancer binding protein-δ (*C/EBPδ*) in pre-adipocytes, which function to stimulate the primary transcription factors of adipogenesis: the nuclear receptor peroxisome proliferator-activated receptor-γ (*PPARγ*) and CCAAT/enhancer binding protein-α (*C/EBPα*) [92]. *C/EBPα* activation inhibits proliferation while

maintaining insulin sensitivity in the maturing adipocyte, and *PPARγ* and *C/EBPα* work in concert via a positive feedback loop in order to sustain high levels of expression necessary to drive maturation and terminal differentiation [93]. These actions collectively lead to lipid accumulation resulting from the upregulation of adipocyte-specific genes such as lipoprotein lipase (*LPL*), fatty acid binding protein-4 (*FABP4* or *aP2*), glucose transporter type 4 (*GLUT4*), fatty acid synthase (*FAS*), malic enzyme, acetyl CoA carboxylase, insulin receptor, and glycerol-3-phosphate dehydrogenase (*GPDH*) [94].

Adipocyte gene expression can also be directly stimulated with synthetic *PPARγ* ligands called thiazolidinediones (TZDs) (e.g. rosiglitazone, pioglitazone, and troglitazone), which are antidiabetic drugs used to increase insulin sensitivity [95]. Upon ligand binding, *PPARγ* undergoes a conformational change to form a heterodimer with retinoid x receptor alpha (RXRα) to allow binding to target DNA regions of particular genes called peroxisome proliferator response elements (PPREs), thus influencing gene transcription [96]. In addition, sterol regulatory element binding protein-1/adipocyte determination and differentiation factor-1 (SREBP1/ADD1) can also directly upregulate *PPARγ* expression, as well as the production of endogenous *PPARγ* ligands such as fatty acids and prostaglandins [97], [98].

A summary of the adipogenic transcriptional cascade is illustrated in Fig. 2.1. Overall, adipogenesis is mediated by a balance between pro-adipogenic and anti-adipogenic factors along various points in the transcriptional cascade, as summarized in Table 2.2. Standard media supplements added to serum-free media formulations to induce *in vitro* adipogenesis depend on the species of interest but often include insulin, 3-isobutyl-1-methylxanthine (IBMX, a phosphodiesterase inhibitor), DEX or hydrocortisone, and troglitazone, which act to promote the upregulation of the key adipogenenic transcription factors and genes [99]–[101].

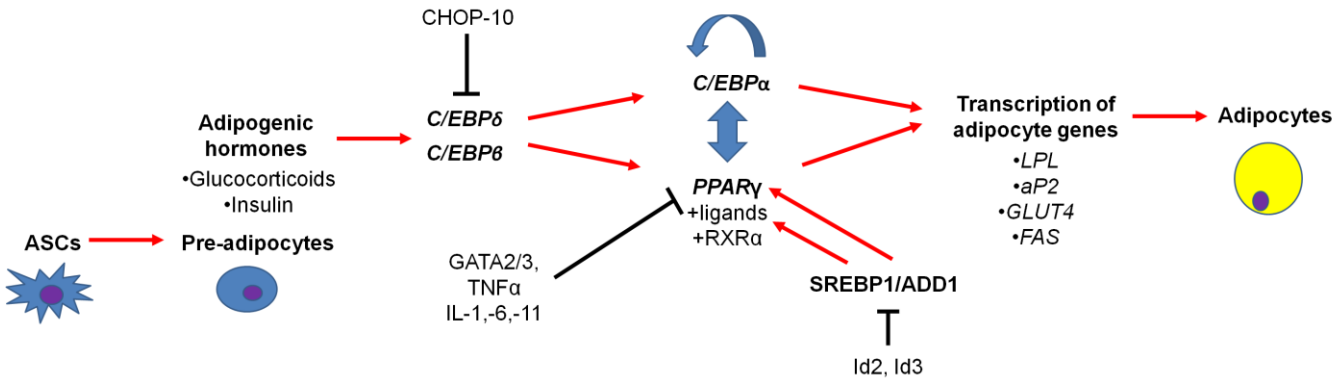

Figure 2.1: Transcriptional control of adipogenesis. Arrows indicate positive effects and solid lines indicate inhibition.

Table 2.2: Factors stimulating and inhibiting adipogenesis [91], [93], [102]–[104]

Factor	Function	Outcome
Insulin-like growth factor-I receptors (IGF-IRs)	Increase insulin sensitivity	+
Macrophage colony-stimulating factor (MCSF)	Involved in adipocyte hyperplasia	+
Fatty acids and prostaglandins	Act as ligands/precursor ligands for *PPARγ* or induce *C/EBPβ* and *C/EBPδ*	+
Glucocorticoids	Activate expression of *C/EBPδ* and *PPARγ*	+
Nuclear co-activators (e.g. PPAR binding protein, PBP)	Function through *PPARγ* to promote adipogenesis	+
Wingless-related integration site (Wnt) signaling	Blocks the induction of *PPARγ* and *C/EBPα*	-
Transforming growth factor- β (TGF-β)	Blocks the induction of *PPARγ* and *C/EBPα*	-
Tumour necrosis factor (TNF-α)	Blocks the induction of *PPARγ* and *C/EBPα*	-
Interleukins (IL-1, IL-6, IL-11)	Blocks the induction of *PPARγ* and *C/EBPα*	-
Prostaglandin F2α (PGF2α)	Inhibits by activation of ERK1/2 pathway in pre-adipocytes	-
C/EBP homologous protein-10 (CHOP-10)	Inhibits *C/EBPβ* expression	-
Inhibitor DNA binding proteins (e.g. Id2, Id3)	Physically blocks SREBP1/ADD1	-
GATA2/3	Inhibits *PPARγ* expression	-
Nuclear co-repressors (e.g. transcriptional co-activator with PDZ-binding motif, (TAZ))	Functions through *PPARγ* to block adipogenesis	-

2.2.4.2 *Osteogenesis*

Osteogenic differentiation of ASCs occurs in several stages starting with a proliferative phase involving the formation of dense cell nodules, followed by the synthesis and secretion of ECM, maturation into osteocytes, and matrix mineralization [105]. The canonical Wnt and bone morphogenetic protein (BMP) signaling pathways play predominant roles throughout the osteogenic cascade in driving proliferation and the maturation of progenitor cells into osteocytes [106]. In particular, BMP-2, -4, -6, -7, and -9 have been recognized as potent inducers of osteogenesis via the signaling mothers against decapentaplegic (SMAD) phosphorylation pathway [107]–[109].

During the early stages, a combination of hormones, growth factors, and cytokines activate transcription of the runt-related transcription factor 2 (*RUNX2*), a primary transcription factor for osteogenesis, which causes the cells to adopt a pre-osteoblast phenotype [106], [110]. In return, *RUNX2* induces the expression of an important secondary transcription factor, zinc finger-containing transcription factor osterix (*OSX*), which is required to sustain commitment to the osteogenic lineage [110], [111]. Through the runt domain, *RUNX2* interacts with the promoters of osteogenic-specific genes such as bone sialoprotein (*BSP*), osteopontin (*OPN*), alkaline phosphatase (*ALP*), osteonectin (*ON*), osteocalcin (*OCN*) as well as the non-specific gene collagen I (*COLL 1*), which leads to matrix production and mineralization [112], [113]. Interestingly, overexpression of *RUNX2* has been shown to have an inhibitory effect during the later stages of differentiation and may be critical only in the beginning phase to induce osteogenesis [114], [115].

The exact mechanisms for controlling *RUNX2* expression remain unclear, however some factors have been elucidated. For example, *RUNX2* transcription has been shown to be upregulated by BMPs, retinoic acid, fibroblast growth factors (FGFs), and 1α,25-dihydroxyvitamin D_3 (vitamin D), while being downregulated by GATA4 and TNF-α [113], [116]–[118]. It has also been reported that there is an inverse relationship between the osteogenic and adipogenic pathways in

MSC differentiation [119], [120]. Related to this, *PPARγ* is a negative regulator of osteogenesis, inhibiting the transcriptional activity of *RUNX2* on the osteocalcin promoter [120]. Typical osteogenic cocktails include the addition of beta-glycerophosphate, ascorbate-2-phosphate, insulin, vitamin D, and DEX to serum-supplemented media to induce matrix production and mineralization [101], [121], [122]. A summary of the progress of osteogenesis is shown in Fig. 2.2.

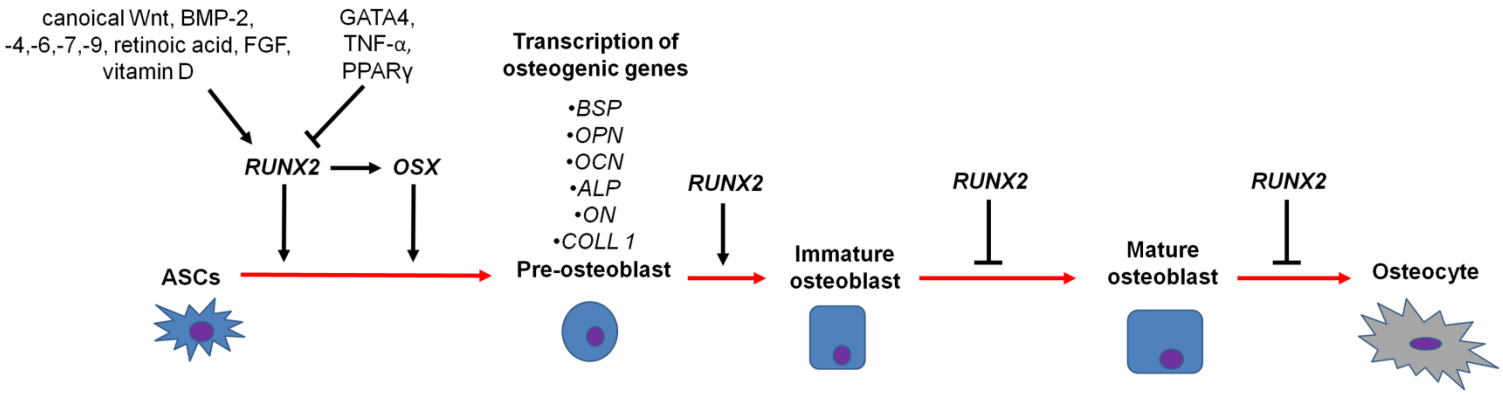

Figure 2.2: Transcriptional control of osteogenesis. Note that collagen I (*COLL 1*) is a non-specific genetic marker for osteogenic differentiation. Arrows indicate positive effects and solid lines indicate inhibition.

2.2.4.3 *Chondrogenesis*

Differentiation towards the chondrogenic lineage requires culturing ASCs in a 3-D conformation to mimic the mesenchymal condensation process during embryogenesis and enhance cell-cell and cell-ECM interactions [123]. In early chondrogenesis, TGF-β as well as BMP-2, -4, -6, and -7 signaling promote cellular condensation, which is important to induce commitment towards a pre-chondrocyte phenotype [123], [124]. Following condensation, the cells begin to differentiate into highly proliferative chondroblasts, initiating a change in matrix composition wherein collagen I expression is reduced and collagen II, collagen IX, collagen XI, aggrecan, and cartilage oligomeric matrix protein (*COMP*) are upregulated [125].

These processes are initiated by the master regulator of chondrogenesis, sex-determining region Y-related high motility group box 9 transcription factor (*SOX9*), which upregulates the

expression of cartilage matrix-specific genes [123]. Furthermore, *SOX9* induces the transcription of the highly homologous pair: *SOX5* and *SOX6* [126], [127]. These two factors play an important role in cartilage-specific matrix production by enhancing *SOX9* activity, which is necessary to maintain the immature phenotype of chondrocytes and prevent premature maturation into hypertrophic cells that is indicative of endochondral ossification [126]–[128]. *SOX9* is also regulated by several factors including FGF, hypoxia inducible factor-1 alpha (HIF-1α), protein kinase A (PKA), which act to upregulate expression, while the canonical Wnt pathway and retinoic acid downregulate expression [128], [129]. Furthermore, IL-1 and TNF-α downregulate *SOX9* expression via the nuclear factor kappa-light-chain-enhancer of activated B cells (NF-κB) pathway and may be involved in the progression of diseased cartilage in inflamed joints [130].

In the late stages, proliferating chondroblasts enlarge and become pre-hypertrophic chondrocytes, followed by terminal differentiation into hypertrophic chondrocytes, thus marking the beginning phase of osteochondrogenesis. During this time, *RUNX2* expression peaks, resulting in the induction of Indian hedgehog (*IHH*) and parathyroid hormone–related protein receptor (*PTHrP-R*) expression, which control chondrocyte hypertrophy leading to the beginning stages of calcification [113], [131]. Together, these processes contribute to the expression of collagen X in hypertrophic chondrocytes followed by apoptosis prior to calcification of the cartilaginous scaffold [123]. Serum-containing chondrogenic media formulations often include insulin, TGF-β1 only or TGF-β3 with BMP-6, DEX, and ascorbate-2-phosphate [121], [132], [133]. A schematic of the chondrogenic pathway is illustrated in Fig. 2.3.

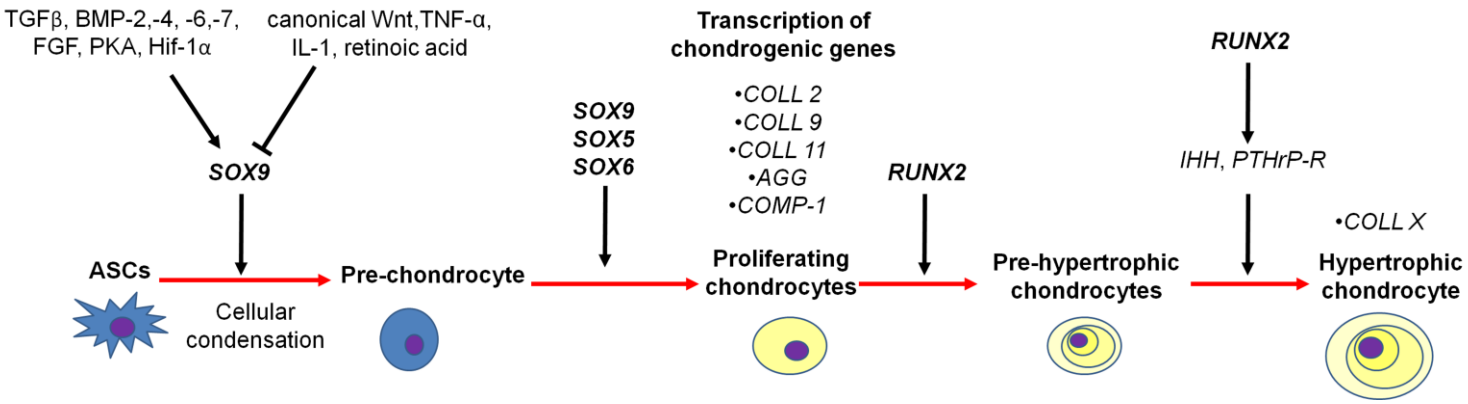

Figure 2.3: Transcriptional control of chondrogenesis. Arrows indicate positive effects and solid lines indicate inhibition.

2.3 The extracellular matrix

The acellular component of tissues in the body is predominantly comprised of a complex protein-rich network known as the ECM. *In vivo*, the ECM is physiologically active and regulates cell fate by guiding processes such as division, growth, and maturation [9], [134]. In addition to providing structural support, the ECM also serves as a local supply of growth factors that can be released through cell-mediated mechanisms [135]. As cells sense and respond to the ECM, they in turn can secrete factors that alter or remodel the environment, demonstrating the dynamic interrelationship between cells and their surroundings [136]. As detailed below, ECM constituents can be broadly classified into: (1) fibrous proteins (e.g. collagens and elastin), (2) glycosaminoglycans (GAGs), (3) proteoglycans, and (4) glycoproteins [137], [138]. Importantly, the variable amounts and arrangements of ECM constituents within different tissues define their structure and function.

2.3.1 Fibrous proteins

2.3.1.1 *Collagens*

Collagen is the most abundant protein in mammals and provides structural integrity, strength, and stability to the ECM [139]. While acting as a biomechanical support, collagen also

plays an important role in biological functions by influencing cellular activities such as attachment, viability, growth, and differentiation through receptor-mediated signaling [140], [141]. A defining feature of all collagens is the right-handed triple helical structure comprised of three α-chain subunits stabilized by hydrogen bonds (Fig. 2.4) [142]. The typical primary structure of each α-chain consists of the repeated amino acid sequences glycine-X-Y, where X and Y are most commonly proline and hydroxyproline residues, respectively, possessing a left-handed coiled conformation [141], [142]. Structurally, the small glycine resides are positioned in the inner coil while the larger proline and hydroxyproline residues are positioned in the outer portions of the triple helix [141]. As a result, steric repulsion between the pyrrolidine rings on the proline and hydroxyproline residues enable stability by allowing tight twists in the molecule [142], [143]. Non-helical N (amino)- and C (carboxyl)- terminal regions flanking the central helical domain are involved in triple helix formation, as well as mediating fibril diameter [141].

A total of 28 different collagen types have been identified to date and can be classified into subtypes as: fibrillar, fibril associated collagen with interrupted triple helices (FACIT), microfibrillar, short chain, and basement membrane [139], [141]. Each of these collagen types possess unique amino acid sequences, assembly, structure, and functional features within specific tissues [141]. For instance, the fibrillar collagens, such as collagen I, are arranged in highly organized aggregates crosslinked at the telopeptide regions by the enzyme lysyl oxidase [144]. This characteristic structure provides tensile strength as well as compressive resistance within skin, bone, tendons, and ligaments [141]. In contrast, basement membrane type collagens such as collagen IV lack a glycine residue in every third amino acid which renders it more flexible [145]. The triple helices of collagen IV are covalently crosslinked and assembled into tetramers to create a sheet-like network in the basement membrane structure [145], [146]. Collagen IV can be found in the lamina densa of skin, as well as in the basal lamina surrounding adipocytes [146], [147].

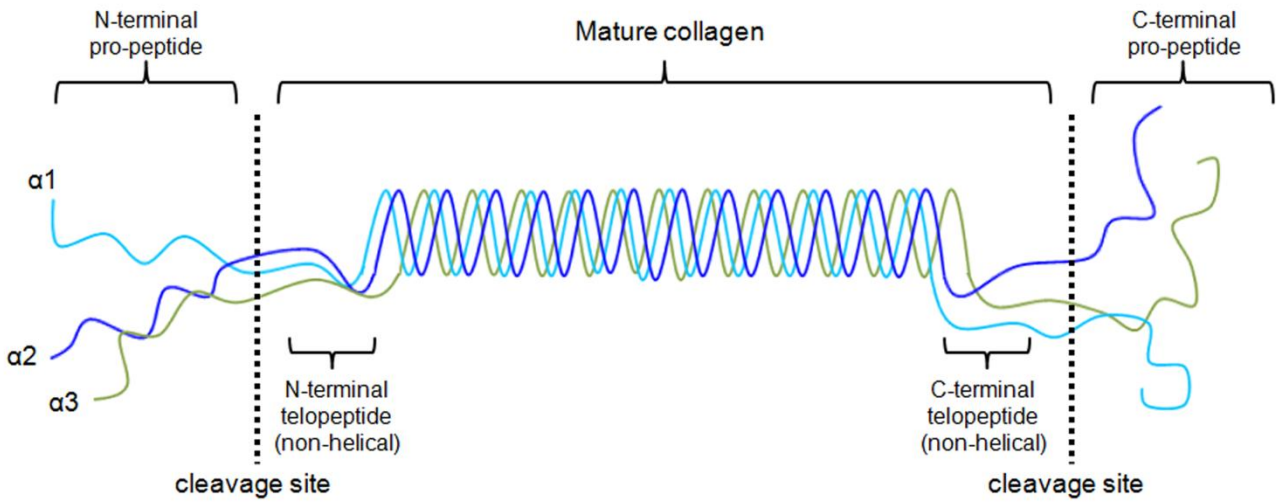

Figure 2.4: Representative structure for fibrillar collagen. Adapted from Fan *et al*.[148].

2.3.1.2 *Elastin*

Elastin is a hydrophobic protein found in many tissues and contributes to elastic properties, particularly in blood vessels, lungs, and skin [149]. Furthermore, elastin is comprised of base sequences of glycine-X, proline-X, glycine-glycine-X, and proline-glycine-X, where X can be glycine, leucine, isoleucine, alanine, and valine residues [149], [150]. Similar to collagen, elastin production starts intracellularly via the transcription of tropoelastin peptides [150]. These tropoelastin molecules are transported into the extracellular space via exocytosis and remain on the cell surface until contacted with an existing elastin fibril [150]. Following this, the tropoelastin molecule is released, crosslinked at the lysine residues by the enzyme lysl oxidase, and integrated via polymerization into the elastin network [150].

2.3.2 Glycosaminoglycans

Glycosaminoglycans (GAGs) are highly anionic linear polysaccharides which aid in the entrapment of growth factors as well as water, thus giving them their distinctive hydrophilic, viscous, lubricating, and shock absorbing properties [151]. GAGs are also involved in range of cellular functions including adhesion, growth, and differentiation, as well as in blood coagulation

[152]. The basic structure is comprised of repeating disaccharide units made up of uronic acid (i.e. iduronate (IdoA) or glucuronate (GlcA)) or galactose (Gal) joined by a glycosidic bond to an amino sugar (i.e. N-acetylgalactosamine (GalNAc), N-acetylglucosamine (GlcNAc), or N-sulphoglucosamine (GlcNS)) [152]. Furthermore, they can be classified into sulphated GAGs as heparin/heparan sulphate (HS), chondroitin sulfate (CS), keratin sulfate (KS), and dermatan sulphates (DS), or the non-sulphated GAG hyaluronic acid (HA) [152]. Unlike sulphated GAGs, HA does not bind to a core protein structure, but it forms the bulk of the interstitial gel that imparts compressive resistance to tissues and provides a backbone for the non-covalent bonding of proteoglycans [152]. Examples of different types of GAGs are shown in Table 2.3.

Table 2.3: Glycosaminoglycans

Glycosaminoglycan	Disaccharide units	Localization
Heparin	L-IdoA(2S)-α(1,4) **or** D-GlcA-β(1,4) **with** D-GlcNS-α(1,4) **or** GlcNAc-α(1,4) **or** D-GlcNS(6S)-α(1,4) **or** GlcNAc(6S)-α(1,4)	Mast cells, arteries of the liver, skin, and lungs
Heparan sulphate	L-IdoA-α(1,4) **or** L-IdoA(2S)-α(1,4) **or** D-GlcA-β(1,4) **with** D-GlcNS-α(1,4) **or** GlcNAc-α(1,4) **or** D-GlcNS(6S)-α(1,4) **or** GlcNAc(6S)-α(1,4)	Basement membrane, cell surface
Chondroitin sulphate	D-GlcA-β(1,3) or D-GlcA(2S)-β(1,3) **with** D-GalNAc-β(1,4) **or** D-GalNAc(4S and/or 6S)-β(1,4)	Cartilage, tendon, ligaments
Keratin sulphate	D-Gal-β(1,4) **or** D-Gal(6S)-β(1,4) **with** D-GalNAc-β(1,3) **or** D-GalNAc(6S)-β(1,3)	Cornea and cartilage
Dermatan sulphate	L-IdoA- β(1,3) **or** L-IdoA(2S)-β(1,3) **or** D-GlcA-β(1,4) **with** D-GalNAc-β(1,4) **or** D-GalNAc(4S and/or 6S)-β(1,4)	Skin, blood vessels, heart valves
Hyaluronic acid	D-GlcA-β(1,3) **with** D-GalNAc-β(1,4)	Skin, load bearing joints

***Nomenclature: α or β and (1,3) or (1,4) denote the location and geometry of the glycosidic bond, respectively. (4S) or (6S) denote the sulphation position while D- and L- denote the configuration of the monosaccharide unit.*

2.3.3 Proteoglycans

Proteoglycans are a class of glycosylated proteins comprised of one or more sulphated GAG chains that are covalently attached to a core protein [153]. Within the ECM, proteoglycans complex with other structures such as collagen, other proteoglycans, and hyaluronic acid, and the network they form helps to regulate the transport of proteins, cells, and molecules within the matrix [149]. To date, several different types of proteoglycans exist and are classified by their size and GAG composition. In particular, the ECM encompasses the largest family of proteoglycans and can be divided into hyalectins and small leucine-rich proteoglycans (SLRPs) [154]. Hyalectins bind to HA and lectin-binding proteoglycans and contain a large protein core attached to CS side chains [155]. Examples include aggrecan in cartilage, versican in soft tissues, as well as neurocan and brevican in the central nervous system [155]. SLRPs, possessing a small protein core attached to CS, KS, or DS side chains, modulate biological functions by interacting with cytokines, growth factors, ECM constituents, and cell surface receptors [156]. Examples of SLRPs include decorin, byglycan, fibromodulin, and lumican [154].

2.3.4 Glycoproteins

Additional fundamental components of the ECM are non-collagenous adhesive glycoproteins, which function to promote cell attachment to the matrix and to link matrix components within the ECM [157]. In particular, cell adhesion to the ECM is predominantly regulated through cellular adhesion molecules (CAMs) known as integrins that are present on the surface of cells and can bind with specific glycoprotein molecules [157]. Two commonly studied glycoproteins are fibronectin and laminin, which have been extensively used in biomaterial synthesis to enhance cell attachment and survival [158]–[160].

Fibronectin facilitates the attachment and migration of cells within the ECM. It exists in a dimer conformation with multiple binding sites along each of the two polypeptide chains, which are

joined at the C-terminus by two disulphide bonds (Fig. 2.5a) [149]. In particular, binding sites along each polypeptide chain are comprised of three repeating globular domains: (1) type I regions binding to heparin, fibrin, or collagen, (2) type II regions binding to collagen, and (3) type III regions binding to cell surface receptors [161]–[163]. Notably, alternative splicing only occurs within the type III regions and has resulted in the generation of 20 known isoforms in humans [164].

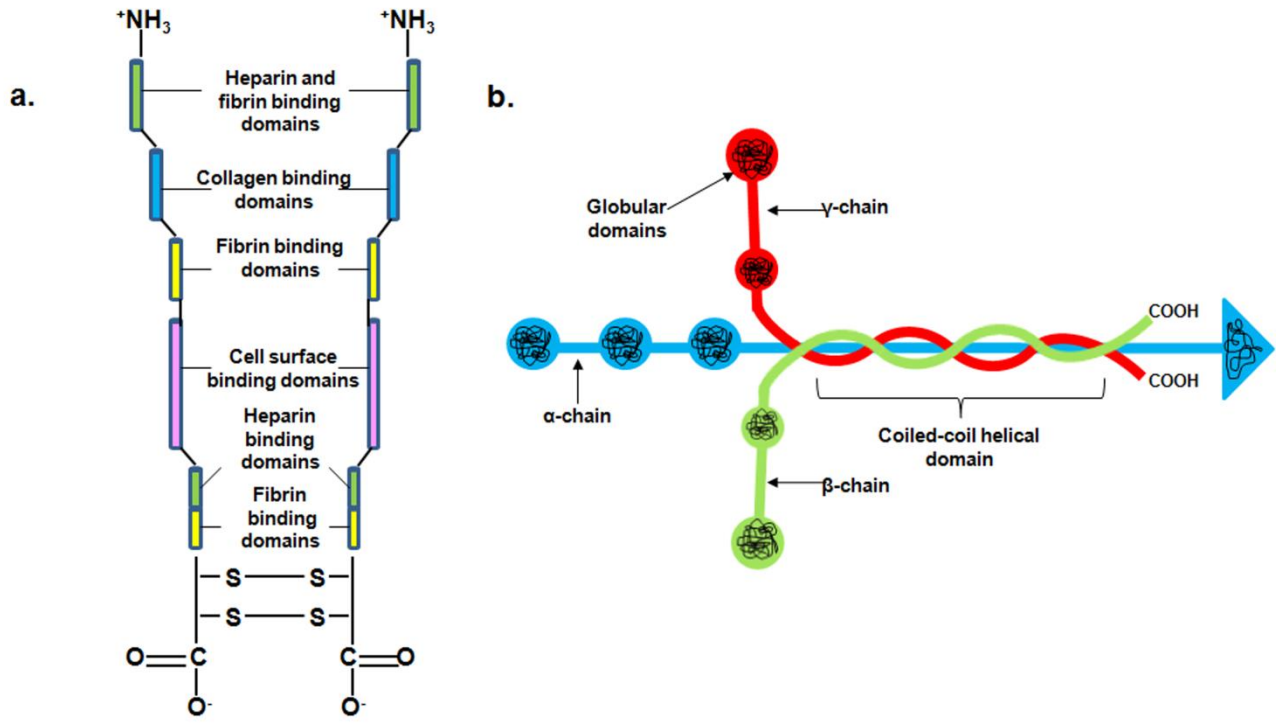

Figure 2.5: Molecular structure of (a) fibronectin and (b) laminin [149].

Laminin has a typical structure comprised of three polypeptide chains (i.e. α-chain, β-chain, and γ-chain) and forms a web-like structural network that is a part of the basement membrane [149]. These chains create a cross-like arrangement bound by disulfide bonds (Fig. 2.5b), each of which contain different isoforms totalling to 45 possible laminin variants [149]. More specifically, the three short arms are located on the N-terminus with three globular domains on the α-chain and two globular domains for the β-chain and γ-chain [165]. On the opposite end, the long arm possesses a

coiled-coil conformation with a large globular domain at the C-terminus [165]. Laminin has been shown to adhere to cell surface integrins as well as to perlecan and nidogens, which are specific to the basement membrane [149]. Together these functions allow laminin to assist in cell motility, proliferation, and differentiation [149].

2.4 ECM-derived biomaterials

Within adult mammalian tissues, the existence of distinct stem cell niches has been well supported since it was first hypothesized in 1978 by Schofield [166]. In particular, Schofield described that stem cell association with the local microenvironment and neighbouring cells is essential in mediating cellular behaviour [166]. As a result, the reciprocal crosstalk between resident stem cells and their niche is a critical factor for maintaining a balanced state of self-renewal and differentiation [166]. Since the ECM is an integral component of the niche, decoupling the unique constituents and properties of the ECM within different tissues is important for rational biomaterials development. In effect, specific cell-ECM interactions may be used to help facilitate *ex vivo* stem cell culture, as well as to regulate stem cell differentiation [11].

Building on these concepts, a plethora of synthetic and natural biomaterials in tissue engineering have been produced with the common goal of promoting constructive regeneration. Regardless of the intended application, all biomaterials should meet the following criteria: (1) biocompatible to support cell survival and prevent an adverse host immune response, (2) biodegradable to allow replacement by the host tissue with non-toxic degradation products, (3) possess mechanical properties suited to the specific tissue of interest, and (4) possess a porous microarchitecture to allow adequate cellular infiltration and diffusion of nutrients for long term stability [167]. While synthetic biomaterials allow for flexible control over biochemical and mechanical properties, it is often difficult to fully replicate the intricate native milieu [168]. Rather than attempting to mimic native tissues synthetically, an emerging strategy is to harness the

potential of naturally occurring constituents in the ECM. As a result, the development of ECM-derived biomaterials as stem cell expansion and delivery platforms has gained significant interest.

To date, ECM-derived biomaterials have been fabricated with ECM components derived from animal or human tissue sources [169]–[173]. Among the diverse ECM-derived materials available, collagen has long been favoured as a natural substrate for cells due to its relative abundance, ease of processing, biodegradability, low antigenicity, and cell-binding properties [169], [174], [175]. Namely, collagen type I is the most predominant form in the ECM and has been used extensively for a wide range of applications in various forms including hydrogels, fibrous sheets, foams, microcarriers, and tubes [141], [169], [174], [176]. Collagen scaffolds can also be further modified with growth factors to improve bioactivity, crosslinked to enhance mechanical properties, and incorporated with other materials to form composites [177]–[180]. Examples of uses include but are not limited to collagen-hydroxyapatite sponges for bone formation, injectable collagen hydrogels for intervertebral disc repair, and collagen dressings for wound healing [181]–[185].

GAG-based materials such as HA and CS are also of interest due to their innate function in the ECM to facilitate cell adhesion, influence cell proliferation and differentiation, entrap growth factors, and provide tissue-like hydration [186]. In particular, the backbone of HA and CS contain carboxyl and hydroxyl functional groups amenable to chemical modification and crosslinking [187], [188]. These sites can be used to incorporate functional groups to allow control over swelling, degradation, growth factor release, and mechanical properties of the resulting hydrogel [188]–[190]. Due to the innate compressive features of HA and CS networks, these types of materials have been investigated as biomaterials for cartilage tissue engineering. For example, chondrocytes encapsulated within injectable composite chitosan-HA or collagen-CS hydrogels have been shown to support chondrocyte viability and phenotype [191], [192]. Furthermore, in terms of wound healing applications, HA oligosaccharide degradation products have also been known to possess proangiogenic properties that can be used to induce vascularization [193], [194].

As discussed previously, elastin is another crucial component of the ECM contributing to tissue elasticity and resilience. Elastin-derived peptides have been demonstrated to modulate cell proliferation, migration, and differentiation [195]–[197]. Although mature elastin is stable it is also highly insoluble which limits its uses, thus soluble forms are prepared via hydrolyzation or in the precursor form as tropoelastin [198]–[200]. Subsequently, these soluble forms of elastin can be crosslinked into sheets, sponges, and tubes [201]. To date, elastin has been used for the creation of skin substitutes by incorporating elastin-laminin peptides into dressings or blending with collagen as in the commercially available matrix MatriDerm® (MedSkin Solutions) [202], [203]. For vascular tissue engineering, it was also demonstrated that tropoelastin fragments coated on synthetic polymers reduced thrombosis, while collagen-elastin tubes supported proliferation and contractility of human SMCs [204], [205] .

2.5 Decellularized tissue bioscaffolds

Within the broad field of ECM-derived biomaterials, focus on the production of decellularized tissue bioscaffolds has been a promising strategy in tissue engineering. This approach provides several advantages by obtaining a higher level of scaffold complexity through the retention of ultrastructural and mechanical properties, as well as the ECM constituents unique to the tissue of interest [206]. Common harvesting depots include, but are not limited to, the urinary bladder matrix (UBM), pericardial matrix, dermal matrix, small intestine submucosa (SIS), liver, and adipose tissue [14], [207]–[211]. Moreover, a range of commercial off-the-shelf decellularized ECM constructs are currently on the market derived from human dermis (AlloDerm®, LifeCell), porcine dermis (Permacol™, Covidien), porcine SIS (Oasis®, Cook Healthpoint), bovine pericardium (Dura-Guard®, Synovis Surgical), porcine UBM (MatriStem®, ACell Inc.), and porcine liver (Miroderm®, Miromatrix Medical Inc.).

In recent studies, tissue-specific ECM from decellularized tissues have instructive properties to direct stem cell differentiation and promote constructive remodeling of native tissues [136]. Pertaining to previous work in the Flynn lab, a detergent-free method for decellularized adipose tissue (DAT) resulted in a highly preserved matrix possessing adipo-inductive and pro-angiogenic properties *in vivo* [14], [26]. In the context of muscle tissue regeneration, decellularized skeletal muscle tissue provided the appropriate architecture and cues to support *de novo* formation of muscle fibers upon implantation in a murine model [212]. Similarly, chondrogenic induction was enhanced *in vitro* when rat BMSCs were cultured in pellets containing decellularized porcine articular cartilage particles, as indicated by higher levels of collagen II production [213]. A similar phenomenon was also observed in the context of bone regeneration, where decellularized trabecular bone induced vascularization and osteogenesis when seeded with human BMSCs and human endothelial cells [214]. Collectively, these studies provide compelling evidence to support that the native physio-mechanical properties, as well as molecular components of the ECM can mediate tissue-specific regeneration for a range of applications.

2.5.1 Decellularization techniques

Decellularization techniques typically involve a combination of chemical, physical, and enzymatic treatments that are appropriate for the tissue or organ of interest. Common chemical reagents include the use of acids or bases and a choice of ionic, non-ionic, and zwitterionic detergents to disrupt cell membranes, nucleic acids, as well as lipid-lipid and lipid-protein interactions [215]. In addition, hypotonic or hypertonic solutions and polar solvents such as alcohol and acetone can be used to induce cell lysis by osmotic shock and solubilize lipids, respectively [215]. Applied physical pressure and force, as well as freezing and thawing cycles, aid in the breakdown of cells and the elimination of cellular debris [215]. Further, enzymatic digestion with trypsin and chelating agents such as EDTA are also used to release cells from the ECM [215].

Decellularization can generally be accomplished in the following ways: (1) by perfusing solutions through an existing vascular network of the tissue or organ, and (2) by immersion and agitation of small tissue sections or blocks in solutions [215]. More specifically, perfusion methods are suitable for denser and larger tissues, such as for heart, liver, and placenta, and can have the advantage of better retaining the original tissue shape and structure [216]–[218]. On the other hand, when vascular cannulation is technically challenging, agitation methods are most commonly used and rely on reagent penetration via diffusion. Numerous protocols have been developed with this latter technique for tissues including adipose, dermis, heart valves, and urinary bladder [14], [219]–[221].

To evaluate the quality of the decellularized tissue, investigators have used a combination of standard histological analysis and biochemical assays. Namely, to visualize the presence of residual lipids oil red O staining is used, while IHC is helpful for visualizing key ECM constituents (e.g. collagen I, IV, III, laminin), growth factors (e.g. VEGF), and to detect potential immunogenic sites (i.e. major histocompatibility complex antigen class I (e.g. MHC-1)) [14], [21], [24]. To assess the presence of cell remnants, DAPI staining is often coupled with DNA quantification with the Quant-iT^{TM} PicoGreen® dsDNA kit [222], [223]. Blyscan, Fastin, and hydroxyproline assays can also be used for the quantification of GAGs, soluble elastin, and collagen content, respectively [224]–[226]. Further, Masson's trichrome staining and SEM are also common tools to help examine the ultrastructure as well as collagen fibril arrangement [223], [226], [227]. As a final step, cytocompatability of the matrix is assessed through *in vitro* cell culture and accompanied with implantation into an *in vivo* animal model to test for host response and tissue remodelling [223].

The integrity of the final decellularized product is dependent upon the choice of reagent and treatment regime employed. More importantly, careful consideration into potential drawbacks of certain reagents is crucial for the development of effective decellularization protocols. While detergents such as sodium dodecyl sulphate (SDS) and Triton X-100 are preferred for the adequate

removal of cells in dense tissues like the heart and dermis, measurable losses in soluble proteins like GAGs, fibronectin, and laminin, as well as changes in ultrastructure have been reported [24], [226], [228], [229]. Incomplete elimination of residual detergents in these tissues could also lead to cytotoxicity and immune rejection, thus multiple washes are necessary to ensure proper extraction [220], [230]. Similarly, acids and bases can weaken the mechanical properties of the tissue and can damage or eliminate growth factors from the ECM [219]. To better preserve the ECM, the use of milder treatments have been documented, with some protocols circumventing the use of detergents altogether, such as for nerve, adipose, gall bladder, and aortic valve tissue [14], [231]–[234]. Overall, the ability to preserve the complex ECM characteristics through decellularization offers a promising strategy to engineer a natural bioscaffold with a microenvironment that would otherwise be challenging to reproduce synthetically.

2.5.2 Methods for fabricating bioscaffolds from decellularized tissues

While decellularized tissues can be used in their intact form, challenges regarding the lack of a well-defined geometry and limited physical properties may narrow their applications. To diversify the utility of decellularized tissue bioscaffolds, it is important to be able to manipulate properties such as stiffness, porosity, and architecture to suit the intended purpose. As a result, current studies have developed methods to process decellularized tissues into powders, pastes, hydrogels, foams, microcarriers, and sheets [19]–[22], [24]. This can be accomplished through a combination of chemical, enzymatic, and mechanical means to achieve the desired final result.

One simple technique is to process decellularized tissues into fine particles to be used directly as a paste or incorporated with other materials as a bioactive component [21], [22], [235]. Following decellularization, the tissue is frozen and lyophilized to produce a dried product. The dried tissue is then mechanically fractured, such as with a cryo-milling apparatus, and subsequently sieved to attain the desired particle sizes [21], [236]. For example, decellularized liver tissue

powders incorporated into fibrin gels exhibited improved neovascularization and host integration within an *in vivo* myocardial infarct model [235].

Another technique employed is to process the decellularized tissue through enzymatic digestion. Similar with the treatment of collagen, acidic pepsin digestion has been used to breakdown the tissue into soluble fragments [237]. Once in this form, the solution can be used to create hydrogels through thermogelation or crosslinked into stable constructs. For example, injectable decellularized cardiac tissue hydrogels capable of gelation at physiological conditions showed improved arteriole formation *in vivo* [238]. In a different application, solubilized decellularized heart, cartilage, and adipose tissue served as bioinks to 3-D print human ASCs and MSCs into highly organized spatial patterns [239]. Furthermore, enzyme-digested decellularized tissues derived from cartilage, tendon, and meniscus have also been functionalized with methacrylamide groups to create photo-polymerizable hydrogels [240].

Decellularized tissues can also be made into porous foams through the use of enzyme digestion, such as the work described in Chapter 4 of this thesis. In particular, the study introduced a novel protocol to create robust non-chemically crosslinked decellularized tissue foams with tunable porosity [20], [241]. In this new approach, intact collagen fibrils in the DAT were preserved following a mild digestion with α-amylase, which results in glycosidic cleavage of carbohydrate groups within the telopeptide regions, rather than the non-specific proteolytic cleavage that occurs when using pepsin [242], [243]. By varying the DAT suspension concentration and freezing conditions, customizable porous constructs can be fabricated through lyophilization that are stable in culture. To date, these techniques have been extended in the Flynn lab to synthesize porous foams from decellularized myocardium [241], bone, and dermis, thus demonstrating the potential of this flexible platform for a vast range of tissue engineering and cell culture applications. Furthermore, decellularized cell sheets may also be formed by casting decellularized tissue suspensions into a shallow mould, followed by lyophilization to yield a thin porous film [244].

2.6 Materials for adipose tissue regeneration

In plastic and reconstructive surgery, soft tissue repair remains prominent each year with approximately 2.2 million soft tissue filler procedures, 4.4 million tumour resections, and 286,000 breast augmentations performed alone in 2014 [245]. Many of these defects have a limited capacity for self-healing due to damage deep in the subcutaneous tissue layer caused by trauma, burns, birth defects, and tumour resections. This disfigurement is often the result of a loss in subcutaneous adipose tissue and the development of adhesion plaques to the muscle and dermis [246]. As such, finding new methods to restore the underlying fat layer including the original appearance and function of the integumentary system has been the main focus among researchers in adipose tissue engineering [247].

Current clinical reconstruction practices encompass a wide range of methods including transplantation of allogenic tissues, synthetic implants, and autologous patient tissue grafts or tissue flaps [248], [249]. For instance, autologous fat transplantation is a common procedure to recover tissue volume and shape loss following a mastectomy [23]. Although there has been partial success with these procedures, many of the methods have proven to be technically challenging with problems associated with immune rejection, graft site tissue morbidity, implant failure, formation of oil cysts, poor volume retention, and necrosis [23], [49], [249]. Often times these complications arise from the fact that adipocytes do not proliferate in their mature form and are susceptible to rupture upon shear force or apoptosis when there is an insufficient blood supply within the implant region [250]. To circumvent these issues, numerous efforts are underway to develop tissue-engineering strategies to prolong implant survival and promote the development of new adipose tissue and vasculature *in situ*.

A preferred approach is to utilize ASCs since they readily differentiate into adipocytes and have been shown to recruit host cells through paracrine signaling to promote vascularization *in vivo* [44]. Furthermore, combining ASCs with an appropriate scaffold is necessary to serve as a delivery

vehicle, improve viability of the cells, as well as to support new fat formation [23]. In terms of scaffold design, porosity is critical to accommodate the enlargement of maturing pre-adipocytes during lipid accumulation, while the mechanical properties should be comparable to native adipose for patient comfort and minimization of capsular fibrosis [251], [252]. Currently, a variety of synthetic and natural materials have been tested in the form of sponges or foams, meshes, as well as injectable hydrogels and microspheres [19], [20], [22], [24], [253].

Regarding synthetic scaffolds, a range of different materials have been demonstrated to be capable of supporting ASC adipogenesis *in vitro* and *in vivo.* In particular, synthetic polymers can be designed to possess specific mechanical properties to match the tissue of interest via crosslinking, while the release of encapsulated growth factors or cytokines and material degradation rate can also be controlled [254]. Examples include the use of biocompatible absorbable polymers such as poly(lactic-co-glycolic acid) (PLGA), polyglycolic acid (PGA), and polylactic acid (PLA) [255]–[261]. Scaffolds synthesized from these materials were capable of supporting stem cell adipogenesis and vascularization; however, long-term stability of the scaffold *in vivo* remains a challenge [258], [262], [263]. For instance, Weiser *et al.* found that PGA woven meshes as a substrate to deliver 3T3-L1 pre-adipocytes were quickly absorbed within 12 weeks of implantation in nude mice, and adipose tissue formation was not present unless cells underwent *in vitro* adipogenic differentiation prior to implantation [263]. A similar observation was also made by Mauney *et al.* in which PLA scaffolds seeded with human BMSCs or ASCs rapidly degraded and were not detectable after 4 weeks in a rat model [258]. In other work, Kang *et al.* investigated the use of PLGA in the form of injectable microspheres for ASCs and found improved cell survival as well as adipose tissue formation after 6 weeks in an athymic mouse [261]. However, an *in vivo* study spanning 1-12 months in a rat model revealed that long-term maintenance of rat pre-adipocyte seeded PLGA scaffolds remains unclear, with adipose tissue volume peaking at no more than 2

months [255]. Other types of synthetics such as poly(ethylene glycol) (PEG) scaffolds as well as polypropylene meshes have also been explored [262], [264], [265].

On the other hand, natural materials for adipose tissue reconstruction have been investigated such as collagen type I, silk, fibrin, alginate, HA, and decellularized tissues [20], [258], [266]–[268]. More specifically, collagen scaffolds have been used to support adipogenesis and vascularization *in vivo* [266], [269]–[271]. For example, Hiraoka *et al.* found that collagen scaffolds embedded with bFGF loaded gelatin microspheres were capable of inducing *in situ* adipose tissue formation in a rat model with and without seeded rat pre-adipocytes after 6 weeks [270]. Interestingly, 3-D silk scaffolds have shown favourable outcomes *in vitro* in terms of supporting adipogenesis and vascularization [272]. The slow resorption and mechanical strength of silk makes it a potential material to achieve sustained volume, as demonstrated in an 18 month *in vivo* study of porous silk sponges seeded with lipoaspirates [273]. In other cases, injectable alginate-based scaffolds in the form of alginate/O-carboxyl methyl chitosan incorporated with fibrin nanoparticles were shown to support *in vitro* human ASC adipogenesis, while porous alginate-RGD was demonstrated to support adipose tissue formation within a subcutaneous sheep model over 3 months [274], [275]. From a commercial standpoint, various naturally based products are also available on the market for adipose tissue reconstructive surgery including the hyaluronic acid gels Hylaform (Biomatrix Corp.) and Restylane (Q-Med), decellularized human dermal tissue AlloDerm (LifeCell), bovine dermal collagen Zyderm I (Collagen Aesthetics), and fibrin gel Fibrel (Mentor Corp.).

Despite these advancements, rapid *in vivo* degradation and resorption resulting from the inability to promote adipose tissue regeneration remain primary challenges for both synthetic and natural materials, thus highlighting the need for further development of strategies that will meet the goal of long-term stable volume retention.

2.6.1 Decellularized adipose tissue scaffolds

In recent years, a growing body of work has centred on the development of DAT scaffolds for applications as a soft tissue filler in plastic and reconstructive surgery, building on the original work from the Flynn lab published in 2010 [14]. More specifically, adipose tissue is an abundant and economical supply of human ECM normally discarded as surgical waste and provides a convenient alternative to xenogenically-sourced materials. With regards to the matrix, the adipose ECM is comprised of collagen I, II, III, IV, laminin, fibronectin, elastin, GAGs, and proteoglycans, in addition to other proteins that lend to its potential to modulate cellular processes [147]. Given these features, adipose ECM is an attractive base material for the design of natural bioactive scaffolds and has resulted in the publication of various adipose tissue decellularization protocols by several groups [14], [21], [24], [253], [276], [277].

Collectively, the majority of decellularization methods described are detergent-based involving the use of either SDS, Triton^{TM} X-100 or sodium deoxycholate to ensure sufficient removal of cellular components [21], [24], [253], [276], [277]. While detergents can aid in the removal of most entrapped lipids within the matrix, additional treatments with isopropanol, as well as the use of the enzyme lipase or colipase are often needed to achieve a fully delipidized material [278]. Hypotonic salt solutions and freeze/thaw cycles are important for initial cell lysis, and other supplementary reagents often include the enzymes trypsin-EDTA, DNase, and RNase to release cells and breakdown nuclear components. Since detergent-based decellularization has been noted to potentially degrade the ECM, the Flynn lab pioneered the field in developing a uniquely detergent-free decellularization protocol in an effort to better preserve properties of the native matrix [14]. More specifically, the method uses a combination of freeze/thaw cycles, washes in hypotonic solutions, trypsin-EDTA, and isopropanol, as well as DNase and RNase treatments to yield an intact bioscaffold [14]. A summary of the different human adipose tissue decellularization protocols reported in literature is shown in Table 2.4.

Table 2.4: Human adipose tissue decellularization protocols

	Reference	Key decellularization steps
Detergent-based	Wang *et al.* [21]	1. Perform 3 freeze/thaw cycles, then wash in deionized (DI) water for 48 h, treat with 0.5 M NaCl then 1 M NaCl for 4 h each. 2. Repeat step 2, treat with 0.25% trypsin/EDTA for 2 h, and wash in DI for 1h. 3. Wash in isopropanol overnight, treat for 3 days in 1% Triton X-100, 2 days in DI water, and 1 day in PBS.
	Choi *et al.*[253]	1. Add DI water to lipoaspirate and homogenize tissue/water (2:1) mixture for 5 min. 2. Centrifuge tissue suspension and remove upper lipid layer. 3. Repeat steps 1 and 2 several times to yield a viscous suspension. 4. Treat suspension with 1 M NaCl for 2 h, rinse with DI water, and wash in 0.5% SDS for 1 h. 5. Rinse with DI water for 24 h, digest with 0.2% DNase and RNase for 1 h, and wash with DI water thoroughly.
	Wu *et al.* [276]	1. Incubate with 0.1%, 1%, 3% or 5% peracetic acid for 3 h. 2. Neutralize to physiological pH and incubate overnight in 1% Triton X-100 in 2 mM EDTA. 3. Treat samples with DNase overnight.
	Young *et al.* [24]	1. Perform one freeze/thaw cycle and wash in 1% SDS or 2.5 mM sodium deoxycholate for 48 h. 2. Rinse with DI water, place in 2.5 mM sodium deoxycholate with lipase and colipase and digest for 24-48 h for a maximum of 72 h. 3. Rinse with DI water for 2 h.
	Brown *et al.* [277]	1. Perform one freeze/thaw cycle, digest in 0.02% trypsin-EDTA for 1 h, and rinse with DI water. 2. Wash in 3% Triton X-100 then in 4% deoxycholate acid solution for 1 h each. 3. Rinse tissue 3 times with DI water.
Non-detergent based	Flynn [14]	1. Perform 3 freeze/thaw cycles and incubate in 0.25% trypsin-EDTA overnight. 2. Wash in isopropanol for 48 h, 3 rinses in buffer solution, and incubate for 6 h in 0.25% trypsin-EDTA. 3. Rinse 3 times in buffer solution and digest overnight with DNase, RNase, and lipase. 4. Wash in isopropanol for 3 h then perform 3 rinses in buffer solution.

Human adipose tissue (Fig. 2.6a) after decellularization has a relatively loose and amorphous appearance in its intact form (Fig. 2.6b). More specifically, the DAT prepared using the Flynn lab protocol demonstrated adipo-inductive properties when seeded with human ASCs as confirmed by the expression of the adipogenic master regulatory genes *PPARγ* and *C/EBPα* in the absence of exogenous differentiation factors [14]. Furthermore, *in vivo* rat studies showed that the DAT supported high levels of stable host-derived adipose tissue regeneration when delivered in

combination with ASCs [88]. However, from a clinical standpoint, the shapeless geometry of intact DAT limits its applicability to a surgical implant. As such, ways to create alternative forms of DAT bioscaffolds have been investigated. In particular, the Flynn lab has made significant contributions to the field in developing a range of DAT-based bioscaffolds. For instance, processing DAT into an injectable format would be beneficial as a minimally invasive soft tissue filler. In this case, methods have been developed in the lab for incorporating milled DAT as a bioactive component for ASCs encapsulated within crosslinked DAT-methacrylated chondroitin sulphate (MCS) and DAT-methacrylated glycol chitosan (MGC) hydrogels [22], [236]. Results from these studies indicated that the adipo-inductive properties of the DAT were also conserved, as demonstrated by both upregulation of the adipogenic master regulator genes as well as intracellular lipid accumulation in proliferation media devoid of differentiation supplements [22], [236]. In addition, physiologically thermoresponsive injectable DAT hydrogels and small injectable 1-ethyl-3-(-3-dimethylaminopropyl) carbodiimide hydrochloride (EDC)-crosslinked DAT have been produced in other studies by Young *et al.* and Wu *et al.*, respectively [24], [276]. Choi *et al.* also demonstrated the versatility of their DAT to be processed into porous sheets, rods, films, hollow tubes, and square moulds [253].

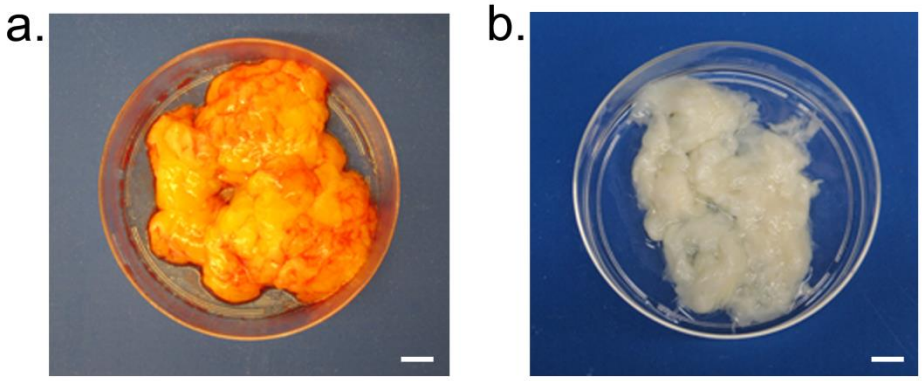

Figure 2.6: Macroscopic images of (a) native adipose and (b) decellularized adipose tissue (DAT). The human adipose tissue shown was processed following the Flynn lab decellularization protocol [14]. Scale bar = 1 cm.

2.7 *Ex vivo* stem cell expansion strategies

2.7.1 3-D bioreactor systems

As discussed previously, cells *in vivo* reside in a 3-D environment and their functions including proliferation, lineage-specific differentiation, and viability are highly influenced by the complex microenvironment. This concept has been increasingly recognized as an integral part in developing new tissue engineering approaches and prompted a change from traditional 2-D monolayer culture to more complex 3-D culture systems [279]. The need for improved culture methods is substantiated by the reduced proliferative capacity and differentiation potential of human MSCs observed upon extended culturing on rigid 2-D tissue culture substrates [280], [281]. It is expected that many cell-based therapies will need to rely on *ex vivo* expansion to obtain relevant cell numbers required for therapeutic efficacy, thus motivating the development of more sophisticated 3-D cell culture strategies that better recapitulate the native cellular milieu [136]. In terms of the design of systems for cell proliferation, the primary goal in these approaches is to be able to expand the cells to obtain large cell populations in a reliable manner while retaining the desired stem cell characteristics [11], [282]. Alternatively, systems are also being designed to provide appropriate conditions to efficiently and predictably induce differentiation, as well as to create suitable tissue models for studying biological processes [279], [283].

Focusing on the development of scalable 3-D expansion methods, an approach allowing flexible control over culturing parameters would enable greater management of growth conditions. This need has led to the design of various bioreactors that can be broadly classified as mixed or perfusion configurations, with each possessing certain advantages and disadvantages [284]. In terms of mixed bioreactors, these come in the form of stirred flasks or rotating wall vessels to enable a more homogenous culture environment and permit efficient exchange of nutrients and oxygen [284]. Scaffolds such as microcarriers can also be suspended within mixed systems, with positive effects reported on stem cell expansion, adipogenesis and osteogenesis, as well as chondrocyte

culture [19], [285], [286]. However, continuous fluid shear stress and collisions with the vessel wall and other scaffolds may have damaging effects on cells [287]. Perfusion bioreactors come in several designs including hollow fiber and microfluidic chambers in which cells are subjected to constant flow and media exchange [287]. Similar to mixed vessels, this arrangement allows for a more uniform culture environment with thorough perfusion of structures to allow cells to grow at high densities comparable to tissues [284]. To date, perfusion arrangements have been used successfully for the culture of hepatocytes, hematopoietic stem cells, and for MSC osteogenic differentiation [288]–[290]. Nonetheless, it is important to note that some current limitations include difficulties in cell retrieval, particularly for hollow fiber arrangements [291].

Within these 3-D culture systems, factors such as hydrodynamic stress, oxygen and nutrient supply, and the monitoring of pH and metabolic changes can be easily overseen [284], [292]. This is particularly important since MSCs are sensitive to external fluid shear stress and strain that could impact proliferative and differentiation potential of the cells [293]. This phenomenon was demonstrated by Zhao *et al.* and Yourek *et al.* in which fluid flow shear stresses induced MSCs towards an osteogenic phenotype [293], [294]. Furthermore, studies on the effect of oxygen tension on MSC behaviour have also shown that greater proliferation and higher retention of stem cell phenotype was generally observed under hypoxia (2% O_2), but that reduced oxygen levels may alter lineage plasticity in comparison to normoxic conditions (20% O_2) [84], [295]. Overall, these parameters must also be considered during the design bioreactors approaches to enable the translation and commercialization of cell-based therapies

2.7.2 Microcarrier technology

The term 'microcarriers' was first coined by A.L. van Wezel in 1967, who used Sephadex particles made up of crosslinked dextran for the cultivation of viruses in large scale production [296]. The simplistic design of the microcarrier suspension system is advantageous by providing an

improved growth surface area to volume ratio, a homogeneous microenvironment, easy sampling and harvesting, and efficient scale up of cell populations by direct cell transfer from confluent microcarriers to freshly added microcarriers without the need for enzymatic release [297]. To date, microcarriers have been used successfully for vaccine production with Chinese hamster ovary (CHO) or Vero cell lines and researchers are now exploring ways to adapt this system for the cultivation of embryonic stem cells (ESCs) and MSCs for various tissue engineering applications [298].

The majority of commercially available collagen- or gelatin-coated microcarriers for cultivating anchorage dependent stem cells are comprised of synthetic materials such as polystyrene and glass [299]–[301]. Since most of these commercial products serve only as a cell expansion system, cells must be removed upon reaching confluence. As ease of clinical application is critical, biocompatible microcarriers overcoming the need to remove adherent cells and enabling direct transplantation via injection may be advantageous [291]. More specifically, when cells are injected into tissues in suspension, high cell death due to anoikis/apoptosis has been reported [302]. By providing an adhesive substrate it has been postulated that this may improve cell viability and localization post-injection. Currently, microcarriers have been fabricated from biocompatible materials including gelatin, chitosan, alginate, and decellularized tissues to act as both cell expansion and delivery vehicles [19], [303], [304]. A summary of synthetic and natural microcarriers reported in the literature to date, ranging from commercial to customized non-commercial options, is shown in Table 2.5.

Table 2.5: Microcarriers used for MSC culture

	Microcarrier	Material	Porosity	Cells supported	Reference
Commercial	Cultispher-G®, Cultispher-S® (Percell, Biolytica AB)	Crosslinked porcine gelatin	Macroporous	Human placental-derived MSCs, rat BMSCs, human BMSCs, human ASCs	[305]–[308]
	Cytodex 1™, Cytodex 3™ (GE Healthcare, Life Sciences)	Crosslinked dextran non-coated or collagen coated	Microporous or nonporous	Rat MSCs, human BMSCs	[305], [309], [310]
	SoloHill® (Pall Corporation)	Polystyrene coated with glass, gelatin, or recombinant proteins	-	Human placental-derived MSCs, human BMSCs, mouse MSCs	[311]
	Synthemax® II, Enhanced Attachment® (Corning Inc.)	Polystyrene coated with synthetic surface	-	Human BMSCs, human ASCs	[312]
	Cytopore 2 (GE Healthcare, Life Sciences)	Positively charged cellulose	Macroporous	Rat BMSCs	[305]
Non-commercial	Decellularized ECM	Dermis, SIS, adipose tissue	Microporous	Human ASCs	[19], [313]
	Alginate	Cartilage ECM coated alginate	-	Human BMSCs	[314]
	Collagen	Equine collagen type I	-	Human BMSCs	[315]

Generally, anchorage-dependent MSCs are cultured on microcarriers in spinner flasks, wherein the contents are kept in dynamic suspension by a rotating magnetic stir bar or paddle [284]. Furthermore, the microcarriers employed should support cell spreading and high-density growth, as well as withstand the mechanical stresses present within the system [291]. Studies have suggested that microcarriers ranging from 100-500 μm in diameter with pore sizes greater than 20 μm can promote diffusion of oxygen and nutrients to support cell viability of most mammalian cell types [316]. Porosity is also an important factor since this also allows for greater available surface area per microcarrier and may protect cells against shear stress upon infiltration [317], [318]. To ensure

a homogeneous environment, low microcarrier densities have been recommended in order to remain in suspension under minimal agitation [291]. In addition, microcarriers need to be readily sterilized to meet Good Manufacturing Practices (GMP), and the cell release methods employed should ensure maximum recovery with minimal damage to cell integrity and viability [291].

During early culture, initial cell attachment efficiency onto the microcarrier surface is critical since this often influences subsequent growth rates [319]. Adherence is also highly dependent on the material properties and microcarriers such as those prepared from dextran or glass often require a coating of gelatin or other ECM-derived proteins such as collagen and fibronectin, or surface modification with cell-adhesive peptide groups (e.g. RGD peptides) [319]. In reviewing various seeding regimes, studies have also highlighted that static or intermittent periods are necessary to maximize initial cell attachment, as poor adherence will affect subsequent growth kinetics [319], [320]. Interestingly, with regards to cell seeding density, a counterintuitive finding was observed by Croughan *et al.* who reported that high cell seeding densities of human FS-4 fibroblasts resulted in reduced growth rates compared to lower seeding densities [321]. The group hypothesized that high cell densities may contribute to the production of growth inhibiting factors, however concrete evidence of these effects remains to be found [321]. This finding also emphasizes that inoculation densities for specific MSC lines must also be optimized. In general, these considerations must be taken into account when defining microcarrier culturing conditions.

In addition to the choice of microcarrier material, appropriate culture conditions are required to ensure proper cell attachment and viability for each specific cell type [291]. In particular, several groups have investigated effects such as shear stress, stirring rate, and inoculation density on human fibroblasts, ASCs, and BMSCs [26], [322], [323]. Most studies have reported using 100-250 mL spinner flasks fitted with a magnetically-driven impeller in the form of either a paddle or bulb-shaped glass shaft geometry [291]. The specific stirring mechanism employed will influence the shear forces generated within the system [322]. Furthermore, the stirring rate and microcarrier

density in a given culture volume can also contribute to the shear forces experienced by the cells [322]. In general, it is important to carefully balance the mechanical forces required to maintain a homogeneous microcarrier suspension, adequate supply of oxygen and nutrients, as well as stable pH, while minimizing the detrimental effects of turbulent forces that could result in cell detachment, damage, or death [324].

It is clear that many parameters could affect stem cell behaviour within microcarrier culture systems. As a result, there is a lack of standardization due to the diverse conditions reported in literature, thus making it difficult to draw comparative conclusions. The future translation of microcarrier-based suspension culture systems for MSCs will be dependent on the capacity to achieve consistent and predictable outcomes in terms of cell yield, phenotype and function. Therefore, further work is needed to develop a deeper understanding of the effects of the complex microenvironment on MSC proliferation in dynamic 3-D culture systems.

2.7.3 Microcarrier culture on stem cell expansion

As discussed, transitioning from 2-D culture systems to 3-D bioreactor systems to obtain large populations of high quality MSCs may significantly advance the progression of some cell-based therapies to the clinic. As many factors within dynamic culture systems can influence MSC phenotype, it is important to assess the potential changes in MSC characteristics following expansion under these conditions including proliferation, immunophenotype, and multipotent differentiation capacity [325]. It has been well documented that microcarrier-based systems can obtain higher expansion of MSCs relative to TCPS, with reported growths as high as 20-fold expansion and conserved multilineage differentiation capacity under prolonged culture [306], [309], [326], [327]. In particular, many studies follow the guidelines provided by the ISCT in assessing the quality of microcarrier-expanded MSCs. As described previously, the ISCT states that the minimal criteria for MSCs are: (1) plastic-adherent under standard culture conditions, (2) exhibit positive

cell surface marker expression of CD105, CD90, and CD73 and negative for CD45, CD14 or CD11b, HLA-DR and CD79α or CD19, and (3) able to differentiate *in vitro* along the adipogenic, osteogenic, and chondrogenic lineages [328]. As a result, the majority of experiments rely on cell counting assays to monitor growth, flow cytometric characterization of MSC immunophenotype, and a combination of gene expression analysis of key lineage-specific markers and histology (e.g. oil red O, von Kossa or Alizarin Red, and toluidine blue stains) for the assessment of differentiation capacity [291]. For example, dos Santos *et al.* demonstrated that human ASCs and MSCs cultured on polystyrene based microcarriers for 2 weeks achieved a 14- and 18-fold expansion, respectively, with retained stem cell phenotype and differentiation capacity towards osteoblasts, adipocytes, and chondroblasts [326]. Similarly, Chang *et al.* concluded that rat BMSCs cultivated on Cultispher-S® microcarriers were superior in growth kinetics compared to conventional planar culture, while still maintaining stem cell marker expression and multipotency after a 16-fold expansion over 14 days [327]. These outcomes highlight the potential for preservation of MSC characteristics post microcarrier expansion for various types of MSCs. However, numerous questions remain including whether the efficiency of differentiation or the pro-regenerative characteristics of the cells are altered following expansion under dynamic conditions.

2.7.4 Microcarrier culture on stem cell differentiation

Several studies have identified that the shift from 2-D surfaces to 3-D scaffolds induces remodelling of the cytoskeleton within the cells, which subsequently affects downstream lineage commitment [329]–[331]. Thus, it is expected that the dynamic 3-D microcarrier culture environment could influence MSC lineage commitment and recent studies looking at changes in cell morphology and differentiation have supported this theory [331]. Examples of microcarrier culture influencing stem cell differentiation towards the adipogenic, osteogenic, and chondrogenic lineages are provided in the following sections.

2.7.4.1 *Adipogenic lineage*

In the context of adipogenesis, there is very limited information on the effects of dynamic microcarrier culture on stem cell adipogenesis. As detailed in Chapter 3, the Flynn lab demonstrated that porous microcarriers fabricated from human DAT seeded with human ASCs exhibited high levels of adipogenic differentiation [19]. This was observed by the presence of lipid accumulation, increased GPDH activity, and elevated adipogenic marker expression compared to gelatin microcarrier controls [19]. It was hypothesized that the adipose ECM in the microcarriers provided ASCs the necessary microenvironmental cues required to promote ASC lineage commitment in a tissue-specific manner.

2.7.4.2 *Osteogenic lineage*

As highlighted previously, several studies have noted positive effects of microcarrier dynamic culture on driving stem cell osteogenesis. For instance, Tseng *et al.* observed spontaneous osteogenic gene expression in four MSC sources (i.e. human BMSCs, human placenta-derived MSCs, human ESC-derived mesenchymal progenitor cells, and mouse MSC cell line C3H10T1/2) cultured on Solohill microcarriers under dynamic conditions without the need for exogenous osteogenic supplements in the medium [311]. Osteogenic capacity was also assessed on Cytodex 3^{TM} microcarriers by Shekaran *et al.*, who found that under static culture microcarrier-bound human fetal BMSCs displayed an upregulation in osteogenic gene marker expression with accelerated matrix mineralization in comparison to the TCPS controls [332]. In this case, it was postulated that direct cell-ECM contact via interactions with the microcarrier surface had a partial role in osteogenic induction [332]. Furthermore, Shekaran *et al*. conducted phenotypic analysis of the BMSCs after cultivation on the microcarriers in comparison to 2-D controls and showed that all groups expressed MSC positive and negative markers in accordance with the ISCT guidelines [332]. Notably, the lack of differences in MSC marker expression between the groups raises the

precaution that other assays must be coupled when evaluating multipotentiality since stem cell marker expression will not necessarily reflect changes in the differentiation capacity of the cells.

In terms of *in vivo* applications, Yang *et al.* tested for apoptosis and ectopic bone formation in a subcutaneous rat model for rat BMSCs seeded on three biodegradable microcarriers: Cytodex 1^{TM}, Cultispher-S®, and Cytopore 2 [305]. Interestingly, *in vitro* cell attachment and expansion was only supported on Cultispher-S® microcarriers and was chosen for subsequent *in vivo* studies [305]. Shortly after subcutaneous transplantation of the seeded microcarriers, terminal deoxynucleotidyl transferase (TdT) dUTP nick-end labeling (TUNEL) assay revealed less apoptosis on the microcarrier groups in comparison to cell suspensions of TCPS expanded BMSCs controls [305]. This observation led to the hypothesis that trypsin release steps may be affecting the viability and quality of cells upon implantation and the ability to deliver the cells via direct injection of cell-seeded microcarriers could be beneficial.

2.7.4.3 *Chondrogenic lineage*

In cartilage tissue engineering, the use of microcarriers has been preferred since the seeded cells naturally adopt a spherical conformation, which has been demonstrated to aid in chondrogenesis as this simulates the high cell-cell contact during mesenchymal condensation in embryonic development [333]. For example, Bertolo *et al.* covalently bound TGF-β1 onto the surface of crosslinked collagen microcarriers to promote human BMSC chondrogenic activity [334]. In this case, an upregulation of mRNA expression as well as protein accumulation of key cartilaginous ECM components (i.e. collagen I, collagen II, and aggrecan) was observed [334]. In another approach, Wu *et al.* used cartilage ECM-coated alginate microcarriers seeded with human BMSCs and also observed improved chondrogenesis in comparison to traditional pellet culture [314].

2.7.5 Current challenges towards clinical translation of microcarrier-based culture systems for MSC expansion

While most studies have reported accelerated MSC propagation on microcarriers, the majority of these experiments are still carried out in medium containing fetal bovine serum. To progress towards the clinical translation of microcarrier cell culture technologies, there is a need to transition to serum-free culture media in order to eliminate downstream xenogenic concerns and batch-to-batch variability of serum [319]. The development of commercially available serum-free formulations is promising; however the documented superior growth kinetics have typically only been explored under 2-D static culture conditions for most MSC sources [335]–[337]. It has also been noted that attachment efficiencies and growth kinetics vary substantially under both static culture and dynamic culture conditions. For instance, in the absence of serum, the cells have been reported to be more sensitive to shear stress and apoptosis [338]. For 2-D static cultures, this is often circumvented by using ECM surface coatings to aid in cellular attachment and subsequent proliferation, however, this strategy may not be sufficient when cells are exposed to the constant mechanical forces generated within a stirred bioreactor system [319]. To date, only a few groups have reported using serum-free or low serum conditions for microcarrier culture [339]–[341], although generally lower MSC expansion has been achieved in these studies with the highest reported at 10-fold [339]. These findings reflect the need to further optimize seeding regimes to improve initial cell attachment, including determining appropriate microcarrier coatings and optimizing agitation rates to minimize shear stress.

Presently, while microcarrier culture studies are commonly performed in small batch bench-top bioreactors, several investigators have highlighted some potential issues in terms of scale up. For instance, a major complication is that oxygen supply via diffusion alone is not adequate in large systems and additional gas sparging techniques are required to ensure cell viability especially in high cell density reactors [342]. As a result, this could introduce more local stress to the cells and

foaming within the system could potentially reduce reactor volume capacity [343]. Anti-foaming agents are available to minimize these effects, but tests must be performed to assess potential cytotoxicity [342]. Another issue that is not often noted is the potential for cell aggregation within the stirred culture system that could impact MSC characteristics, heterogeneity, proliferation, and differentiation [310]. More specifically, Ferrari *et al.* found that agitation speed and seeding density contributed most to cell aggregation on Cytodex-1™ microcarriers seeded with porcine BMSCs [310]. To avoid this problem it is recommended that fresh microcarriers should be added to the system immediately before the onset of aggregation [310]. Schop *et al.* also used this technique to limit goat MSC aggregation and found improved homogeneous cell distribution across the Cytodex-1™ microcarrier surface [344].

In addition to these considerations, it will be crucial to thoroughly investigate other factors that may impact large-scale production. For example, impeller location, shape, and geometry, as well as probes within the vessel must be considered when modelling shear forces experienced by the cells [345]. Promisingly, Schirmaier *et al.* was able to carefully optimize translatable engineering parameters to expand ASCs under low serum conditions from a 100 mL vessel to a pilot scale 35 L vessel and to obtain yields of 30 million and 10 billion cells, respectively [341]. This work marks key progress towards the realization of using microcarriers for large-scale stem cell production, but many challenges still remain in developing robust MSC culture conditions for applications in a broad range of cell-based therapies.

2.8 Summary

Towards the advancement of future stem cell-based therapies, there is a need for instructive substrates that could be tuned to drive desired cellular processes, such as proliferation versus differentiation, coupled with the establishment of robust translatable cell culture strategies. In particular, taking advantage of the dynamic reciprocity between stem cells and their local

microenvironment has been viewed as a promising approach for the development of novel scaffolds in tissue engineering and regenerative medicine. The ECM within tissues plays a predominant role in modulating cellular activities, thus harnessing specific ECM properties has formed the basis for the production of many synthetic and natural biomaterials to date. While synthetic biomaterials are studied extensively, naturally derived biomaterials in the form of decellularized tissues have also gained wide interest due to the ability to retain complex features of the native matrix as well as their intrinsic biocompatibility. More specifically, there is now growing interest on the use of human adipose tissue as a rich source of ECM and ASCs among researchers and clinicians. Many studies have also highlighted the natural inductive properties of tissue-specific ECM on stem cells, therefore DAT bioscaffolds combined with ASCs represents a potential platform for the creation of translatable cell-based treatments for soft tissue regeneration. Currently, few studies have examined the use of DAT bioscaffolds beyond their intact form. As a result, this thesis aimed to develop and characterize novel 3-D DAT bioscaffolds possessing well-defined physical properties to further explore DAT as tissue-specific ECM substrates for adipose tissue regeneration and the expansion of human ASCs.

Chapter 3

The Performance of Decellularized Adipose Tissue Microcarriers as an Inductive Substrate for Human Adipose-Derived Stem Cells
Biomaterials (2012), 33(18), 4490-4499.

3.1 Introduction

A variety of synthetic, naturally-derived, and composite biomaterials have been investigated as carriers for the expansion and delivery of adipose-derived stem/stromal cells (ASCs) for use in an array of cell-based therapies, including for soft tissue reconstruction [23], [346], [347]. Recent research indicates that a tissue-specific approach holds immense potential for the development of bioscaffolds that are capable of directing the cell response to promote the regeneration of specific tissues of interest [348]–[350]. The complex and dynamic microenvironment of the extracellular matrix (ECM) mediates a wide range of cellular behaviors including survival, proliferation, differentiation, and migration [135], [351]. Subtle differences in the composition and properties of the ECM can dramatically alter processes such as stem cell lineage specification, both *in vitro* and *in vivo* [348]. While individual ECM components including collagen, laminin, and fibronectin are commercially-available, the native ECM provides many complex cues that are difficult to replicate using a bottom-up scaffold design approach [352]. As a result, there is significant interest in using decellularized tissues as base scaffold materials, as decellularization can preserve the natural tissue-specific ECM, while removing cellular and antigenic components that would initiate an immune response [137], [206].

Moving towards the aim of regenerating adipose tissue, previous research in the Flynn lab focused on the development of a protocol for the decellularization of human fat, which yields a well-preserved and highly purified form of the adipose matrix [14]. *In vitro* studies investigating the ASC response to the decellularized adipose tissue (DAT) scaffolds demonstrated that the DAT provided an adipogenic microenvironment for the ASCs, even in the absence of exogenous

differentiation factors [14]. As a result, the adipo-inductive nature of the DAT renders it a highly promising biomaterial for use in adipose tissue engineering applications.

Limited research has been conducted on the development of an adipo-inductive microcarrier with a tailored microgeometry. Promisingly, past work in the Flynn lab demonstrated that microcarriers prepared from solubilized DAT demonstrated enhanced attachment and proliferation of human ASCs relative to gelatin microcarriers and tissue culture polystyrene (TCPS) controls [26]. Based on the adipo-inductive nature of the intact DAT scaffolds [14], it was hypothesized that the DAT microcarriers may also provide a highly adipogenic, injectable tissue engineering substrate to promote soft tissue regeneration.

The focus of this Chapter was to investigate the potential for the DAT microcarriers to support the adipogenic differentiation of seeded human ASCs, as compared to gelatin microcarrier controls. The selection of gelatin as the scaffold control was based on the fact that the bulk of the DAT matrix is comprised of collagens [14]. Further, the adipo-inductive nature of the DAT microcarriers in culture was explored through characterizing the ASC response in the presence and absence of exogenous adipogenic differentiation factors. Detailed *in vitro* cell studies were conducted including gene expression analyses, enzyme activity quantification, and oil red O staining of intracellular lipid content. Finally, preliminary *in vivo* studies were conducted in a subcutaneous rat model to assess the biocompatibility of the DAT microcarriers (unseeded or seeded with allogenic rat ASCs) as compared to gelatin microcarrier controls.

3.1.1 Materials

Unless otherwise stated, all chemicals were purchased from Sigma-Aldrich Canada Ltd. (Oakville, ON, Canada), and were used as received.

3.1.2 Adipose tissue procurement

Freshly excised adipose tissue samples were obtained from female patients undergoing elective lipo-reduction surgery involving the abdomen or breast at the Kingston General Hospital or Hotel Dieu Hospital in Kingston, ON, Canada. The tissues were transported to the laboratory on ice in sterile cation-free Dulbecco's phosphate buffered saline (D-PBS; Thermo Scientific HyClone, Cat. # SH30028, Fisher Scientific, Oakville, ON, Canada) supplemented with 20 mg/mL bovine serum albumin (BSA). The donor age, weight, height, and explant site were recorded. Within 2 h of harvesting, the adipose tissue samples were processed using established protocols for (i) ASC extraction, or (ii) adipose tissue decellularization [14]. An overview of the project scope is provided in Fig. 3.1. Research ethics board approval for this study was obtained from Queen's University (REB# CHEM-002-07).

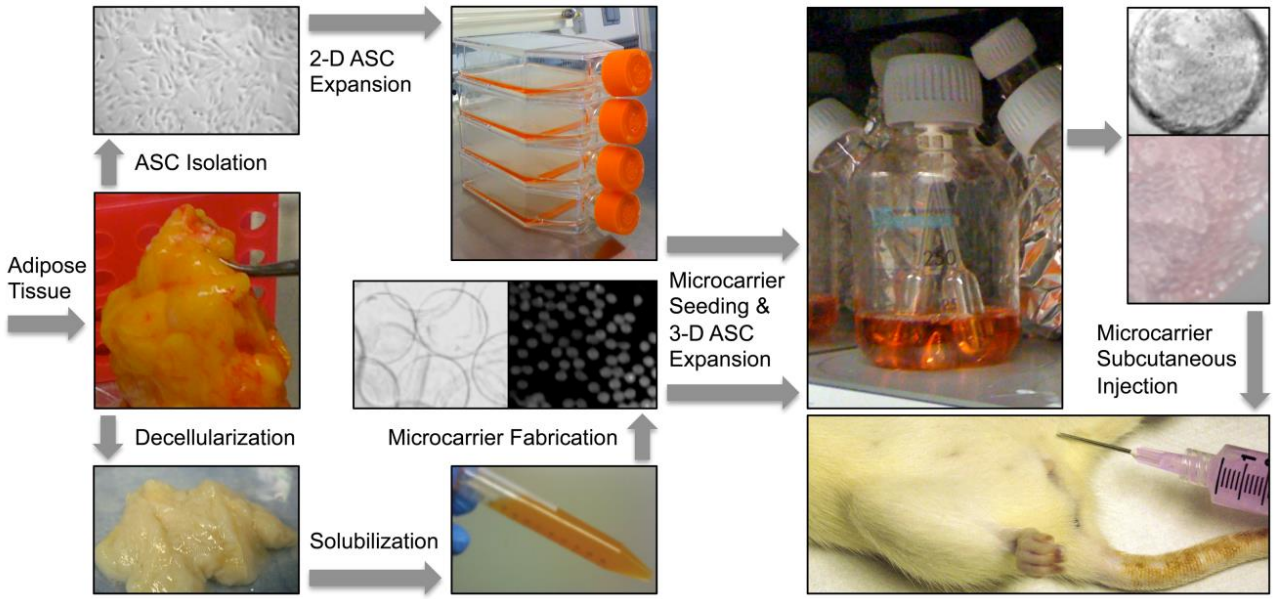

Figure 3.1: Schematic overview of the experimental methodology.

3.1.3 Microcarrier fabrication

Sterile DAT microcarriers were fabricated using published methods [26]. In brief, DAT samples from multiple patients were pooled (n=5) and solubilized via pepsin digestion (50 mg

pepsin/g DAT) in 0.5 M acetic acid for 20 h (37 °C, 150 rpm). The solubilized DAT samples were concentrated through air drying to obtain a final protein concentration in the range of 2-4 mg/mL, as measured using the Bio-Rad Protein Assay with an albumin standard (Bio-Rad Laboratories, Inc., Cat. # 500-0002, Hercules, CA, USA) [26]. The solubilized DAT was combined with 3% (w/v) sodium alginate solution in a volumetric ratio of 3:2, and the mixture was added drop-wise through a blunt-ended 21-gauge Punctur-Guard® needle (ICU Medical, Inc., Vernon, CT, USA) into 1.5% (w/v) $CaCl_2$ solution (pH 7.2) using a syringe pump (0.25 mL/min) in the presence of a compressed nitrogen jet (5 psi). The composite microcarriers were photo-chemically stabilized using 0.01% (w/v) rose bengal solution, with exposure to visible light for 8 h. Finally, the alginate phase was extracted by incubation in 50 mM sodium citrate for 15 min, to yield porous DAT microcarriers. As a control, gelatin microcarriers were fabricated with 50 mg/mL gelatin (Type B from bovine skin) in place of the DAT using identical methods [26].

3.1.4 Adipose-derived stem cell culture

Primary human ASCs were isolated and expanded on tissue culture polystyrene (TCPS) using established methods [218]. Fresh proliferation medium, comprised of DMEM:Ham's F-12 medium supplemented with 10% fetal bovine serum (FBS; Thermo Scientific Hyclone, Cat. # SH30396) and 100 U/mL penicillin and 0.1 mg/mL streptomycin (1% pen-strep), was provided every 2-3 days, and the cells were passaged at 80% confluence. For all microcarrier studies, passage 2 (P2) ASCs were employed. To facilitate comparative analyses, ASCs sourced from a single donor were used to seed the DAT microcarrier, gelatin microcarrier, and TCPS control samples for all time points in each trial of an assay. All *in vitro* studies were repeated with cells from different donors (N =2-3) to verify the trends.

3.1.5 Microcarrier seeding and ASC expansion

The ASC response on the DAT and gelatin microcarriers was investigated under dynamic conditions in a CELLSPIN spinner flask system (INTEGRA Biosciences AG, Switzerland). The microcarriers were seeded with P2 ASCs at an initial density of 20,000 cells/mg of microcarriers, and subjected to 2 min of intermittent stirring at 15 rpm every 30 min for 3 h, followed by 6 h of static operation, and an additional 3 h of intermittent stirring at 15 rpm [26]. After seeding, the system was operated continuously at 15 rpm (37 °C, 5% CO_2), and the proliferation medium was replaced every 2-3 days for a period of 14 days. As a control for each time point in all assays, ASCs were seeded onto 6-well TCPS plates (20,000 cells/well; n=6) and cultured in proliferation medium for 14 days.

3.1.6 Adipogenic differentiation

After the 14 day proliferation phase, adipogenic differentiation on the DAT and gelatin microcarriers was induced under dynamic conditions (15 rpm, 37 °C, 5% CO_2) by culturing in serum-free adipogenic differentiation medium comprised of DMEM:Ham's F12 supplemented with 33 μM biotin, 17 μM pantothenate, 66 nM human insulin, 1 nM triiodothyronine, 10 μg/mL transferrin, 100 nM hydrocortisone, and 1% pen-strep [353]. For the first 72 h, the medium was supplemented with 1 μg/mL of troglitazone and 0.25 mM isobutylmethylxanthine (IBMX). For each time point of an assay, TCPS controls were cultured in adipogenic differentiation medium (positive controls; n =3) or proliferation medium (negative controls; n=3). Fresh medium was provided to all samples every 2-3 days for up to 14 days after induction.

To probe the adipo-inductive nature of the DAT microcarriers, an additional set of trials was conducted to assess adipogenic marker expression in the ASC-seeded DAT microcarriers maintained in proliferation medium for the culture period, as compared to those cultured in adipogenic differentiation medium, as well as TCPS controls.

3.1.7 End-point RT-PCR analysis

End-point RT-PCR was used to assess the expression of the adipogenic markers peroxisome proliferator-activated receptor-γ (*PPARγ*), CCAAT/enhancer binding protein-α (*C/EBPα*), and lipoprotein lipase (*LPL*) at 72 h, 7 days, and 14 days after the induction of differentiation, with glyceraldehyde-3-phosphate dehydrogenase (*GAPDH*) as the housekeeping gene (n =3, N=2) [354]. Each sample was homogenized in 1 mL of TRIzol® reagent (Invitrogen, Burlington, ON, Canada) with a sonic dismembrator (Model-100, Fisher Scientific) and total RNA was extracted using standard protocols [14]. The RNA concentration and purity were measured using a NanoDrop spectrophotometer (ND1000, Fisher Scientific), and the 260/280 ratio generally ranged between 1.9 and 2.0.

First-strand cDNA was synthesized from 1 μg of total RNA in a 20 μL working volume with first-strand buffer (50 mM Tris-HCl, 75 mM KCl, 3 mM $MgCl_2$; Invitrogen), 10 mM dithiothreitol (DTT; Invitrogen), 0.09 OD260 units of random primers (Invitrogen, Cat. # 48190-011), 0.5 mM of each dNTP (Invitrogen, Cat. # 18427-013), and 200 units of SuperScript II RT (Invitrogen, Cat. # 18064-104). For each sample, minus-RT controls were prepared. The gene-specific primers (50 nM, desalted, Invitrogen) (Table 3.1) had a melting point of 60 °C and were designed using Primer3 software.

PCR was conducted in a 50 μL reaction volume, with 2.0 μL of synthesized cDNA, 1x Taq buffer (10 mM Tris-HCl, 50 mM KCl, 0.08% Nonidet P40; Fermentas, Cat. # EP0404), 250 nM forward primer, 250 nM reverse primer, 250 nM of each dNTP, 2.5 mM $MgCl_2$, and 0.375 units of recombinant Taq DNA Polymerase (Fermentas, Cat. # EP0404). For the PCR reactions, a Bio-Rad C1000 thermal cycler was used, with conditions of 95 °C for 5 min, 40 cycles of 30 s at 95 °C (denaturation), 30 s at 58 °C (annealing), and 30 s at 72 °C (elongation). Minus-RT and no-template controls were included on every plate. The PCR products were separated via electrophoresis on 5%

agarose gels (High Resolution Agarose, Sigma-Aldrich, Cat. # A4718), stained with ethidium bromide, and detected under ultraviolet light (G:Box Chemi HR16, Syngene).

Table 3.1: Human gene-specific primers for DAT microcarrier adipogenesis study

Gene	Description	Accession No.	Primer	Fragment length (bp)
PPARγ	Peroxisome proliferator-activated receptor gamma	NM_138712	F: TTCAGAAATGCCTTGCAGTG R: CCAACAGCTTCTCCTTCTCG	84
C/EBPα	CCAAT-enhancer-binding protein alpha	NM_004363	F:CAGAGGGACCGGAGTTATGA R: TTCACATTGCACAAGGCACT	107
LPL	Lipoprotein lipase	NM_000237	F: GTCCGTGGCTACCTGTCATT R: TGGCACCCAACTCTCATACA	94
GAPDH	Glyceraldehyde-3-phosphate dehydrogenase	NM_002046	F: ACAGTCAGCCGCATCTTCTT R: ACGACCAAATCCGTTGACTC	94

3.1.8 Glycerol-3-phosphate dehydrogenase (GPDH) quantification

To quantitatively assess the adipogenic response, GPDH enzyme activity levels were measured in the DAT and gelatin microcarrier samples at 72 h, 7 days, and 14 days after adipogenic induction, as well as in the controls, using a GPDH Activity Measurement Kit (Kamiya Biomedical Corporation, Cat. # KT-010, Seattle, WA, USA) (n=3, N=3) [355]. To normalize the GPDH activity levels, each sample was assayed in triplicate for total cytosolic protein using the Bio-Rad Protein Assay (Bio-Rad Laboratories, Inc.) with an albumin standard. At each time point, triplicate samples from each group were rinsed 3 times in PBS and transferred into 1 mL of enzyme extracting reagent provided with the kit. The cells were lysed using a sonic dismembrator (Model-100, Fisher Scientific), and each sample was centrifuged (12,800 xg, 5 min, 4 °C) to obtain the cytosolic fraction containing the intracellular GPDH. The samples were immediately assayed for GPDH activity and total protein content according to the manufacturers' instructions. For the GPDH studies, 1 Unit is defined as the activity required to oxidize 1 μmole of NADH in 1 min.

3.1.9 Oil red O staining

Oil red O histological staining was performed to stain intracellular lipid in the ASCs at 72 h, 7 days, and 14 days after adipogenic induction. At each time point, triplicate samples of approximately 10 microcarriers (n=3, N=3) were fixed for 2 h in 4% glutaraldehyde, and then rinsed 3 times with cation-free D-PBS. TCPS controls were fixed for 30 min in 10% neutral-buffered formalin and thoroughly rinsed with D-PBS. Oil red O stock solution was prepared in 99.9% isopropanol at a concentration of 3 g/L. Immediately prior to staining, a mixture of 3 parts oil red O stock solution and 2 parts deionized water (v/v) was filtered through a Whatman type I filter paper (Whatman, Cat. # 1001-150). Each sample was incubated at room temperature in 2 mL of the filtered oil red O solution for 5 min, followed by multiple rinses in deionized water to remove excess dye. The TCPS controls were counterstained with hematoxylin for 2 min, and then rinsed 3 times in deionized water. All samples were examined using a Zeiss Invertoskop 40C optical microscope, with digital image capturing (Lumenera, Infinity 2.1, Ottawa, ON, Canada).

3.1.10 *In vivo* assessment of DAT and gelatin microcarriers

A preliminary study was conducted to compare the unseeded and ASC-seeded DAT and gelatin microcarriers in a subcutaneous implant model in 12-week old female Wistar rats at 14 and 28 days. For the seeding experiments, primary rat ASCs were isolated from the epididymal fat pads of 8-week old male Wistar rats (n=2). The allogenic rat ASCs were cultured in proliferation medium on TCPS, with passaging at 80% confluence, and P2 cells were used for the microcarrier seeding. Canadian Council on Animal Care (CCAC) guidelines for the care and use of laboratory animals were followed, and the protocols for this study were reviewed and approved by the University Animal Care Committee (UACC) at Queen's University (Protocol # Flynn-2009-059 & Flynn-2010-053).

For the seeded microcarriers, P2 rat ASCs were dynamically seeded onto the DAT or gelatin microcarriers within the CELLSPIN system at an initial seeding density of 20,000 ASCs/mg of microcarriers, as described, and expanded in proliferation medium for 14 days. Immediately prior to implantation, the microcarrier samples were collected using wide-bore serological pipettes, rinsed in sterile D-PBS, and filtered through 100 μm nylon mesh to remove excess medium. The concentrated microcarrier samples (seeded and unseeded) were then gently transferred into 1 mL syringes.

The female rats were anesthetized with 2% isoflurane in 2 L/min of O_2, and were administered 5 mg/kg ketoprofen subcutaneously as a pre-operative analgesic. A total of 10 rats were used in the study, with 3 rats implanted with DAT microcarriers and 2 rats implanted with gelatin microcarriers per time point. For each rat, a 0.5 mL ASC-seeded microcarrier sample was injected through an 18-gauge hypodermic needle into the right subcutaneous space in the lower abdominal region (Fig. 3.1). For comparison, 0.5 mL unseeded microcarriers were injected into the same region in the left side of the rat. At 14 and 28 days post-implantation, the rats were sacrificed by CO_2 overdose, and the microcarriers were explanted within the surrounding tissues for histological analysis.

3.1.11 Histological staining

The explanted microcarriers were fixed in 4% paraformaldehyde for 12 h, rinsed with 70% ethanol, paraffin-embedded, and sectioned (5 μm sections). Representative sections were stained with Masson's trichrome, to characterize the collagen structure and to assess cellular distribution and angiogenesis throughout the explanted grafts, with visualization using a Zeiss Axio Imager 2 optical microscope.

3.1.12 Statistical analysis

Data are expressed as means ± standard deviations (SDs). All statistical analyses were performed by ANOVA with a Tukey's post-hoc comparison of the means. Differences were considered statistically significant at $p < 0.05$.

3.2 Results

3.2.1 Microcarrier fabrication and ASC seeding

In concordance with previous work in the Flynn lab, stable DAT and gelatin microcarriers were fabricated using the air-jet droplet technique and photo-crosslinking with rose bengal [26]. The diameter of the DAT and gelatin microcarriers used in all studies typically ranged from 900 to 950 μm. Using optical microscopy, it was confirmed that the seeded ASCs attached and proliferated on the microcarriers over the 14-day cell expansion period.

3.2.2 Adipogenic gene expression

End-point RT-PCR was conducted to qualitatively analyze the expression of the master adipogenic regulators *PPARγ* and *C/EBPα,* as well as the early adipogenic marker *LPL* in human ASCs cultured on the microcarriers. Representative agarose gel electrophoresis staining bands are shown in Fig. 3.2. During the initial RT-PCR study, comparing the induced DAT and gelatin microcarriers to the TCPS controls (Fig. 3.2a), all of the adipogenic genes were expressed in the induced DAT microcarrier samples at all times points (72 h, 7 days, and 14 days). In contrast, no detectable levels of adipogenic gene expression were observed at any time point for the induced gelatin microcarrier samples. In the second RT-PCR study, comparing the induced (cultured in differentiation medium) and non-induced (cultured in proliferation medium) DAT microcarriers (Fig. 3.2b), *PPARγ*, *C/EBPα*, and *LPL* were expressed in the induced DAT microcarrier samples at all time points. There was generally a trend for increasing expression over time, particularly for

LPL, consistent with a progression in adipogenic differentiation [356]. Interestingly, all three of the adipogenic genes were also expressed in the non-induced DAT microcarrier samples. For both of the studies, similar *PPARγ*, *C/EBPα*, and *LPL* expression patterns were detected in the TCPS control samples (Fig. 3.2c), with increasing levels of expression over time in the positive controls and lower levels detected in the negative controls, particularly for *C/EBPα* and *LPL*. In general, more intense bands for the adipogenic gene markers were found in the ASCs cultured on the DAT microcarriers as compared to the TCPS and gelatin controls.

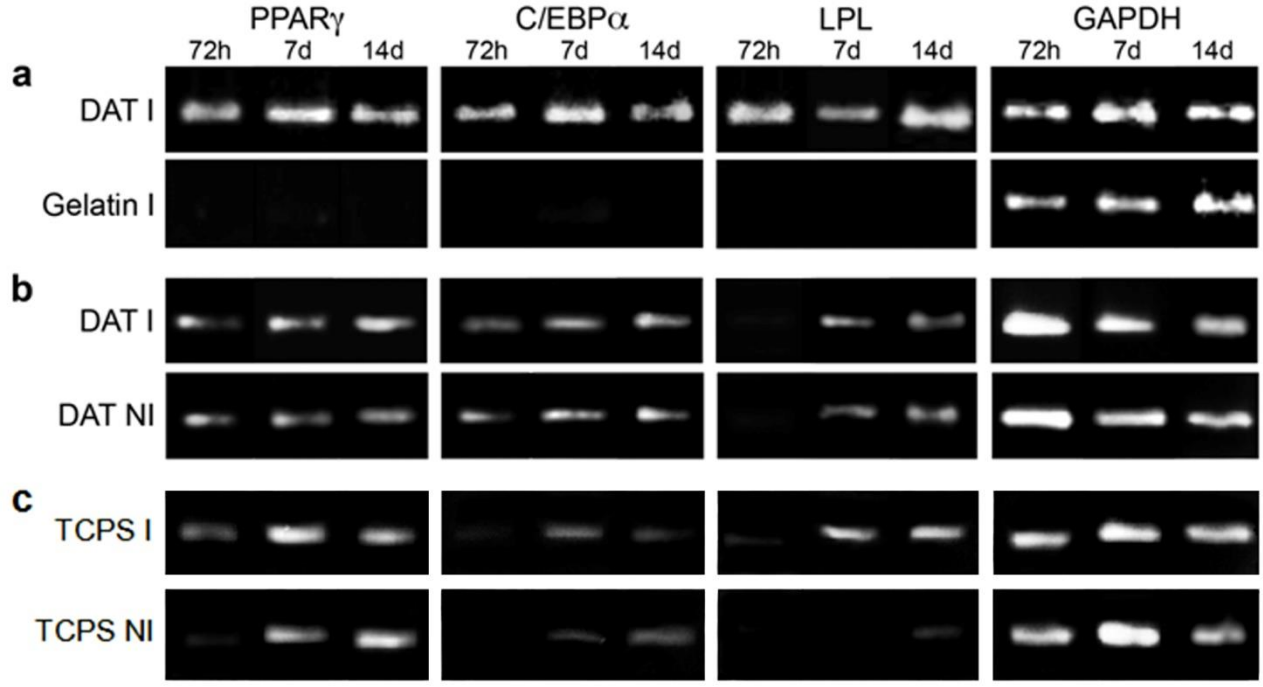

Figure 3.2: Representative end-point RT-PCR gene expression patterns of the adipogenic markers *PPARγ, C/EBPα,* and *LPL*, with *GAPDH* as the housekeeping gene, at 72 h, 7 days, and 14 days after adipogenic induction. I = induced (cultured in adipogenic differentiation medium). NI = not induced (cultured in proliferation medium). (a) DAT and gelatin microcarrier study, induced culturing conditions. (b) DAT microcarrier study, induced and non-induced culturing conditions. (c) TCPS controls. *PPARγ, C/EBPα*, and *LPL* were all expressed in the induced and non-induced ASCs cultured on the DAT microcarriers. No significant adipogenic gene expression was observed for the gelatin microcarrier controls. Staining patterns are representative of all samples analyzed (n= 3, N=2).

3.2.3 GPDH enzyme activity

The GPDH enzyme activity studies quantitatively confirmed the gene expression results, showing an increase in adipogenic activity in the DAT microcarrier samples (Figs. 3.3 and 3.4) as compared to the gelatin microcarrier or TCPS controls. In the first GPDH study, induced DAT and gelatin microcarriers were compared to TCPS controls (Fig. 3.3). At the 72 h time point, the induced DAT microcarriers demonstrated statistically higher GPDH activity (4.1 ± 0.1 mU/mg) than all other samples, including the induced TCPS controls (2.9 ± 1.6 mU/mg). No significant elevation in GPDH activity was detected for the induced gelatin microcarriers (0.5 ± 0.1 mU/mg). At 7 days, the GPDH activity on the induced DAT microcarriers (15.3 ± 2.2 mU/mg) was statistically greater than at 72 h, and higher than all other 7 day samples. No significant difference was detected for the gelatin microcarriers or the induced TCPS. At the 14 day time point, the induced DAT microcarrier GPDH activity (32.3 ± 3.4 mU/mg) was statistically greater than at all other time points, and higher than the other samples assayed at 14 days. GPDH activity detected on the induced gelatin microcarriers at 14 days (1.7 ± 0.6 mU/mg) was statistically greater than at 72 h and 7 days, but remained at a low level. No significant increase in activity was measured for the induced TCPS control. As anticipated, low GPDH activity levels were detected for the non-induced TCPS controls at all time points.

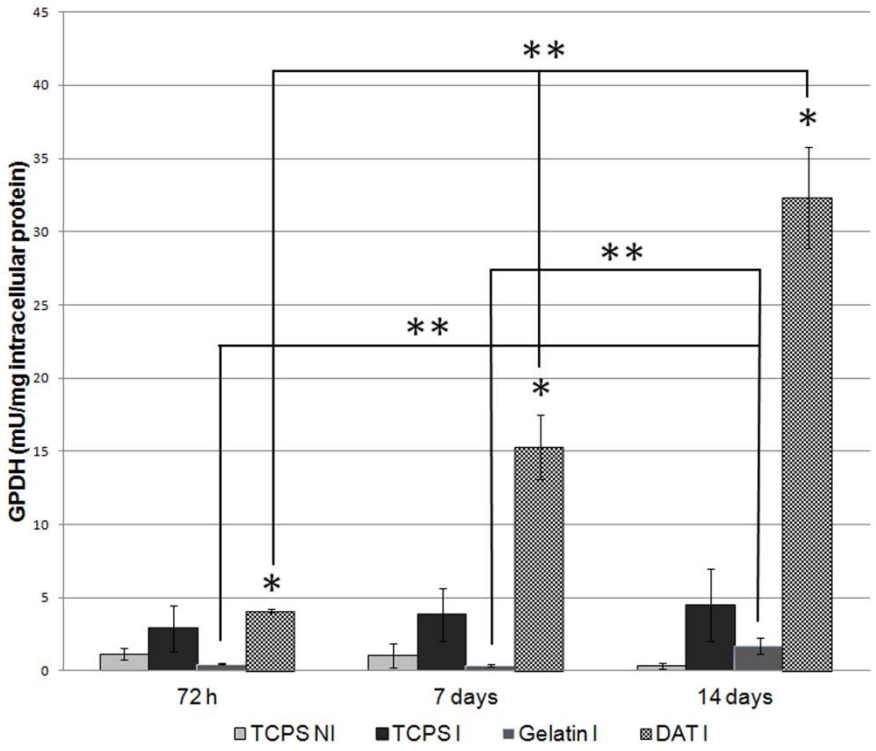

Figure 3.3: GPDH enzyme activity measured for DAT and gelatin microcarriers, as compared to non-induced (NI) and induced (I) TCPS controls, at 72 h, 7 days, and 14 days after inducing adipogenic differentiation. Data are expressed as mean GPDH activity ± SD and considered significant at $p < 0.05$. * = statistically different from other groups at same time point. ** = statistically different between time points. (n = 3, N =1).

In the second GPDH study, both induced and non-induced DAT microcarriers were compared to TCPS controls, to quantitatively assess the adipo-inductive potential of the DAT microcarriers (Fig. 3.4a). Overall, the induced DAT microcarriers demonstrated the highest GPDH activity levels over the course of the study. Interestingly, the non-induced DAT microcarrier GPDH activity levels were also elevated at all time points. After 72 h, the induced DAT microcarrier activity (3.9 ± 0.2 mU/mg) was statistically greater than all other samples, and the non-induced DAT microcarrier activity (2.7 ± 0.4 mU/mg) was statistically comparable to the induced TCPS activity (2.3 ± 0.7 mU/mg). At the 7-day time point, the GPDH activity for the induced DAT microcarriers (11.5 ± 2.4 mU/mg) was statistically higher than all other samples, and the GPDH activity for the non-induced DAT microcarriers (6.1 ±0.1 mU/mg) was statistically greater than the induced TCPS control (3.4 ± 0.4 mU/mg). Between 72 h and 7 days, the induced and non-

induced DAT microcarrier GPDH activity levels statistically increased over time. After 14 days, the induced DAT microcarriers had the statistically highest GPDH activity value (17.1 ± 1.5 mU/mg). The non-induced DAT microcarriers had a statistically elevated GPDH activity (5.2 ± 1.1 mU/mg) over the induced TCPS (3.2 ± 1.3 mU/mg) and comparable activity to the non-induced DAT microcarriers at 7 days (6.1 ± 0.1 mU/mg). No significant changes in GPDH activity were detected for the non-induced TCPS controls. The trend of elevated GPDH activity on the induced and the non-induced DAT microcarriers remained consistent, despite variability exhibited between cell donors with differing body mass indices (BMIs) (Fig. 3.4b).

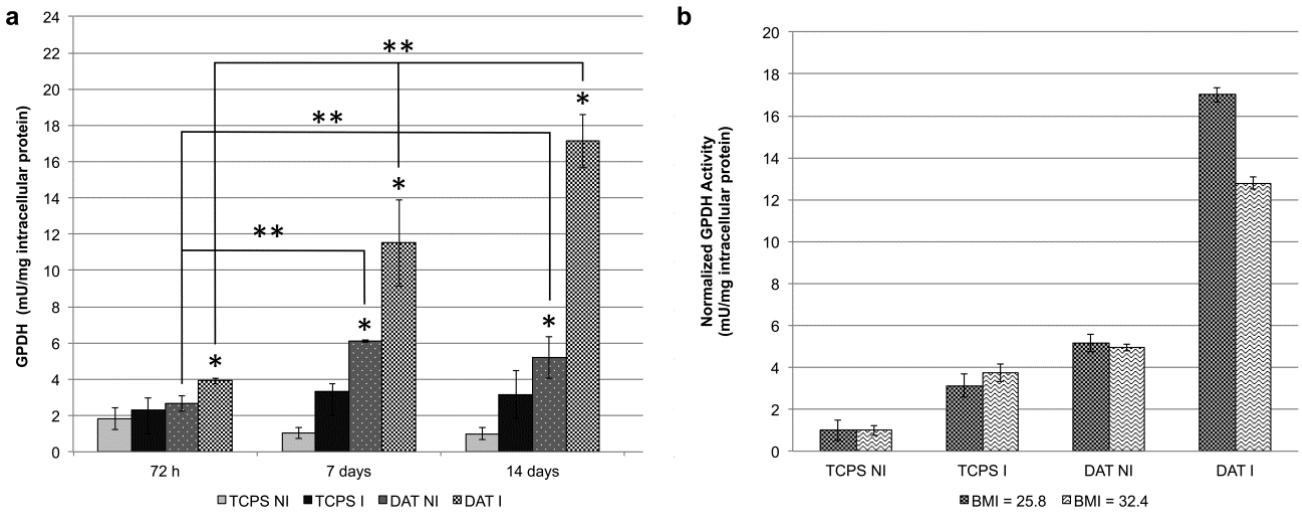

Figure 3.4: GPDH enzyme activity measured for induced (I) and non-induced (NI) DAT microcarriers, as compared to TCPS controls (I and NI). Data are expressed as mean GPDH activity ± SD and considered significant at $p < 0.05$. (a) Representative GPDH activity measured at 72 h, 7 days, and 14 days after inducing adipogenic differentiation (n =3, N=1). * = statistically different from other groups at same time point. ** = statistically different between time points. (b) Normalized GPDH activity at t = 14 days, relative to the non-induced TCPS control (n= 3, N =2), for two different cell donors.

3.2.4 Intracellular lipid accumulation

Representative oil red O images at 14 days of ASCs differentiating on DAT microcarriers and relevant controls are shown in Fig. 3.5.

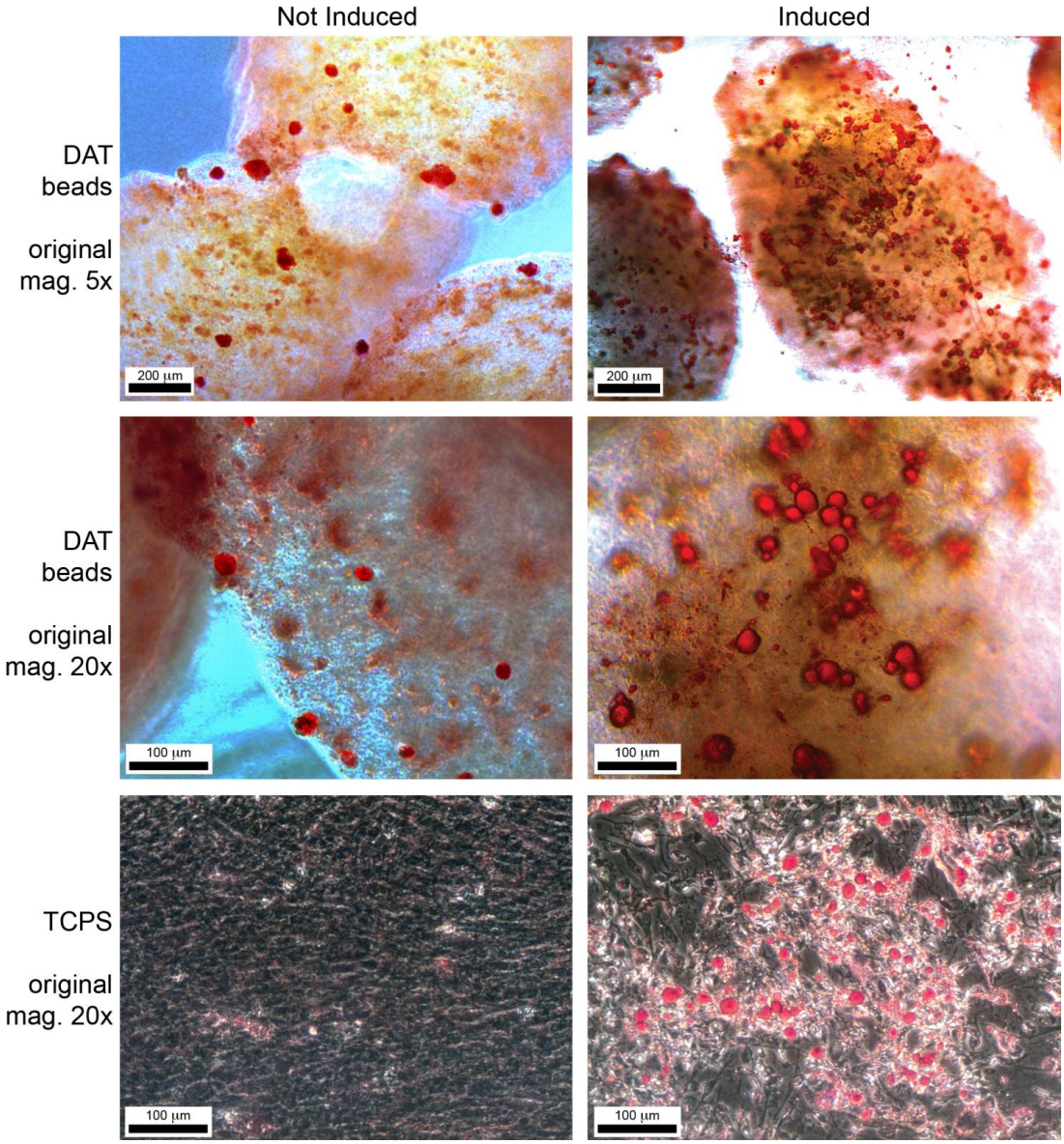

Figure 3.5: Representative oil red O staining for intracellular lipid accumulation within seeded ASCs at 14 days after inducing adipogenic differentiation. Induced = cultured in adipogenic differentiation medium. Not Induced = cultured in proliferation medium. DAT beads = DAT microcarriers seeded with ASCs and dynamically cultured. Cell visualization was performed using optical microscopy. Overall, the DAT microcarriers promoted ASC lipid uptake for both induced and non-induced culturing conditions.

Lipid loading was detected in ASCs cultured on induced DAT microcarriers as early as 72 h after inducing differentiation, with extensive oil red O staining at 14 days. Intracellular lipid accumulation was also observed on non-induced DAT microcarriers at the 14-day time point. The gelatin microcarriers did not stain positively for lipid loading at any time point. For the TCPS controls, intracellular lipid was detected in induced ASCs starting at 7 days. Non-induced TCPS controls remained devoid of intracellular lipid droplets at all time points. Qualitatively, the ASCs that differentiated on the induced DAT microcarriers demonstrated comparable levels of lipid uptake as the ASCs differentiated in 2-D on TCPS. In general, the staining patterns on the induced DAT microcarriers were more homogeneous, with differentiating cells distributed over the entire surface of the beads, as compared to the TCPS samples, which demonstrated a more cluster-like arrangement of differentiating cells over the surface of the plates.

3.2.5 *In vivo* injectablity and biocompatibility testing

During injection, the microcarriers were readily implanted into the subcutaneous space in the rat via an 18-gauge needle. All injection sites appeared to heal normally, without visible signs of macroscopic inflammation or infection. Over the course of the 28-day study, the injected microcarrier grafts remained localized and were easily identified for explantation.

Macroscopically, the excised DAT microcarrier (Fig. 3.6) and gelatin microcarrier (Fig. 3.7) grafts retained their volume over the course of the study, and no detectable differences were observed between the seeded and the unseeded DAT microcarrier grafts over time (Fig. 3.6a,b). Upon explantation at both time points, the injected DAT microcarriers were closely integrated with the host tissues, and formed a uniform, compressible tissue-like structure (Fig. 3.6a). In contrast, the gelatin microcarriers were encapsulated by a dense layer of fibrous tissues, and did not integrate well with each other or the surrounding host tissues (Fig. 3.7). Macroscopically, no visible

differences were observed between the seeded and the unseeded gelatin microcarrier grafts (Fig. 3.7a,b).

Masson's trichrome histological staining confirmed the integration of the seeded and unseeded DAT microcarriers with the host tissues, with evidence of remodeling of the DAT microcarriers and tissue infiltration (Fig. 3.6). In general, a higher degree of cellularity and enhanced angiogenesis were observed in the seeded DAT microcarrier grafts (Fig. 3.6d,f), as compared to the unseeded grafts (Fig. 3.6c,e), at both time points. The injected gelatin microcarriers remained individually distinguishable from one another within the grafts over the course of the study, with no cellular infiltration observed (Fig. 3.7). Increased cellularity and collagen deposition were detected in interstices between the seeded gelatin microcarriers (Fig. 3.7d,f), as compared to the unseeded gelatin microcarriers (Fig. 3.7c,e), at both time points. There was no evidence of a strong immune or inflammatory response to the DAT or gelatin microcarriers, with staining patterns consistent with normal wound healing.

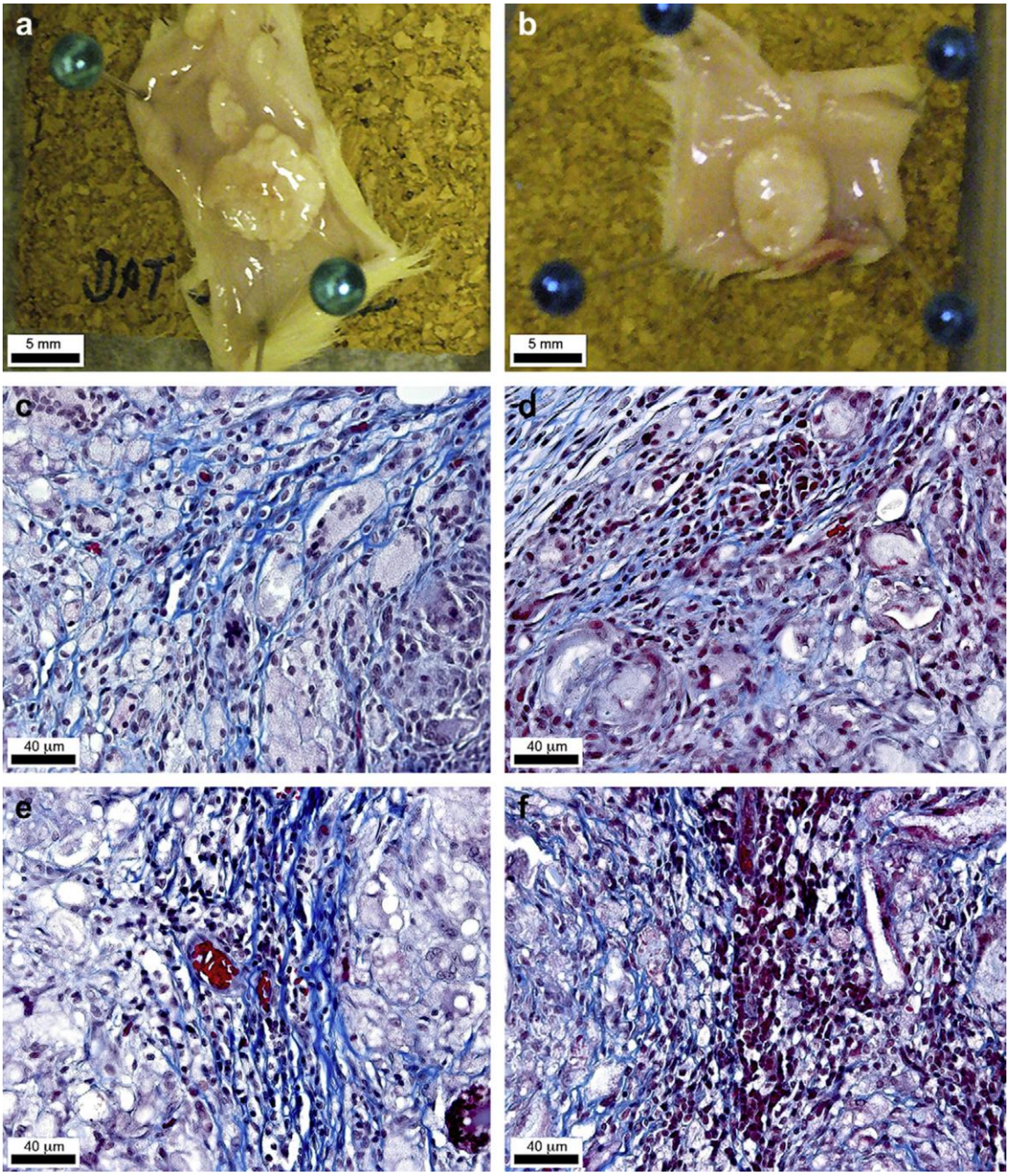

Figure 3.6: Decellularized adipose tissue (DAT) microcarriers injected subcutaneously into the lower abdomen of female Wistar rats. Macroscopic images of (a) unseeded DAT microcarriers and (b) DAT microcarriers seeded with allogenic rat ASCs, at 14 days after injection. The samples showed no macroscopic differences between the two groups. Masson's trichrome staining of (c) unseeded DAT and (d) ASC-seeded DAT at 14 days after injection, and (e) unseeded DAT and (f) ASC-seeded DAT at 28 days after injection. The DAT microcarriers were well integrated into the surrounding tissues. Under histological analysis, seeding the DAT microcarriers with allogenic ASCs enhanced the degree of cellularity and angiogenesis at both time points.

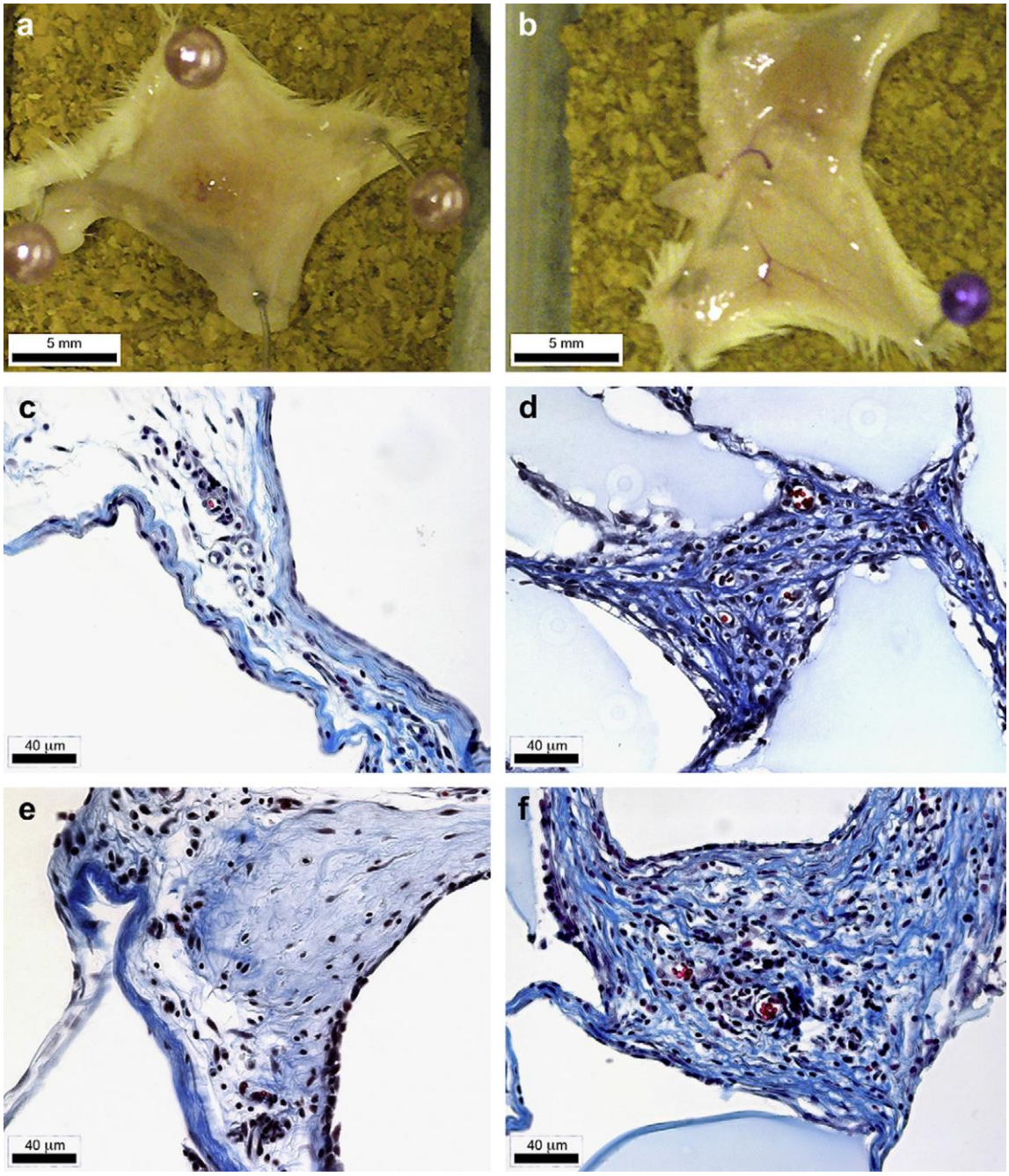

Figure 3.7: Gelatin microcarriers injected subcutaneously into the lower abdomen of female Wistar rats. (a) Unseeded gelatin microcarriers and (b) gelatin microcarriers seeded with allogenic rat ASCs, at 14 days after injection. Masson's trichrome staining of (c) unseeded gelatin and (d) ASC-seeded gelatin at 14 days after injection, and (e) unseeded gelatin and (f) ASC-seeded gelatin at 28 days after injection. There was no observable cell infiltration into the gelatin microcarriers (clear or light blue regions). Seeding the gelatin microcarriers with allogenic ASCs qualitatively appeared to increase the cellularity and amount of collagen deposition in the interstices between the microcarriers at both time points.

3.3 Discussion

In the culture of stem cells, the ECM microenvironment plays a critical role in mediating stem cell lineage commitment and differentiation [325]. There is strong evidence to support that this regulation occurs through both receptor ligand interactions, as well as mechanical signaling events, which influence the key signal transduction pathways that control the cellular response [254], [357], [358]. The complexity of these cell-ECM interactions points to the need for a tissue-specific approach to re-engineering the native stem cell niche. Much research has focused on the modification of biomaterials in a bottom-up approach to more closely mimic the compositional and/or mechanical properties of the native cellular microenvironment, and thereby direct proliferation and/or differentiation [359], [360]. More recent studies have highlighted the potential for decellularized ECM bioscaffolds to naturally direct stem cell differentiation and maintain the phenotype of mature cell populations in a tissue-specific manner [361], [362].

With this view, the objective of the current study was to explore the adipogenic potential of human ASCs cultured on microcarriers fabricated from decellularized human adipose ECM. Using previously-optimized microcarrier seeding and expansion protocols as a basis [26], human ASCs were seeded at low density and allowed to proliferate under dynamic conditions for a period of 14 days. This design was selected as a clinically-relevant model, where small tissue biopsies could be used to extract ASCs that would subsequently be expanded on allogenic microcarriers, which could be available as off-the-shelf bioscaffolds. Ideally, this approach would ultimately eliminate the need for cell expansion on TCPS, which can profoundly affect the characteristics of the stem cells [75]. Adipogenic differentiation has been shown to correlate with growth arrest, and is typically enhanced under high-density conditions where the cells have a more rounded morphology [363]. As such, the 14 day proliferation period was an important phase prior to the induction of differentiation to support adipogenesis in any of the culture groups.

The initial studies focused on comparing the levels of ASC adipogenesis on the DAT microcarriers, relative to gelatin microcarriers fabricated using similar methods. For all of the assays, the results indicated that the DAT microcarriers were strongly supportive of ASC adipogenesis. In contrast, no appreciable adipogenic activity was detected on the gelatin microcarriers, emphasizing the advantage of the complex matrix composition in mediating the stem cell response. Based on these promising initial results, a second set of studies was conducted to compare adipogenesis on the DAT microcarriers under dynamic culture in proliferation medium and adipogenic differentiation medium, to investigate whether the DAT microcarriers were adipo-inductive for the human ASCs. In previous work, it was found that ASCs cultured on intact (i.e. non-solubilized) DAT bioscaffolds expressed the adipogenic gene markers *PPARγ* and *C/EBPα* after 10 days of culture under proliferation conditions, without the need for standard exogenous differentiation factors [14]. During adipogenesis, *PPARγ* and *C/EBPα* act as the master regulators of differentiation. These two transcription factors are required for the expression and maintenance of the genes that are required for ASC maturation into adipocytes, including the early adipogenic marker *LPL* [94], [364], which is an enzyme involved in fatty acid transport during lipogenesis [365]. Previous results indicated that the intact DAT provided a naturally conducive environment for fat formation, although it was unclear whether the matrix effects on the ASCs were compositional and/or structural in nature [14].

The investigation of the DAT microcarriers provided an opportunity to further explore this potential, by investigating scaffolds incorporating the composition of the DAT, after solubilization and fabrication into a controlled geometry. Interestingly, the RT-PCR analysis revealed that the adipogenic markers were all expressed in the non-induced DAT microcarrier samples. These patterns indicated that the adipo-inductive properties of the DAT were conserved through the enzyme solubilization and microcarrier fabrication processes. From a more quantitative standpoint, the GPDH enzyme activity levels indicated that while the highest levels of expression were

measured in the ASCs cultured on the DAT microcarriers in adipogenic medium, elevated levels were also detected for the non-induced DAT microcarrier samples. The differentiation factors supplied during the *in vitro* experiments provide a potent mixture of adipogenic cues, but the GPDH results suggest that there are elements of the DAT matrix that are also adipo-inductive, supporting the application of a tissue-specific approach for adipose regeneration. The GPDH results were further corroborated by the oil red O staining which showed that in contrast to the TCPS positive controls, a very homogeneous response was observed on the induced DAT microcarriers, with differentiating cells distributed over the entire surface of the beads rather than in localized clusters. Further, there was evidence of intracellular lipid accumulation on the non-induced DAT microcarriers cultured in proliferation medium, visually confirming that the DAT was inducing ASC adipogenesis.

Overall, the combination of the DAT microcarriers with adipogenic medium *in vitro* resulted in the highest levels of differentiation in the seeded ASCs. However, the results confirmed that it is feasible to engineer microenvironments that naturally stimulate differentiation towards the adipogenic lineage. With further optimization, this tailored culturing environment may help to reduce the need for costly growth factors and hormones to support differentiation, which could minimize the risk of undesirable systemic side effects *in vivo* and support the clinical translatability of ASCs cultured using this approach for adipose tissue engineering. Promisingly, consistent results were obtained with the DAT microcarriers in all of the assays, regardless of the cell donor source. Future research could focus on identifying those factors within the DAT scaffolds and microcarriers that are contributing to the unique adipo-inductive properties of the adipose matrix. The ability to harness this potential would have broad implications in the fields of adipose tissue engineering, obesity, and diabetes research.

A preliminary *in vivo* study was conducted to assess the DAT microcarriers as injectable cell delivery vehicles in an immunocompetent subcutaneous rat model. Similar to previous results with

other types of decellularized scaffolds, there was no evidence of strong inflammatory or immune response to the DAT microcarriers, with staining patterns consistent with normal wound healing. The Masson's trichrome staining of the DAT microcarrier grafts showed evidence of cellular infiltration, angiogenesis, and matrix remodeling, with the microcarriers forming an integrated tissue-like structure. More importantly, for soft tissue regeneration, there was macroscopic preservation of the implant volume over the course of the study.

The enhanced cellularity and vascularization achieved in this work by pre-seeding the DAT microcarriers with ASCs are consistent with the recognized wound healing and angiogenic properties of these unique regenerative cells [366]. ASCs are known to secrete a broad range of factors that modulate cell migration, ECM synthesis, inflammation, and angiogenesis [366]–[368], although the detailed mechanisms of how ASCs modulate these responses are not yet fully understood. Over the time frame of the current study, there was no evidence of mature adipose tissue formation within the implant regions. However, these results confirm that ASCs, together with DAT microcarriers, enhanced the overall regenerative response at both time points. Future work could probe longer time frames, which are typically required to support adipose tissue remodeling *in vivo*, as well as the effects of pre-differentiating the ASCs on the DAT microcarriers prior to implantation.

Overall, the *in vitro* and *in vivo* results support the use of DAT microcarriers as both cell expansion and delivery vehicles for adipose tissue engineering. The differentiation studies clearly emphasize the critical role of the ECM in modulating the ASC response, and suggest that adipose-derived ECM has compositional properties that naturally induce adipogenesis. Clinically, the DAT microcarriers hold promise as injectable cell carriers and bioscaffolds for the correction of small-volume soft tissue defects. Human adipose tissue routinely discarded during lipo-reduction surgery could readily be collected, processed into DAT microcarriers at a centralized facility, lyophilized, and stored as an allogenic off-the-shelf biomaterial. On demand, the microcarriers could be seeded

and implanted with autologous ASCs isolated using minimally-invasive techniques, to enhance the regeneration of damaged or missing soft tissues.

3.4 Conclusions

In the current study, the DAT-based microcarriers were investigated as injectable adipose tissue-specific scaffolds for ASC adipogenesis within a dynamic culture system. Promisingly, the results demonstrated that the microcarriers fabricated from solubilized DAT provided a naturally adipo-inductive substrate that supported the adipogenic differentiation of human ASCs *in vitro*, corroborating previous work with intact DAT scaffolds. More specifically, gene expression analyses indicated that the DAT microcarriers induced the expression of *PPARγ*, *C/EBPα*, and *LPL*, without the need for exogenous adipogenic differentiation factors. Quantification of GPDH activity confirmed the adipo-inductive capacity of the DAT microcarriers. The highest levels of the adipogenic genes and proteins were observed in the ASCs dynamically cultured on the DAT microcarriers in adipogenic differentiation medium. The results of the gene and protein expression assays were confirmed by oil red O visualization of extensive intracellular lipid accumulation on the induced DAT microcarriers, as well as lower levels in the non-induced group. In the *in vivo* subcutaneous Wistar rat model, the DAT microcarriers showed good biocompatibility as compared to the gelatin microcarriers, with enhanced integration, cellularity, and angiogenesis, as well as soft tissue volume retention and no evidence of a negative immunogenic reaction over 28 days. Overall, the results from this work emphasize the importance of the ECM in mediating ASC adipogenesis and point to the potential of the adipo-inductive DAT microcarriers for use in soft tissue regeneration, including applications in plastic and reconstructive surgery.

Chapter 4

Porous Decellularized Adipose Tissue Foams for Soft Tissue Regeneration
Biomaterials (2013), 34(13), 3290-330.

4.1 Introduction

To facilitate soft tissue regeneration and implant integration into the host tissues, bioscaffolds are typically designed to be highly porous to improve cellular infiltration and viability, to be structurally robust, and ideally, to promote normal cell signaling processes. In this context, recent studies have focused on natural collagenous foams as they have the potential to provide a cost effective, biologically active and highly customizable base material that can be adapted for use in a variety of tissue engineering applications [24], [81], [244], [369]. Standard foam fabrication methods often involve freezing acid-solubilized collagen in a preformed mould, followed by lyophilization to yield a homogenous porous matrix [370]–[372]. Typically, pore sizes larger than 100 μm are required to facilitate extensive cellular infiltration, which may not be easily achieved using this approach [371], [373]. As an alternative, solid free form (SFF) technology has been investigated in which 3-D printers fabricate custom casting moulds to achieve deep channelling microarchitecture [374]. Similarly, other methods have been presented including a foaming/freeze drying technique or incorporating large ice particulates into the collagen solution before lyophilization [375], [376].

To date, the majority of natural foams have been prepared using purified animal collagens or gelatin, which have limitations associated with their xenogenic sourcing [375], [377], [378]. Prior to the publication of this study, the use of human extracellular matrix (ECM) had not yet been extensively studied for the fabrication of tissue-specific ECM-derived foams. Decellularized human tissues provide an interesting alternative for bioscaffold fabrication, as the complex microenvironment of the ECM mediates a wide range of cellular behaviour in a tissue-specific

manner including survival, proliferation, migration, and differentiation, all of which are critical for tissue regeneration [135], [351].

Recently, adipose tissue has emerged as an abundant and accessible source of human ECM that is enriched with basement membrane, which can be collected from either excised tissue blocks or from processed lipoaspirates through a range of decellularization techniques [14], [24]. As described in Chapter 3, both DAT and injectable DAT-based microcarriers provide an adipo-inductive substrate for human adipose-derived stem/stromal cells (ASCs) that hold great promise as bioscaffolds for adipose regeneration [14], [19]. Other groups have investigated adipose-derived ECM in the form of powders, sheets and injectable gels, with positive results in terms of cell adhesion, proliferation, and integration following *in vivo* implantation [16], [24], [244], [379].

Building on this previous work, the objective of this Chapter was to develop improved DAT bioscaffold fabrication methods to circumvent the need for chemical crosslinking to ensure stability. In particular, α-amylase digested DAT was used to synthesize non-chemically crosslinked DAT bioscaffolds, and bioactivity was assessed in the form of porous DAT foams with a focus on ASC adipogenesis as well as soft tissue regeneration and wound healing. Moreover, novel methods were established to create macroporous "bead foams", comprised of a network of interconnected porous DAT microcarriers. When the DAT was α-amylase digested to form a suspension and prepared via freeze-drying techniques, the DAT foams and bead foams were stable *in vitro* without the need for additional chemical crosslinking [242]. By varying the freezing temperatures and concentrations of the DAT suspension, a range of foam and bead foam constructs were prepared and their physical properties were characterized. Subsequently, the *in vitro* adipogenic differentiation response of human ASCs seeded on the DAT-based foams was assessed in terms of adipogenic gene expression and enzymatic activity. Finally, the *in vivo* response to the DAT-based foams was characterized in a subcutaneous Wistar rat model to evaluate scaffold biocompatibility, angiogenesis, adipogenesis and implant integration over 12 weeks.

4.1.1 Materials

Unless otherwise indicated, chemical reagents for this study were obtained and used as received from Sigma Aldrich Canada Ltd. (Oakville, ON, Canada).

4.1.2 Adipose tissue acquisition

In collaboration with surgeons from the Kingston General Hospital and Hotel Dieu Hospital (Kingston, ON, Canada), human adipose tissue samples were sourced from female patients undergoing elective lipo-reduction surgery of the breast or abdomen and transported to the lab on ice in sterile cation-free Dulbecco's phosphate buffered saline (D-PBS; Thermo Scientific HyClone, Cat. # SH30028, Fisher Scientific, Oakville, ON, Canada) supplemented with 20 mg/mL bovine serum albumin (BSA). The patient information was recorded (donor age, weight, height, and excision site) and the tissue was processed within 2 h for ASC isolation or decellularization, using published protocols [14]. Research ethics board approval for this study was obtained from Queen's University (REB# CHEM-002-07) and an experimental outline of the overall project scope is shown in Fig. 4.1.

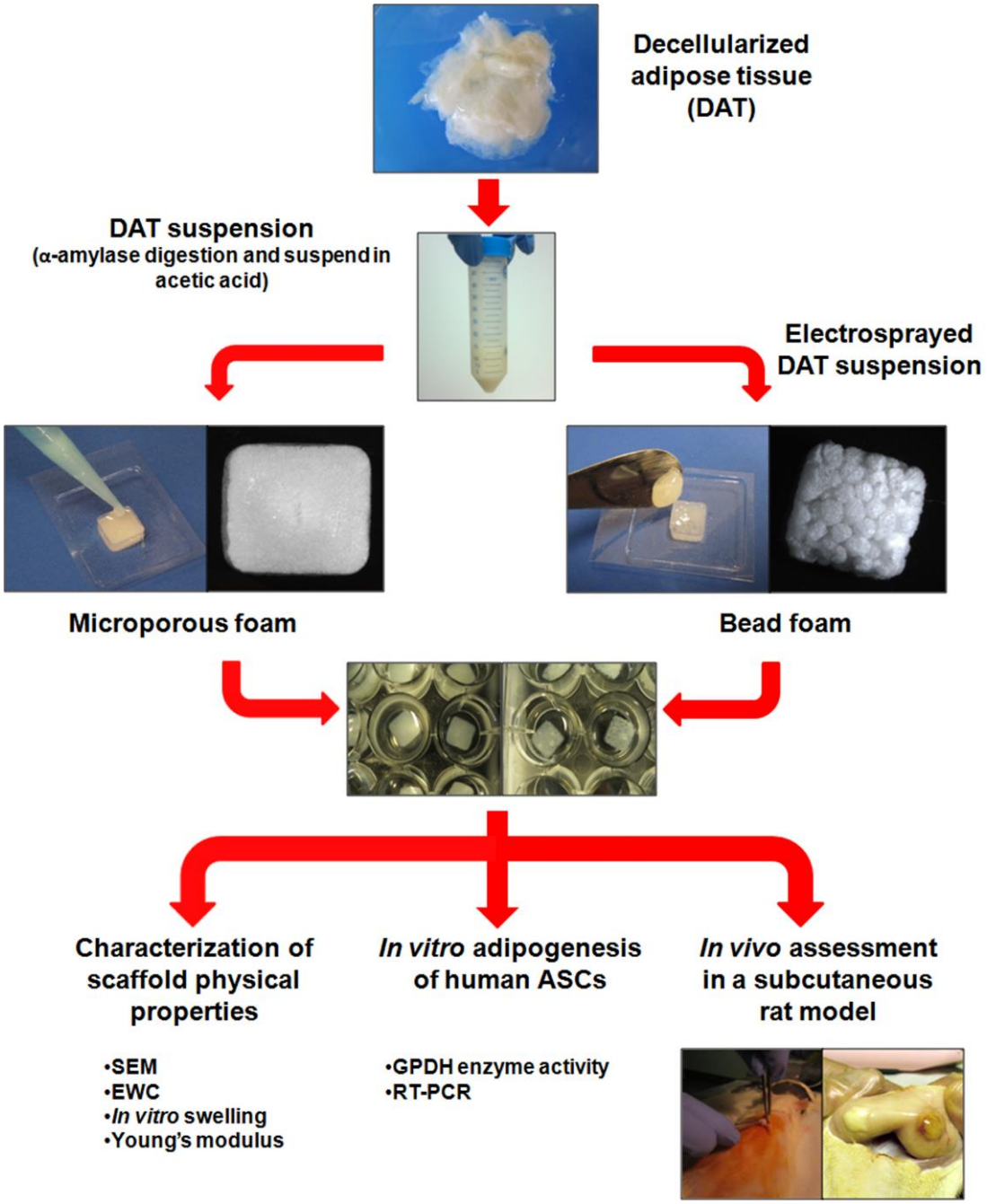

Figure 4.1: Schematic overview of the experimental scope and methods.

4.1.3 DAT suspension

DAT samples were pooled from multiple patients (n =5) and processed into a suspension using methods adapted from Stevens *et al.* [242]. Collective samples of DAT (2 g, wet weight) were repeatedly washed in 5% (w/v) NaCl solution followed by distilled water. The DAT was resuspended in 0.22 M NaH_2PO_4, the pH was adjusted to 5.4, and 0.3% (w/w) α-amylase was added

to the tissue. The tissue was digested by agitating continuously at room temperature for 72 h, after which the DAT was washed repeatedly with 5% (w/v) NaCl solution followed by distilled water. The DAT was then minced finely (~0.5 cm^3 fragments) and resuspended in 0.2 M acetic acid and allowed to agitate continuously at 37 °C for 48 h, with periodic homogenization (PowerGen Model 125 homogenizer, Fisher Scientific, Ottawa, ON, Canada). The liquefied DAT suspension was then centrifuged (12,000 xg, 5 min, 4 °C) and the ECM-rich supernatant was collected. The DAT residue was subjected to an additional extraction with acetic acid and the supernatants were pooled. The concentration of the DAT suspension was estimated based on the initial mass of the DAT and the volume of acetic acid added.

4.1.4 Foam fabrication

The microporous DAT foams were prepared by pipetting 500 μL of DAT suspension into a cryomould (Tissue-Tek ®Biopsy Cryomold 10 x10 x 5mm; VWR, Cat. # 25608-922, Batavia, IL), freezing the scaffolds completely, and lyophilizing overnight. The combined effects of varying the DAT suspension concentration (25 mg/mL, 50 mg/mL, and 100 mg/mL) and freezing temperature (-20 °C, -80 °C) on the properties of the DAT foams were explored.

The “bead foams” were prepared using microporous DAT microcarriers fabricated using an electrospraying method adapted from Kim *et al.* [303]. Briefly, via a syringe pump set at a rate of 0.5 mL/min, the DAT beads were synthesized by electrospraying DAT suspension (25 mg/mL or 50 mg/mL) through a 25-gauge infusion needle (SURFLO®, Cat. # SV-25BLK, Terumo, Somerset, NJ) with an applied voltage of 10 kV into a bath of liquid nitrogen at a working distance of 15 cm. The frozen DAT microcarriers were collected and allowed to thaw completely at room temperature before they were transferred into the cryomould, followed by freezing (-20 °C, -80 °C) and lyophilization, to create a stable 3-D bead foam comprised of an interconnected network of packed DAT microcarriers.

4.1.5 Characterization of foam stability and structure

Characterization studies were conducted to assess the physical properties of a range of DAT foams and bead foams as summarized in Table 4.1. Scanning electron microscopy (SEM) was used to visualize the microarchitecture of each foam formulation. To prepare the samples for SEM, the foams were fixed overnight in 2.5% glutaraldehyde, rinsed extensively in D-PBS and then freeze-fractured using liquid nitrogen to assess the internal microstructure. The samples were then subjected to an established chemical drying protocol using hexamethyldisilazane (HDMS) [14]. The dried samples were mounted and pulse coated with gold, and visualized with a JOEL JSM-840 microscope with an accelerating voltage of 10 kV and a working distance of 15 mm.

To measure the equilibrium water content (EWC), the dry weights (W_D) were recorded for all lyophilized foam samples prior to rehydration in deionized water. After 72 h, the foams were carefully blotted to remove excess liquid prior to recording the wet weight (W_W). The EWC was determined using the following formula:

$$EWC = \frac{W_w - W_D}{W_w} \times 100\%$$

Macroscopic images of the foams were taken using a stereomicroscope to quantitatively assess changes in the dimensions of the foams using ImageJ analysis software. Using these measurements, a swelling ratio for each type of foam was calculated according to the following equation:

$$Swelling\ ratio = \frac{A_w}{A_D} \times 100\%$$

Where A_W represents the surface area of the foam in the hydrated state, and A_D represents the surface area in the lyophilized form.

Table 4.1: DAT foam formulations

Formulation	
Microporous foam	25 mg/mL DAT suspension, frozen at -20 °C 25 mg/mL DAT suspension, frozen at -80 °C
	50 mg/mL DAT suspension, frozen at -20 °C 50 mg/mL DAT suspension, frozen at -80 °C
	100 mg/mL DAT suspension, frozen at -20 °C 100 mg/mL DAT suspension, frozen at -80 °C
Bead foam	25 mg/mL DAT suspension, frozen at -20 °C 25 mg/mL DAT suspension, frozen at -80 °C
	50 mg/mL DAT suspension, frozen at -20 °C 50 mg/mL DAT suspension, frozen at -80 °C

4.1.6 Mechanical testing

Foam materials with various DAT suspension concentrations were prepared in cylindrical moulds with a diameter of 23 mm. To characterize the mechanical properties, the instantaneous compressive Young's modulus of each cylindrical foam sample was measured using an unconstrained indentation technique, performed by Dr. Abbas Samani in his lab at the University of Western Ontario. In this technique, the cylindrical sample is indented using a small indenter while its wall is unconfined (Fig. 4.2a). Compared to a standard uniaxial test, this indentation test is advantageous as it is capable of assessing the homogeneity of the sample material. In this investigation, a custom-made indentation mechanical testing machine was used, as shown in Fig. 4.2a. As described by Samani *et al.* [380], the indenter was connected to a linear LAL-30 servo motor (SMAC, Carlsbad, CA, USA) driven by a 6K2 motor controller device (Parker Hannifin Corporation, Rohnert Park, CA, USA) which has a motion range of 25 mm and resolution of 0.5 mm. The controller can be programmed to provide a user-defined indenter motion profile. To measure the indentation force profile corresponding to the applied user-defined indentation profile, a high precision LCL-113 model load cell (Omega, Quebec, Canada) with a capacity of 113 g was used. To enhance force measurement, the load cell data was sampled at 1000 samples/s. Each

sample was carefully moved out of its mould and placed in the indentation machine's sample holder, which contained a thin layer of PBS to reduce sample friction with the holder and to prevent sample dehydration. In this study, a plane-ended indenter was used with a 3 mm diameter, while the indentation motion was set to sinusoidal with a peak-to-peak amplitude of 0.5 mm. Prior to indentation, a small preloading from 0.1 g to 0.2 g was applied to each sample to ensure full contact. This was followed by 10 indentation loading cycles at the sample's center for preconditioning, which is necessary for exhibiting repeatable response by biological tissues [381]. After preconditioning, 4 more cycles were applied while the corresponding indentation displacement and force data were acquired. A typical graph showing force versus displacement data acquired over 4 cycles is shown in Fig. 4.2b. To calculate the sample's Young's modulus, the slope, S, of the loading part of the indentation force versus displacement data was used. The slope S was obtained by linearly fitting that part of the data using a least squares fitting algorithm. To obtain each sample's Young's modulus, E, the following equation was used, described in detail by Samani *et al.*:

$$E = \kappa S$$

In this equation, κ is a conversion factor that depends on the sample geometry and its mechanical boundary conditions. As described by Samani *et al.*, κ of each sample was calculated using an inverse Finite Element (FE) algorithm [380]. Note that in this study, all samples were cylindrical with a diameter of 23 mm and height ranging from 2.5 mm to 5.0 mm. In order to calculate κ for each sample, the actual height of the sample was measured to construct its FE model used in the inverse FE algorithm.

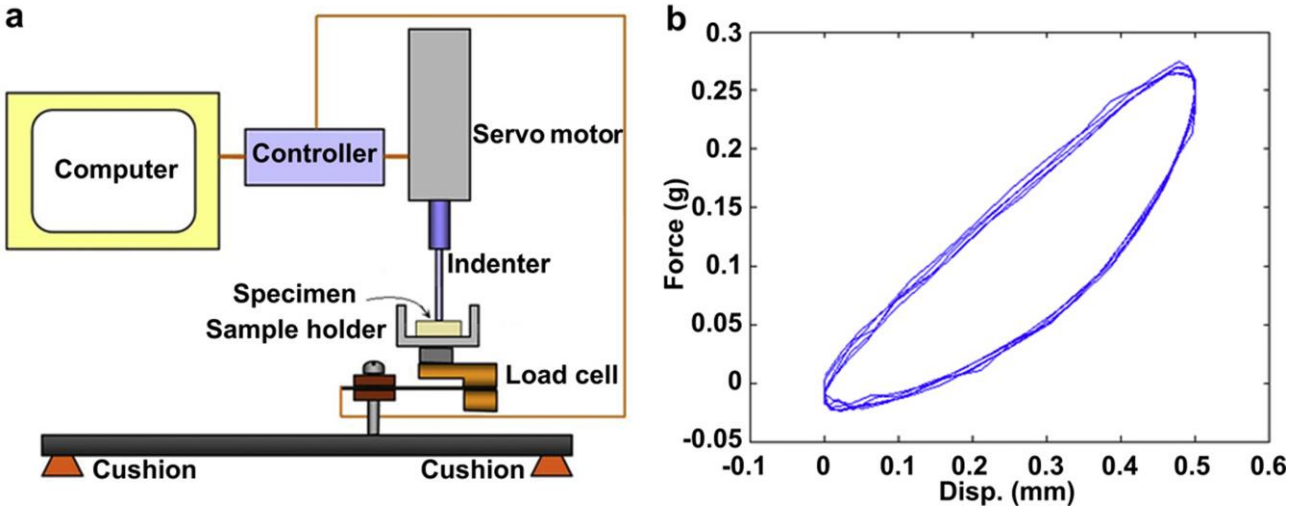

Figure 4.2: Schematic of the indentation system used to measure the Young's modulus of the foam samples and force displacement curve. (a) The indentation system consists of a linear servo motor and a motion control unit that measures the applied indentation displacement in addition to a high precision load cell to measure the corresponding forces over the indentation time. Indenter motion and data acquisition was coordinated using a LabVIEW program. (b) A typical force displacement curve corresponding to a foam (50 mg/mL DAT suspension, frozen at -20 ºC). The height of this sample was measured at 5 mm. Data of 4 cycles are shown, where the top part corresponds to the loading part of the cycles, which was used for the slope (S) calculation.

4.1.7 Adipose-derived stem cell culture

Following established methods [355], human ASCs were extracted and expanded on tissue culture polystyrene (TCPS) in proliferation medium containing DMEM:Ham's F-12 medium supplemented with 10% fetal bovine serum (FBS; Thermo Scientific HyClone, Cat. # SH30396) and 100 U/mL penicillin and 0.1 mg/mL streptomycin (1% pen-strep), with medium changes every 2-3 days. Passage 2 (P2) ASCs were used for all cell studies. To minimize donor variability within each experiment, ASCs from a single donor were used to seed all foams, bead foams, non-digested intact DAT, and TCPS control samples in triplicate (n=3) for each assay across all time points. Trends were verified in the main *in vitro* studies with cells sourced from different donors (N =2-3).

4.1.8 Foam seeding

For all cell culture experiments, the foams were decontaminated through repeated rinsing in 70% ethanol and then rehydrated in sterile D-PBS. The rehydrated foams were equilibrated overnight (37 °C, 5% CO_2) in proliferation medium prior to seeding. Each scaffold was transferred into a 12-well tissue culture insert (ThinCert^{TM}, Cat. # 665640, Greiner Bio-One, North Carolina, USA) and seeded with $1x10^6$ ASCs in 350 μL of medium by carefully distributing the cell suspension over the surface of the foam. Next, 2 mL of proliferation medium was gently added to the outside of the insert for each sample. After 48 h to allow for cell attachment, the foams were removed from the inserts and cultured directly within the 12-well plates for the remainder of the study (37 °C, 5% CO_2).

An adipogenic differentiation study was conducted comparing glycerol-3-phosphate dehydrogenase (GPDH) enzyme activity for all of the microporous scaffold formulations outlined in Table 4.1, to select the most promising conventional foam for further investigation (n =3). Based on the combined results of the stability study and this cell culture trial, the subsequent *in vitro* studies characterized ASC adipogenesis in the conventional DAT foams and macroporous DAT bead foams fabricated with a DAT suspension concentration of 50 mg/mL and a freezing temperature of -20 °C. For comparative purposes, all trials included non-digested intact DAT samples (50 mg DAT/scaffold) seeded in the same manner, as well as additional controls on TCPS, seeded at a density of 50,000 cells/cm^2 in 12-well plates.

4.1.9 Induction of adipogenic differentiation

At 48 h after seeding, the ASCs were differentiated using serum-free adipogenic differentiation medium consisting of DMEM:Ham's F12 supplemented with 33 μM biotin, 17 μM pantothenate, 66 nM human insulin, 1 nM triiodothyronine, 10 μg/mL transferrin, 100 nM hydrocortisone, and 1% pen-strep [26]. In inducing differentiation, 1 μg/mL of troglitazone and

0.25 mM isobutylmethylxanthine (IBMX) were added to the medium for the first 72 h. For all assays, each time point included positive TCPS controls (n=3) cultured in adipogenic differentiation medium and negative TCPS controls (n=3) cultured in proliferation medium. Throughout the culture period, the medium was changed every 2-3 days for all samples.

4.1.10 GPDH enzyme activity

To quantitatively assess the adipogenic response, GPDH enzyme activity levels were measured at 72 h, 7 days, and 14 days after adipogenic induction, using established protocols with a GPDH Activity Measurement Kit (Kamiya Biomedical Corporation, Cat# KT-010, Seattle, WA, USA) (n=3) [25]. The data was normalized to the total intracellular protein content measured using the Bio-Rad Protein Assay. For the GPDH studies, 1 Unit is defined as the activity required to oxidize 1 μmole of NADH in 1 min.

4.1.11 End-point RT-PCR analysis

To evaluate ASC expression of key adipogenic markers, end-point RT-PCR was performed at 72 h, 7 days, and 14 days post adipogenic induction. Expression of peroxisome proliferator-activated receptor-γ (*PPARγ*), CCAAT/enhancer binding protein-α (*C/EBPα*), and lipoprotein lipase (*LPL*) was analysed in addition to the housekeeping gene glyceraldehyde-3-phosphate dehydrogenase (*GAPDH*) (n =3, N=2) [354]. Gene-specific primers (50 mM, desalted, Invitrogen) designed with Primer3 software (Table 3.1) with a melting temperature of 60 °C were employed. Subsequent RNA extraction, cDNA synthesis, PCR amplification, and gel electrophoresis were performed as described previously, using standard protocols [19].

4.1.12 ASC distribution on foams

Masson's trichrome staining was performed to assess the ASC distribution within the DAT foams *in vitro* at 72 h, 7 days, and 14 days after adipogenic induction. At each time point, samples of the foams (n=3, N=3) were fixed for 2 h in 4% paraformaldehyde, rinsed 3 times with cation-free D-PBS. The samples were then paraffin-embedded and sectioned (5 µm sections), and stained with Masson's trichrome using established protocols [19]. Each sample was examined using a Zeiss Invertoskop 40C optical microscope, with digital image capturing (Lumenera, Infinity 2.1, Ottawa, ON, Canada).

4.1.13 *In vivo* assessment of the DAT-based bioscaffolds

An *in vivo* study was conducted to assess the tissue response to the microporous DAT foams (25 mg/mL DAT suspension, 50 mg/mL DAT suspension, and 100 mg/mL DAT suspension samples, frozen at -20 °C) and DAT bead foams (50 mg/mL DAT suspension, frozen at -20 °C) over 12 weeks using a subcutaneous Wistar rat model (12-week old female rats, Charles River Laboratories). Intact DAT samples were included as a control group for the study. The effects of seeding the scaffolds with allogenic rat ASCs (rASCs) were also explored. For these experiments, the rASCs were isolated from the epididymal fat pads of 8-week old male Wistar rats and were expanded in proliferation medium on TCPS to P2. For the seeded samples, $1x10^6$ rASCs were seeded on each scaffold using the previously described methods, and allowed to adhere for 36 h prior to implantation. Immediately before implantation, the seeded samples were rinsed in sterile D-PBS to remove residual proliferation medium. Canadian Council on Animal Care (CCAC) guidelines for the care and use of laboratory animals were followed, and all protocols were approved by the University Animal Care Committee (UACC) at Queen's University (Protocol # Flynn-2009-059 & Flynn-2010-053).

For the implantation surgeries, the female rats were anesthetized with 2% isofluorane in 2 L/min of O_2 and were administered 5 mg/kg ketoprofen subcutaneously as a pre-operative analgesic. A 1 cm incision was made in the dorsal dermis of the rats and the scaffolds were carefully positioned in the subcutaneous space. Each rat received either 4 or 5 implants (randomized, with a maximum of 1 per scaffold group), and both the seeded and unseeded scaffolds were assessed in triplicate (n=3) at each time point, with a total of 30 rats in the study. At 1, 3, 8, and 12 weeks post implantation, the rats were sacrificed by CO_2 overdose and the scaffolds were explanted within the surrounding tissues for histological analysis.

4.1.14 Histological Staining

Foams and intact DAT samples were fixed in 4% paraformaldehyde for 12 h, rinsed with 70% ethanol, paraffin-embedded, and sectioned (5 μm sections). Representative sections were stained with Masson's trichrome, to examine the collagen organization and scaffold integration into the host tissues, including analysis of cellular infiltration, angiogenesis, and adipogenesis. Visualization was performed using a Zeiss Axio Imager 2 optical microscope.

4.1.15 Statistical analysis

All data are expressed as the mean ± standard deviation (SD) and statistical analyses were performed by ANOVA with a Tukey's post-hoc comparison of means using OriginPro Software. Differences were considered statistically significant at $p < 0.05$.

4.2 Results

4.2.1 Foam fabrication and characterization

Microporous foams were prepared by freeze-drying human DAT suspensions within moulds, yielding soft porous sponges with a well-defined 3-D architecture (Fig. 4.3a). Similarly,

bead foams were fabricated through lyophilizing packed arrangements of the DAT microcarriers (1-2 mm in diameter), to produce scaffolds comprised of interconnected beads (Fig. 4.3b). Macroscopically, the pore size and porosity of the foams could be tuned to some degree by varying the freezing temperature and DAT suspension concentration. More specifically, conventional foams fabricated at lower DAT suspension concentrations and frozen more slowly (i.e. at a higher freezing temperature) were generally more porous, likely due to the formation of larger ice crystals during processing (Fig. 4.4). The foams prepared with 25 mg/mL DAT suspension were very soft, with more structural heterogeneity observed under SEM. For the microporous foam formulations, the foams synthesized with 50 mg/mL DAT suspension and frozen at -20 °C appeared to have a more homogenous network organization with larger open pores.

Microscopic examination of the bead foams (Figs. 4.3 and 4.4) showed that the microporous DAT beads were fused at junction points that stabilized the overall structure, with more macroporous regions found in the interstices between the beads. The most uniform and structurally robust bead foams were comprised of the DAT microcarriers synthesized with 50 mg/mL DAT suspension and frozen at -20 °C before lyophilization. In general, the bead foams synthesized at the lower freezing temperature produced more densely packed constructs. Interestingly, while all of the foams had high equilibrium water contents, ranging between 95 and 98%, they did not swell extensively (Table 4.2) and maintained their original geometry, as defined by the shape of the fabrication mould.

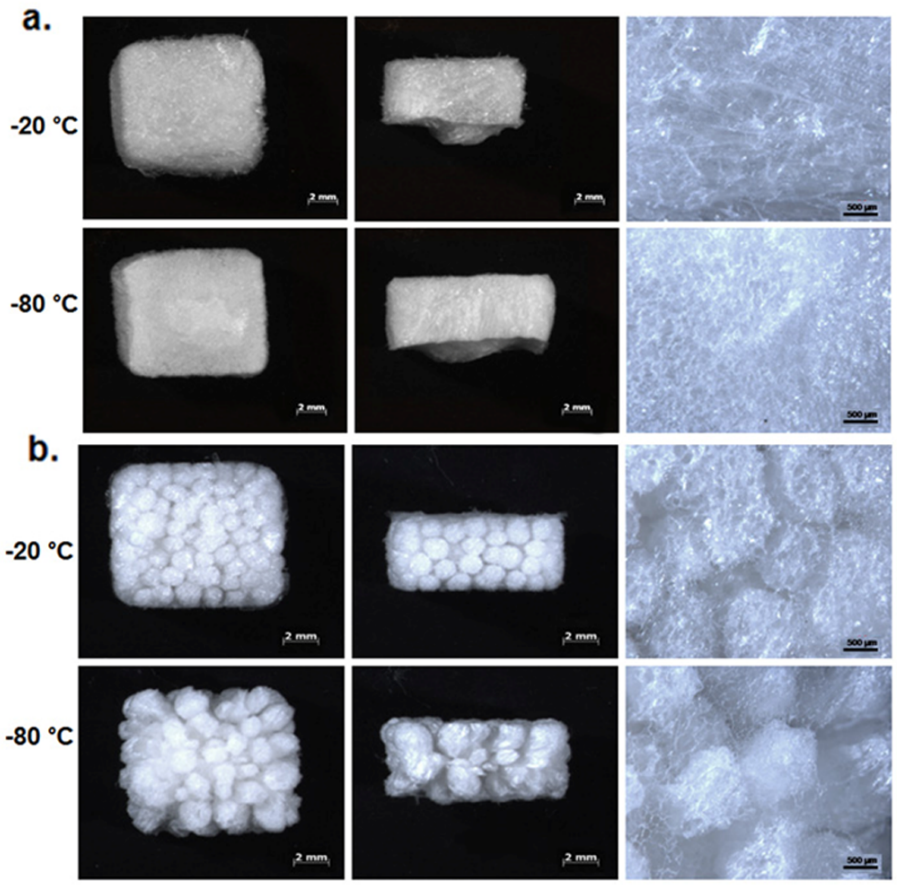

Figure 4.3: Representative stereomicroscopic images of lyophilized (a) DAT foams and (b) DAT bead foams comprised of an interconnected network of microporous DAT microcarriers, prepared using 50 mg/mL DAT suspension and frozen at either -20 ºC or -80 ºC. Both types of foams retained their shape, as defined by the fabrication mould, following rehydration.

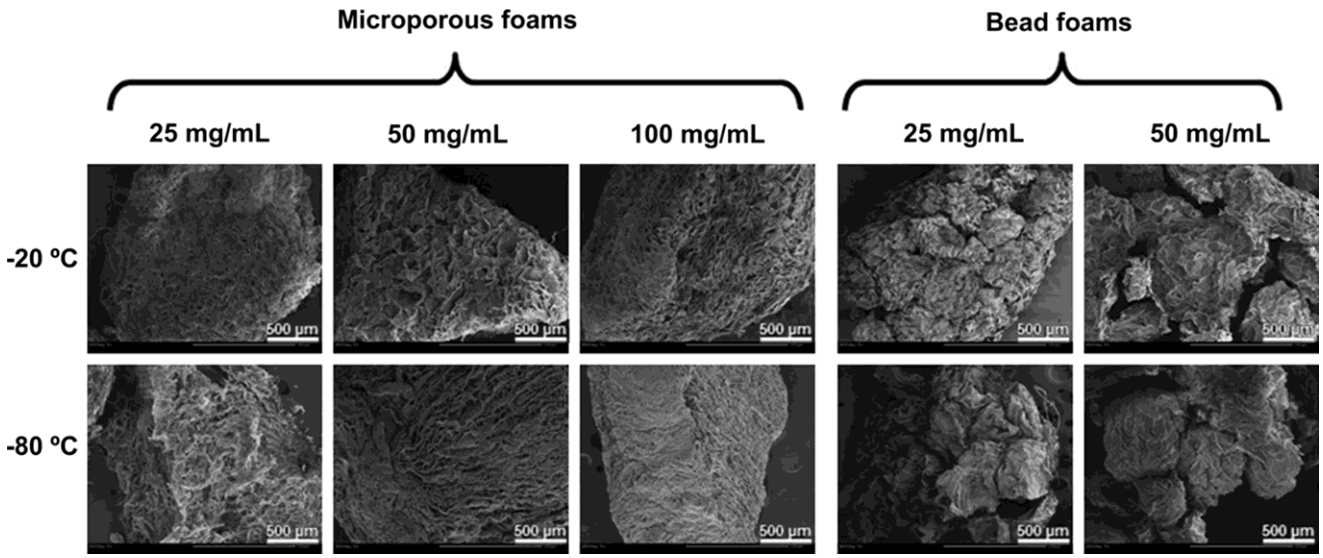

Figure 4.4: Representative SEM images of freeze-fractured DAT foams and bead foams prepared using various DAT suspension concentrations and freezing temperatures. In general, the foams fabricated with lower DAT suspension concentrations and frozen more slowly to promote ice crystal formation (i.e. at a higher freezing temperature) had a more porous ultrastructure.

Table 4.2: Foam formulation and properties.

	Formulation	Swelling ratio (%)	Equilibrium water content (%)	Young's modulus (kPa)
Microporous foam	25 mg/mL DAT suspension, frozen at -20 °C	97 ± 1	97.7 ± 0.3	n.d.
	25 mg/mL DAT suspension, frozen at -80 °C	100 ± 2	97.4 ± 0.4	n.d.
	50 mg/mL DAT suspension, frozen at -20 °C	103 ± 3	97.5 ± 0.1	3.67 ± 0.38
	50 mg/mL DAT suspension, frozen at -80 °C	99 ± 4	97.0 ± 0.4	2.42 ± 0.65
	100 mg/mL DAT suspension, frozen at -20 °C	103 ± 8	97.3 ± 0.3	4.00 ± 0.38
	100 mg/mL DAT suspension, frozen at -80 °C	110 ± 4	95.2 ± 0.6	4.01 ± 0.46
Bead foam	25 mg/mL DAT suspension, frozen at -20 °C	108 ± 2	97.4 ± 0.1	n.d.
	25 mg/mL DAT suspension, frozen at -80 °C	99 ± 2	96.4 ± 0.5	n.d.
	50 mg/mL DAT suspension, frozen at -20 °C	111 ± 5	97.7 ± 0.2	n.d.
	50 mg/mL DAT suspension, frozen at -80 °C	92 ± 2	95.8 ± 0.6	n.d.

4.2.2 Mechanical properties and adipogenesis

As described, inverse FE models were developed to assess the mechanical properties of the hydrated foams, which were extremely soft and required a sensitive load cell to accurately measure the compressive moduli. Due to the natural heterogeneity in the samples, there was significant

variability in the measurements for the conventional 25 mg/mL DAT suspension foams, as well as for the bead foams, and it was not possible to accurately calculate an average modulus for these groups. Macroscopically, the 25 mg/mL DAT suspension foams were the softest of all of the scaffolds investigated in the current study. The Young's moduli determined for the conventional foams fabricated with either 50 mg/mL or 100 mg/mL DAT suspension are shown in Table 4.2. With the exception of the 50 mg/mL DAT suspension, -80 °C group, which had a slightly lower modulus, all of the foams had similar moduli, within the 3-4 kPa range previously measured for normal human adipose tissue [382].

Building from these results, a differentiation study was conducted to compare ASC adipogenic differentiation on the conventional foams, measured in terms of GPDH enzyme activity (Fig. 4.5). At 72 h following the induction of differentiation, there were no significant differences in the GPDH activity of the human ASCs seeded on the various microporous foams. At 7 days, the 100 mg/mL DAT suspension, -20 °C foams had a higher mean GPDH activity level (30.4 ± 9.0 mU/mg) as compared to all of the other groups. Moreover, there was a significant increase in the GPDH activity for the 100 mg/mL DAT suspension foams (-20 °C and -80 °C) from 72 h to 7 days. At 14 days, the 50 mg/mL DAT suspension, -20 °C foams (59.3 ± 9.3 mU/mg), the 100 mg/mL DAT suspension, -80 °C foams (69.5 ± 2.8 mU/mg), and the 100 mg/mL DAT suspension, -20 °C foams (58.3 ± 3.8 mU/mg) had comparable levels of GPDH activity, which were statistically different from the other formulations at the same time point. Interestingly, the highest levels of adipogenic differentiation were observed for the foams with the Young's moduli that most closely approximated that of native human fat. Notably, the GPDH activity at 14 days for all formulations was statistically different than at 72 h or 7 days, consistent with a progression in differentiation.

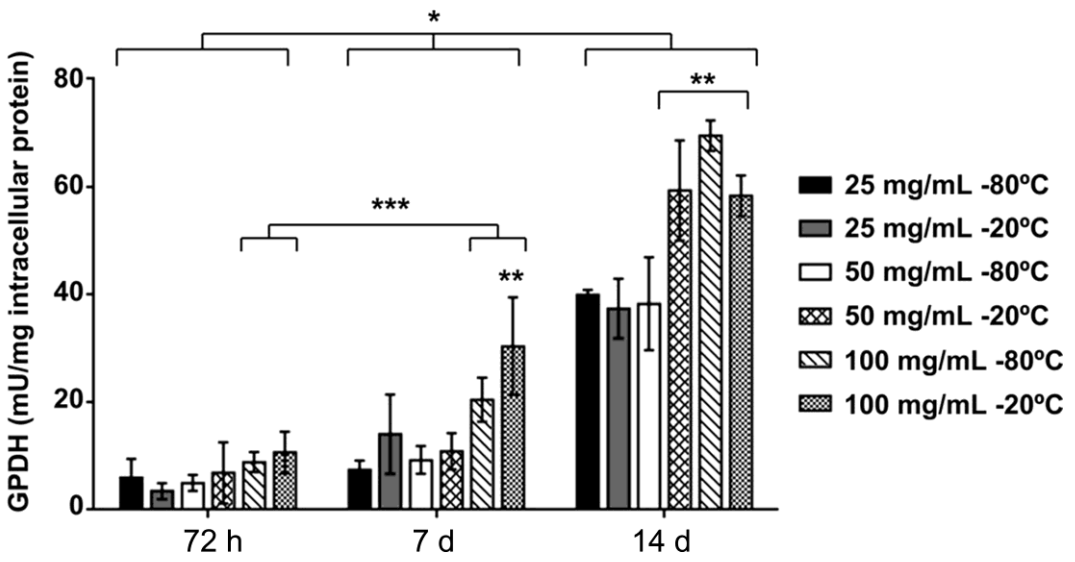

Figure 4.5: GPDH enzyme activity of ASCs seeded on a range of microporous DAT foams and cultured under adipogenic differentiation conditions. Data is expressed as a mean GPDH activity ± SD with significance considered at $p<0.05$. * = statistically different at 14 days as compared to the other time points. ** = statistically different than the other scaffold groups at the same time point. *** = statistically different between 72 h and 7 days. (n=3).

4.2.3 GPDH enzyme activity comparison for conventional and bead foams

Based on the initial characterization studies, the 50 mg/mL DAT suspension, -20 °C foams were selected for further analysis, as this formulation yielded stable foams with (i) a highly uniform structure of open pores that could theoretically support cellular infiltration, (ii) similar mechanical properties to native fat, and (iii) enhanced ASC adipogenesis at 14 days. For comparison, the bead foams were fabricated from DAT microcarriers synthesized with 50 mg/mL DAT suspension that were frozen at -20 °C. Adipogenic differentiation of seeded human ASCs was quantitatively assessed in terms of GPDH enzyme activity in comparison to intact DAT and TCPS controls (Fig. 4.6a). The experiment was repeated with ASCs from two different donors (ASC donor 1 BMI = 31.5, ASC donor 2 BMI = 23.3), with consistent levels observed for all groups, and the data represents the combined results from both trials. At 72 h, all induced microporous foams, bead foams, and intact DAT controls had statistically higher GPDH activity (12.4 ± 2.7 mU/mg, 10.0 ± 4.1 mU/mg, and 11.8 ± 1.7 mU/mg, respectively) than the non-induced scaffolds and TCPS controls. At 7 days, the induced microporous foams, bead foams, and intact DAT (20.0 ± 4.9

mU/mg, 17.5 ± 3.8 mU/mg, and 14.1 ± 5.6 mU/mg, respectively) exhibited similar elevated GPDH activity levels. At 14 days, the induced microporous foams (36.1 ± 8.0 mU/mg) had the highest GPDH activity level, statistically different from all other samples at this time point. The induced bead foams (21.7 ± 2.9 mU/mg) and intact DAT (16.2 ± 4.6 mU/mg) also demonstrated enhanced GPDH activities that were statistically different from the non-induced scaffolds and TCPS controls. In general, for the induced scaffold groups, there was an increasing trend in GPDH activity from 72 h to 14 days. Interestingly, the non-induced foams, bead foams, and intact DAT demonstrated comparable levels of GPDH activity as the induced TCPS controls at all time points, with a trend for slightly higher levels on the non-induced foams and bead foams.

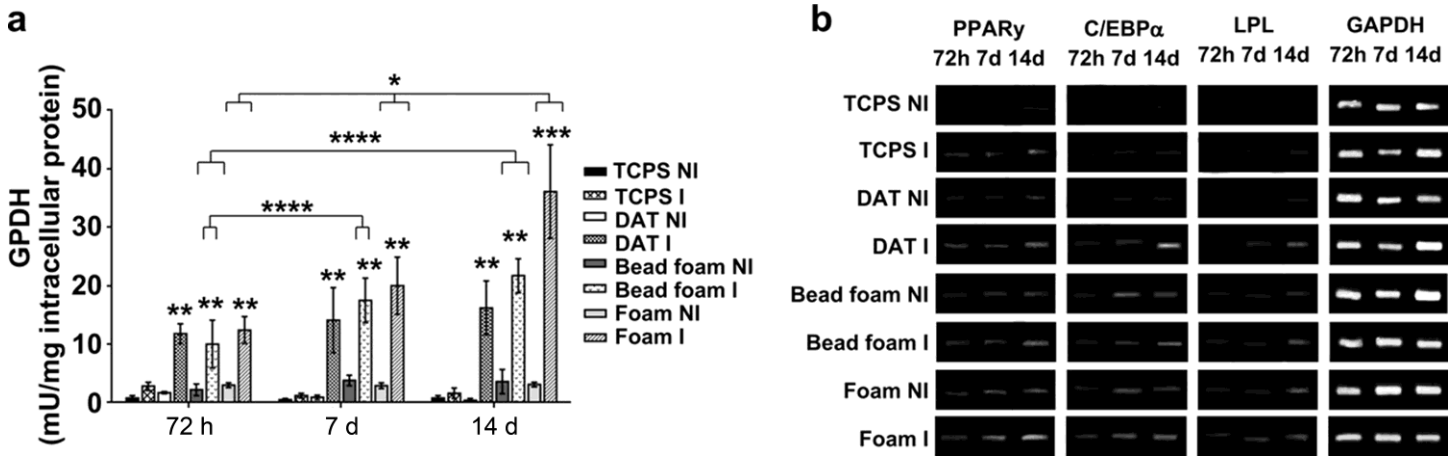

Figure 4.6: *In vitro* analysis of ASC adipogenic differentiation on the DAT foams and bead foams (50 mg/mL, DAT suspension -20 ºC), in comparison to intact DAT and TCPS controls. (a) GPDH enzyme activity expressed as mean ± SD and considered significant at $p<0.05$ (n =3, N =2). * = statistically different at 14 days compared to the other time points. ** = statistically different than the non-induced scaffold groups and TCPS controls at the same time point. *** = statistically different than all other groups at the same time point. **** = statistically different than at 72 h. (b) Endpoint RT-PCR analysis of adipogenic gene expression (*PPARγ*, *C/EBPα*, and *LPL*), with *GAPDH* as the housekeeping gene. Staining patterns are representative of all samples analysed (n =3, N= 2). I = induced (cultured in adipogenic differentiation medium). NI = non-induced (cultured in proliferation medium).

4.2.4 Adipogenic gene expression

To support the GPDH activity data, end-point RT-PCR studies were performed to assess the expression of the master adipogenic regulators *PPARγ* and *C/EBPα*, as well as the early adipogenic marker *LPL*, in the induced and non-induced foams, bead foams, intact DAT and TCPS controls. The representative agarose gel electrophoresis results are shown in Fig. 4.6b. Overall, the induced and non-induced foam and bead foam samples all demonstrated expression of the adipogenic genes at all time points, suggesting that the foams were both "adipo-conductive" and "adipo-inductive". The adipogenic markers were also observed in the induced intact DAT controls, although *LPL* expression was not detected at 72 h. In comparison to the DAT-based foams, the non-induced intact DAT samples cultured in proliferation medium showed qualitatively lower levels of *PPARγ* and *C/EBPα* expression at all time points, combined with low expression of *LPL* at 14 days. The gene expression trends in the induced TCPS controls showed increased expression of the adipogenic markers over time, consistent with a progression in differentiation. Overall, the levels of *PPARγ*, *C/EBPα* and *LPL* gene expression for the cells differentiated on TCPS were qualitatively lower than for the DAT foams and bead foams under either differentiation or proliferation conditions.

4.2.5 Cellular distribution

Histological assessment of the cellular distribution in the foams through Masson's trichrome staining demonstrated that the majority of the ASCs were localized on the surface of the foams and bead foams, with only a few cells penetrating into the interior regions of the scaffolds over 14 days in culture (Fig. 4.7). In general, the ASCs grew in a layer across the surface of the foams, with the degree of confluence increasing over time. On the bead foams, the cell distribution was somewhat less uniform, potentially due to the more uneven topography and interstices between the microcarriers. On a microscopic level, there was evidence of collagen contraction in the most superficial layers of the foams at 14 days (Fig. 4.7), particularly for the conventional foams.

However, there were no significant macroscopic changes in the overall dimensions of the scaffolds during the culture period.

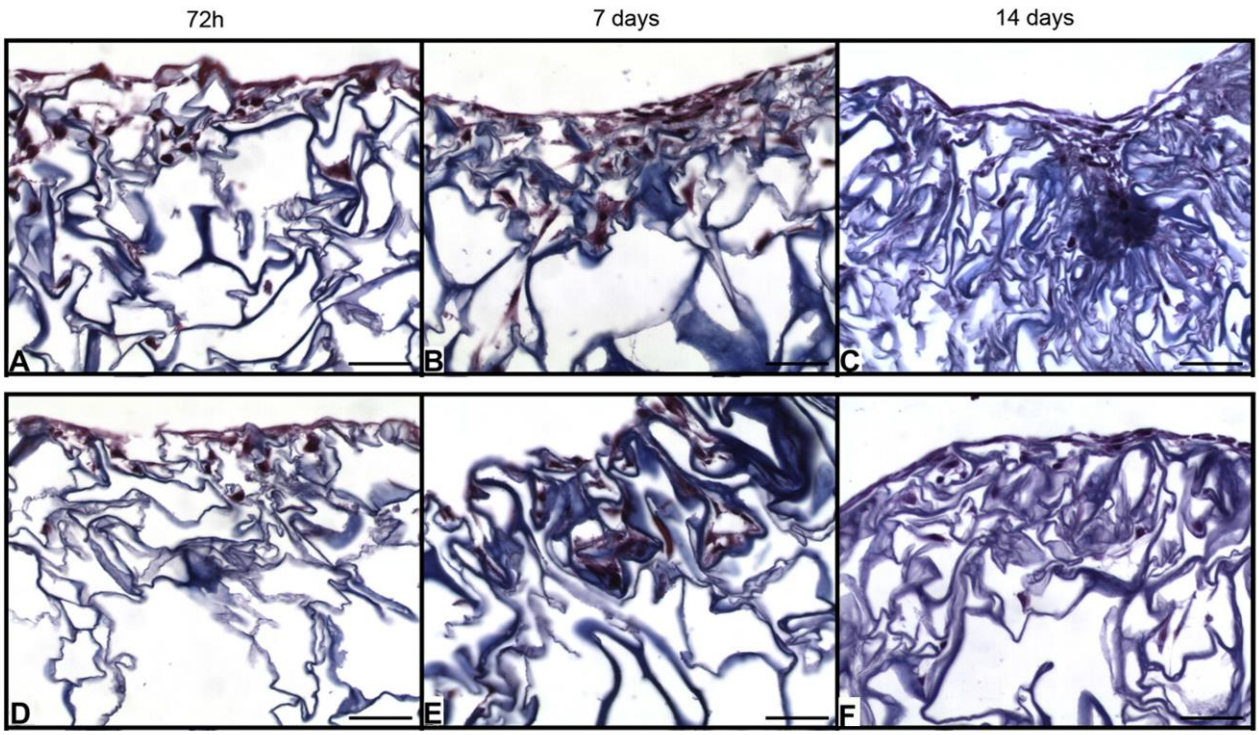

Figure 4.7: Masson's trichrome staining of cell distribution in the DAT foams (A, B, C) and bead foams (D, E, F) after 72 h, 7 days, and 14 days of *in vitro* cell culture. Generally, there was limited ASC infiltration into the interior of the foams. Scale bars =50 µm.

4.2.6 *In vivo* characterization and biocompatibility

In the implantation study, the foam, bead foam and intact DAT samples were easy to handle and position within the subcutaneous space in the rat model. The incisions healed well over the course of the first week, with no detectable signs of inflammation or irritation in any of the animals. A blinded comparative histological assessment of the foams and bead foams demonstrated that there were no discernible differences in terms of the host response, tissue organization, and implant integration between these two scaffold groups at any of the time points in the current study. Similarly, seeding the foams, bead foams, and intact DAT with allogenic rASCs did not significantly impact the *in vivo* response observed in this model.

At 1 week, the shape and dimensions of the foam and bead foam samples were macroscopically well conserved and there was evidence that the scaffolds induced a potent angiogenic response in the host tissues (Fig. 4.8A). In contrast, very little vascularization was visualized on the surface of the intact DAT scaffolds at any time point (Fig. 4.9). Masson's trichrome staining indicated that there was inflammatory cell infiltration into the periphery of the foam and bead foam samples at 1 week, with relatively few cells visualized within the open porous network maintained in the central regions of the scaffolds (Fig. 4.8B,C). At 3 weeks, there was a marked reduction in the volume of the foam and bead foam samples (approximately 50%), combined with extensive cellular infiltration, consistent with a host inflammatory response (Fig. 4.8D,E,F). In contrast to the foams, there was reduced inflammatory cell infiltration observed in the intact DAT scaffolds, which macroscopically maintained their volume over the course of the 12-week study (Fig. 4.9). In addition, functional blood vessels could be visualized within the intact DAT scaffolds as early as 3 weeks (Fig. 4.9F). At 8 weeks, there was a further reduction in the volume of the foams and bead foams (Fig. 4.8G,H), although the inflammatory response had subsided. There was also evidence of tissue remodelling, with alignment of the collagen fibres in the foams parallel to the collagen within the host tissues (Fig. 4.8I). By 12 weeks, the foams had resorbed significantly, but were well integrated into the host tissues (Fig. 4.8J,K). Mature adipocytes and functional blood vessels were visualized within the central regions of the foam, bead foam, and intact DAT samples at both 8 and 12 weeks (Fig. 4.8I,L & Fig. 4.9I,L).

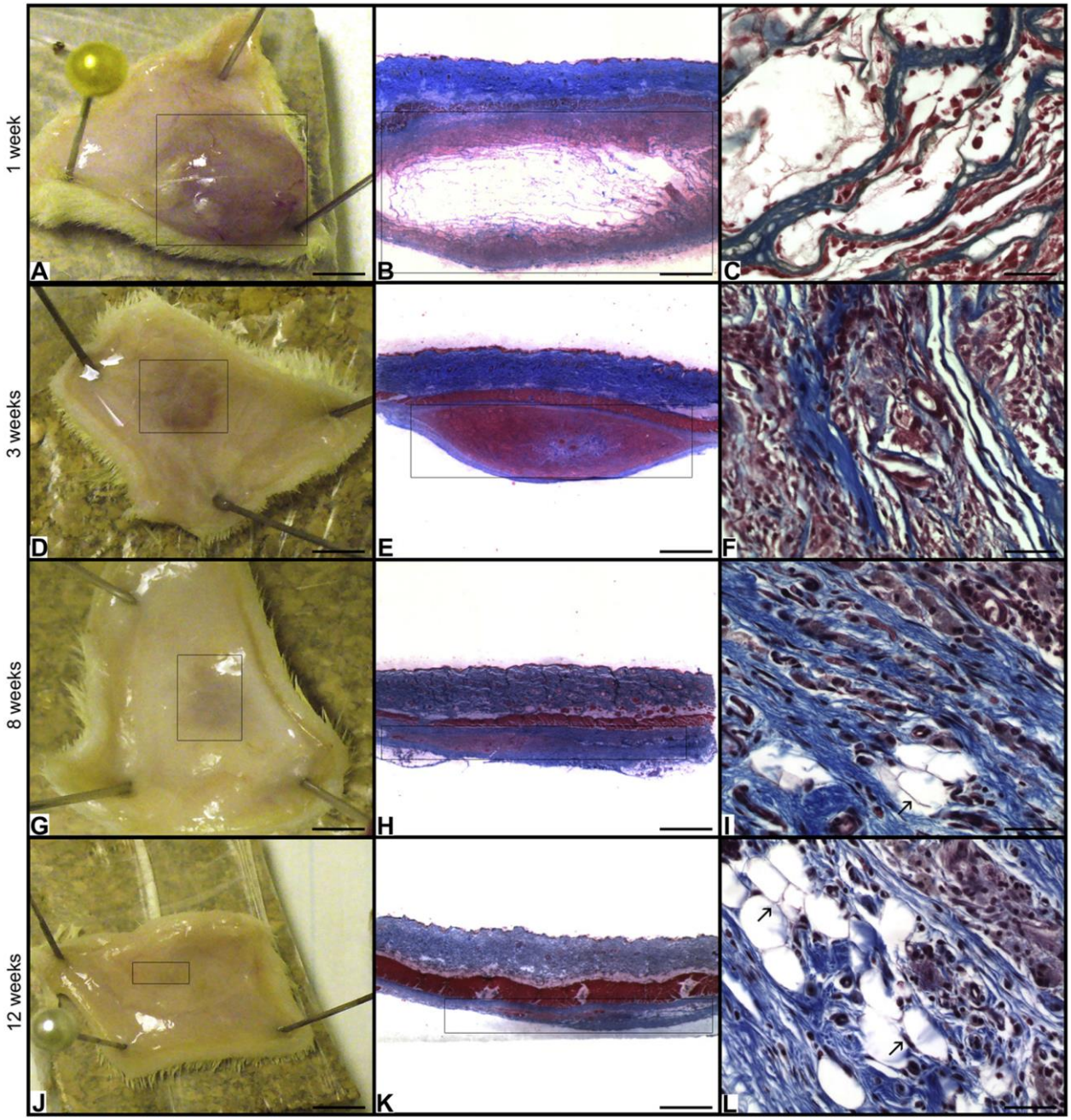

Figure 4.8: *In vivo* response to the DAT foams and bead foams in the subcutaneous Wistar rat model. All of the foams exhibited very similar *in vivo* behaviour, including for the seeded and unseeded groups, and representative images for each time point are shown. Macroscopically, the excised foams (A, D, G, J) induced a strong initial angiogenic response in the host, followed by resorption over the course of the study. Scale bars = 500 µm. Representative stereomicroscopic images of Masson's trichrome stained cross-sections (B, E, H, K) showed cellular infiltration into the foams over time, with volume reduction as the foams (boxed regions) became integrated into the host tissues. Scale bars = 250 µm Microscopically, Masson's trichrome staining (C, F, I, L) indicated there was early inflammatory cell infiltration into the foams, which stabilized over time. At 8 and 12 weeks, mature adipocytes (black arrows) and functional blood vessels were visualized in the foams, and reorganization of the collagen in the foams was evident. Scale bars = 50 µm.

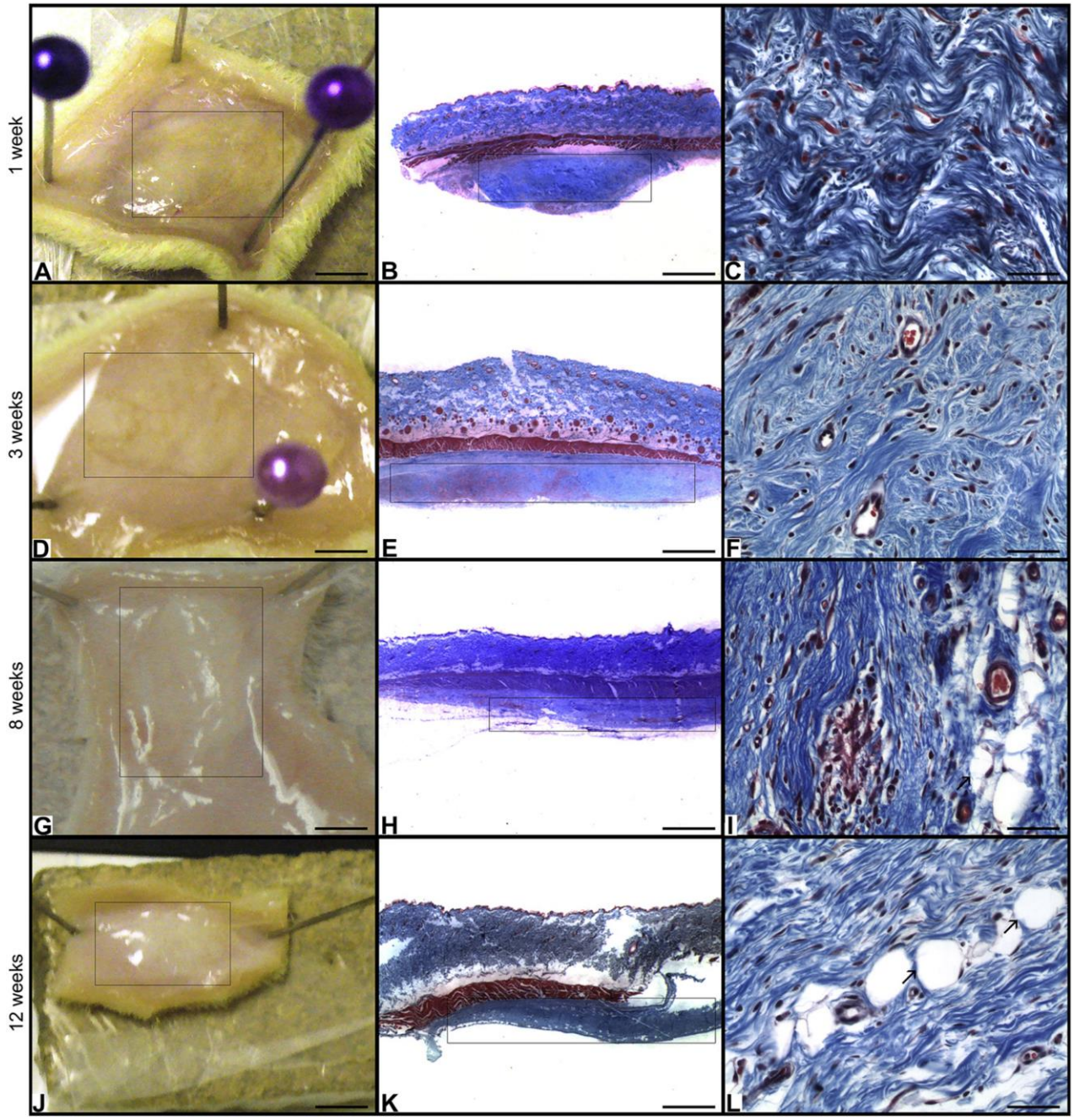

Figure 4.9: *In vivo* response to the intact DAT controls in the subcutaneous Wistar rat model. No distinguishable differences were observed in the rASC seeded and unseeded groups, and representative images are shown. Macroscopically, compared to the DAT foams, the intact DAT scaffolds (A, D, G, J) showed less surface vascularization, as well as no detectable changes in volume over time. Scale bars = 500 µm. Representative stereomicroscopic images of Masson's trichrome stained cross-sections (B, E, H, K) confirmed that there was superior volume retention of the intact DAT (boxed regions) over the course of the study. Scale bars = 250 µm. Microscopically, the Masson's trichrome staining (C, F, I, L) showed a lower initial inflammatory response to the intact DAT as compared to the foams. Developing blood vessels could be visualized within the central regions of the DAT scaffolds at 3 weeks. At 8 and 12 weeks, mature adipocytes (black arrows) were present in the grafts, along with mature functional blood vessels. Scale bars = 50 µm.

4.3 Discussion

Orchestrating stem cell fate has been tightly linked to cell-ECM interactions mediated through transmembrane adhesion receptors, which in turn induce a cascade of cellular events that can regulate proliferation, differentiation, migration, and survival [10], [383]. Subtle differences in ECM constituents and mechanical properties within the stem cell microenvironment have been demonstrated to drive lineage commitment and differentiation in a tissue-specific manner [12], [348], [357]. With this as a guiding principle, recent cell-based strategies have focused on incorporating naturally-derived ECM factors within bioscaffolds engineered to mimic both the biochemical and biomechanical properties of the native cell niche [384]. While synthetic biomaterials can be modified with specific peptide sequences or proteins of interest, decellularized ECM derived from human tissues provides an alternative scaffolding source, in which the complex matrix composition and ultrastructure can be retained to closely replicate the natural cellular milieu [348], [385]. Similar to the osteo-conductive and osteo-inductive properties of demineralized bone matrix [386], previous work has demonstrated that intact DAT matrices and DAT-based microcarriers are highly supportive of ASC adipogenesis. Further, DAT-based bioscaffolds can naturally induce the differentiation of human ASCs into mature adipocytes in the absence of exogenous differentiation factors, supporting that DAT is both adipo-conductive and adipo-inductive in nature [14], [19].

In this Chapter, methods were developed for fabricating porous foams from enzyme-digested human DAT for use as scaffolds in soft tissue reconstruction and wound healing. In particular, enzymatic digestion with α-amylase results in glycosidic cleavage of carbohydrate groups compared to non-specific proteolytic cleavage with pepsin [387], [388]. As a result, this milder digestion protocol better preserved the integrity of the collagen fibres so they can be readily dispersed into dilute acetic acid, and fabricated into well-defined 3D foams that were stable *in vitro* without the need for chemical crosslinking.

In addition to more conventional microporous sponges formed through controlled freeze-drying techniques, an approach was established for synthesizing macroporous bead foams comprised of a network of fused porous DAT microcarriers [389]. Within the bead foams, there was a secondary level of porosity resulting from the formation of pores and channels between the individual microcarriers, which could be adjusted by varying the size, shape, and packing density of the beads. The techniques in the current study could readily be adapted to produce foams derived from various collagen sources, including decellularized ECM from other tissues, and custom moulds could be implemented to define the overall scaffold geometry.

The distribution of ASCs on the microporous foams and bead foams was assessed to examine the influence of porosity on *in vitro* cellular migration. Typically, pore sizes greater than 100 μm are required to support extensive cellular infiltration, to allow for diffusion of oxygen and nutrients, and to accommodate the expansion of maturing adipocytes following *in vivo* implantation [246]. Histological analysis of the *in vitro* cultured foams revealed that the majority of the cells were localized within a layer on the outer surface of the foams despite the high porosity and large pore sizes in the scaffolds. It is probable that the combination of a high seeding density and static culture conditions resulted in the formation of a cell layer on the surface that obstructed the pores in the DAT-based foams [390]. The limited cellular infiltration may also explain why no significant differences were observed between the unseeded and seeded scaffolds in the *in vivo* study.

In assessing cellular responses to biomaterials, matrix stiffness has emerged as an important factor in mediating mesenchymal stem/stromal cell (MSC) lineage commitment [360]. More specifically, culturing MSCs on softer matrices (~1 kPa) with a modulus more similar to native soft tissues promotes a rounder cell morphology and enhances adipogenic differentiation [363], [391], [392]. Mechanical testing of the hydrated conventional DAT foams synthesized with 50 mg/mL or 100 mg/mL of DAT suspension indicated that the Young's moduli were similar between the formulations, in agreement with previous mechanical studies on hydrated collagen-

glycosaminoglycan scaffolds, where stiffness was shown to be independent of physical crosslinking density and pore size [393]. Inhomogeneities in the conventional foams fabricated with the lowest concentration (25 mg/mL DAT suspension), likely resulting from greater variability in ice crystal formation during foam fabrication, interfered with the mechanical assessment of the macroscopically softest groups of foams. Interestingly, at 14 days, where the cells had formed a confluent surface layer in all of the scaffold groups, adipogenic differentiation was enhanced on the stiffer scaffolds that had initial moduli that were most similar to the properties of mature human adipose tissue [380].

In the subsequent *in vitro* studies probing ASC adipogenesis on representative DAT foams and bead foams, both types of scaffolds were shown to strongly support ASC adipogenesis. Consistent with the findings in Chapter 3 for the crosslinked DAT microcarriers and previous results with intact DAT scaffolds, the GPDH activity and adipogenic gene expression results for the non-induced foams and bead foams cultured in proliferation medium supported that these scaffolds are also adipo-inductive in nature [14], [19]. In comparing the relative levels of differentiation observed in the induced foam, bead foam, and intact DAT samples, the results indicate that adipogenesis was enhanced on the conventional foams. Based on the histological assessment of the scaffolds, it was hypothesized that the uniform architecture of the foams allowed for a more homogenous distribution of the ASCs in a confluent layer on the surface of the scaffolds, promoting cell-cell interactions, which have been shown to enhance adipogenic differentiation [363], [384]. While it is challenging to decouple the influence of the physical, biochemical, and biomechanical properties of the DAT scaffolds, the results of this study highlight the importance of all of these factors in mediating ASC adipogenesis.

In vivo testing of the DAT foams, bead foams, and intact DAT bioscaffolds in an immunocompetent subcutaneous rat model yielded interesting results. The foams, which were fabricated from enzyme-digested DAT, induced a strong angiogenic response and promoted higher

levels of inflammatory cell migration at early time points relative to the intact DAT. These results may be related to alterations in the collagen structure and density following enzymatic digestion that stimulate cell migration [394], or potentially to the increased availability of angiogenic growth factors naturally found within the adipose ECM [277] after enzymatic digestion. Macroscopically, there was a substantial reduction in the volume of the foams and bead foams over the course of the 12-week study, but no significant changes in volume observed for the intact DAT controls. Overall, the DAT-based biomaterials integrated well into the host tissues over time, with functional blood vessels visualized in the central regions of the scaffolds, along with mature adipocytes at 8 and 12 weeks, indicating that the DAT-based scaffolds supported the formation of new adipose tissue.

The differences in the properties of the foams versus the intact DAT scaffolds potentially point to their suitability for use in different applications in plastic and reconstructive surgery. More specifically, the angiogenic capacity, enhanced cell migration, and biodegradation characteristics of the foams suggest that they could be useful in wound healing, such as for the treatment of diabetic wounds and ulcers. If required, the resorption rate of the foams could potentially be tuned through chemical crosslinking [395]. In comparison, the stable and non-immunogenic intact DAT, with its naturally adipogenic capacity, could be an appropriate bioscaffold for use in 3-D volume augmentation and adipose replacement. Overall, decellularized human adipose tissue is a promising source of ECM that can be used to fabricate a broad range of bioscaffolds that promote soft tissue regeneration.

4.4 Conclusions

In this study, stable non-crosslinked porous ECM derived foams that had a defined shape and volume were developed from enzyme-digested DAT for use as soft tissue replacements. In addition, a technique for fabricating bead foams comprised of an integrated network of porous DAT microcarriers was introduced. Characterization studies demonstrated that all foams remained stable

under *in vitro* culturing conditions over 2 weeks. GPDH activity results indicated that mechanically matching the DAT foam stiffness to the native tissues might enhance adipogenesis. Further *in vitro* differentiation studies confirmed that the DAT foams are both adipo-conductive and adipo-inductive. These findings were shown through the expression of the adipogenic genes *PPARγ*, *C/EBPα*, and *LPL* in both the induced and non-induced foam samples, and supported by the quantitative GPDH activity results. *In vivo* studies using a subcutaneous Wistar rat model demonstrated that the DAT foams, bead foams, and intact DAT were well tolerated and promoted angiogenesis, adipogenesis, and tissue remodelling. In comparison to the intact DAT, the foams and bead foams induced a stronger angiogenic response in the host tissues, promoted more extensive inflammatory cell infiltration, and resorbed more rapidly over the course of the 12-week study. In general, DAT-based biomaterials are promising bioscaffolds for soft tissue regeneration in plastic and reconstructive surgery as well as for *in vitro* adipogenic cell culture platforms.

Chapter 5

Tissue-Specific Decellularized Adipose Tissue Microcarriers for Adipose-Derived Stem Cell Expansion

5.1 Introduction

A rise in research efforts involving the use of mesenchymal stem/stromal cells (MSCs) for the treatment of degenerative diseases has been motivated in part by their identification within various adult and neo-natal tissues including the bone marrow, adipose tissue, synovium, skeletal muscle, umbilical cord, and placenta [18], [35], [396]–[399]. In particular, adipose-derived stem/stromal cells (ASCs) are an accessible and uniquely expendable regenerative cell source derived from human fat of interest for a broad range of applications in tissue engineering. In addition to demonstrated multipotency towards the adipogenic, osteogenic and chondrogenic lineages, ASCs can also secrete an array of beneficial paracrine factors that can help to establish a more pro-regenerative microenvironment within host tissues [400]. Currently, there is a need to develop robust cultivation methods to obtain sufficient cell numbers for clinical applications while maintaining the stem cell phenotype and multilineage differentiation capacity [291]. In this respect, the ability to produce large ASC populations from small patient biopsies would represent a clinical advantage for the translation of innovative autologous or allogenic therapies from the 'benchtop to bedside'.

Typical cultivation practices commonly involve monolayer culture on tissue culture flasks for small-scale laboratory operations or larger-scale multilayer stacked trays capable of producing up to 50 million cells per 40-layer stack via automated or manual handling [401]. Although convenient, these systems do not possess the complex cellular microenvironment found in native tissues, which may contribute to the reduced ASC proliferation and multilineage differentiation capacities reported upon extended culturing [2], [3], [402]. Furthermore, other concerns regarding scale-up include the low surface area-to-volume ratio offered on 2-D culture flasks, material costs,

labour intensiveness, the risk of contamination with repeated passaging, and the lack of control over culture parameters and monitoring of the system [291].

To address the limitations of conventional static culture methods, various techniques have been explored to efficiently expand and deliver high quality stem cells in the form of stirred or perfusion bioreactor culture systems [307], [403]–[405]. In particular, the use of microcarriers in suspension culture has been widely documented due to the potential for continuous rapid expansion of adherent cell populations and simple collection through gravity settling. Bioresorbable microcarriers have been fabricated from materials including collagen I, poly(lactic-co-glycolic acid) (PLGA), chitosan, and decellularized tissues and may also serve as direct injectable cell delivery vehicles [19], [313], [315], [377], [406]. As discussed in Chapters 3 and 4, the latter approach using decellularized matrices may retain complex biochemical and biophysical elements of the extracellular matrix (ECM), which have been shown to modulate cell behaviour and promote constructive regeneration [137], [407], [408]. The favourable biological characteristics of decellularized ECM provide a strong rationale for their use as natural bioactive substrates in microcarrier development.

Although the chemically crosslinked DAT microcarriers described in Chapter 3 served as a promising adipo-inductive substrate, it was recognized that improvements could be made to the fabrication process. In particular, the composite approach using alginate as a stabilizer and porogen with photo-crosslinking of the pepsin-solubilized DAT resulted in low porosity (~30%) and poor stability below a size range of 900-950 μm [19], [26]. In this final Chapter, these limitations were addressed by using the α-amylase digestion method established in Chapter 4 to generate porous non-chemically crosslinked DAT microcarriers as a potential ASC expansion platform. More specifically, microcarriers within a target size range of 350-500 μm were fabricated via electrospraying, as studies have established that microcarriers ranging between 100-500 μm in diameter are recommended to support cell viability of most mammalian cell types [20]. Upon

characterizing the physical properties of these refined DAT microcarriers, ASC proliferation on the DAT microcarriers within a spinner flask culture system was compared to commercially-available Cultispher-S microcarriers. Cultispher-S microcarriers were chosen for this study based on their natural composition (crosslinked porcine gelatin), ability to support MSC adhesion and growth, and macroporous architecture [306]–[308], [326]. Subsequently, the ASC immunophenotype, expression of lineage-specific genes (fat, bone, and cartilage) prior to differentiation, and multilineage differentiation potential towards the adipogenic, osteogenic, and chondrogenic lineages was assessed following expansion on the DAT microcarriers, Cultispher-S microcarriers, and conventional tissue culture polystrene (TCPS).

5.2 Methods

5.2.1 Materials

All chemical reagents for this work were obtained from Sigma-Aldrich Canada Ltd. (Oakville, ON, Canada) and were used as received unless otherwise indicated. Cultispher-S microcarriers were purchased from Percell Biolytica AB, (Åstorp, Sweden).

5.2.2 Adipose tissue procurement and decellularization

Excised subcutaneous human adipose tissue was acquired from female patients undergoing routine breast and abdominal reduction surgeries at the Kingston General Hospital and Hotel Dieu Hospital in Kingston, Canada or from the University Hospital in London, Canada. All studies were reviewed and approved by the Research Ethics Boards at Queen's University (REB # CHEM-002-07) or Western University (REB # 105426). ASC isolation was performed within 2 h of collection following established methods, while adipose tissue to be further processed for decellularization was stored in a hypotonic cell lysis buffer solution at -80 ºC [14]. An overview of the project scope is provided in Fig. 5.1.

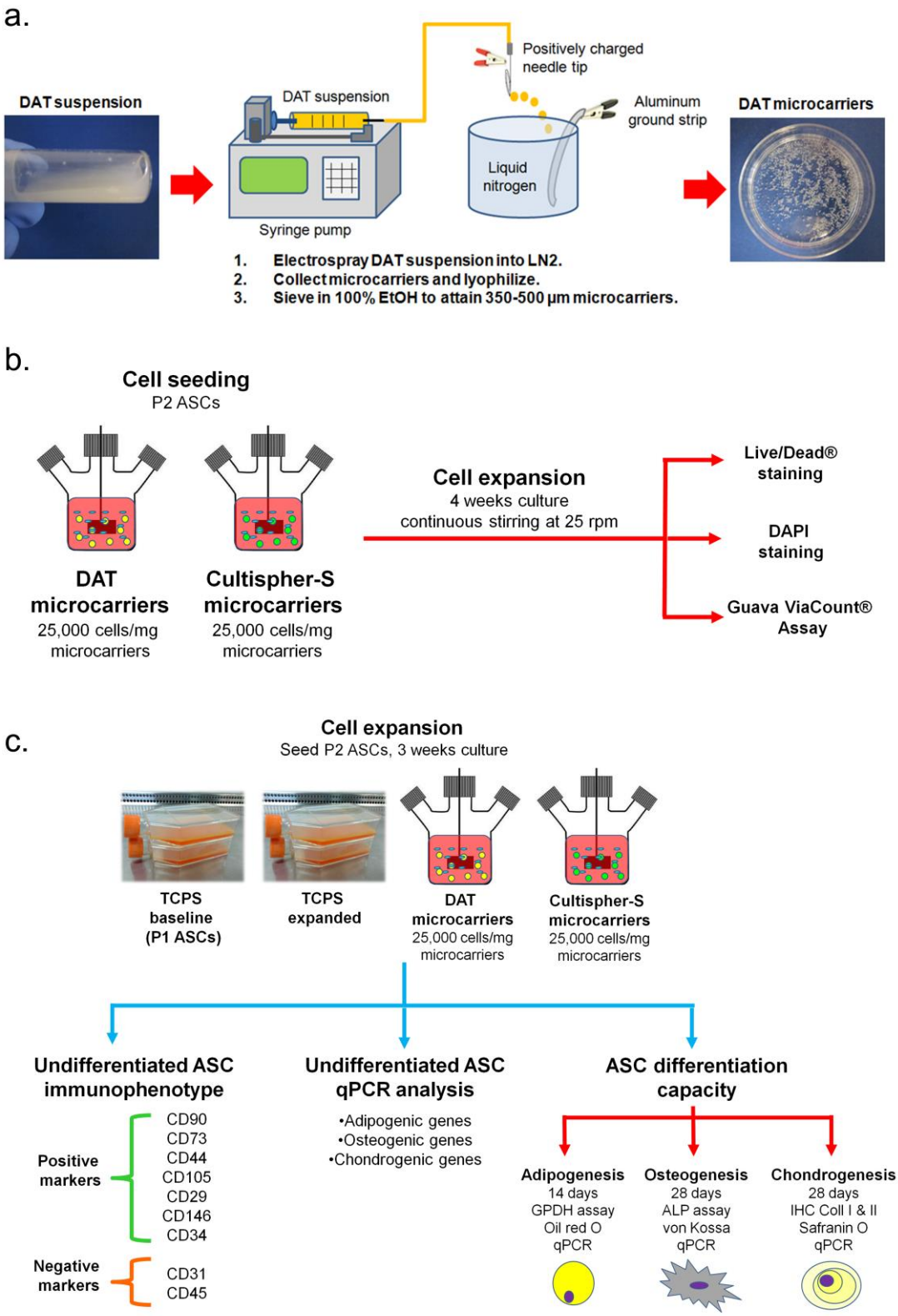

Figure 5.1: Schematic of experimental methods. a) DAT microcarrier fabrication, b) ASC proliferation study, and c) ASC multilineage differentiation capacity study.

5.2.3 Non-chemically crosslinked DAT microcarrier fabrication

DAT was prepared using published protocols and stored in 70% ethanol at 4 ºC [14]. Prior to microcarrier fabrication, DAT was pooled from a minimum of 5 donors and lyophilized for 48 h. The lyophilized DAT was minced finely with scissors (1-2 mm^3 pieces) and placed into a Retsch MM400 milling chamber, submerged in liquid nitrogen for 3 min, and milled continuously for 3 min at 1800 rpm to yield a fine DAT powder.

The milled DAT was subsequently digested with α-amylase to generate a homogenous DAT suspension using methods adapted from Steven *et al*. [20], [242]. Briefly, 250 mg of cryo-milled DAT was placed into a 15 mL conical tube and 5 mL of 0.22 M NaH_2PO_4 (pH 5.3) supplemented with 0.3% (w/w of dry tissue) α-amylase (Sigma, Cat. # 10065) was added. The DAT was digested at room temperature for 72 h under continuous agitation at 300 rpm, followed by centrifugation at 1500 xg for 10 min. The processed DAT was rinsed twice with 10 mL of 5% NaCl solution and once with distilled water by agitating vigorously at room temperature for 10 min, with centrifuging at 1500 xg for 10 min between each rinse. Finally, 0.2 M acetic acid was added to obtain a total volume of 5 mL, yielding a 50 mg/mL DAT suspension stock. The DAT suspension was agitated at 37 ºC overnight at 120 rpm and then homogenized (PowerGen Model 125 homogenizer, Fisher Scientific, Ottawa, ON, Canada), prior to being stored at 4 °C until needed.

Prior to microcarrier fabrication, the 50 mg/mL DAT suspension stock was diluted with distilled water to produce 35 and 17.5 mg/mL concentrations. The DAT suspension was then loaded into a 3 mL syringe and secured in a syringe pump. The electrospray apparatus used consisted of a positive probe attached to the tip of a 25G infusion needle connected to the loaded syringe, and a ground probe attached to a strip of aluminum foil immersed in a dewar of liquid nitrogen (Fig. 5.1a). The DAT microcarriers were synthesized by electrospraying the DAT suspension directly into the liquid nitrogen at a height of 5 cm, with an infusion rate of 0.5 mL/min and an applied voltage of 20 kV. The microcarriers were collected, immediately lyophilized overnight,

resuspended in 100% ethanol, and strained through a 1000 µm sieve to remove aggregated microcarriers. Afterwards, the microcarriers were stored in 100% ethanol at 4 ºC and gradually rehydrated with sterile Dulbecco's phosphate buffered saline (D-PBS) (Lonza, Cat. # CA12001-664) when needed.

5.2.4 Microcarrier characterization

5.2.4.1 *Swelling, equilibrium water content, and porosity measurements*

Microcarrier swelling and equilibrium water content (EWC) were evaluated in triplicate samples to determine the stability of DAT microcarriers fabricated with 17.5, 35, and 50 mg/mL DAT suspensions. Swelling was assessed by immersing approximately 100 microcarriers per well (n=3) in a 12-well plate with 2 mL of Ringer's physiological solution at 37 °C. Over 1 month, the microcarriers were photographed with a stereomicroscope and the diameter was measured using ImageJ analysis software at 24 h, 72 h, 1 week, 2 week, 3 week, and 4 week time points. The swelling ratio was calculated based on the following equation, where D_w and D_D are the hydrated and dry diameters, respectively.

$$\%\, Swelling\ ratio = \frac{D_w}{D_D} \times 100$$

EWC was determined by placing 200 mg (wet weight) of DAT microcarriers in ethanol for each formulation in a 2 mL eppendorf tube (n=3). The microcarriers were rehydrated with distilled water and resuspended in a final volume of 2 mL of distilled water followed by incubation at 37 °C for 72 h. Afterwards, the water was carefully removed, the wet weight was recorded, and the tubes were frozen at -80 °C overnight and lyophilized for 24 h to obtain the dry weight. EWC was calculated using the following equation, where W_w is the wet weight and W_D is the dry weight.

$$\% \, EWC = \frac{(W_w - W_D)}{W_w}$$

Porosity of the DAT and Cultispher-S microcarriers were determined using a modified Archimedes method [409]. Duplicate microcarrier samples of equal volume were placed in a 1.5 mL eppendorf tube and immersed in 100% isopropanol. Trapped bubbles were removed by sonicating briefly and then placing the samples under light vacuum for 1 h at room temperature. The excess isopropanol was carefully removed and the wet mass (m_{wet}) of the microcarriers was recorded. Next, the microcarriers were allowed to completely air dry overnight and the dry mass (m_{dry}) was recorded. The following equations were used to calculate the porosity where ρ and ν are density (g/cm^3) and volume (cm^3), respectively. The density of isopropanol is 0.79 g/cm^3 and it was assumed that the DAT and Cultispher-S microcarriers were composed primarily of collagen with a density of 1.343 g/cm^3 [410].

$$Porosity \, (\%) = \frac{\nu_{pores}}{\nu_{pores} + \nu_{collagen}} \times 100\%$$

$$\nu_{pores} = \frac{m_{wet} - m_{dry}}{\rho_{isopropanol}}$$

$$\nu_{collagen} = \frac{m_{dry}}{\rho_{collagen}}$$

5.2.4.2 *Scanning electron microscopy*

DAT microcarrier surface microarchitecture was visualized by scanning electron microscopy (SEM) using published protocols [14]. Briefly, the microcarriers were chemically dried and gold coated prior to imaging with a JOEL JSM-840 microscope at an accelerating voltage of 10 kV and working distance of 15 mm.

5.2.4.3 *Immunohistochemical characterization of ECM components*

Immunohistochemistry (IHC) was performed to detect the presence of key adipose ECM components in the 50 mg/mL DAT microcarriers by fluorescence microscopy. In brief, microcarrier samples were fixed overnight in 4% paraformaldehyde, paraffin embedded, and sectioned into 5 µm thickness. Primary antibodies were purchased from ABCAM (Toronto, Canada) as follows: monoclonal mouse anti-collagen I (Cat. # ab90395), polyclonal rabbit anti-collagen IV (Cat. # ab6586), monoclonal mouse anti-fibronectin (Cat. # ab6328), and polyclonal rabbit anti-laminin (Cat. # ab11575). Complimentary secondary antibodies used were: Alexa Fluor® 555 goat anti-mouse (Cat. # A-21422, Life Technologies, Burlington, Canada, dilute 1:200) and Alexa Fluor® 488 goat anti-rabbit (Cat. # A-11008, Life Technologies, Burlington, Canada). IHC staining conditions are summarized in Table 5.1 [241]. No primary and tissue-positive controls were included for each antibody to confirm staining specificity.

Table 5.1: Summary of immunostaining methods

Antibody	Antigen retrieval method	Primary/Secondary antibody dilution
Collagen I	Heat mediated (DAKO)	1:500/1:500
Collagen IV	Enzymatic (0.05% trypsin/EDTA)	1:100/1:200
Fibronectin	Enzymatic (20 µg/mL Proteinase K)	1:100/1:200
Laminin	Enzymatic (0.05% trypsin/EDTA)	1:100/1:200

5.2.4.4 *Mechanical testing*

The Young's modulus of the 50 mg/mL DAT microcarriers and Cultispher-S microcarriers were determined using a CellScale MicroSquisher system (Waterloo, ON, Canada). A micro-scale parallel-plate compression configuration fitted with a 154 µm diameter cantilever was used for the DAT microcarriers, while a 308 µm cantilever diameter was chosen for the Cultispher-S microcarriers. Briefly, samples of hydrated microcarriers were placed in a D-PBS fluid bath at 37 ºC and the cantilever was lowered until the upper compression plate made contact with the top of the microcarrier. A total of 6 samples for each of the DAT and Cultispher-S microcarriers were tested, with compression to 50% and 20% strain, respectively, for a duration of 20 s, held at constant deformation for 5 s, and released for 20 s. After preconditioning, data from 3 consecutive cycles was collected per sample. To calculate the Young's modulus of the microcarriers the force (F) versus deformation$^{3/2}$ ($d^{3/2}$) was plotted. Following the Hertzian theory for non-adhesive elastic contact, a linear regression was fitted at the 20% and 8% strain data point for the DAT and Cultispher-S microcarriers, respectively. Upon determining the tangential slope, the initial radius of the microcarrier (R) was used to calculate the Young's modulus (E) using the following expression [411], [412]:

$$F = \frac{4}{3}E \times R^{1/2} \times d^{3/2}$$

5.2.5 ASC isolation, seeding, and dynamic culture

ASCs were isolated from human adipose tissue (female donors) following established methods and cultured in proliferation media comprised of Dulbecco's Modified Eagle's medium (DMEM):Ham's F12 supplemented with 10% fetal bovine serum (FBS) (Wisent Inc., Cat. # 080-150, US origin), and 100 U/mL penicillin and 0.1 mg/mL streptomycin (1% pen-strep) (Life Technologies, Cat. # 15140122) [14]. Passage 2 (P2) ASCs were used for all subsequent *in vitro*

culture experiments and a summary of the cell donor information for each study is described in Table 5.2.

Table 5.2: Summary of cell donor information for all *in vitro* studies

Study	Cell donor information	
Proliferation study	**Donor 1**: 39 y, BMI = 30.9 **Donor 2**: 54 y, BMI = 34.8	
Immunophenotype analysis	**Donor 3**: 63 y, BMI = 34.6 **Donor 4**: 36 y, BMI = 27.1 **Donor 5**: 53 y, BMI = 30.9 **Donor 6**: 17 y, BMI = 34.3	
Differentiation study	Adipogenesis & osteogenesis	**Donor 4**: 36 y, BMI = 27.1 **Donor 5**: 53 y, BMI = 30.9 **Donor 6**: 17 y, BMI = 34.3
	Chondrogenesis	**Donor 6**: 17 y, BMI = 34.3
Gene expression analysis*	**Donor 6**: 17 y, BMI = 34.3	

**For qPCR analyses of undifferentiated and differentiated ASCs*

To prepare the microcarriers for culture, DAT microcarriers (125 mg dry weight) were decontaminated in 100% ethanol followed by gradual rehydration with sterile D-PBS, while Cultispher-S microcarriers (125 mg dry weight) were rehydrated in D-PBS and sterilized by autoclaving as per the manufacturer's instructions. Prior to the proliferation studies, all microcarriers were labeled with Alexa Fluor® 350 NHS Ester (Succinimidyl Ester) (Life Technologies, Cat. # A10168) following the manufacturer's instructions to aid in subsequent visualization via confocal imaging.

On the day before seeding, the microcarriers were resuspended in 62.5 mL of proliferation media in a 250 mL CELLSPIN flask (INTEGRA Biosciences, AG, Switzerland) and equilibrated overnight in an incubator (37 ºC, 5% CO_2). The next day, ASCs were seeded onto the microcarriers at 25,000 cells/mg microcarriers dry weight, and the previously established 12 h seeding regimen was performed: 2 min of stirring at 25 rpm followed by 30 min rest over a period of 3 h, 6 h rest, and then 2 min of stirring at 25 rpm followed by 30 min rest over a period of 3 h [26]. Note that the

seeding density of 25,000 cells/mg microcarrier was chosen based on previous pilot work, where inoculation densities less than 25,000 cells/mg microcarrier resulted in too few cells for accurate counting with the Guava ViaCount® Assay. After seeding, the culture volume was topped up to 125 mL and the CELLSPIN flasks were stirred continuously at 25 rpm for up to 1 month. This seeding and culturing procedure was performed for all subsequent proliferation and differentiation studies.

5.2.6 Cell proliferation assessment

ASC proliferation on the DAT versus Cultispher-S microcarriers was assessed over 1 month (Fig. 5.1b), with duplicate samples of 1 mL microcarrier suspensions taken at 24 h, 72 h, 1 week, 2 week, 3 week, and 4 week time points (n=2, N=2). Cellular attachment on the microcarriers was visualized after Live/Dead® staining (Life Technologies, Cat. # L-3224) using an Olympus FluoView^{TM} FV1000 confocal microscope. Cellular infiltration at each time point was also assessed by fixing the microcarriers in 4% paraformaldehyde overnight, paraffin embedding, and staining 5 µm sections with DAPI fluoroshield mounting medium. Afterwards, the microcarrier sections were visualized using an EVOS® FL Imaging System (Thermo Fisher Scientific, Cat. # AMF4300).

Cell counts were performed with the Guava Viacount® Assay (EMD Millipore, Cat. # 4000-0040) using the Guava easyCyte 8HT Benchtop flow cytometer (EMD Millipore), following the manufacturer's protocol. Different cell detachment methods were employed for the DAT and Cultispher-S microcarriers to maximize cell recovery. DAT microcarrier samples were digested at 37 °C under constant agitation at 120 rpm for 45 min with periodic pipetting every 15 min in 600 µL of sterile-filtered collagenase digest solution (94% Krebs Ringer Buffer Solution, 5.7% bovine serum albumin (35%), 3 mM glucose, 2 mg/mL collagenase type I (Worthington, Cat. # LS004196), and 25 mM HEPES). Meanwhile, Cultispher-S microcarrier samples were detached with 600 uL of 0.25% trypsin-EDTA as recommended by the manufacturer's instructions and

agitated at 37 °C for 5 min at 120 rpm. After cell release, an equal volume of proliferation media was added and the samples were strained through a 40 µm filter. The ASCs were centrifuged at 1200 xg for 5 min and plated in a 6 well-plate for 24 h to allow for attachment. After 24 h, ASCs were detached with trypsin-EDTA and stained with the Guava Viacount® assay for counting with the Guava easyCyte 8HT flow cytometer. Unseeded DAT and Cultispher-S microcarriers controls were treated in the same manner and counted to subtract for false positive readings from residual debris.

5.2.7 Flow cytometry analysis

Single colour flow cytometry analysis of ASCs was performed using the Guava easyCyte 8HT Benchtop flow cytometer (n=3, N=4) to assess changes in the ASC immunophenotype prior to and post expansion under 3-D dynamic versus 2-D static culture conditions. Briefly, P1 ASCs were analyzed as TCPS baseline controls in comparison to ASCs expanded for 3 weeks to confluence on DAT microcarriers and Cultispher-S microcarriers as well as on TCPS, where cells were repeatedly passaged at 80% confluence and plated at a constant initial seeding density of 5000 cells/cm^2 with each new passage. ASCs were extracted from each group via trypsin release and stained using published methods [62] with the following monoclonal fluorochrome-conjugated antibody markers (eBioscience, San Diego,CA): CD105-PE (Cat. # 12-1057-41), CD90 (Thy-1)-FITC (Cat. #11-0909-41), CD73-FITC (Cat. # 11-0739-41), CD44-PeCy7 (Cat. # 25-0441-81), CD29 (Integrin β1)-PE (Cat. # 12-0299-41), CD34-APC (Cat. # 17-0349-41), CD146-FITC (Cat. #11-1469-41), CD31-PE (Cat. #12-0319-42), and CD45-FITC (Cat. # 11-0459-41). Unstained controls were included and isotype controls were performed for each antibody to confirm specificity.

5.2.8 ASC differentiation and assessment

To assess the multilineage differentiation capacity of the ASCs following 3 weeks expansion to confluence on the DAT and Cultispher-S microcarriers, a differentiation study was conducted where P1 ASCs cultured on TCPS served as baseline controls for all trials. In the second and third repeat of the study (i.e. cell donors 5 and 6), an additional control group of ASCs expanded on TCPS for 3 weeks was included. Differentiation studies initially focused on the more well-established adipogenic and osteogenic lineages, and then analysis was extended for the final cell donor to also probe for the chondrogenic lineage. A summary of the experimental overview is shown in Fig. 5.1c and the cell donor information is described in Table 5.1.

Briefly, ASCs cultured on the DAT and Cultispher-S microcarriers were collected using identical protocols described in the proliferation section to maximize cell recovery, whereas ASCs from the TCPS expanded and TCPS baseline groups were trypsin released. The harvested ASCs were either plated or pelleted for differentiation along the adipogenic, osteogenic, and chondrogenic lineages, described in detail below, using the inductive media formulations in Table 5.3 [2], [14], [62]. All differentiation supplements were added to DMEM:Ham's F12 with 1% pen-strep. For all assays, non-induced controls cultured in proliferation media were included for each group. Media was exchanged every 2-3 days for the adipogenic and osteogenic groups, while half media changes every 2 days were performed for the chondrogenic groups.

Table 5.3: Summary of differentiation media formulations.

Lineage	Supplements
Adipogenesis	33 µM biotin 17 µM pantothenate 10 µg/mL transferrin 100 nM hydrocortisone 66 nM human insulin 1 nM triiodothryonine 0.25 mM isobutylmethylxanthine (IBMX) * 1 µg/mL troglitazone *
Osteogenesis	10% FBS 50 µM ascorbic acid 10 mM β-glycerolphosphate 100 nM dexamethasone 0.01 µM 1,25-dihydroxyvitamin D3
Chondrogenesis	10% FBS 50 µg/mL ascorbic acid 6.25 µg/mL human insulin 100 nM dexamethasone 10 ng/mL TGF-β1 (R&D Systems, Cat. # 100-B-001)

** = only in the first 72 h.*

For adipogenesis, ASCs were plated at 50,000 cells/cm^2 on 12-well plates and induced for 14 days [14]. The level of adipogenesis was quantified using the glycerol-3-phosphate dehydrogenase (GPDH) Activity Measurement Kit (Kamiya Biomedical Inc., Cat. # KT-010, Seattle, WA, USA) according to established methods (n=3, N=3) [14]. One Unit of GPDH activity is defined as the consumption of 1 µmole of NADH in 1 min for a 1 mL sample and is normalized to the total intracellular protein content measured using the BioRad Protein Assay. Oil red O staining was used to visualize intracellular lipid accumulation within each of the groups following standard methods previously described (n=3, N=3) [26].

For osteogenesis, ASCs were seeded at 20,000 cells/cm^2 on laminin-coated (Sigma, Cat. # L2020; concentration 1.6 µg/cm^2) plates and induced for 28 days [62]. Osteogenic differentiation was assessed in terms of alkaline phosphatase (ALP) activity normalized to the total intracellular protein content determined with the BioRad Protein Assay, following published methods (n=3,

N=3) [2], [413]. In addition, matrix mineralization was visualized by von Kossa staining following established protocols (n=3, N=3) [2].

For chondrogenesis, ASCs were cultured in 3-D pellets comprised of 250,000 ASCs/pellet within 15 mL vented cap conical tubes. The ASC pellets were generated by centrifuging the cells at 300 xg for 5 min and allowing them to self-aggregate for 48 h in proliferation media prior to induction in 1 mL of chondrogenic media [2]. Immunohistochemistry (IHC) was performed for collagen I and II on unfixed cryo-preserved ASC pellets (n=2, N=1). At each time point, pellets were immediately embedded in Tissue-Tek® O.C.T.™ Compound (Sakura), sectioned into 5 µm thickness, and stored at -20 °C until further processing. In preparation for IHC, the cryosectioned slides were warmed to room temperature for 10-20 min followed by rehydration in D-PBS for 10 min. All sections were then blocked with 10% goat serum in PBST (D-PBS + 0.2% Tween 20 (v/v)) for 1 h at room temperature. The following primary antibodies used were diluted in 10% goat serum in PBST: collagen I anti-mouse (ABCAM, Cat. # ab90395, diluted 1:500) and collagen II anti-rabbit (ABCAM, Cat. # ab34712, diluted 1:200). Primary collagen I was incubated for 1 h at room temperature, while primary collagen II was incubated at 4 ºC overnight. Following incubation, the sections were rinsed 3 times with D-PBS for 5 min each and the following secondary antibodies were incubated in the dark for 1 h at room temperature: goat anti-mouse IgG H&L (Dylight® 650) (ABCAM, Cat. # ab96882, diluted 1:500) and goat anti-rabbit IgG H&L (Dylight® 650) (ABCAM, Cat. # ab96902, diluted 1:500). The sections were rinsed 3 times with D-PBS for 5 min each and mounted with DAPI fluoroshield mounting medium prior to fluorescence imaging with an EVOS® FL Imaging System (Thermo Fisher Scientific, Cat. # AMF4300). No primary and tissue-positive controls were included to confirm staining specificity. To assess proteoglycan accumulation, additional ASC pellets were fixed overnight in 4% paraformaldehyde, paraffin embedded, and sectioned into 5 µm thickness (n=2, N=1). The sections were then deparaffinized and stained with Weigert's iron hematoxylin working solution for 10 min and washed under running tap water for 10

min. Next, the sections were stained with 0.1% safranin O solution for 5 min, and quickly dehydrated and cleared by 2 changes each for 2 min of 95% ethanol, 100% ethanol, and xylene followed by mounting with resinous medium.

5.2.9 Quantitative RT-PCR analysis

To obtain insight on whether 3 weeks of dynamic microcarrier or static TCPS expansion primed the ASCs towards a particular lineage, quantitative RT-PCR analysis was performed to evaluate the expression of key lineage-specific markers prior to plating the cells for differentiation (Fig. 5.1c). Similarly, to further characterize the cells in the multilineage differentiation study (cell donor 6), quantitative RT-PCR analysis was performed in additional samples prepared as described in the previous section, to assess the expression of adipogenic markers at 14 days (n=3), as well as osteogenic (n=3) and chondrogenic (n=2, with each replicate containing 4 pooled pellets) markers at 28 days. The TaqMan® Gene Expression Assay (Invitrogen) human gene-specific primers conjugated with FAM-MGB probes used in this study are presented in Table 5.4. Two stable human housekeeping genes for each lineage were selected using a predesigned 384-well panel Reference Genes H384 plate (Bio-Rad. Cat. # 10025899) and calculated with the Bio-Rad CFX Manager 3.1 Software.

Briefly, total RNA was isolated using established protocols [19] and the samples were treated with the TURBO DNA-free™ kit (Invitrogen, Cat. # AM1907) to eliminate possible genomic contamination. The cDNA was then synthesized from 500 ng of input RNA using the iScript™ Reverse Transcription Supermix kit (Invitrogen, Cat. # 1708840) according to the manufacturer's protocol. For quantitative PCR, samples were prepared using the TaqMan® Fast Advanced Master Mix (Invitrogen, Cat. # 444965) in the recommended 10 µL reaction volume for a 384-well plate. Amplification was carried out in a CFX384 Touch™ Real-Time PCR Detection System (Bio-Rad, Cat. # 1855485), with the following cycling conditions: incubation at 50 ºC for 2

min, activation at 95 ºC for 20 s, and 40 cycles of denaturing at 95 ºC for 3 s and annealing/extension at 60 ºC for 30 s. For each gene of interest, the C_t values were normalized to the geometric mean C_t of the two housekeeping genes. A comparative C_t method was then used to calculate the relative fold change in gene expression to a reference group. In this case, the TCPS expanded group and induced TCPS baseline group served as the calibrator for the undifferentiated and differentiated ASC gene analysis studies, respectively. No-RT controls and no template controls were included on every plate.

Table 5.4: Human gene-specific primers for DAT microcarrier multilineage differentiation study

Lineage	Gene	Description	Product No.
Adipogenesis	*PPARγ*	Peroxisome proliferator-activated receptor gamma	Hs00234592_m1
	LPL	Lipoprotein lipase	Hs00173425_m1
	ADIPOQ	Adiponectin	Hs00605917_m1
	*GAPDH**	Glyceraldehyde-3-phosphate dehydrogenase	Hs02758991_g1
	*IPO8**	Importin 8	Hs00183533_m1
Osteogenesis	*RUNX2*	Runt-related transcription factor 2	Hs01047973_m1
	ON	Osteonectin	Hs00234160_m1
	OCN	Osteocalcin	Hs01587814_g1
	*PGK1**	Phosphoglycerate kinase 1	Hs00943178_g1
	*UBC**	Ubiquitin C	Hs01871556_s1
Chondrogenesis	*SOX9*	Sex-determining region Y-related high motility group box 9 transcription factor	Hs01001343_g1
	COLL 2	Collagen 2	Hs00264051_m1
	COMP	Cartilage oligomeric matrix protein	Hs00164359_m1
	AGG	Aggrecan	Hs00153936_m1
	*RPL13A**	Ribosomal protein L13A	Hs04194366_g1
	*UBC**	Ubiquitin C	Hs01871556_s1

** = housekeeping genes selected for each lineage.*

5.2.10 Statistical analysis

Statistical analyses were performed using GraphPad Prism 6 Software by one-way or two-way ANOVA with Tukey's post-hoc comparison of means. All data values are expressed as a mean ± standard deviation (SD) and significant differences considered when $p < 0.05$.

5.3 Results

5.3.1 Microcarrier characterization and mechanical properties

DAT microcarriers were prepared by electrospraying the DAT suspension into liquid nitrogen followed by lyophilization, which produced spherical microcarriers that were robust when hydrated (Fig. 5.2). DAT suspension concentrations of 17.5, 35, and 50 mg/mL were used to fabricate microcarriers to evaluate stability over a range of formulations as summarized in Table 5.5, with no significant differences observed for each property.

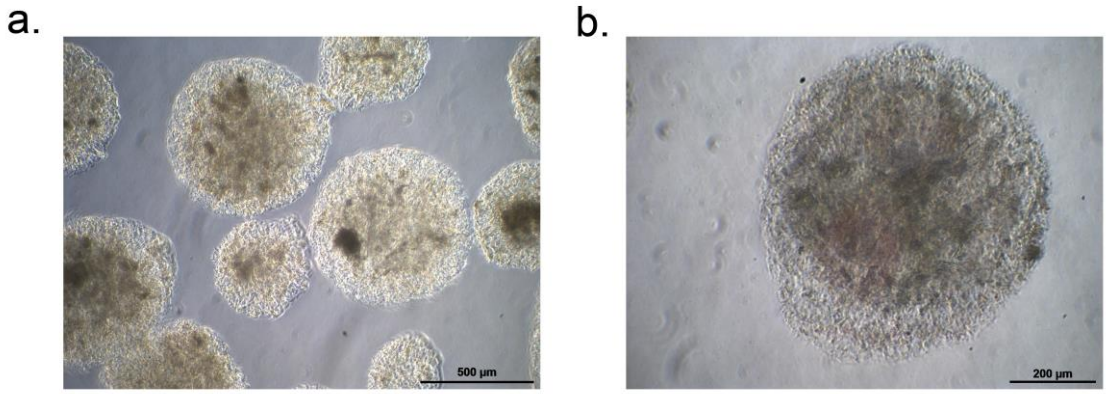

Figure 5.2: Representative images of electrosprayed DAT microcarriers. Optical images of 50 mg/mL DAT microcarriers hydrated in D-PBS at (a) 10x (scale bar = 500 µm) and (b) 20x magnification (scale bar = 200 µm).

Table 5.5: Summary of DAT microcarrier characterization

DAT suspension (mg/mL)	Mean diameter (µm)*	Swelling ratio (%)*	EWC (%)*	Porosity (%)
17.5	436 ± 15	110 ± 5	96.9 ± 0.9	99.1 ± 0.2
35	435 ± 5	106 ± 1	96.5 ± 0.2	98.9 ± 0.1
50	428 ± 2	105 ± 1	96.4 ± 0.5	98.9 ± 0.1

**Measurements taken at 72 h.*

All DAT microcarrier mean diameters after 72 h were within the target range of 350-500 µm. Diameter measurements over 28 days revealed similar trends for each microcarrier, showing a slight increase in diameter from 24 h to 72 h, followed by stabilization from 7 days to 28 days

(Fig. 5.3). Interestingly, while all DAT microcarrier formulations possessed a high EWC (>96%) and porosity (>98%), they did not swell extensively from their original size with no macroscopic changes in sphericity observed during the study. From the SEM images, the DAT microcarriers have a rough surface topography and the ECM fibers appear more densely packed when fabricated at the higher DAT suspension concentrations (Fig. 5.4a). In terms of ECM components, IHC staining of the DAT microcarriers qualitatively showed the presence of collagen I and IV, however, fibronectin and laminin were not detected (Fig. 5.4b).

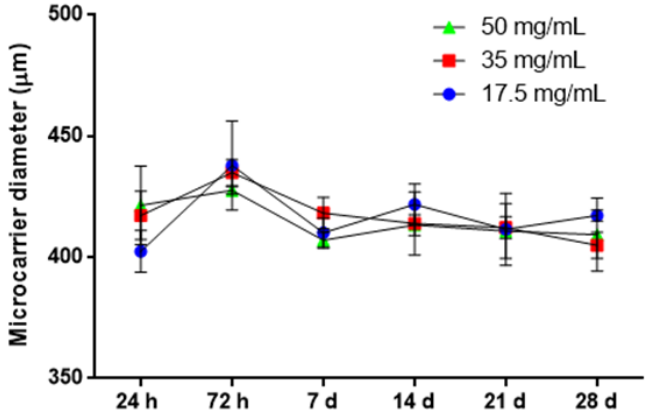

Figure 5.3: Mean DAT microcarrier diameter over 28 days in Ringer's physiological solution at 37°C. Data are expressed as a mean ± SD and significant differences considered when $p < 0.05$. Approximately 100 microcarriers were averaged at each time point per formulation (n=3).

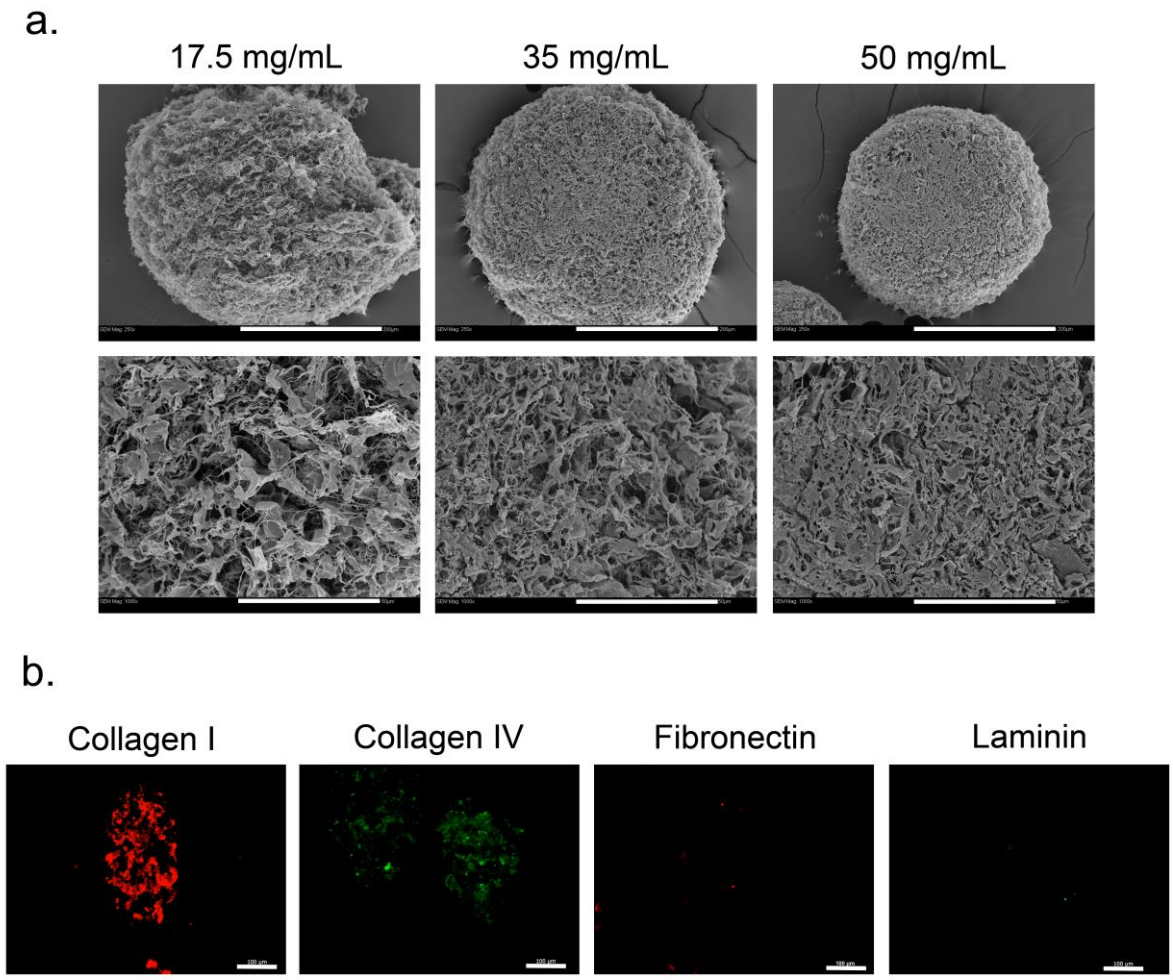

Figure 5.4: Representative SEM and IHC images of DAT microcarriers. a) SEM imaging showing a porous ultrastructure fabricated from different DAT suspension concentrations (top row scale bars = 200 µm, bottom row scale bars = 20 µm). b) IHC staining of ECM components in the 50 mg/mL DAT microcarriers. Scale bars = 100 µm. Refer to Fig. A.1 in the Appendix for positive tissue controls.

The 50 mg/mL DAT suspension concentration was chosen for subsequent *in vitro* studies since it was postulated that the denser structure would better resist ASC contraction forces during prolonged culture. Prior to conducting subsequent cultivation studies, the porosity and mechanical properties of the 50 mg/mL DAT microcarriers and commercial Cultispher-S microcarriers were compared. DAT microcarriers were determined to be significantly more porous than the Cultispher-S microcarriers with a porosity of 98.9 ± 0.1% and 69.2 ± 0.2 %, respectively. Mechanical testing was performed using a highly-sensitive CellScale MicroSquisher apparatus which was used to

determine the force required to compress the hydrated microcarriers. From the force versus deformation curves (Fig. 5.5), the calculated Young's modulus was considerably greater for the Cultispher-S microcarriers (131.3 ± 42.2 kPa) relative to the DAT microcarriers (0.5 ± 0.2 kPa). Furthermore, higher hysteresis was shown in Fig. 5.5 for the DAT microcarriers than the Cultispher-S microcarriers, which is indicative of a more viscoelastic response. These observations are likely attributed to the highly crosslinked nature of the porcine gelatin Cultispher-S microcarriers as opposed to the non-chemically crosslinked DAT microcarriers.

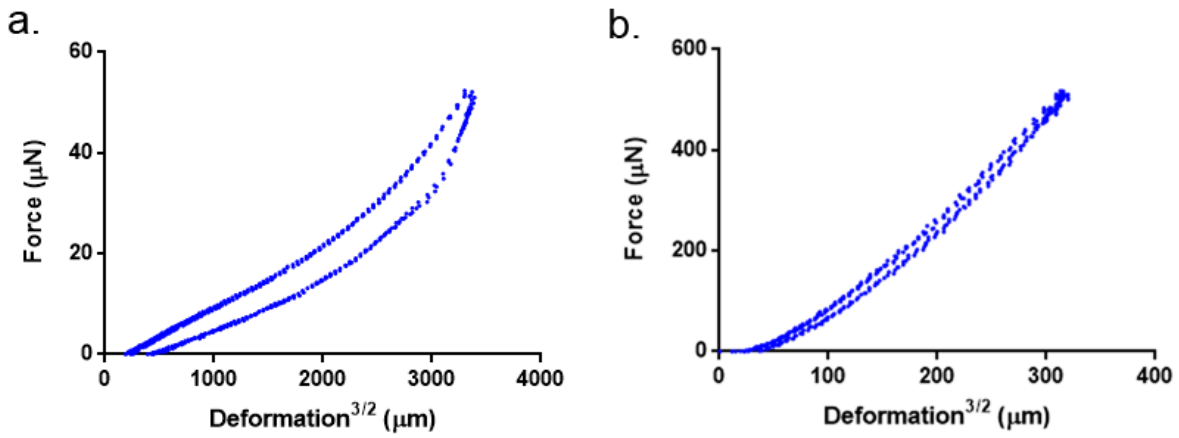

Figure 5.5: Typical force versus deformation curves for a) 50 mg/mL DAT microcarrier and b) Cultispher-S microcarrier. A total of 3 cycles is shown where the top portion corresponds to the compression part of the cycle and was used to calculate the tangential slope required to solve for the Young's modulus.

5.3.2 ASC proliferation on the microcarriers

Upon selecting the 50 mg/mL DAT microcarrier formulation, ASC proliferation was assessed on the DAT and Cultispher-S microcarriers under dynamic culture within a CELLSPIN system. In culture, both microcarriers remained structurally intact and supported ASC expansion over 4 weeks. Confocal images of Live/Dead^{TM} stained ASCs (Fig. 5.6a) qualitatively showed enhanced cell attachment at 24 h on the DAT microcarriers compared to the Cultispher-S microcarriers. For both DAT and Cultispher-S microcarriers, the ASCs proliferated evenly across

the surface over time with microcarrier aggregation observed at 3 and 4 weeks. In addition, the presence of infiltrating ASCs within both microcarriers at 4 weeks was also detected by DAPI stained sections (Fig. 5.6b).

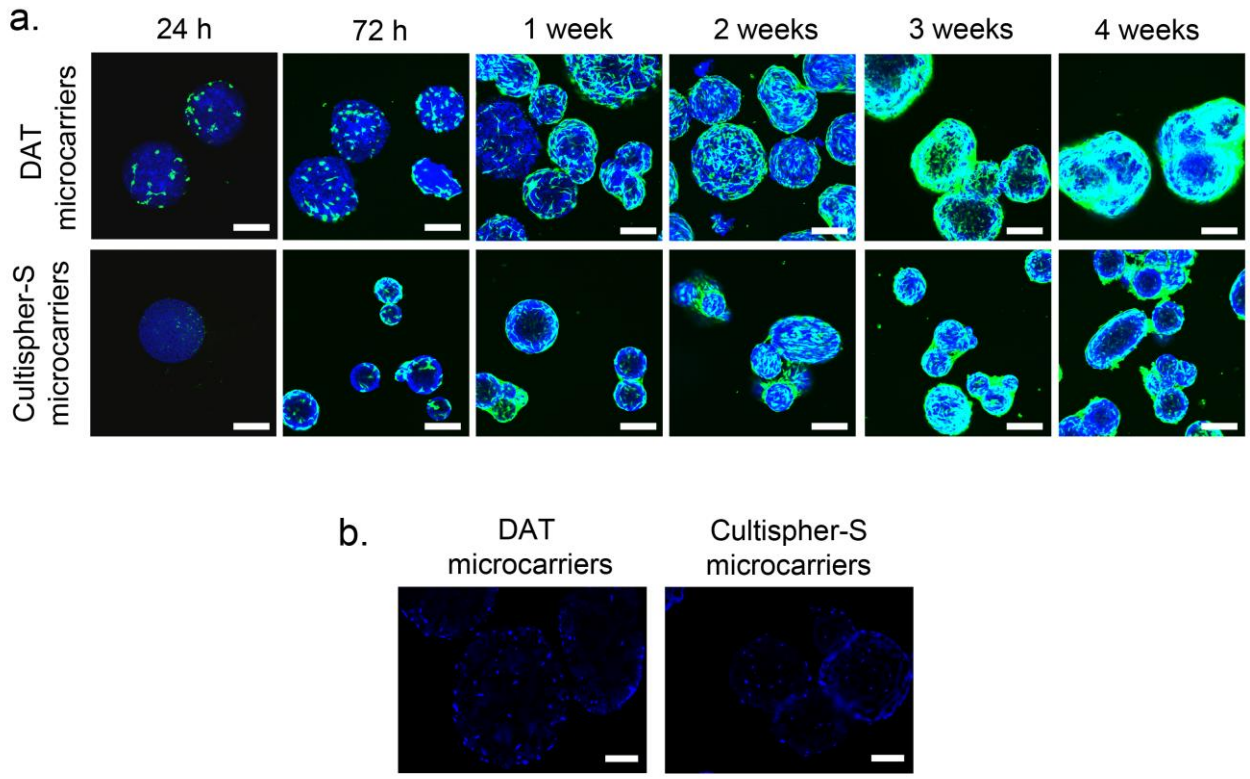

Figure 5.6: Representative images of ASCs on DAT and Cultispher-S microcarriers over 4 weeks dynamic culture. a) Live/Dead™ (green/red) stained ASCs and Alexa Fluor® 350 (blue) stained microcarriers. Scale bars = 200 µm. b) DAPI staining showing the presence of cells within the DAT and Cultispher-S microcarriers at 4 weeks. Scale bars = 100 µm.

Quantification of viable ASCs on the microcarriers showed similar growth patterns between the donors with significantly greater cell numbers recovered from the DAT microcarriers in comparison to the Cultispher-S microcarriers at 2, 3, and 4 weeks (Fig. 5.7). To evaluate the efficacy of ASC expansion on each of the microcarriers, the population fold change was calculated based on the ratio of cells recovered at 4 weeks relative to cells recovered at the 24 h condition (Table 5.6). Interestingly, a consistent trend was observed for both cell donors showing the DAT

microcarriers supporting a significantly higher ASC population fold change than the Cultispher-S microcarriers after 4 weeks of expansion.

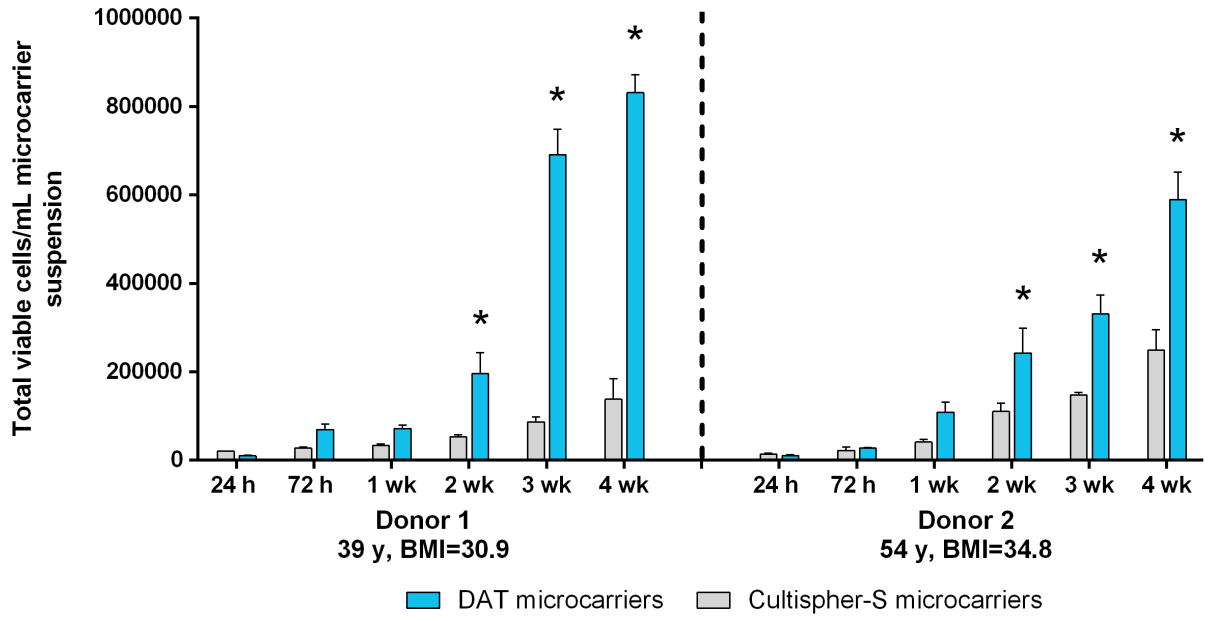

Figure 5.7: ASC proliferation on DAT and Cultispher-S microcarriers over 4 weeks. Data are expressed as a mean ± SD and significant differences considered when $p < 0.05$. Total viable cells were counted with the Guava Viacount® Assay at each time point. * = significant to Cultispher-S microcarrier within the time point. (n=2, N=2).

Table 5.6: ASC population fold change at 4 weeks relative to 24 h

Microcarrier	Donor 1 39 y, BMI=30.9	Donor 2 54 y, BMI=34.8
DAT	90.0 ± 14.7	59.4 ± 8.9
Cultispher-S	6.7 ± 2.2	17.6 ± 2.5

5.3.3 ASC stem cell immunophenotype expression

To determine if expansion culture conditions resulted in immunophenotype changes, ASC surface marker expression was analyzed following 3 weeks expansion on DAT microcarriers, Cultispher-S microcarriers, or TCPS in comparison to a subset of P1 ASCs from the same donor as a TCPS baseline control (Table 5.7). In general, the results from the TCPS baseline group

confirmed that the starting ASC population is consistent with the expected ASC immunophenotype. Interestingly, for positive marker expression, ASCs cultured under dynamic conditions on both microcarriers exhibited a decrease in CD73, CD105, and CD29 relative to the TCPS expanded and TCPS baseline groups. Furthermore, the lowest expression for CD34 (progenitor associated marker) was observed for ASCs expanded on the DAT microcarriers. In terms of negative marker expression, ASCs expanded on TCPS, DAT microcarriers, and Cultispher-S microcarriers showed negligible expression for CD31 (endothelial marker) and CD45 (haematopoietic cell marker).

Table 5.7: Immunophenotype of expanded ASCs relative to TCPS baseline controls

	Antigen	TCPS Baseline (%) (N=4)	TCPS Expanded (%) (N=3)	DAT Microcarrier (%) (N=4)	Cultispher-S Microcarrier (%) (N=4)
Positive markers	CD90	99.9 ± 0.1	99.6 ± 0.5	94.8 ± 3.6	96.2 ± 3.1
	CD73	99.2 ± 1.0	99.4 ± 0.4	86.5 ± 9.1	88.2 ± 8.2
	CD44	98.3 ± 0.1	99.8 ± 0.2	94.7 ± 3.9	99.8 ± 0.2
	CD105	97.1 ± 0.4	97.9 ± 2.9	85.9 ± 4.9	82.6 ± 19.1
	CD29	95.9 ± 2.1	98.0 ± 2.7	89.9 ± 7.0	78.3 ± 34.2
	CD146	4.2 ± 7.3	2.9 ± 4.4	1.4 ± 0.8	0.8 ± 0.8
	CD34	17.3 ± 20.5	11.9 ± 20.2	2.2 ± 2.5	10.1 ± 18.7
Negative markers	CD31	0.6 ± 0.2	0.3 ± 0.2	0.2 ± 0.2	0.5 ± 0.3
	CD45	1.5 ± 1.1	0.5 ± 0.3	0.6 ± 0.2	0.3 ± 0.4

5.3.4 Effect of expansion conditions on ASC lineage-specific gene expression

To probe whether the cell expansion culture conditions were priming the ASCs towards a particular lineage, quantitative RT-PCR analysis of lineage-specific markers was performed on ASCs cultured for 3 weeks on the DAT and Cultispher-S microcarriers or on TCPS (Fig. 5.8). For the adipogenic lineage, a statistically significant upregulation in the adipogenic transcription factor *PPARγ* was observed on the ASCs expanded on the DAT (3.3 ± 0.5 fold change) relative to the

TCPS expanded controls. Interestingly, there was also significantly higher expression of the early marker *LPL* observed in both the DAT (18.4 ± 8.9 fold change) and Cultispher-S (6.0 ± 3.4 fold change) microcarrier groups. However, no expression of the mature adipocyte marker *ADIPOQ* was detected for all groups. For osteogenesis, a trend for enhanced expression of the transcription factor *RUNX2* was observed in both the DAT (3.2 ± 1.2 fold change) and Cultispher-S (3.0 ± 1.4 fold change) groups relative to the TCPS expanded group, but was not statistically significant. Similarly, no significant differences were observed in the expression levels of the early-stage osteogenic marker *ON* or late-stage marker *OCN* between any of the groups. For chondrogenesis, the early transcription factor *SOX9* and mature marker *AGG* were expressed at similar levels under all conditions. Notably, while *COLL2* was not detectable in any of the groups, the early marker *COMP* was detected at higher levels in ASCs cultured on both microcarriers with significant enhancement following expansion on the Cultispher-S microcarriers (18.8 ± 8.4 fold change).

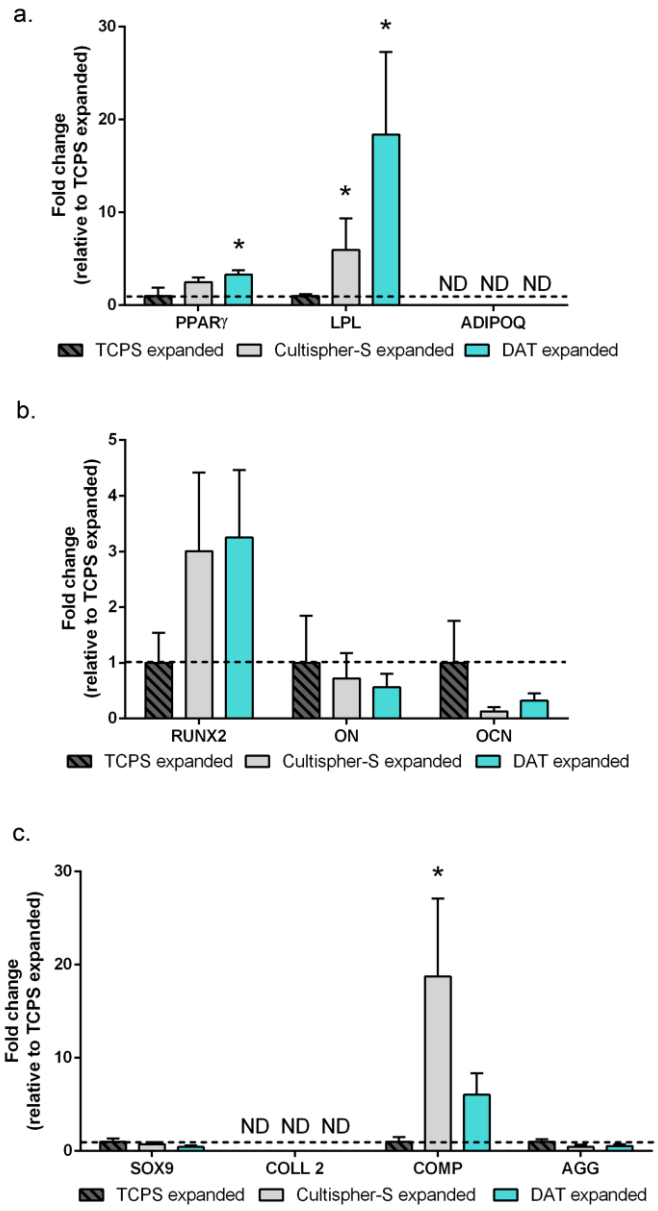

Figure 5.8: Comparison of gene expression profile of ASCs after 3 weeks expansion on TCPS, Cultispher-S microcarriers, or DAT microcarriers for donor 6. Data are expressed as a mean ± SD and significant differences considered when $p < 0.05$. ND = not detected. a) Adipogenic marker expression where * = significant to TCPS expanded group for *PPARγ* and *LPL*. b) Osteogenic marker expression. c) Chondrogenic marker expression where *= significant to all other groups for *COMP*. (n=3).

5.3.5 ASC multilineage capacity post-expansion

Following 3 weeks expansion on the microcarriers or TCPS, the multilineage differentiation capacity of ASCs was evaluated to confirm the maintenance of stem cell phenotype relative to

TCPS baseline controls. For the final differentiation study with cell donor 6, the population fold change during the expansion phase was calculated for each group prior to inducing differentiation to more fully compare observed differences in differentiation capacity potentially due to increased proliferation (Table 5.8).

Table 5.8: ASC population fold change after 3 weeks expansion for donor 6

Expansion condition	Population fold change
TCPS	96.4 ± 4.8
Cultispher-S microcarriers	12.4 ± 2.0
DAT microcarriers	53.4 ± 3.0

5.3.5.1 *Adipogenesis*

To quantitatively assess the level of adipogenic differentiation between the two microcarrier groups, GPDH enzyme activity was measured at 14 days post induction (Fig. 5.9a). With the exception of the donor 4 samples, where there was slightly enhanced activity measured in the Cultispher-S group, similar GPDH activity levels were observed between the DAT and Cultispher-S microcarrier groups. As expected, low GPDH activity levels were measured in the non-induced controls for all conditions. To compare trends in adipogenic differentiation between the dynamic microcarrier groups and static TCPS controls across all cell donors, the GPDH activity was normalized to the TCPS baseline controls for all induced groups (Fig. 5.9b). In this case, a significant decrease in ASC adipogenic activity was observed among all expanded groups after 3 weeks of culture. Despite a decline in GPDH activity post expansion, oil red O staining showed positive intracellular lipid accumulation in all of the induced groups (Fig. 5.9c). Consistent with the observed trend in GPDH activity, qualitatively higher levels of staining were observed in the TCPS baseline group. Interestingly, for all donors the lipid accumulation in the DAT microcarrier expanded ASCs appeared to be more uniform across the population while the Cultispher-S microcarrier expanded ASCs were more clustered. No positive oil red O staining was detected in the non-induced controls for all conditions.

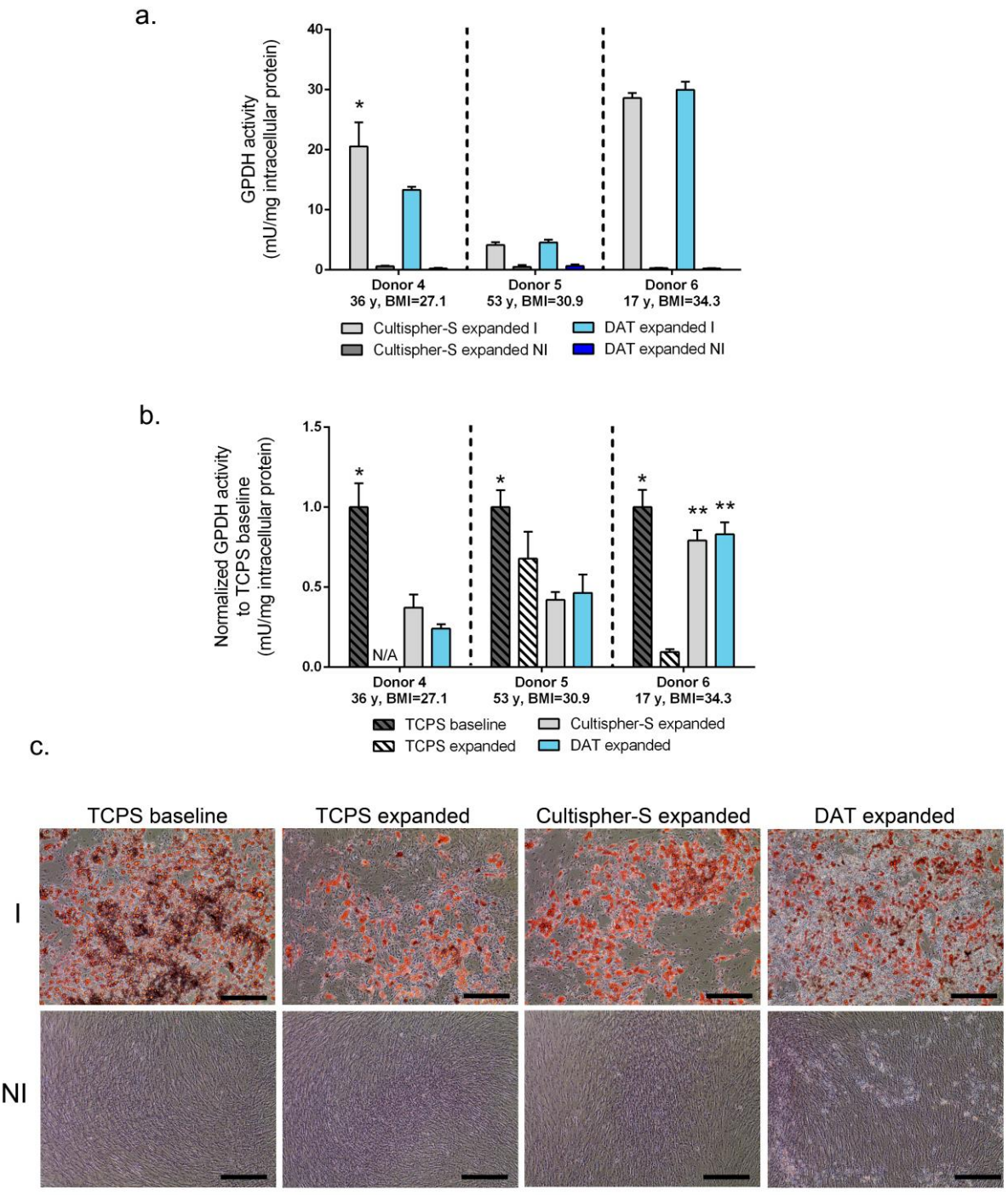

Figure 5.9: GPDH enzyme activity and oil red O staining of ASCs after 14 days adipogenic induction. Data are expressed as mean GPDH activity ± SD and significant differences considered when $p < 0.05$. Adipogenesis was quantified by GPDH activity and normalized to the total intracellular protein content for (a) DAT compared to Cultispher-S microcarriers and (b) all induced expanded groups normalized to induced TCPS baseline controls. * = significant to all other groups, ** = significant to TCPS expanded group. (c) Representative oil red O staining from donor 6 of intracellular lipid accumulation. Scale bars = 100 µm. I = induced and NI= non-induced. (n=3, N=2-3).

For cell donor 6, gene expression analysis was also conducted to assess the expression of key adipogenic markers using quantitative RT-PCR. The data presented for the expanded ASC groups was normalized to the induced TCPS baseline controls (Fig. 5.10). Overall, the expression patterns observed in the induced groups are consistent with adipogenic differentiation as shown by measurable expression levels observed for both early-stage and late-stage adipogenic markers. Relative to the TCPS baseline, all induced expanded groups exhibited reduced expression levels of *PPARγ*, *LPL*, and *ADIPOQ*, with the lowest expression detected in the TCPS expanded controls. Low levels of expression were observed in the non-induced groups for all genes.

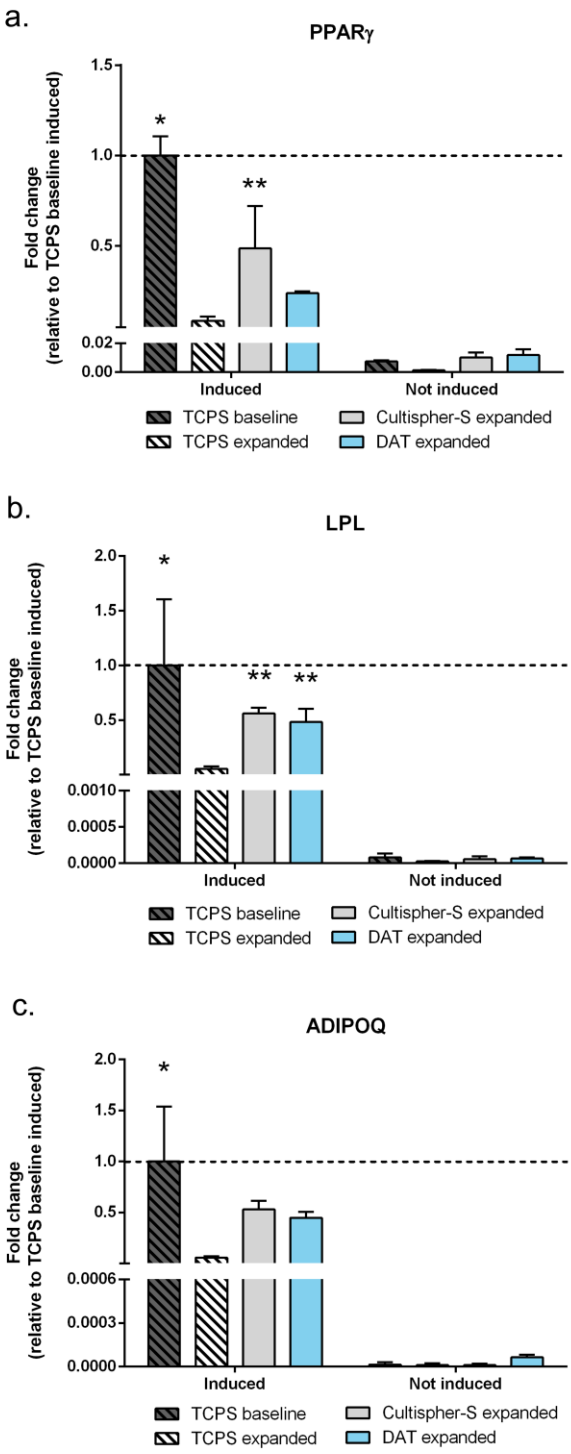

Figure 5.10: Adipogenic gene expression of ASCs after 14 days induction. Data are expressed as a mean ± SD and significant differences considered when $p < 0.05$. a) *PPARγ* expression where * = significant to all other groups and ** = significant to TCPS expanded induced and all non-induced groups, b) Lipoprotein lipase (*LPL*) expression where * = significant to TCPS expanded induced and all non-induced groups and ** = significant to all non-induced groups. c) Adiponectin (*ADIPOQ*) expression where * = significant to TCPS expanded induced and all non-induced groups. (n=3).

5.3.5.2 *Osteogenesis*

Osteogenic differentiation of ASCs expanded on both types of microcarriers revealed a consistent trend for higher ALP activity in the induced DAT microcarrier group relative to the Cultispher-S microcarriers, although the differences were not statistically significant (Fig. 5.11a). When ALP activities of the induced ASC expanded sets were normalized to the induced TCPS baseline controls, a significant decrease was observed for all of the expanded groups for donors 4 and 5, with the exception of the DAT microcarrier expanded group in donor 5 (Fig. 5.11b). Von Kossa staining confirmed matrix mineralization in the induced DAT and Cultispher-S microcarrier expanded ASCs and TCPS baseline controls, however, no positive staining was detected in the TCPS expanded ASCs (Fig. 5.11c). Interestingly, for donors 5 and 6 more matrix mineralization was observed in the DAT microcarrier expanded ASCs relative to the Cultispher-S and TCPS baseline controls, which correlated to the levels of ALP activity. As expected, no positive von Kossa stains were observed in all non-induced controls.

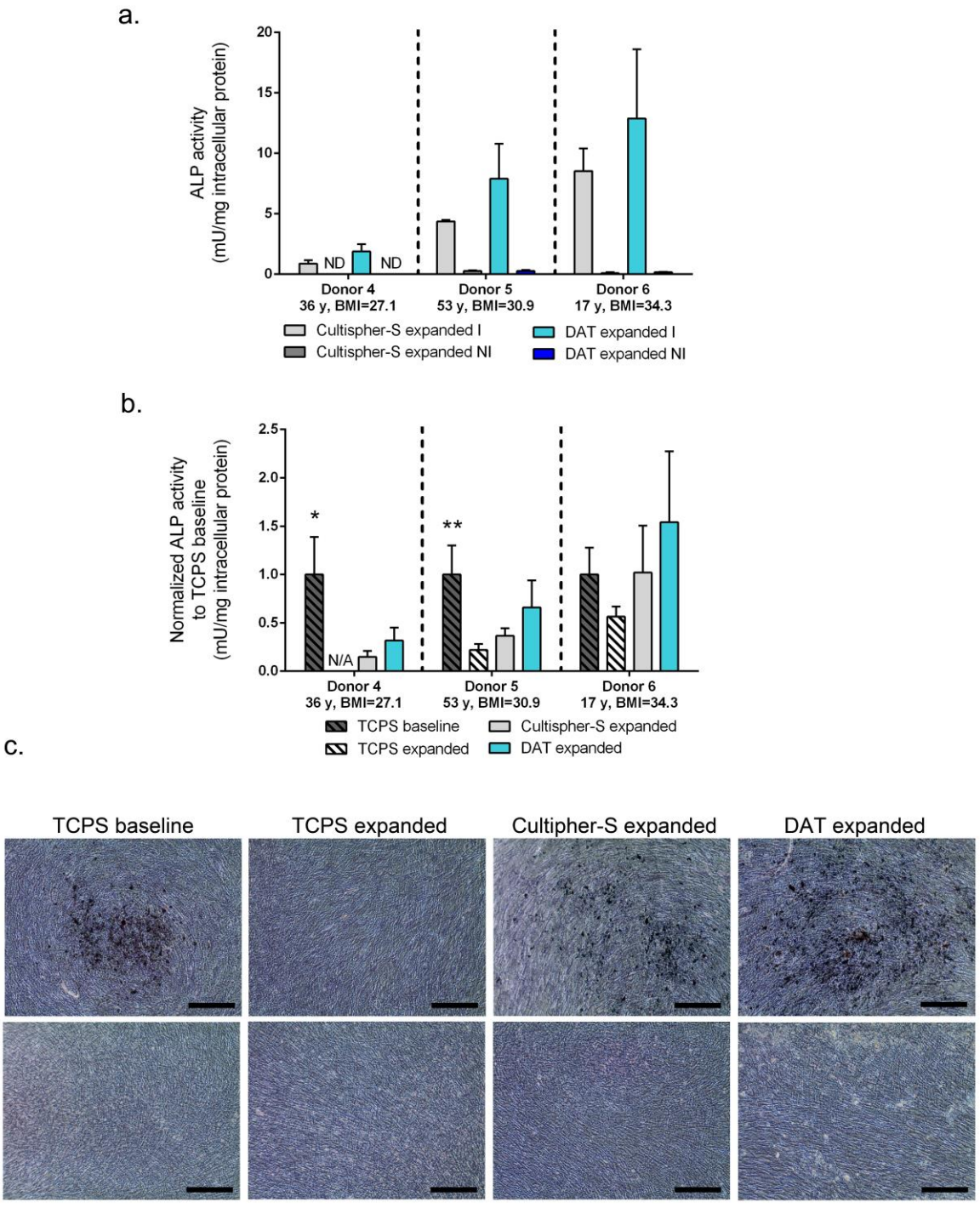

Figure 5.11: ALP activity and von Kossa staining of ASCs after 28 days osteogenic induction. Data are expressed as mean ALP activity ± SD and significant differences considered when $p < 0.05$. Osteogenesis was quantified by ALP activity and normalized to the total intracellular protein content for (a) DAT compared to Cultispher-S microcarriers and (b) all induced expanded groups normalized to induced TCPS baseline control. * = significant to all other groups, ** = significant to TCPS expanded and Cultispher-S expanded. (c) Representative von Kossa staining from donor 6 of matrix mineralization. Scale bar = 100 µm. I = induced and NI= non-induced**.** (n=3, N=2-3).

To further validate these trends, osteogenic gene expression analysis was performed on donor 6 samples for each condition (Fig. 5.12). Overall, this data confirmed that the induced expanded ASCs underwent osteogenesis in terms of early-stage and late-stage osteogenic gene expression. The induced DAT microcarrier group was found to have significantly higher levels of *RUNX2* expression relative to the non-induced TCPS baseline groups, as well as a significant increase in *ON* expression relative to the non-induced DAT microcarrier group. Interestingly, in comparing the non-induced sets, detectable levels of *RUNX2* and *ON* were observed in all groups while *OCN* expression was observed in the DAT microcarrier group.

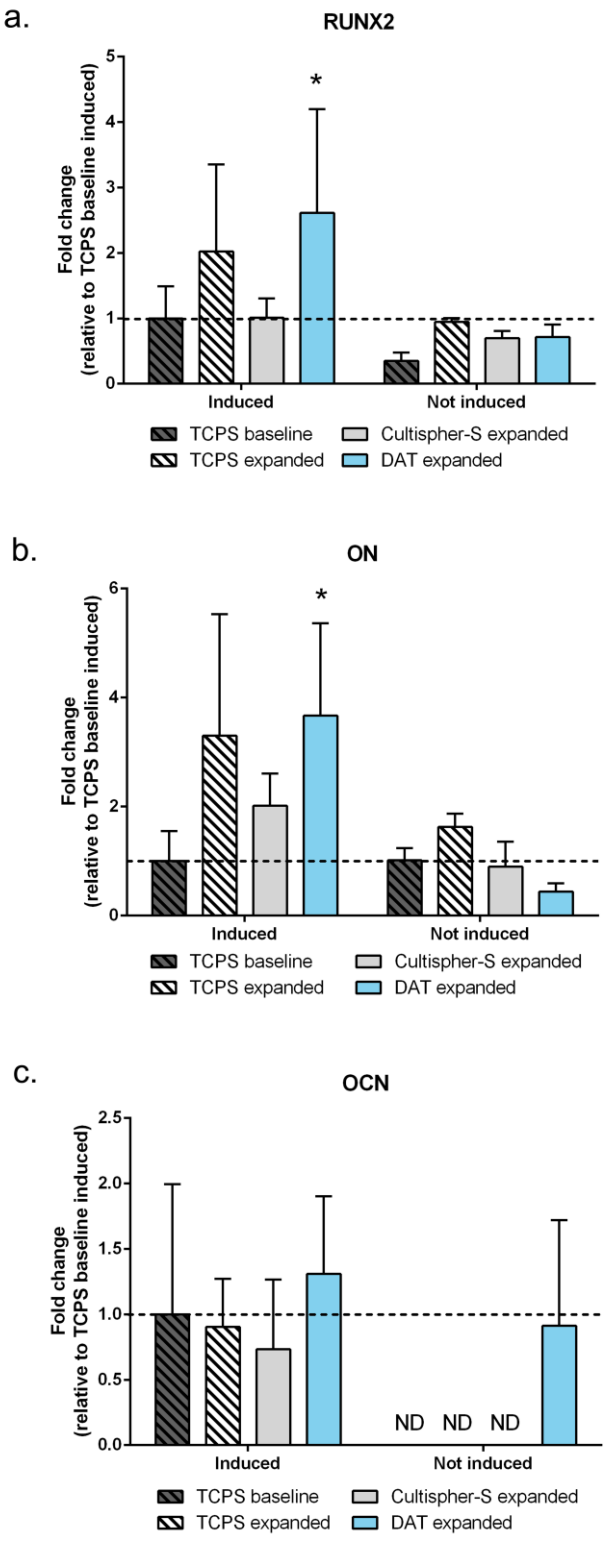

Figure 5.12: Osteogenic gene expression of ASCs after 28 days induction. Data expressed as a mean ± SD and significant differences considered when $p < 0.05$. a) *RUNX2* expression where * = significant to TCPS baseline non-induced. b) Osteonectin (*ON*) expression where * = significant to DAT expanded non-induced group. c) Osteocalcin (*OCN*) expression. ND = not detected. (n=3).

5.3.5.3 *Chondrogenesis*

Building on the results from the adipogenesis and osteogenic lineages, chondrogenic differentiation was evaluated for cell donor 6 samples to further investigate the multilineage differentiation capacity of the expanded ASCs. Collagen type II is an abundant protein found in native articular cartilage and a shift from collagen I to collagen II production has been shown to indicate chondrogenic differentiation [414]. Based on qualitative IHC analysis (Fig. 5.13) evidence of positive chondrogenesis was most prominently visualized in the induced DAT microcarrier and TCPS baseline groups, as shown by the increased relative staining intensity of collagen II to collagen I. Interestingly, uniform positive staining for collagen II was also detected in the non-induced DAT microcarrier samples. However, the relatively intense collagen I staining also observed suggests that the level of chondrogenesis was not as high as the induced DAT microcarrier group. The accumulation of proteoglycan, which is highly abundant in native cartilage ECM, was visualized by safranin O staining on the ASC pellets as shown in Fig. 5.13. In general, all conditions stained positive for safranin O, with subtle differences in intensity observed between the induced and non-induced controls. Qualitatively, differences in safranin O staining intensity were most apparent for the induced DAT expanded group when compared to its non-induced counterpart.

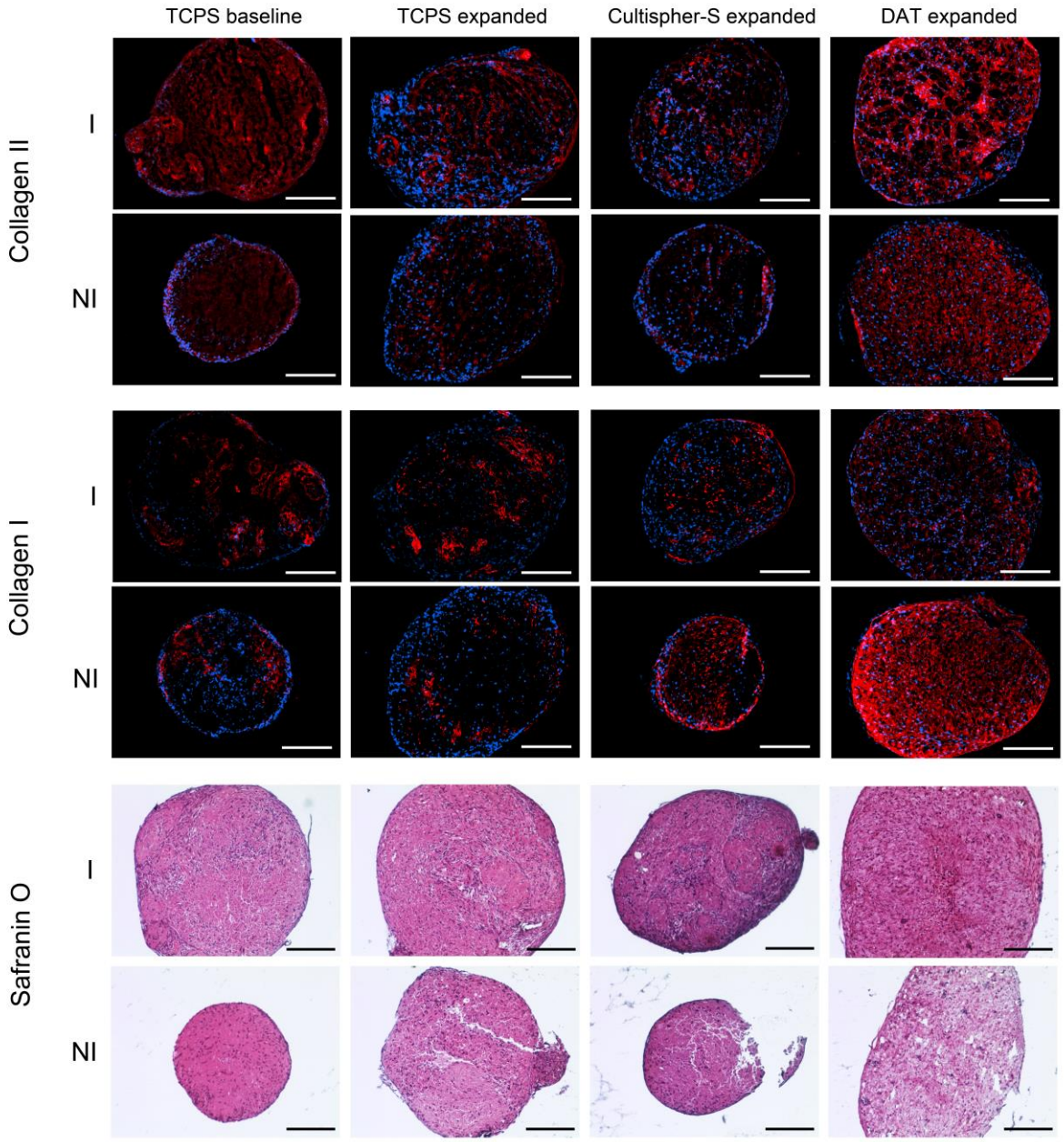

Figure 5.13: Representative IHC and safranin O staining on ASC pellets after 28 days chondrogenic induction. a) IHC was used to visualize collagen II and I (red) with DAPI counterstaining (blue), scale bars = 100 µm. b) Safranin O staining was used to visualize proteoglycan content, scale bars = 100 µm. Positive and negative controls can be found in Fig. A.2 in the Appendix. I = induced and NI = non-induced.

To confirm these qualitative observations, quantitative RT-PCR analysis of key chondrogenic genes was performed (Fig. 5.14). Notably, the induced DAT microcarrier expanded ASCs had significantly higher expression levels of *SOX9*, *COLL2*, *COMP* and *AGG* relative to all other groups, with the exception of *SOX9*, suggesting that chondrogenesis was enhanced in this

group. Higher levels of *SOX9* and *COMP* expression were also observed in the induced Cultispher-S microcarrier group relative to the TCPS baseline. In this case, non-induced ASCs expanded on both microcarrier types had significant expression of *SOX9* relative to the TCPS baseline, while DAT microcarriers also had a significant increase in the expression of *COMP* relative to the TCPS baseline.

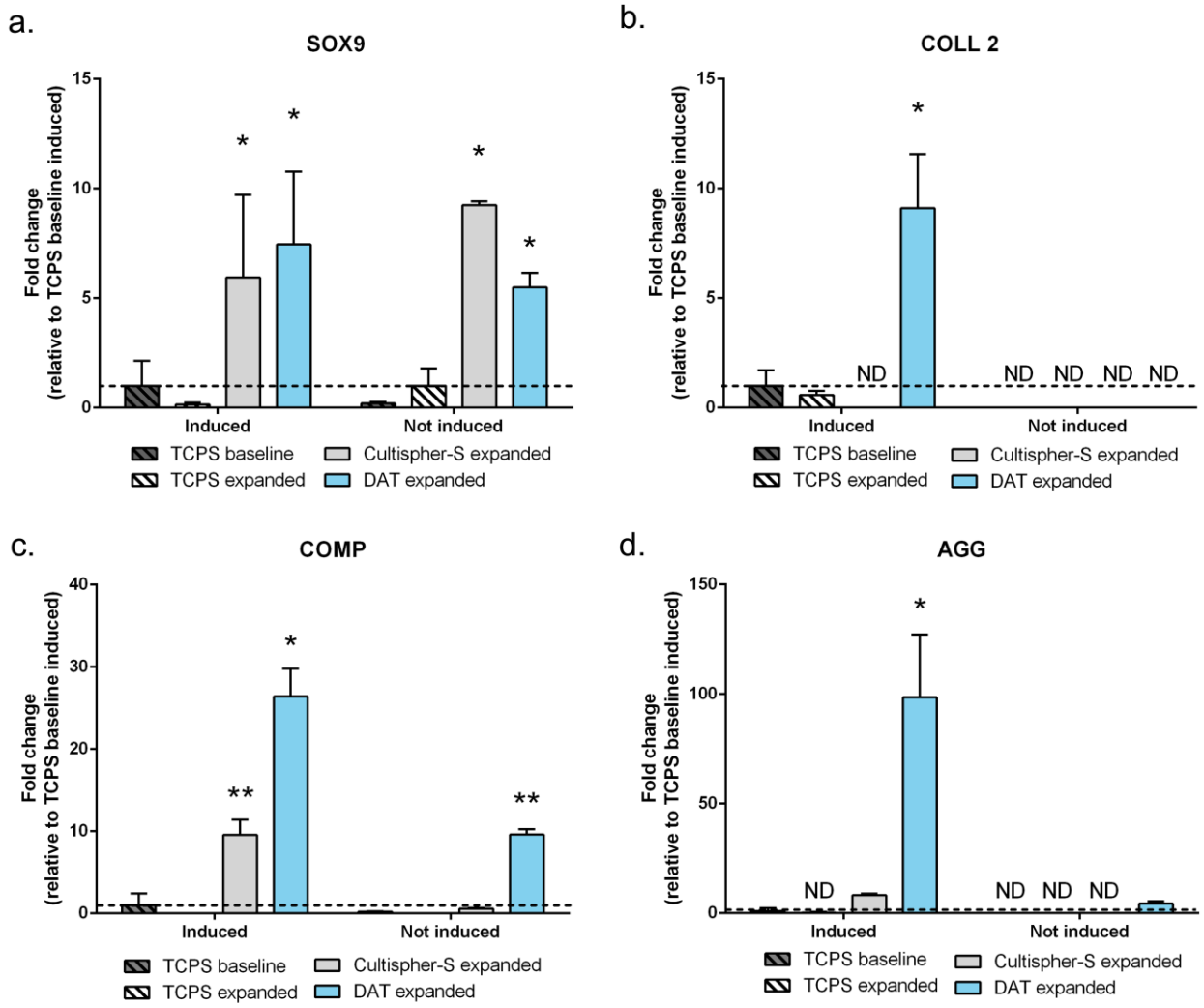

Figure 5.14: Chondrogenic gene expression of ASCs after 28 days induction. Data are expressed as a mean ± SD and significant differences considered when $p < 0.05$. a) *SOX9* expression where * = significant to TCPS baseline and TCPS expanded induced and non-induced groups. b) collagen II (*COLL 2*) expression where * = significant to all other groups. c) cartilage oligomeric complex protein (*COMP*) where * = significant to all groups and ** = significant to TCPS baseline and TCPS expanded induced and non-induced groups. d) aggrecan (*AGG*) expression where * = significant to all other groups. ND = not detected. (n=2, with each replicate containing 4 pooled pellets).

5.4 Discussion

Cell fate is highly influenced by the dynamic microenvironment and this fundamental concept has led to advancements in engineered bioinstructive materials, as well as controlled culture systems in the fields of tissue engineering and regenerative medicine. Through understanding the cross-talk that occurs between cells and their extracellular microenvironment both *in vitro* and *in vivo*, the effect of key elements like biochemical, biochemical, and biophysical cues on cellular functions including proliferation, differentiation, and migration may be elucidated [7], [9]. With this knowledge, strategies to recapitulate these complex cell-matrix interactions may include careful tuning of bioreactor conditions combined with the design of novel synthetic or naturally-derived scaffolds with bioactive properties [7], [136], [415]. In particular, the use of decellularized matrices has gained significant interest as a strategy to better mimic intricate features of the native tissue milieu and serve as instructive biomaterials for tissue engineering.

Building upon these concepts, the aim of the present study was to perform a detailed investigation into the potential use of tissue-specific DAT microcarriers within a scalable stirred bioreactor system to enhance ASC proliferation while preserving the multilineage differentiation capacity. In particular, a novel technique was established to create non-chemically crosslinked DAT microcarriers to improve upon the previous composite fabrication strategy using pepsin-solubilized DAT described in Chapter 3 [20]. Applying the α-amylase digestion approach described in Chapter 4 [242] to form a DAT suspension enabled the fabrication of DAT microcarriers without the need for additional stabilizing agents or crosslinkers, which could potentially alter the physical and biological properties of the ECM [416]. In this new approach, collagen fibrils were more highly preserved following glycosidic cleavage of carbohydrate groups with α-amylase, in contrast to the lack of intact collagen fibrils following non-specific proteolytic cleavage with pepsin [242], [243]. The intact collagen fibrils present in α-amylase digested DAT readily dispersed in dilute acetic acid

and allowed for the production of stable microcarriers via physical entanglement during electrospraying.

The DAT microcarriers were structurally robust and supported ASC attachment while also demonstrating the potential to be remodelled by the cells to enable infiltration, as indicated by the presence of ASCs in the interior of the microcarriers after 4 weeks in culture. In terms of ECM composition, collagen type I and collagen type IV were identified in the DAT microcarriers. Given the important biological functions of fibrillar collagen type I and the basement membrane component collagen type IV in facilitating cell adhesion, these constituents may help to support cell attachment and growth [140], [141], [417]. It is postulated that the cryo-milling step during fabrication contributed to the loss of detectable fibronectin and laminin epitopes in the DAT microcarriers, which is supported by previous work showing lower staining intensities of these ECM components in milled DAT foams relative to intact DAT and non-cryo-milled DAT foams [418].

The initial study involved examining ASC proliferation on the DAT microcarriers in comparison to commercially available Cultispher-S microcarriers within a stirred CELLSPIN system. Qualitatively, cell viability and growth on both microcarrier types were well supported throughout the one-month study. With regards to cell yields, the data clearly indicated that the DAT microcarriers supported higher levels of initial cell attachment and population fold change than the Cultispher-S microcarriers. The observed differences between the microcarriers could be due to a myriad of possible effects including microcarrier composition, surface topography, chemical crosslinking, and mechanical properties [136], [325], [419], [420]. In particular, the non-chemically crosslinked nature of the DAT microcarriers compared to the highly crosslinked Cultispher-S microcarriers could be a contributing factor to cell adherence. A similar effect was observed by Grover *et al.,* where carbodiimide crosslinking improved the mechanical stiffness of collagen-based scaffolds, but resulted in decreased myoblast adhesion [416]. In addition, the tissue-specific ECM

composition of the DAT microcarriers may have also contributed to enhanced ASC proliferation, as supported by the work of Zhang *et al.* where higher proliferation levels for liver, skin, and muscle cells were observed when cultured on tissue-matched ECM coatings [421]. Interestingly, the non-chemically crosslinked DAT microcarriers fabricated in the current study supported qualitatively higher levels of ASC attachment and proliferation compared to previously published work from the Flynn lab on the chemically crosslinked microcarriers fabricated from pepsin-digested DAT [26]. These differences could potentially be due to the more porous surface topography and intact ECM fibrils resulting from the milder α-amylase treatment, as well as the non-chemically crosslinked nature of the DAT microcarriers used in this study [26]. From a clinical perspective, the natural composition and cell-supportive qualities of these novel DAT microcarriers could also make them well-suited as a direct injectable cell delivery platform for autologous or allogenic cell-based therapies.

Upon confirming expansion of the ASCs on the microcarriers, the focus of the subsequent work was to assess the maintenance of ASC immunophenotype and multilineage differentiation capacity after prolonged dynamic culture in comparison to conventional static culture on TCPS. According to the International Society for Cellular Therapy (ISCT) guidelines, ASCs are defined by greater than 80% positive stromal marker expression and less than 2% negative marker expression, with reported variable expression for CD146 (pericyte-associated marker) and CD34 (progenitor associated marker) [67]. Generally, ASC immunophenotype was preserved for all groups. An interesting trend was observed for both the DAT and Cultispher-S microcarrier expanded ASCs, with reduced expression of CD73 (ecto-5'-nucleotidase), CD105 (endoglin), and CD29 (β1-integrin), which are adhesion molecules involved in cell-cell and cell-ECM interactions [51], [422]. These findings suggest that mechanical effects within the dynamic 3-D culture environment may have modulated the stem cell immunophenotype profile, which has been supported by other studies demonstrating a downregulation of these cell surface markers upon mechanical stimulation via

loading and shear effects. For example, Ode *et al.* showed reduced CD73 and CD29 expression for rat bone marrow-derived stem cells (BMSCs) after mechanical loading at 20% strain, while Kang *et al.* found that increasing cyclic uniaxial mechanical stimulation up to 10% strain resulted in decreased CD105 and CD73 expression in human umbilical cord-derived MSCs [422], [423]. In addition, Frith *et al.* observed a loss in expression of CD29 and CD105 of human MSC spheroids upon shear stress within a spinner flask and rotating wall vessel as compared to monolayer cultures [403]. Based on these findings, it is possible that the shear stress generated within the CELLSPIN system may have contributed to the decreased adhesion marker expression in ASCs. In terms of CD34 and CD146 expression, studies characterizing ASC immunophenotype have shown higher expression in early passages, followed by a decline with continued culture [75], which is generally consistent with the CD146 and CD34 expression patterns in this study. However, the uniformly reduced CD34 expression within the DAT microcarrier group may suggest that the DAT microenvironment and dynamic culturing conditions could be selective for specific subpopulations within the heterogeneous ASC population [424].

With the knowledge that the microenvironment could directly influence cell response and fate [325], [425], quantitative RT-PCR analysis was performed to elucidate the expression of key lineage-specific genes upon 3-D dynamic microcarrier expansion versus 2-D static TCPS expansion of ASCs. The findings suggest that dynamic microcarrier expansion may have been an important factor in the upregulation of some early markers observed. For example, mechanical stimulation from shear stress effects may have contributed to the increased *COMP* expression for ASCs expanded on both types of microcarriers. This is consistent with the observed upregulation of *COMP* expression in bovine chondrocytes after prolonged cyclic compression [426]. In contrast, the significant upregulation of both *PPARγ* and *LPL* for the ASCs expanded on the DAT microcarriers may suggest potential compositional and/or biomechanical effects, similar to the early stages of adipogenesis observed previously on the chemically crosslinked DAT microcarriers and non-

chemically crosslinked DAT foams cultured in proliferation medium [19], [20]. However, while the data suggests that the DAT microcarriers provided a mildly pro-adipogenic microenvironment, the absence of the late-stage marker *ADIPOQ* indicates that the ASCs did not have a mature phenotype. Overall, while there was an upregulation of early adipogenic markers immediately following ASC expansion on the DAT microcarriers, the cells retained the expected ASC immunophenotype and trilineage differentiation capacity following induction, supporting the application of this platform as a generalized ASC expansion strategy.

Currently, the multipotentiality and differentiation efficiency of MSCs harvested after microcarrier expansion has not been extensively characterized [309], [332], [427]. In 2-D culture, MSC proliferation has been reported to decline with time as well as losing their capacity to differentiate towards the adipogenic, osteogenic, and chondrogenic lineages with repeated passaging [2], [3], [280], [281], [428]. This trend was observed in the TCPS expanded group in the current study, which showed significantly reduced levels of adipogenic, osteogenic, and chondrogenic marker expression, including a notable lack of mineralization in the osteogenic differentiation study. Importantly, the ASCs expanded on the DAT microcarriers in this study retained their trilineage differentiation capacity, despite having undergone more than a 50-fold increase in population size. Relative to the Cultispher-S microcarrier group, which had a consistently lower population fold change, the ASCs expanded on the DAT microcarriers demonstrated similar levels of adipogenesis and osteogenesis, as well as enhanced levels of chondrogenesis. Interestingly, the histological results in terms of oil red O and von Kossa staining also suggested that the cells expanded on the DAT microcarriers demonstrated a more uniform differentiation response than those expanded on either the Cultispher-S microcarriers or TCPS, which may be favourable for the application of these cells in differentiation-based cell therapy strategies. The lower stiffness of the DAT microcarriers may have contributed to this enhanced proliferation with preserved differentiation capacity, since mechanical properties of the ECM have

been demonstrated to regulate stem cell self-renewal and differentiation [430], [431]. More specifically, Winer *et al.* showed that human BMSCs cultured on hydrogels possessing an elastic modulus of 0.25 kPa similar to that of bone marrow increased their capacity for self-renewal with maintained multipotentiality as opposed to culturing on stiffer substrates [432]. Compositional factors including cell-ECM and cell-cell interactions during the expansion phase may have also influenced the differentiation potential of the cells. Overall, this study demonstrates the promising use of non-chemically crosslinked DAT microcarriers as a scalable and clinically relevant cell expansion strategy for diverse applications in regenerative medicine.

5.5 Conclusions

The work presented demonstrates that the application of DAT microcarriers in a 3-D stirred bioreactor system is a promising strategy to obtain large populations of ASCs from small tissue biopsies. In particular, a novel fabrication method was developed to synthesize non-chemically crosslinked DAT microcarriers with long-term stability in culture. Proliferation data indicated enhanced ASC attachment and growth on the DAT microcarriers as compared to commercially-available Cultispher-S controls, potentially due to their complex tissue-specific ECM composition, non-chemically crosslinked nature, mechanical properties, and complex surface topography. Flow cytometry confirmed the maintenance of stem cell immunophenotype for all expanded ASCs, with reduced expression levels of the adhesion markers CD73, CD105, and CD29 noted under dynamic culture conditions. Quantitative RT-PCR analysis indicated that dynamic cultivation on the DAT microcarriers upregulated the expression of early adipogenic (*PPARγ* and *LPL*) and chondrogenic (*COMP*) markers following expansion without inducing a mature phenotype. Furthermore, differentiation studies confirmed that the ASCs expanded on the DAT microcarriers retained their multilineage differentiation capacity upon harvesting and subsequent induction with differentiation medium. While ASCs had undergone a significantly higher population fold change when cultured

on the DAT microcarriers, similar levels of adipogenesis and osteogenesis to the Cultispher-S microcarrier expanded ASCs was achieved, with histological data suggesting a more uniform cellular response in the DAT microcarrier group. Interestingly, the highest levels of chondrogenic markers were observed in the DAT microcarrier expanded ASCs relative to all other groups including the TCPS baseline control, suggesting that this platform may be favourable for generating cells for cartilage tissue engineering applications. Overall, these findings help advance current knowledge on the effect of the microenvironment on stem cell behaviour and differentiation potential, and the ASCs expanded using this novel system may hold potential for a range of applications for fat, bone, and cartilage therapies.

.

Chapter 6

Conclusions and Future Work

6.1 Summary and conclusions

With the development of translational cell-based therapies, multipotent adipose-derived stem/stromal cells (ASCs) have surfaced as a promising autologous or allogenic stem cell source [18]. Furthermore, ASCs are clinically practical since significant quantities can be harvested using minimally invasive techniques from relatively small volumes of human fat as compared to bone marrow-derived stem/stromal cells (BMSCs) [433]. While investigation into the broad applications of ASCs has grown over the years, there has also been increasing research into adipose-derived scaffolds in the form of decellularized adipose tissue (DAT). This natural approach arises from knowledge that the native extracellular matrix (ECM) is a key player in mediating cellular responses and can facilitate constructive regeneration upon implantation [325], [434]. Moreover, while there are numerous types of ECM within the body, subtle differences in composition and physical properties have led to the concept that cell processes, such as proliferation and differentiation, can be driven by appropriate cues within the tissue-specific ECM [349]. As a result, these observations provide a strong basis for the combined use of DAT and ASCs in tissue engineering.

In the context of adipose tissue regeneration, tissue-specific approaches integrating DAT and ASCs have been investigated by several groups [14], [16], [19], [21], [22], [276]. More specifically, these studies have shown positive effects in the inductive capabilities of intact DAT bioscaffolds to drive ASC adipogenesis *in vitro*, as well as to promote vascularization and fat formation *in vivo*. Ongoing efforts are now focusing on methods to manipulate the amorphous intact DAT into structured formats that would be advantageous for the creation of reproducible and customizable cell delivery platforms. Enzymatic digestion of DAT has been previously applied by multiple groups to form injectable hydrogels, however, studies into the potential use of well-defined

porous 3-D DAT constructs for soft tissue regeneration remains an area to be further explored [22]–[24].

The rapid progression of ASC-based therapies also points to the need for scalable culture systems to meet the high cell demands in future clinical stem cell-based treatments. To address challenges regarding reduced stem cell proliferation and differentiation capacities with conventional 2-D culture systems on rigid tissue culture polystyrene, the application of custom-designed microcarriers within dynamic bioreactor systems may be a promising approach for the cultivation of ASCs [19], [312], [313]. Bioreactors offer great flexibility, as culturing parameters can be tuned and monitored to more closely mimic the native microenvironment and drive desired cellular responses. Moreover, microcarriers fabricated from biodegradable materials may also serve as an injectable ASC delivery platform. Towards the advancement of microcarrier culture strategies, it is critical to develop a better understanding of how the microenvironment affects ASC behaviour and differentiation potential. Namely, no studies to date have examined the use of a clinically relevant tissue-specific ECM approach using adipose-derived microcarriers for ASC expansion and evaluating the maintenance of multilineage capacity upon extended cultivation within a dynamic culture system.

With regards to the challenges described, this thesis focused on broadening the applications of DAT-based bioscaffolds for the fields of adipose tissue engineering and as a platform for ASC expansion. In particular, novel techniques were developed to process intact DAT into structurally defined 3-D DAT microcarriers and foams applicable for soft tissue repair and/or large-scale bioreactor culture. These studies confirmed the preservation of the adipo-inductive properties of intact DAT following enzymatic digestion with pepsin and α-amylase, thus contributing new insight into the importance of the ECM in mediating ASC adipogenesis *in vitro* and *in vivo.* In addition, this work also demonstrated promising evidence that tissue-specific ECM can be applied to enhance ASC propagation while maintaining multilineage plasticity.

6.2 Significant findings and contributions

1. Investigation of chemically-crosslinked DAT microcarriers as an adipo-inductive substrate for ASCs

The work presented in Chapter 3 showed for the first time the potential of chemically crosslinked DAT microcarriers, prepared from pepsin-digested human DAT, as an adipogenic substrate for human ASCs cultured within a low shear stirred bioreactor system. The results suggested that the native ECM composition may play an important role in mediating ASC differentiation, as demonstrated by the high levels of adipogenesis and the adipo-inductive properties of the DAT microcarriers in comparison to gelatin microcarrier controls. This was confirmed by the observed increase in GPDH activity, lipid accumulation, and expression of adipogenic genes. Furthermore, short term *in vivo* results showed macroscopically stable volume retention, as well as improved tissue remodeling, integration, cellularity, and angiogenesis for the DAT microcarriers relative to the gelatin microcarriers. These findings indicate that the chemically crosslinked DAT microcarriers may represent a potential injectable strategy for soft tissue repair.

2. Development of porous DAT foams for applications in soft tissue regeneration

In Chapter 4, a technique was pioneered to fabricate 3-D porous foams derived from α-amylase-digested human DAT with well-defined properties and were stable in culture without the need for chemical crosslinking. In addition, a novel method was established to fabricate bead foams comprised of interconnected networks of porous DAT beads fused through a controlled freeze-thawing and lyophilization procedure. In support of the previous work in Chapter 3 with the chemically crosslinked DAT microcarriers, the DAT foams and beads foams strongly supported adipogenesis during *in vitro* culture with human ASCs, as demonstrated by GPDH activity and adipogenic gene expression. Furthermore, the foams also had conserved adipo-inductive properties as shown by elevated levels of adipogenic genes in the absence of exogenous differentiation factors.

Interestingly, ASCs cultured on foams possessing a Young's modulus most similar to native fat exhibited enhanced GPDH activity, suggesting that stiffness influenced adipogenic differentiation on the foams. Long term *in vivo* assessment showed that the foams were well-tolerated, integrated into the host tissues, and supported fat formation and angiogenesis. The rapid resorption and strong angiogenic response elicited by the foams as compared to the intact DAT suggests that the foams may be more applicable as biological dressings for wound healing, as opposed to scaffolds for volume augmentation in plastic and reconstructive surgery.

3. Development of non-chemically crosslinked DAT microcarriers for ASC expansion

In Chapter 5, a novel technique was introduced to synthesize non-chemically crosslinked DAT microcarriers by adapting fabrication methods using α-amylase-digested DAT established in Chapter 4. Physical characterization studies confirmed that the DAT microcarriers were highly porous and hydrophilic, possessed both collagen I and IV, and were soft and compliant while remaining stable in long-term culture. *In vitro* studies conducted within a stirred culture system showed significantly higher ASC proliferation on the DAT microcarriers compared to commercially-sourced Cultispher-S microcarriers, with cell infiltration in both microcarrier types at 4 weeks. Moreover, ASC immunophenotype was maintained in all expanded groups and the results also indicated that dynamic culture conditions may have reduced expression levels of the adhesion markers CD73, CD105, and CD29. Insight into the upregulation of some early lineage-specific genes (i.e. *PPARγ, LPL*, and *COMP*) in ASCs expanded on the DAT microcarriers also provided evidence on the possible effects of the culture environment towards cell fate. Upon probing the multilineage differentiation capacity of the expanded ASCs, similar levels of adipogenesis and osteogenesis was measured between the DAT and Cultispher-S microcarrier expanded ASCs, even though the ASCs underwent a higher population fold change on the DAT microcarriers. Furthermore, chondrogenic differentiation was highest in the DAT microcarrier expanded ASCs

relative to all other expanded groups and TCPS baseline controls, which suggests that these ASCs could have potential in cartilage tissue engineering. Towards the development of large scale cell expansion strategies, the data obtained highlighted potential effects of the microenvironment on stem cell proliferation and differentiation capacity and demonstrates the promising use of DAT microcarriers as an ASC expansion platform for diverse applications in regenerative medicine.

6.3 Future recommendations

In terms of short-term goals for the work presented in Chapter 5, the quantitative RT-PCR and chondrogenic differentiation studies should be repeated on additional donors to further validate the observed trends. Furthermore, while TCPS expanded ASCs served as an interesting 2-D control, future studies could consider using frozen stocks of ASCs to be able to match the population fold change for the TCPS expanded group to each of the DAT and Cultispher-S microcarriers for a more direct comparison. It would also be worthwhile to explore a time course in gene expression for each of the lineages to more fully interpret the progression of differentiation among the expanded groups relative to the TCPS baseline control. Other markers such as *FABP4* which is primarily expressed in mature adipocytes, osteopontin which is important in bone remodeling, and collagen VI which is a component of the pericellular matrix in mature chondrocytes could also be included to compliment the current gene panels for each lineage. In terms of long term goals, the following paragraphs discuss some possible future directions for the studies outlined in this thesis.

Several groups have demonstrated that ECM-derived substrates can provide an instructive microenvironment for directing stem cell differentiation in a tissue-specific manner [14], [26], [212], [213]. For instance, Zhang *et al.* found that tissue-specific ECM coatings prepared from decellularized skin, liver, and muscle tissues were able to promote lineage-specific differentiation of tissue-matched cell types [348]. This observation is further supported from the results obtained in this thesis, showing the natural inductive properties of DAT bioscaffolds to promote ASC

adipogenesis. In extension of these findings, it would be worthwhile to apply the foam and microcarrier fabrication methods to create other tissue-specific ECM scaffolds, such as from the dermis, heart, cartilage, and bone. By combining these constructs with the appropriate tissue-matched cells, it would be interesting to examine whether the inductive properties of these ECM scaffolds would enhance the maintenance of the native phenotype within a 3-D environment.

Alternatively, rather than using tissue-matched cells, ASCs could also be cultivated on different decellularized tissue scaffolds to promote desired cell phenotypes (e.g. osteogenesis and chondrogenesis) for applications beyond adipose tissue engineering. For example, other studies in the Flynn lab have previously shown that decellularized non-chemically crosslinked cardiac foams served as a mildly inductive substrate for the cardiomyogenesis of pericardial fat ASCs [241]. By exploring the response of ASCs cultured on a variety of different ECM constructs, the importance of the tissue-specific ECM can be further elucidated. These studies are important to more fully support the rationale of using tissue-specific ECM since most work to date, including the Flynn lab, have focused on using ECM from the tissue source they are trying to regenerate [14], [88], [213], [349].

While scaffold properties are important, the mechanical environment is also critical in providing external cues to influence stem cell fate [357]. More specifically, *in vitro* ASC osteogenesis can be modulated dynamically by fluid shear stress and/or passively by responding to the scaffold elastic modulus, ultrastructure, and biochemical composition [435]. Namely, this phenomenon has been demonstrated by several studies showing enhanced osteogenic differentiation when ASCs were cultured dynamically on microcarriers [311], [332]. Further, hypoxic conditions have been shown to enhance ASC proliferative capacity as well as influence differentiation, thus this would also be a worthwhile parameter to investigate [436]. In this context, it would be interesting to build upon the work in Chapter 3 and explore ASC multilineage differentiation directly on the microcarriers within a CELLSPIN system. More specifically, shear stress and

oxygen tension could be tuned in separate proliferation and differentiation stages to drive growth followed by lineage-specific differentiation.

With the development of cell-based therapies it is crucial to ensure culture methods are compliant with GMP guidelines for clinical translation and commercialization. One aspect that was not explored in this work was the use of serum-free media to overcome potential issues of xenogenicity and disease transmission associated with fetal bovine serum. To date, limited studies have examined the use of serum-free media culture in a microcarrier culture system for MSCs [339]–[341]. Thus, applying serum-free conditions to the DAT microcarrier culture system would represent a more clinically relevant approach for large-scale ASC propagation. While ASC expansion was the primary focus in this thesis, direct seeding of the adipose stromal vascular fraction (SVF) population would also be of clinical value to streamline processes by avoiding the need for pre-selection on tissue culture polystyrene [46]. Thus, it would be interesting to elucidate differences in proliferation and differentiation between the heterogeneous SVF versus the more homogeneous ASC population.

In terms of future *in vivo* work, while the DAT foams and bead foams were capable of promoting adipogenesis, their fast resorption rate in comparison to intact DAT suggests that they may not be well suited for soft tissue augmentation. More specifically, the enhanced cellularity and the strong angiogenic response elicited by the DAT foams and bead foams presented a potential alternative use as a wound healing substrate, such as for diabetic foot ulcers. Namely, the constituents of the ECM could promote the recruitment of host cells and drive a pro-regenerative cascade, while the porous network could provide a permissive environment for the migration of resident endothelial cells and fibroblasts during tissue remodelling. In this regard, *in vivo* studies using a diabetic mouse model may possibly shed light on the efficacy of porous DAT foams for the treatment of chronic wounds.

References

[1] P. K. T. Subbanna, “Mesenchymal stem cells for treating GVHD: in-vivo fate and optimal dose.,” *Med. Hypotheses*, vol. 69, no. 2, pp. 469–70, Jan. 2007.

[2] Y. Zhao, S. D. Waldman, and L. E. Flynn, “The effect of serial passaging on the proliferation and differentiation of bovine adipose-derived stem cells.,” *Cells. Tissues. Organs*, vol. 195, no. 5, pp. 414–27, Jan. 2012.

[3] M. E. Wall, S. H. Bernacki, and E. G. Loboa, “Effects of serial passaging on the adipogenic and osteogenic differentiation potential of adipose-derived human mesenchymal stem cells.,” *Tissue Eng.*, vol. 13, no. 6, pp. 1291–8, Jun. 2007.

[4] M. Wagner, B. Hampel, D. Bernhard, M. Hala, W. Zwerschke, and P. Jansen-Dürr, “Replicative senescence of human endothelial cells in vitro involves G1 arrest, polyploidization and senescence-associated apoptosis,” *Exp. Gerontol.*, vol. 36, no. 8, pp. 1327–1347, Aug. 2001.

[5] X.-F. Tian, B.-C. Heng, Z. Ge, K. Lu, A. J. Rufaihah, V. T.-W. Fan, J.-F. Yeo, and T. Cao, “Comparison of osteogenesis of human embryonic stem cells within 2D and 3D culture systems.,” *Scand. J. Clin. Lab. Invest.*, vol. 68, no. 1, pp. 58–67, Jan. 2008.

[6] H. Shin, S. Jo, and A. G. Mikos, “Biomimetic materials for tissue engineering.,” *Biomaterials*, vol. 24, no. 24, pp. 4353–64, Nov. 2003.

[7] M. Liu, N. Liu, R. Zang, Y. Li, and S.-T. Yang, “Engineering stem cell niches in bioreactors.,” *World J. Stem Cells*, vol. 5, no. 4, pp. 124–35, Oct. 2013.

[8] R. Peerani and P. W. Zandstra, “Enabling stem cell therapies through synthetic stem cell-niche engineering.,” *J. Clin. Invest.*, vol. 120, no. 1, pp. 60–70, Jan. 2010.

[9] K. A. Moore, “Stem Cells and Their Niches,” *Science*, vol. 311, no. 5769, pp. 1880–85, Mar. 2006.

[10] M. F. Brizzi, G. Tarone, and P. Defilippi, “Extracellular matrix, integrins, and growth factors as tailors of the stem cell niche.,” *Curr. Opin. Cell Biol.*, pp. 1–7, Aug. 2012.

[11] S. M. Dellatore, A. S. Garcia, and W. M. Miller, “Mimicking stem cell niches to increase stem cell expansion.,” *Curr. Opin. Biotechnol.*, vol. 19, no. 5, pp. 534–40, Oct. 2008.

[12] M. Votteler, P. J. Kluger, H. Walles, and K. Schenke-Layland, “Stem cell microenvironments--unveiling the secret of how stem cell fate is defined.,” *Macromol. Biosci.*, vol. 10, no. 11, pp. 1302–15, Nov. 2010.

[13] C. R. Nuttelman, M. C. Tripodi, and K. S. Anseth, “Synthetic hydrogel niches that promote hMSC viability.,” *Matrix Biol.*, vol. 24, no. 3, pp. 208–18, May 2005.

[14] L. E. Flynn, “The use of decellularized adipose tissue to provide an inductive microenvironment for the adipogenic differentiation of human adipose-derived stem cells.,” *Biomaterials*, vol. 31, no. 17, pp. 4715–24, Jun. 2010.

[15] J. S. Choi, H.-J. Yang, B. S. Kim, J. D. Kim, S. H. Lee, E. K. Lee, K. Park, Y. W. Cho, and H. Y. Lee, “Fabrication of porous extracellular matrix scaffolds from human adipose tissue.,” *Tissue Eng. Part C. Methods*, vol. 16, no. 3, pp. 387–96, Jun. 2010.

[16] B. N. Brown, J. M. Freund, L. Han, J. P. Rubin, J. E. Reing, E. M. Jeffries, M. T. Wolf, S.

Tottey, C. A. Barnes, B. D. Ratner, and S. F. Badylak, “Comparison of three methods for the derivation of a biologic scaffold composed of adipose tissue extracellular matrix.,” *Tissue Eng. Part C. Methods*, vol. 17, no. 4, pp. 411–21, Apr. 2011.

[17] P. A. Zuk, M. Zhu, P. Ashjian, D. A. De Ugarte, J. I. Huang, H. Mizuno, Z. C. Alfonso, J. K. Fraser, P. Benhaim, and M. H. Hedrick, “Human adipose tissue is a source of multipotent stem cells.,” *Mol. Biol. Cell*, vol. 13, no. 12, pp. 4279–95, Dec. 2002.

[18] P. A. Zuk, M. Zhu, H. Mizuno, J. Huang, J. W. Futrell, A. J. Katz, P. Benhaim, H. P. Lorenz, and M. H. Hedrick, “Multilineage cells from human adipose tissue: implications for cell-based therapies.,” *Tissue Eng.*, vol. 7, no. 2, pp. 211–28, Apr. 2001.

[19] A. E. B. Turner, C. Yu, J. Bianco, J. F. Watkins, and L. E. Flynn, “The performance of decellularized adipose tissue microcarriers as an inductive substrate for human adipose-derived stem cells.,” *Biomaterials*, vol. 33, no. 18, pp. 4490–9, Jun. 2012.

[20] C. Yu, J. Bianco, C. Brown, L. Fuetterer, J. F. Watkins, A. Samani, and L. E. Flynn, “Porous decellularized adipose tissue foams for soft tissue regeneration.,” *Biomaterials*, vol. 34, no. 13, pp. 3290–302, Apr. 2013.

[21] L. Wang, J. A. Johnson, Q. Zhang, and E. K. Beahm, “Combining decellularized human adipose tissue extracellular matrix and adipose-derived stem cells for adipose tissue engineering.,” *Acta Biomater.*, vol. 9, no. 11, pp. 8921–31, Nov. 2013.

[22] H. K. Cheung, T. T. Y. Han, D. M. Marecak, J. F. Watkins, B. G. Amsden, and L. E. Flynn, “Composite hydrogel scaffolds incorporating decellularized adipose tissue for soft tissue engineering with adipose-derived stem cells.,” *Biomaterials*, vol. 35, no. 6, pp. 1914–23, Feb. 2014.

[23] J. H. Choi, J. M. Gimble, K. Lee, K. G. Marra, J. P. Rubin, J. J. Yoo, G. Vunjak-Novakovic, and D. L. Kaplan, “Adipose tissue engineering for soft tissue regeneration.,” *Tissue Eng. Part B. Rev.*, vol. 16, no. 4, pp. 413–26, Aug. 2010.

[24] D. A. Young and K. L. Christman, “Injectable biomaterials for adipose tissue engineering.,” *Biomed. Mater.*, vol. 7, no. 2, p. 024104, Apr. 2012.

[25] Y. C. Choi, J. S. Choi, C. H. Woo, and Y. W. Cho, “Stem cell delivery systems inspired by tissue-specific niches,” *J. Control. Release*, vol. 193, pp. 42–50, Nov. 2014.

[26] A. E. B. Turner and L. E. Flynn, “Design and characterization of tissue-specific extracellular matrix-derived microcarriers.,” *Tissue Eng. Part C. Methods*, vol. 18, no. 3, pp. 186–97, Mar. 2012.

[27] J. B. Hansen and K. Kristiansen, “Regulatory circuits controlling white versus brown adipocyte differentiation.,” *Biochem. J.*, vol. 398, no. 2, pp. 153–68, Sep. 2006.

[28] M. H. Fonseca-Alaniz, J. Takada, M. I. C. Alonso-Vale, and F. B. Lima, “Adipose tissue as an endocrine organ: from theory to practice,” *J. Pediatr. (Rio. J).*, vol. 83, no. 5 Suppl, pp. S192–203, Nov. 2007.

[29] P. Trayhurn and J. H. Beattie, “Physiological role of adipose tissue: white adipose tissue as an endocrine and secretory organ.,” *Proc. Nutr. Soc.*, vol. 60, no. 3, pp. 329–39, Aug. 2001.

[30] P. Trayhurn and I. S. Wood, “Adipokines: inflammation and the pleiotropic role of white adipose tissue,” *Br. J. Nutr.*, vol. 92, no. 3, p. 347, Mar. 2007.

[31] P. Seale and M. A. Lazar, “Brown fat in humans: turning up the heat on obesity.,” *Diabetes*,

vol. 58, no. 7, pp. 1482–4, Jul. 2009.

[32] B. Cannon and J. Nedergaard, “Brown adipose tissue: function and physiological significance.,” *Physiol. Rev.*, vol. 84, no. 1, pp. 277–359, Jan. 2004.

[33] W. D. van Marken Lichtenbelt, J. W. Vanhommerig, N. M. Smulders, J. M. A. F. L. Drossaerts, G. J. Kemerink, N. D. Bouvy, P. Schrauwen, and G. J. J. Teule, “Cold-activated brown adipose tissue in healthy men.,” *N. Engl. J. Med.*, vol. 360, no. 15, pp. 1500–8, May 2009.

[34] A. J. Friedenstein, I. I. Piatetzky-Shapiro, and K. V. Petrakova, “Osteogenesis in transplants of bone marrow cells,” *J Embryol Exp Morphol*, vol. 16, no. 3, pp. 381–90, Dec. 1966.

[35] A. J. Friedenstein, K. V Petrakova, A. I. Kurolesova, and G. P. Frolova, “Heterotopic of bone marrow. Analysis of precursor cells for osteogenic and hematopoietic tissues.,” *Transplantation*, vol. 6, no. 2, pp. 230–47, Mar. 1968.

[36] P. A. Zuk, M. Zhu, P. Ashjian, D. A. De Ugarte, J. I. Huang, H. Mizuno, Z. C. Alfonso, J. K. Fraser, P. Benhaim, and M. H. Hedrick, “Human adipose tissue is a source of multipotent stem cells.,” *Mol. Biol. Cell*, vol. 13, no. 12, pp. 4279–95, Dec. 2002.

[37] M. J. Griffiths, D. Bonnet, and S. M. Janes, “Stem cells of the alveolar epithelium,” *Lancet*, vol. 366, no. 9481, pp. 249–60, Jul. 2005.

[38] A. P. Beltrami, L. Barlucchi, D. Torella, M. Baker, F. Limana, S. Chimenti, H. Kasahara, M. Rota, E. Musso, K. Urbanek, A. Leri, J. Kajstura, B. Nadal-Ginard, and P. Anversa, “Adult cardiac stem cells are multipotent and support myocardial regeneration.,” *Cell*, vol. 114, no. 6, pp. 763–76, Sep. 2003.

[39] P.-P. Chong, L. Selvaratnam, A. A. Abbas, and T. Kamarul, “Human peripheral blood derived mesenchymal stem cells demonstrate similar characteristics and chondrogenic differentiation potential to bone marrow derived mesenchymal stem cells.,” *J. Orthop. Res.*, vol. 30, no. 4, pp. 634–42, Apr. 2012.

[40] J. G. Toma, M. Akhavan, K. J. L. Fernandes, F. Barnabé-Heider, A. Sadikot, D. R. Kaplan, and F. D. Miller, “Isolation of multipotent adult stem cells from the dermis of mammalian skin,” *Nat. Cell Biol.*, vol. 3, no. 9, pp. 778–84, Sep. 2001.

[41] S. A. Wexler, C. Donaldson, P. Denning-Kendall, C. Rice, B. Bradley, and J. M. Hows, “Adult bone marrow is a rich source of human mesenchymal ‘stem’ cells but umbilical cord and mobilized adult blood are not.,” *Br. J. Haematol.*, vol. 121, no. 2, pp. 368–74, Apr. 2003.

[42] M. M. Bonab, K. Alimoghaddam, F. Talebian, S. H. Ghaffari, A. Ghavamzadeh, and B. Nikbin, “Aging of mesenchymal stem cell in vitro.,” *BMC Cell Biol.*, vol. 7, p. 14, Jan. 2006.

[43] C. H. Hollenberg and A. Vost, “Regulation of DNA synthesis in fat cells and stromal elements from rat adipose tissue.,” *J. Clin. Invest.*, vol. 47, no. 11, pp. 2485–98, Nov. 1969.

[44] J. M. Gimble, A. J. Katz, and B. A. Bunnell, “Adipose-derived stem cells for regenerative medicine.,” *Circ. Res.*, vol. 100, no. 9, pp. 1249–60, May 2007.

[45] B. M. Strem, K. C. Hicok, M. Zhu, I. Wulur, Z. Alfonso, R. E. Schreiber, J. K. Fraser, and M. H. Hedrick, “Multipotential differentiation of adipose tissue-derived stem cells.,” *Keio J. Med.*, vol. 54, no. 3, pp. 132–41, Sep. 2005.

[46] J. M. Gimble, B. A. Bunnell, E. S. Chiu, and F. Guilak, “Concise review: Adipose-derived stromal vascular fraction cells and stem cells: let’s not get lost in translation.,” *Stem Cells*,

vol. 29, no. 5, pp. 749–54, May 2011.

[47] B. Peterson, J. Zhang, R. Iglesias, M. Kabo, M. Hedrick, P. Benhaim, and J. R. Lieberman, “Healing of critically sized femoral defects, using genetically modified mesenchymal stem cells from human adipose tissue.,” *Tissue Eng.*, vol. 11, no. 1–2, pp. 120–9, Jan. 2005.

[48] M. Oedayrajsingh-Varma, S. van Ham, M. Knippenberg, M. Helder, J. Klein-Nulend, T. Schouten, M. Ritt, and F. van Milligen, “Adipose tissue-derived mesenchymal stem cell yield and growth characteristics are affected by the tissue-harvesting procedure,” *Cytotherapy*, vol. 8, no. 2, pp. 166-77, Jul. 2009.

[49] A. Schäffler and C. Büchler, “Concise review: adipose tissue-derived stromal cells--basic and clinical implications for novel cell-based therapies.,” *Stem Cells*, vol. 25, no. 4, pp. 818–27, Apr. 2007.

[50] W. Wagner and A. D. Ho, “Mesenchymal stem cell preparations--comparing apples and oranges.,” *Stem Cell Rev.*, vol. 3, no. 4, pp. 239–48, Dec. 2007.

[51] F. Haasters, W. C. Prall, D. Anz, C. Bourquin, C. Pautke, S. Endres, W. Mutschler, D. Docheva, and M. Schieker, “Morphological and immunocytochemical characteristics indicate the yield of early progenitors and represent a quality control for human mesenchymal stem cell culturing.,” *J. Anat.*, vol. 214, no. 5, pp. 759–67, May 2009.

[52] P. C. Baer and H. Geiger, “Adipose-derived mesenchymal stromal/stem cells: tissue localization, characterization, and heterogeneity.,” *Stem Cells Int.*, vol. 2012, p. 812693, Jan. 2012.

[53] F. Guilak, K. E. Lott, H. A. Awad, Q. Cao, K. C. Hicok, B. Fermor, and J. M. Gimble, “Clonal analysis of the differentiation potential of human adipose-derived adult stem cells.,” *J. Cell. Physiol.*, vol. 206, no. 1, pp. 229–37, Jan. 2006.

[54] M. S. Choudhery, M. Badowski, A. Muise, J. Pierce, and D. T. Harris, “Donor age negatively impacts adipose tissue-derived mesenchymal stem cell expansion and differentiation.,” *J. Transl. Med.*, vol. 12, p. 8, Jan. 2014.

[55] M. Zhu, E. Kohan, J. Bradley, M. Hedrick, P. Benhaim, and P. Zuk, “The effect of age on osteogenic, adipogenic and proliferative potential of female adipose-derived stem cells.,” *J. Tissue Eng. Regen. Med.*, vol. 3, no. 4, pp. 290–301, Jun. 2009.

[56] L. de Girolamo, S. Lopa, E. Arrigoni, M. F. Sartori, F. W. Baruffaldi Preis, and A. T. Brini, “Human adipose-derived stem cells isolated from young and elderly women: their differentiation potential and scaffold interaction during in vitro osteoblastic differentiation.,” *Cytotherapy*, vol. 11, no. 6, pp. 793–803, Jan. 2009.

[57] T. P. Frazier, J. M. Gimble, J. W. Devay, H. A. Tucker, E. S. Chiu, and B. G. Rowan, “Body mass index affects proliferation and osteogenic differentiation of human subcutaneous adipose tissue-derived stem cells.,” *BMC Cell Biol.*, vol. 14, p. 34, Jan. 2013.

[58] V. van Harmelen, T. Skurk, K. Röhrig, Y.-M. Lee, M. Halbleib, I. Aprath-Husmann, and H. Hauner, “Effect of BMI and age on adipose tissue cellularity and differentiation capacity in women.,” *Int. J. Obes. Relat. Metab. Disord.*, vol. 27, no. 8, pp. 889–95, Aug. 2003.

[59] A. Mojallal, C. Lequeux, C. Shipkov, A. Duclos, F. Braye, R. Rohrich, S. Brown, and O. Damour, “Influence of age and body mass index on the yield and proliferation capacity of adipose-derived stem cells.,” *Aesthetic Plast. Surg.*, vol. 35, no. 6, pp. 1097–105, Dec. 2011.

[60] G. Yu, X. Wu, M. A. Dietrich, P. Polk, L. K. Scott, A. A. Ptitsyn, and J. M. Gimble, “Yield

and characterization of subcutaneous human adipose-derived stem cells by flow cytometric and adipogenic mRNA analyzes.," *Cytotherapy*, vol. 12, no. 4, pp. 538–46, Jul. 2010.

[61] B. M. Schipper, K. G. Marra, W. Zhang, A. D. Donnenberg, and J. P. Rubin, "Regional anatomic and age effects on cell function of human adipose-derived stem cells.," *Ann. Plast. Surg.*, vol. 60, no. 5, pp. 538–44, May 2008.

[62] V. Russo, C. Yu, P. Belliveau, A. Hamilton, and L. E. Flynn, "Comparison of human adipose-derived stem cells isolated from subcutaneous, omental, and intrathoracic adipose tissue depots for regenerative applications.," *Stem Cells Transl. Med.*, vol. 3, no. 2, pp. 206–17, Feb. 2014.

[63] A. E. Aksu, J. P. Rubin, J. R. Dudas, and K. G. Marra, "Role of gender and anatomical region on induction of osteogenic differentiation of human adipose-derived stem cells.," *Ann. Plast. Surg.*, vol. 60, no. 3, pp. 306–22, Mar. 2008.

[64] M. Corselli, C.-W. Chen, M. Crisan, L. Lazzari, and B. Péault, "Perivascular ancestors of adult multipotent stem cells.," *Arterioscler. Thromb. Vasc. Biol.*, vol. 30, no. 6, pp. 1104–9, Jun. 2010.

[65] G. Lin, M. Garcia, H. Ning, L. Banie, Y.-L. Guo, T. F. Lue, and C.-S. Lin, "Defining stem and progenitor cells within adipose tissue.," *Stem Cells Dev.*, vol. 17, no. 6, pp. 1053–63, Dec. 2008.

[66] J. T. Wright and G. J. Hausman, "Monoclonal antibodies against cell surface antigens expressed during porcine adipocyte differentiation.," *Int. J. Obes.*, vol. 14, no. 5, pp. 395–409, May 1990.

[67] P. Bourin, B. A. Bunnell, L. Casteilla, M. Dominici, A. J. Katz, K. L. March, H. Redl, J. P. Rubin, K. Yoshimura, and J. M. Gimble, "Stromal cells from the adipose tissue-derived stromal vascular fraction and culture expanded adipose tissue-derived stromal/stem cells: a joint statement of the International Federation for Adipose Therapeutics and Science (IFATS) and the International So," *Cytotherapy*, vol. 15, no. 6, pp. 641–8, Jun. 2013.

[68] M. F. Pittenger, A. M. Mackay, S. C. Beck, R. K. Jaiswal, R. Douglas, J. D. Mosca, M. A. Moorman, D. W. Simonetti, S. Craig, and D. R. Marshak, "Multilineage potential of adult human mesenchymal stem cells.," *Science*, vol. 284, no. 5411, pp. 143–7, Apr. 1999.

[69] K. McIntosh, S. Zvonic, S. Garrett, J. B. Mitchell, Z. E. Floyd, L. Hammill, A. Kloster, Y. Di Halvorsen, J. P. Ting, R. W. Storms, B. Goh, G. Kilroy, X. Wu, and J. M. Gimble, "The immunogenicity of human adipose-derived cells: temporal changes in vitro.," *Stem Cells*, vol. 24, no. 5, pp. 1246–53, May 2006.

[70] D. O. Traktuev, S. Merfeld-Clauss, J. Li, M. Kolonin, W. Arap, R. Pasqualini, B. H. Johnstone, and K. L. March, "A population of multipotent CD34-positive adipose stromal cells share pericyte and mesenchymal surface markers, reside in a periendothelial location, and stabilize endothelial networks.," *Circ. Res.*, vol. 102, no. 1, pp. 77–85, Jan. 2008.

[71] M. Higuchi, G. J. Dusting, H. Peshavariya, F. Jiang, S. T.-F. Hsiao, E. C. Chan, and G.-S. Liu, "Differentiation of Human Adipose-Derived Stem Cells into Fat Involves Reactive Oxygen Species and Forkhead Box O1 Mediated Upregulation of Antioxidant Enzymes.," *Stem Cells Dev.*, vol. 22, no. 6, pp. 878-88, Nov. 2012.

[72] S. Gronthos, D. M. Franklin, H. A. Leddy, P. G. Robey, R. W. Storms, and J. M. Gimble, "Surface protein characterization of human adipose tissue-derived stromal cells.," *J. Cell. Physiol.*, vol. 189, no. 1, pp. 54–63, Oct. 2001.

[73] P. C. Baer, “Adipose-derived mesenchymal stromal/stem cells: An update on their phenotype in vivo and in vitro.,” *World J. Stem Cells*, vol. 6, no. 3, pp. 256–65, Jul. 2014.

[74] A. Scherberich, N. Di Di Maggio, and K. M. McNagny, “A familiar stranger: CD34 expression and putative functions in SVF cells of adipose tissue.,” *World J. Stem Cells*, vol. 5, no. 1, pp. 1–8, Jan. 2013.

[75] J. B. Mitchell, K. McIntosh, S. Zvonic, S. Garrett, Z. E. Floyd, A. Kloster, Y. Di Halvorsen, R. W. Storms, B. Goh, G. Kilroy, X. Wu, and J. M. Gimble, “Immunophenotype of human adipose-derived cells: temporal changes in stromal-associated and stem cell-associated markers.,” *Stem Cells*, vol. 24, no. 2, pp. 376–85, Feb. 2006.

[76] E. Y. Lee, Y. Xia, W.-S. Kim, M. H. Kim, T. H. Kim, K. J. Kim, B.-S. Park, and J.-H. Sung, “Hypoxia-enhanced wound-healing function of adipose-derived stem cells: increase in stem cell proliferation and up-regulation of VEGF and bFGF.,” *Wound Repair Regen.*, vol. 17, no. 4, pp. 540–7, Jan. .

[77] W.-S. Kim, B.-S. Park, J.-H. Sung, J.-M. Yang, S.-B. Park, S.-J. Kwak, and J.-S. Park, “Wound healing effect of adipose-derived stem cells: a critical role of secretory factors on human dermal fibroblasts.,” *J. Dermatol. Sci.*, vol. 48, no. 1, pp. 15–24, Oct. 2007.

[78] S. P. Blaber, R. A. Webster, C. J. Hill, E. J. Breen, D. Kuah, G. Vesey, and B. R. Herbert, “Analysis of in vitro secretion profiles from adipose-derived cell populations.,” *J. Transl. Med.*, vol. 10, p. 172, Jan. 2012.

[79] R. Yañez, A. Oviedo, M. Aldea, J. A. Bueren, and M. L. Lamana, “Prostaglandin E2 plays a key role in the immunosuppressive properties of adipose and bone marrow tissue-derived mesenchymal stromal cells.,” *Exp. Cell Res.*, vol. 316, no. 19, pp. 3109–23, Nov. 2010.

[80] J. Rehman, D. Traktuev, J. Li, S. Merfeld-Clauss, C. J. Temm-Grove, J. E. Bovenkerk, C. L. Pell, B. H. Johnstone, R. V Considine, and K. L. March, “Secretion of angiogenic and antiapoptotic factors by human adipose stromal cells.,” *Circulation*, vol. 109, no. 10, pp. 1292–8, Mar. 2004.

[81] M. P. Francis, P. C. Sachs, P. a Madurantakam, S. a Sell, L. W. Elmore, G. L. Bowlin, and S. E. Holt, “Electrospinning adipose tissue-derived extracellular matrix for adipose stem cell culture.,” *J. Biomed. Mater. Res. A*, vol. 100, no. 7, pp. 1716–24, Jul. 2012.

[82] J. Rehman, D. Traktuev, J. Li, S. Merfeld-Clauss, C. J. Temm-Grove, J. E. Bovenkerk, C. L. Pell, B. H. Johnstone, R. V Considine, and K. L. March, “Secretion of angiogenic and antiapoptotic factors by human adipose stromal cells.,” *Circulation*, vol. 109, no. 10, pp. 1292–8, Mar. 2004.

[83] W.-S. Kim and J.-H. Sung, “Hypoxic Culturing Enhances the Wound-Healing Potential of Adipose-Derived Stem Cells,” *Adv. Wound Care*, vol. 1, no. 14, pp. 172-76, Aug. 2012.

[84] W. L. Grayson, F. Zhao, B. Bunnell, and T. Ma, “Hypoxia enhances proliferation and tissue formation of human mesenchymal stem cells.,” *Biochem. Biophys. Res. Commun.*, vol. 358, no. 3, pp. 948–53, Jul. 2007.

[85] E. Potier, E. Ferreira, R. Andriamanalijaona, J.-P. Pujol, K. Oudina, D. Logeart-Avramoglou, and H. Petite, “Hypoxia affects mesenchymal stromal cell osteogenic differentiation and angiogenic factor expression.,” *Bone*, vol. 40, no. 4, pp. 1078–87, May 2007.

[86] S. T.-F. Hsiao, A. Asgari, Z. Lokmic, R. Sinclair, G. J. Dusting, S. Y. Lim, and R. J. Dilley, “Comparative analysis of paracrine factor expression in human adult mesenchymal stem cells

derived from bone marrow, adipose, and dermal tissue.," *Stem Cells Dev.*, vol. 21, no. 12, pp. 2189–203, Aug. 2012.

[87] C. N. Manning, C. Martel, S. E. Sakiyama-Elbert, M. J. Silva, S. Shah, R. H. Gelberman, and S. Thomopoulos, "Adipose-derived mesenchymal stromal cells modulate tendon fibroblast responses to macrophage-induced inflammation in vitro.," *Stem Cell Res. Ther.*, vol. 6, p. 74, Jan. 2015.

[88] T. T. Y. Han, S. Toutounji, B. G. Amsden, and L. E. Flynn, "Adipose-derived stromal cells mediate in vivo adipogenesis, angiogenesis and inflammation in decellularized adipose tissue bioscaffolds.," *Biomaterials*, vol. 72, pp. 125–37, Dec. 2015.

[89] K.-S. Cho, H.-K. Park, H.-Y. Park, J. S. Jung, S.-G. Jeon, Y.-K. Kim, and H. J. Roh, "IFATS collection: Immunomodulatory effects of adipose tissue-derived stem cells in an allergic rhinitis mouse model.," *Stem Cells*, vol. 27, no. 1, pp. 259–65, Jan. 2009.

[90] J. Gimble and F. Guilak, "Adipose-derived adult stem cells: isolation, characterization, and differentiation potential.," *Cytotherapy*, vol. 5, no. 5, pp. 362–9, Jan. 2003.

[91] O. A. MacDougald and S. Mandrup, "Adipogenesis: forces that tip the scales," *Trends Endocrinol. Metab.*, vol. 13, no. 1, pp. 5–11, Jan. 2002.

[92] T. M. Loftus and M. D. Lane, "Modulating the transcriptional control of adipogenesis.," *Curr. Opin. Genet. Dev.*, vol. 7, no. 5, pp. 603–8, Oct. 1997.

[93] Q. Q. Tang and M. D. Lane, "Role of C/EBP homologous protein (CHOP-10) in the programmed activation of CCAAT/enhancer-binding protein-beta during adipogenesis.," *Proc. Natl. Acad. Sci. U. S. A.*, vol. 97, no. 23, pp. 12446–50, Nov. 2000.

[94] E. D. Rosen, C. J. Walkey, P. Puigserver, and B. M. Spiegelman, "Transcriptional regulation of adipogenesis," *Genes & Dev.*, vol. 14, no. 11, pp. 1293–1307, Jun. 2000.

[95] "A new selective peroxisome proliferator-activated receptor gamma antagonist with antiobesity and antidiabetic activity.," *Mol. Endocrinol.*, vol. 16, no. 11, pp. 2628–44, Nov. 2002.

[96] S. Tyagi, P. Gupta, A. S. Saini, C. Kaushal, and S. Sharma, "The peroxisome proliferator-activated receptor: A family of nuclear receptors role in various diseases.," *J. Adv. Pharm. Technol. Res.*, vol. 2, no. 4, pp. 236–40, Oct. 2011.

[97] J. B. Kim, H. M. Wright, M. Wright, and B. M. Spiegelman, "ADD1/SREBP1 activates PPARgamma through the production of endogenous ligand.," *Proc. Natl. Acad. Sci. U. S. A.*, vol. 95, no. 8, pp. 4333–7, Apr. 1998.

[98] M. J. Reginato, S. L. Krakow, S. T. Bailey, and M. A. Lazar, "Prostaglandins promote and block adipogenesis through opposing effects on peroxisome proliferator-activated receptor," *J. Biol. Chem.*, vol. 273, no. 4, pp. 1855–58, Jan. 1998.

[99] M. A. Scott, V. T. Nguyen, B. Levi, and A. W. James, "Current methods of adipogenic differentiation of mesenchymal stem cells.," *Stem Cells Dev.*, vol. 20, no. 10, pp. 1793–804, Oct. 2011.

[100] B. Galateanu, S. Dinescu, A. Cimpean, A. Dinischiotu, and M. Costache, "Modulation of adipogenic conditions for prospective use of hADSCs in adipose tissue engineering.," *Int. J. Mol. Sci.*, vol. 13, no. 12, pp. 15881–900, Jan. 2012.

[101] B. A. Bunnell, M. Flaat, C. Gagliardi, B. Patel, and C. Ripoll, "Adipose-derived stem cells:

isolation, expansion and differentiation.," *Methods*, vol. 45, no. 2, pp. 115–20, Jun. 2008.

[102] J. A. Levine, M. D. Jensen, N. L. Eberhardt, and T. O'Brien, "Adipocyte macrophage colony-stimulating factor is a mediator of adipose tissue growth.," *J. Clin. Invest.*, vol. 101, no. 8, pp. 1557–64, Apr. 1998.

[103] M. Moldes, M. Boizard, X. L. Liepvre, B. Fève, I. Dugail, and J. Pairault, "Functional antagonism between inhibitor of DNA binding (Id) and adipocyte determination and differentiation factor 1/sterol regulatory element-binding protein-1c (ADD1/SREBP-1c) trans-factors for the regulation of fatty acid synthase promoter in adipocyte," *Biochem. J.*, vol. 344 Pt 3, pp. 873–80, Dec. 1999.

[104] J.-E. Lee and K. Ge, "Transcriptional and epigenetic regulation of PPARγ expression during adipogenesis.," *Cell Biosci.*, vol. 4, p. 29, Jan. 2014.

[105] B. E. Grottkau and Y. Lin, "Osteogenesis of Adipose-Derived Stem Cells.," *Bone Res.*, vol. 1, no. 2, pp. 133–45, Jun. 2013.

[106] S. Marcellini, J. P. Henriquez, and A. Bertin, "Control of osteogenesis by the canonical Wnt and BMP pathways in vivo: cooperation and antagonism between the canonical Wnt and BMP pathways as cells differentiate from osteochondroprogenitors to osteoblasts and osteocytes.," *Bioessays*, vol. 34, no. 11, pp. 953–62, Nov. 2012.

[107] Y. Honda, X. Ding, F. Mussano, A. Wiberg, C.-M. Ho, and I. Nishimura, "Guiding the osteogenic fate of mouse and human mesenchymal stem cells through feedback system control.," *Sci. Rep.*, vol. 3, p. 3420, Jan. 2013.

[108] M. Phimphilai, Z. Zhao, H. Boules, H. Roca, and R. T. Franceschi, "BMP signaling is required for RUNX2-dependent induction of the osteoblast phenotype.," *J. Bone Miner. Res.*, vol. 21, no. 4, pp. 637–46, Apr. 2006.

[109] J. A. Jadlowiec, A. B. Celil, and J. O. Hollinger, "Bone tissue engineering: recent advances and promising therapeutic agents.," *Expert Opin. Biol. Ther.*, vol. 3, no. 3, pp. 409–23, Jun. 2003.

[110] K. Nakashima and B. de Crombrugghe, "Transcriptional mechanisms in osteoblast differentiation and bone formation.," *Trends Genet.*, vol. 19, no. 8, pp. 458–66, Aug. 2003.

[111] H. Zheng, Z. Guo, Q. Ma, H. Jia, and G. Dang, "Cbfa1/osf2 transduced bone marrow stromal cells facilitate bone formation in vitro and in vivo.," *Calcif. Tissue Int.*, vol. 74, no. 2, pp. 194–203, Feb. 2004.

[112] P. Ducy, R. Zhang, V. Geoffroy, A. L. Ridall, and G. Karsenty, "Osf2/Cbfa1: a transcriptional activator of osteoblast differentiation.," *Cell*, vol. 89, no. 5, pp. 747–54, May 1997.

[113] T. Komori, "Regulation of skeletal development by the Runx family of transcription factors.," *J. Cell. Biochem.*, vol. 95, no. 3, pp. 445–53, Jun. 2005.

[114] W. Liu, S. Toyosawa, T. Furuichi, N. Kanatani, C. Yoshida, Y. Liu, M. Himeno, S. Narai, A. Yamaguchi, and T. Komori, "Overexpression of Cbfa1 in osteoblasts inhibits osteoblast maturation and causes osteopenia with multiple fractures.," *J. Cell Biol.*, vol. 155, no. 1, pp. 157–66, Oct. 2001.

[115] M. H. Lee, A. Javed, H. J. Kim, H. I. Shin, S. Gutierrez, J. Y. Choi, V. Rosen, J. L. Stein, A. J. van Wijnen, G. S. Stein, J. B. Lian, and H. M. Ryoo, "Transient upregulation of CBFA1 in response to bone morphogenetic protein-2 and transforming growth factor beta1 in C2C12

myogenic cells coincides with suppression of the myogenic phenotype but is not sufficient for osteoblast differentiation.," *J. Cell. Biochem.*, vol. 73, no. 1, pp. 114–25, Apr. 1999.

[116] I. Song, K. Kim, J. H. Kim, Y.-K. Lee, H.-J. Jung, H.-O. Byun, G. Yoon, and N. Kim, "GATA4 negatively regulates osteoblast differentiation by downregulation of Runx2.," *BMB Rep.*, vol. 47, no. 8, pp. 463–8, Aug. 2014.

[117] H. Kaneki, R. Guo, D. Chen, Z. Yao, E. M. Schwarz, Y. E. Zhang, B. F. Boyce, and L. Xing, "Tumor necrosis factor promotes Runx2 degradation through up-regulation of Smurf1 and Smurf2 in osteoblasts.," *J. Biol. Chem.*, vol. 281, no. 7, pp. 4326–33, Feb. 2006.

[118] R. Paredes, G. Arriagada, F. Cruzat, A. Villagra, J. Olate, K. Zaidi, A. van Wijnen, J. B. Lian, G. S. Stein, J. L. Stein, and M. Montecino, "Bone-specific transcription factor Runx2 interacts with the 1alpha,25-dihydroxyvitamin D3 receptor to up-regulate rat osteocalcin gene expression in osteoblastic cells.," *Mol. Cell. Biol.*, vol. 24, no. 20, pp. 8847–61, Oct. 2004.

[119] J. M. Gimble, S. Zvonic, Z. E. Floyd, M. Kassem, and M. E. Nuttall, "Playing with bone and fat.," *J. Cell. Biochem.*, vol. 98, no. 2, pp. 251–66, May 2006.

[120] M. J. Jeon, J. A. Kim, S. H. Kwon, S. W. Kim, K. S. Park, S.-W. Park, S. Y. Kim, and C. S. Shin, "Activation of peroxisome proliferator-activated receptor-gamma inhibits the Runx2-mediated transcription of osteocalcin in osteoblasts.," *J. Biol. Chem.*, vol. 278, no. 26, pp. 23270–7, Jun. 2003.

[121] R. Ogawa, H. Mizuno, A. Watanabe, M. Migita, T. Shimada, and H. Hyakusoku, "Osteogenic and chondrogenic differentiation by adipose-derived stem cells harvested from GFP transgenic mice," *Biochem. Biophys. Res. Commun.*, vol. 313, no. 4, pp. 871–877, Jan. 2004.

[122] P. Niemeyer, M. Kornacker, A. Mehlhorn, A. Seckinger, J. Vohrer, H. Schmal, P. Kasten, V. Eckstein, N. P. Südkamp, and U. Krause, "Comparison of immunological properties of bone marrow stromal cells and adipose tissue-derived stem cells before and after osteogenic differentiation in vitro.," *Tissue Eng.*, vol. 13, no. 1, pp. 111–21, Jan. 2007.

[123] M. B. Goldring, K. Tsuchimochi, and K. Ijiri, "The control of chondrogenesis.," *J. Cell. Biochem.*, vol. 97, no. 1, pp. 33–44, Jan. 2006.

[124] A. E. Denker, A. R. Haas, S. B. Nicoll, and R. S. Tuan, "Chondrogenic differentiation of murine C3H10T1/2 multipotential mesenchymal cells: I. Stimulation by bone morphogenetic protein-2 in high-density micromass cultures.," *Differentiation.*, vol. 64, no. 2, pp. 67–76, Jan. 1999.

[125] J. Frith and P. Genever, "Transcriptional control of mesenchymal stem cell differentiation.," *Transfus. Med. Hemother.*, vol. 35, no. 3, pp. 216–27, Jun. 2008.

[126] V. Lefebvre, R. R. Behringer, and B. de Crombrugghe, "L-Sox5, Sox6 and Sox9 control essential steps of the chondrocyte differentiation pathway," *Osteoarthr. Cartil.*, vol. 9, pp. S69–75, Aug. 2001.

[127] V. Lefebvre, P. Li, and B. de Crombrugghe, "A new long form of Sox5 (L-Sox5), Sox6 and Sox9 are coexpressed in chondrogenesis and cooperatively activate the type II collagen gene.," *EMBO J.*, vol. 17, no. 19, pp. 5718–33, Oct. 1998.

[128] E. Kozhemyakina, A. B. Lassar, and E. Zelzer, "A pathway to bone: signaling molecules and transcription factors involved in chondrocyte development and maturation.," *Development*,

vol. 142, no. 5, pp. 817–31, Mar. 2015.

[129] T. Maruyama, A. J. Mirando, C.-X. Deng, and W. Hsu, “The balance of WNT and FGF signaling influences mesenchymal stem cell fate during skeletal development.,” *Sci. Signal.*, vol. 3, no. 123, p. ra40, Jan. 2010.

[130] S. Murakami, “Potent inhibition of the master chondrogenic factor Sox9 gene by interleukin-1 and tumor necrosis factor-alpha,” *J. Biol. Chem.*, vol. 275, no. 5, pp. 3687–92, Feb. 2000.

[131] E.-J. Kim, S.-W. Cho, J.-O. Shin, M.-J. Lee, K.-S. Kim, and H.-S. Jung, “Ihh and Runx2/Runx3 signaling interact to coordinate early chondrogenesis: a mouse model.,” *PLoS One*, vol. 8, no. 2, p. e55296, Jan. 2013.

[132] B. T. Estes, B. O. Diekman, and F. Guilak, “Monolayer cell expansion conditions affect the chondrogenic potential of adipose-derived stem cells.,” *Biotechnol. Bioeng.*, vol. 99, no. 4, pp. 986–95, Mar. 2008.

[133] T. Hennig, H. Lorenz, A. Thiel, K. Goetzke, A. Dickhut, F. Geiger, and W. Richter, “Reduced chondrogenic potential of adipose tissue derived stromal cells correlates with an altered TGFbeta receptor and BMP profile and is overcome by BMP-6.,” *J. Cell. Physiol.*, vol. 211, no. 3, pp. 682–91, Jun. 2007.

[134] O. Naveiras and G. Q. Daley, “Stem cells and their niche: a matter of fate.,” *Cell. Mol. Life Sci.*, vol. 63, no. 7–8, pp. 760–6, Apr. 2006.

[135] H. K. Kleinman, D. Philp, and M. P. Hoffman, “Role of the extracellular matrix in morphogenesis.,” *Curr. Opin. Biotechnol.*, vol. 14, no. 5, pp. 526–32, Oct. 2003.

[136] B. N. Brown and S. F. Badylak, “Extracellular matrix as an inductive scaffold for functional tissue reconstruction.,” *Transl. Res.*, vol. 163, no. 4, pp. 268–85, Apr. 2014.

[137] S. F. Badylak, D. O. Freytes, and T. W. Gilbert, “Extracellular matrix as a biological scaffold material: Structure and function.,” *Acta Biomater.*, vol. 5, no. 1, pp. 1–13, Jan. 2009.

[138] C. Frantz, K. M. Stewart, and V. M. Weaver, “The extracellular matrix at a glance.,” *J. Cell Sci.*, vol. 123, no. Pt 24, pp. 4195–200, Dec. 2010.

[139] M. K. Gordon and R. A. Hahn, “Collagens.,” *Cell Tissue Res.*, vol. 339, no. 1, pp. 247–57, Jan. 2010.

[140] G. S. Schultz and A. Wysocki, “Interactions between extracellular matrix and growth factors in wound healing.,” *Wound Repair Regen.*, vol. 17, no. 2, pp. 153–62, Jan. .

[141] K. Gelse, “Collagens—structure, function, and biosynthesis,” *Adv. Drug Deliv. Rev.*, vol. 55, no. 12, pp. 1531–46, Nov. 2003.

[142] M. D. Shoulders and R. T. Raines, “Collagen structure and stability.,” *Annu. Rev. Biochem.*, vol. 78, pp. 929–58, Jan. 2009.

[143] J. A. Ramshaw, N. K. Shah, and B. Brodsky, “Gly-X-Y tripeptide frequencies in collagen: a context for host-guest triple-helical peptides.,” *J. Struct. Biol.*, vol. 122, no. 1–2, pp. 86–91, Jan. 1998.

[144] J. P. Orgel, T. J. Wess, and A. Miller, “The in situ conformation and axial location of the intermolecular cross-linked non-helical telopeptides of type I collagen,” *Structure*, vol. 8, no. 2, pp. 137–142, Feb. 2000.

[145] J. Khoshnoodi, V. Pedchenko, and B. G. Hudson, “Mammalian collagen IV.,” *Microsc. Res.*

Tech., vol. 71, no. 5, pp. 357–70, May 2008.

[146] A. M. Abreu-Velez and M. S. Howard, “Collagen IV in normal skin and in pathological processes.,” *N. Am. J. Med. Sci.*, vol. 4, no. 1, pp. 1–8, Jan. 2012.

[147] E. C. M. Mariman and P. Wang, “Adipocyte extracellular matrix composition, dynamics and role in obesity.,” *Cell. Mol. Life Sci.*, vol. 67, no. 8, pp. 1277–92, Apr. 2010.

[148] D. Fan, A. Takawale, J. Lee, and Z. Kassiri, “Cardiac fibroblasts, fibrosis and extracellular matrix remodeling in heart disease.,” *Fibrogenesis Tissue Repair*, vol. 5, no. 1, p. 15, Jan. 2012.

[149] B. Alberts, A. Johnson, J. Lewis, M. Raff, K. Roberts, and P. Walter, “The Extracellular Matrix of Animals.” Garland Science, 2002.

[150] L. Debelle and A. M. Tamburro, “Elastin: molecular description and function.,” *Int. J. Biochem. Cell Biol.*, vol. 31, no. 2, pp. 261–72, Mar. 1999.

[151] M. Yanagishita, “Function of proteoglycans in the extracellular matrix,” *Pathol. Int.*, vol. 43, no. 6, pp. 283–93, Jun. 1993.

[152] N. S. Gandhi and R. L. Mancera, “The Structure of Glycosaminoglycans and their Interactions with Proteins,” *Chem. Biol. Drug Des.*, vol. 72, no. 6, pp. 455–82, Dec. 2008.

[153] M. Yanagishita, “Function of proteoglycans in the extracellular matrix.,” *Acta Pathol. Jpn.*, vol. 43, no. 6, pp. 283–93, Jun. 1993.

[154] R. V Iozzo and L. Schaefer, “Proteoglycan form and function: A comprehensive nomenclature of proteoglycans.,” *Matrix Biol.*, vol. 42, pp. 11–55, Mar. 2015.

[155] H. V. C. Wight Thomas N., Toole Bryan P., *The Extracellular Matrix: an Overview*. Springer Science & Business Media, 2011.

[156] R. Merline, R. M. Schaefer, and L. Schaefer, “The matricellular functions of small leucine-rich proteoglycans (SLRPs).,” *J. Cell Commun. Signal.*, vol. 3, no. 3–4, pp. 323–35, Dec. 2009.

[157] H. Lodish, A. Berk, S. L. Zipursky, P. Matsudaira, D. Baltimore, and J. Darnell, “Cell-Matrix Adhesion.” W. H. Freeman, 2000.

[158] J. Zhu, J. A. Beamish, C. Tang, K. Kottke-Marchant, and R. E. Marchant, “Extracellular Matrix-like Cell-Adhesive Hydrogels from RGD-Containing Poly(ethylene glycol) Diacrylate,” *Macromolecules*, vol. 39, no. 4, pp. 1305–07, Feb. 2006.

[159] S. K. Seidlits, C. T. Drinnan, R. R. Petersen, J. B. Shear, L. J. Suggs, and C. E. Schmidt, “Fibronectin-hyaluronic acid composite hydrogels for three-dimensional endothelial cell culture.,” *Acta Biomater.*, vol. 7, no. 6, pp. 2401–9, Jun. 2011.

[160] A. T. Francisco, R. J. Mancino, R. D. Bowles, J. M. Brunger, D. M. Tainter, Y.-T. Chen, W. J. Richardson, F. Guilak, and L. A. Setton, “Injectable laminin-functionalized hydrogel for nucleus pulposus regeneration.,” *Biomaterials*, vol. 34, no. 30, pp. 7381–8, Oct. 2013.

[161] E. A. Lenselink, “Role of fibronectin in normal wound healing.,” *Int. Wound J.*, vol. 12, no. 3, pp. 313–6, Jun. 2015.

[162] W. S. To and K. S. Midwood, “Plasma and cellular fibronectin: distinct and independent functions during tissue repair.,” *Fibrogenesis Tissue Repair*, vol. 4, p. 21, Jan. 2011.

[163] E. S. White and A. F. Muro, “Fibronectin splice variants: understanding their multiple roles

in health and disease using engineered mouse models.," *IUBMB Life*, vol. 63, no. 7, pp. 538–46, Jul. 2011.

[164] C. Ffrench-Constant, "Alternative splicing of fibronectin--many different proteins but few different functions.," *Exp. Cell Res.*, vol. 221, no. 2, pp. 261–71, Dec. 1995.

[165] K. Beck, I. Hunter, and J. Engel, "Structure and function of laminin: anatomy of a multidomain glycoprotein," *FASEB J*, vol. 4, no. 2, pp. 148–60, Feb. 1990.

[166] R. Schofield, "The relationship between the spleen colony-forming cell and the haemopoietic stem cell.," *Blood Cells*, vol. 4, no. 1–2, pp. 7–25, Jan. 1978.

[167] F. J. O'Brien, "Biomaterials & scaffolds for tissue engineering," *Mater. Today*, vol. 14, no. 3, pp. 88–95, Mar. 2011.

[168] J. Zhu and R. E. Marchant, "Design properties of hydrogel tissue-engineering scaffolds.," *Expert Rev. Med. Devices*, vol. 8, no. 5, pp. 607–26, Sep. 2011.

[169] J. Glowacki and S. Mizuno, "Collagen scaffolds for tissue engineering.," *Biopolymers*, vol. 89, no. 5, pp. 338–44, May 2008.

[170] W. Daamen, "Preparation and evaluation of molecularly-defined collagen–elastin–glycosaminoglycan scaffolds for tissue engineering," *Biomaterials*, vol. 24, no. 22, pp. 4001–9, Oct. 2003.

[171] A. Y. Rioja, R. T. Annamalai, S. Paris, A. J. Putnam, and J. P. Stegemann, "Endothelial sprouting and network formation in collagen- and fibrin-based modular microbeads.," *Acta Biomater.*, vol. 29, pp. 33-41, Jan. 2016.

[172] M. N. Collins and C. Birkinshaw, "Hyaluronic acid based scaffolds for tissue engineering--a review.," *Carbohydr. Polym.*, vol. 92, no. 2, pp. 1262–79, Feb. 2013.

[173] H. W. Kang, Y. Tabata, and Y. Ikada, "Fabrication of porous gelatin scaffolds for tissue engineering.," *Biomaterials*, vol. 20, no. 14, pp. 1339–44, Jul. 1999.

[174] B. Chevallay and D. Herbage, "Collagen-based biomaterials as 3D scaffold for cell cultures: applications for tissue engineering and gene therapy," *Med. Biol. Eng. Comput.*, vol. 38, no. 2, pp. 211–18, Mar. 2000.

[175] C. H. Lee, A. Singla, and Y. Lee, "Biomedical applications of collagen.," *Int. J. Pharm.*, vol. 221, no. 1–2, pp. 1–22, Jun. 2001.

[176] D. W. Hutmacher, J. C. Goh, and S. H. Teoh, "An introduction to biodegradable materials for tissue engineering applications.," *Ann. Acad. Med. Singapore*, vol. 30, no. 2, pp. 183–91, Mar. 2001.

[177] L. I. F. Moura, A. M. A. Dias, E. Suesca, S. Casadiegos, E. C. Leal, M. R. Fontanilla, L. Carvalho, H. C. de Sousa, and E. Carvalho, "Neurotensin-loaded collagen dressings reduce inflammation and improve wound healing in diabetic mice.," *Biochim. Biophys. Acta*, vol. 1842, no. 1, pp. 32–43, Jan. 2014.

[178] S. M. Choi, H. A. Ryu, K.-M. Lee, H. J. Kim, I. K. Park, W. J. Cho, H.-C. Shin, W. J. Choi, and J. W. Lee, "Development of Stabilized Growth Factor-Loaded Hyaluronate- Collagen Dressing (HCD) matrix for impaired wound healing.," *Biomater. Res.*, vol. 20, p. 9, Jan. 2016.

[179] L. Meng, O. Arnoult, M. Smith, and G. E. Wnek, "Electrospinning of in situ crosslinked collagen nanofibers," *J. Mater. Chem.*, vol. 22, no. 37, p. 19412, Aug. 2012.

[180] J. M. Ruijgrok, J. R. de Wijn, and M. E. Boon, “Glutaraldehyde crosslinking of collagen: effects of time, temperature, concentration and presoaking as measured by shrinkage temperature.,” *Clin. Mater.*, vol. 17, no. 1, pp. 23–7, Jan. 1994.

[181] I. Tcacencu and M. Wendel, “Collagen-hydroxyapatite composite enhances regeneration of calvaria bone defects in young rats but postpones the regeneration of calvaria bone in aged rats.,” *J. Mater. Sci. Mater. Med.*, vol. 19, no. 5, pp. 2015–21, May 2008.

[182] M. Geiger, R. H. Li, and W. Friess, “Collagen sponges for bone regeneration with rhBMP-2.,” *Adv. Drug Deliv. Rev.*, vol. 55, no. 12, pp. 1613–29, Nov. 2003.

[183] D. Macaya, K. K. Ng, and M. Spector, “Injectable Collagen-Genipin Gel for the Treatment of Spinal Cord Injury: In Vitro Studies,” *Adv. Funct. Mater.*, vol. 21, no. 24, pp. 4788–97, Dec. 2011.

[184] B. Borde, P. Grunert, R. Härtl, and L. J. Bonassar, “Injectable, high-density collagen gels for annulus fibrosus repair: An in vitro rat tail model.,” *J. Biomed. Mater. Res. A*, vol. 103, no. 8, pp. 2571–81, Aug. 2015.

[185] C. A. Fleck and R. Simman, “Modern collagen wound dressings: function and purpose.,” *J. Am. Col. Certif. Wound Spec.*, vol. 2, no. 3, pp. 50–4, Sep. 2010.

[186] R. L. Jackson, S. J. Busch, and A. D. Cardin, “Glycosaminoglycans: molecular properties, protein interactions, and role in physiological processes,” *Physiol Rev*, vol. 71, no. 2, pp. 481–539, Apr. 1991.

[187] J. A. Burdick and G. D. Prestwich, “Hyaluronic acid hydrogels for biomedical applications.,” *Adv. Mater.*, vol. 23, no. 12, pp. H41–56, Mar. 2011.

[188] I. Strehin, Z. Nahas, K. Arora, T. Nguyen, and J. Elisseeff, “A versatile pH sensitive chondroitin sulfate-PEG tissue adhesive and hydrogel.,” *Biomaterials*, vol. 31, no. 10, pp. 2788–97, Apr. 2010.

[189] S. A. Zawko, S. Suri, Q. Truong, and C. E. Schmidt, “Photopatterned anisotropic swelling of dual-crosslinked hyaluronic acid hydrogels.,” *Acta Biomater.*, vol. 5, no. 1, pp. 14–22, Jan. 2009.

[190] J. A. Burdick, C. Chung, X. Jia, M. A. Randolph, and R. Langer, “Controlled degradation and mechanical behavior of photopolymerized hyaluronic acid networks.,” *Biomacromolecules*, vol. 6, no. 1, pp. 386–91, Jan. .

[191] H. Tan, C. R. Chu, K. A. Payne, and K. G. Marra, “Injectable in situ forming biodegradable chitosan-hyaluronic acid based hydrogels for cartilage tissue engineering.,” *Biomaterials*, vol. 30, no. 13, pp. 2499–506, May 2009.

[192] J. L. van Susante, J. Pieper, P. Buma, T. H. van Kuppevelt, H. van Beuningen, P. M. van der Kraan, J. H. Veerkamp, W. B. van den Berg, and R. P. . Veth, “Linkage of chondroitin-sulfate to type I collagen scaffolds stimulates the bioactivity of seeded chondrocytes in vitro,” *Biomaterials*, vol. 22, no. 17, pp. 2359–69, Sep. 2001.

[193] C.-K. Perng, Y.-J. Wang, C.-H. Tsi, and H. Ma, “In vivo angiogenesis effect of porous collagen scaffold with hyaluronic acid oligosaccharides.,” *J. Surg. Res.*, vol. 168, no. 1, pp. 9–15, Jun. 2011.

[194] E. L. Pardue, S. Ibrahim, and A. Ramamurthi, “Role of hyaluronan in angiogenesis and its utility to angiogenic tissue engineering.,” *Organogenesis*, vol. 4, no. 4, pp. 203–14, Oct. 2008.

[195] A. Kamoun, J.-M. Landeau, G. Godeau, J. Wallach, A. Duchesnay, B. Pellat, and W. Hornebeck, “Growth stimulation of human skin fibroblasts by elastin-derived peptides,” *Cell Commun. Adhes.*, vol. 3, no. 4, pp. 273–81, Jul. 2009.

[196] S. Mochizuki, B. Brassart, and A. Hinek, “Signaling pathways transduced through the elastin receptor facilitate proliferation of arterial smooth muscle cells.,” *J. Biol. Chem.*, vol. 277, no. 47, pp. 44854–63, Nov. 2002.

[197] N. Fujimoto, S. Tajima, and A. Ishibashi, “Elastin peptides induce migration and terminal differentiation of cultured keratinocytes via 67 kDa elastin receptor in vitro: 67 kDa elastin receptor is expressed in the keratinocytes eliminating elastic materials in elastosis perforans serpiginosa.,” *J. Invest. Dermatol.*, vol. 115, no. 4, pp. 633–9, Oct. 2000.

[198] W. F. Daamen, S. T. M. Nillesen, T. Hafmans, J. H. Veerkamp, M. J. A. van Luyn, and T. H. van Kuppevelt, “Tissue response of defined collagen-elastin scaffolds in young and adult rats with special attention to calcification.,” *Biomaterials*, vol. 26, no. 1, pp. 81–92, Jan. 2005.

[199] S. G. Wise, S. M. Mithieux, and A. S. Weiss, “Engineered tropoelastin and elastin-based biomaterials.,” *Adv. Protein Chem. Struct. Biol.*, vol. 78, pp. 1–24, Jan. 2009.

[200] Z. Indik, W. R. Abrams, U. Kucich, C. W. Gibson, R. P. Mecham, and J. Rosenbloom, “Production of recombinant human tropoelastin: characterization and demonstration of immunologic and chemotactic activity.,” *Arch. Biochem. Biophys.*, vol. 280, no. 1, pp. 80–6, Jul. 1990.

[201] S. M. Mithieux, J. E. J. Rasko, and A. S. Weiss, “Synthetic elastin hydrogels derived from massive elastic assemblies of self-organized human protein monomers.,” *Biomaterials*, vol. 25, no. 20, pp. 4921–7, Sep. 2004.

[202] T. Hashimoto, Y. Suzuki, M. Tanihara, Y. Kakimaru, and K. Suzuki, “Development of alginate wound dressings linked with hybrid peptides derived from laminin and elastin.,” *Biomaterials*, vol. 25, no. 7–8, pp. 1407–14, Jan. .

[203] W. Haslik, L.-P. Kamolz, G. Nathschläger, H. Andel, G. Meissl, and M. Frey, “First experiences with the collagen-elastin matrix Matriderm as a dermal substitute in severe burn injuries of the hand.,” *Burns*, vol. 33, no. 3, pp. 364–8, May 2007.

[204] K. A. Woodhouse, P. Klement, V. Chen, M. B. Gorbet, F. W. Keeley, R. Stahl, J. D. Fromstein, and C. M. Bellingham, “Investigation of recombinant human elastin polypeptides as non-thrombogenic coatings.,” *Biomaterials*, vol. 25, no. 19, pp. 4543–53, Aug. 2004.

[205] P. Buijtenhuijs, L. Buttafoco, A. A. Poot, W. F. Daamen, T. H. van Kuppevelt, P. J. Dijkstra, R. A. I. de Vos, L. M. T. Sterk, B. R. H. Geelkerken, J. Feijen, and I. Vermes, “Tissue engineering of blood vessels: characterization of smooth-muscle cells for culturing on collagen-and-elastin-based scaffolds.,” *Biotechnol. Appl. Biochem.*, vol. 39, no. Pt 2, pp. 141–9, Apr. 2004.

[206] T. W. Gilbert, T. L. Sellaro, and S. F. Badylak, “Decellularization of tissues and organs.,” *Biomaterials*, vol. 27, no. 19, pp. 3675–83, Jul. 2006.

[207] D. M. Hoganson, E. M. O’Doherty, G. E. Owens, D. O. Harilal, S. M. Goldman, C. M. Bowley, C. M. Neville, R. T. Kronengold, and J. P. Vacanti, “The retention of extracellular matrix proteins and angiogenic and mitogenic cytokines in a decellularized porcine dermis.,” *Biomaterials*, vol. 31, no. 26, pp. 6730–7, Oct. 2010.

[208] S. Wu, Y. Liu, S. Bharadwaj, A. Atala, and Y. Zhang, “Human urine-derived stem cells

seeded in a modified 3D porous small intestinal submucosa scaffold for urethral tissue engineering.," *Biomaterials*, vol. 32, no. 5, pp. 1317–26, Mar. 2011.

[209] S. Mirsadraee, H. E. Wilcox, S. A. Korossis, J. N. Kearney, K. G. Watterson, J. Fisher, and E. Ingham, "Development and characterization of an acellular human pericardial matrix for tissue engineering.," *Tissue Eng.*, vol. 12, no. 4, pp. 763–73, May 2006.

[210] Y. Wang, C.-B. Cui, M. Yamauchi, P. Miguez, M. Roach, R. Malavarca, M. J. Costello, V. Cardinale, E. Wauthier, C. Barbier, D. A. Gerber, D. Alvaro, and L. M. Reid, "Lineage restriction of human hepatic stem cells to mature fates is made efficient by tissue-specific biomatrix scaffolds.," *Hepatology*, vol. 53, no. 1, pp. 293–305, Jan. 2011.

[211] D. J. Rosario, G. C. Reilly, E. Ali Salah, M. Glover, A. J. Bullock, and S. Macneil, "Decellularization and sterilization of porcine urinary bladder matrix for tissue engineering in the lower urinary tract.," *Regen. Med.*, vol. 3, no. 2, pp. 145–56, Mar. 2008.

[212] B. Perniconi, A. Costa, P. Aulino, L. Teodori, S. Adamo, and D. Coletti, "The pro-myogenic environment provided by whole organ scale acellular scaffolds from skeletal muscle.," *Biomaterials*, vol. 32, no. 31, pp. 7870–82, Nov. 2011.

[213] A. J. Sutherland, E. C. Beck, S. C. Dennis, G. L. Converse, R. A. Hopkins, C. J. Berkland, and M. S. Detamore, "Decellularized cartilage may be a chondroinductive material for osteochondral tissue engineering.," *PLoS One*, vol. 10, no. 5, p. e0121966, Jan. 2015.

[214] C. Correia, W. L. Grayson, M. Park, D. Hutton, B. Zhou, X. E. Guo, L. Niklason, R. A. Sousa, R. L. Reis, and G. Vunjak-Novakovic, "In vitro model of vascularized bone: synergizing vascular development and osteogenesis.," *PLoS One*, vol. 6, no. 12, p. e28352, Jan. 2011.

[215] P. M. Crapo, T. W. Gilbert, and S. F. Badylak, "An overview of tissue and whole organ decellularization processes.," *Biomaterials*, vol. 32, no. 12, pp. 3233–43, Apr. 2011.

[216] J. Bao, Q. Wu, J. Sun, Y. Zhou, Y. Wang, X. Jiang, L. Li, Y. Shi, and H. Bu, "Hemocompatibility improvement of perfusion-decellularized clinical-scale liver scaffold through heparin immobilization.," *Sci. Rep.*, vol. 5, p. 10756, Jan. 2015.

[217] H. C. Ott, T. S. Matthiesen, S.-K. Goh, L. D. Black, S. M. Kren, T. I. Netoff, and D. A. Taylor, "Perfusion-decellularized matrix: using nature's platform to engineer a bioartificial heart.," *Nat. Med.*, vol. 14, no. 2, pp. 213–21, Feb. 2008.

[218] L. Flynn, J. L. Semple, and K. A. Woodhouse, "Decellularized placental matrices for adipose tissue engineering.," *J. Biomed. Mater. Res. A*, vol. 79, no. 2, pp. 359–69, Nov. 2006.

[219] J. E. Reing, B. N. Brown, K. A. Daly, J. M. Freund, T. W. Gilbert, S. X. Hsiong, A. Huber, K. E. Kullas, S. Tottey, M. T. Wolf, and S. F. Badylak, "The effects of processing methods upon mechanical and biologic properties of porcine dermal extracellular matrix scaffolds.," *Biomaterials*, vol. 31, no. 33, pp. 8626–33, Nov. 2010.

[220] S. Cebotari, I. Tudorache, T. Jaekel, A. Hilfiker, S. Dorfman, W. Ternes, A. Haverich, and A. Lichtenberg, "Detergent decellularization of heart valves for tissue engineering: toxicological effects of residual detergents on human endothelial cells.," *Artif. Organs*, vol. 34, no. 3, pp. 206–10, Mar. 2010.

[221] B. Yang, Y. Zhang, L. Zhou, Z. Sun, J. Zheng, Y. Chen, and Y. Dai, "Development of a porcine bladder acellular matrix with well-preserved extracellular bioactive factors for tissue engineering.," *Tissue Eng. Part C. Methods*, vol. 16, no. 5, pp. 1201–11, Oct. 2010.

[222] T. W. Gilbert, J. M. Freund, and S. F. Badylak, “Quantification of DNA in biologic scaffold materials.,” *J. Surg. Res.*, vol. 152, no. 1, pp. 135–9, Mar. 2009.

[223] P. M. Crapo, T. W. Gilbert, and S. F. Badylak, “An overview of tissue and whole organ decellularization processes.,” *Biomaterials*, vol. 32, no. 12, pp. 3233–43, Apr. 2011.

[224] Y. C. Choi, J. S. Choi, D. Ph, B. S. Kim, J. D. Kim, H. I. Yoon, and Y. W. Cho, “Decellularized extracellular matrix derived from porcine adipose tissue as a xenogeneic biomaterial for tissue engineering,” vol. 18, no. 11, pp. 866-76, Jul. 2012.

[225] T. H. Petersen, E. A. Calle, M. B. Colehour, and L. E. Niklason, “Matrix composition and mechanics of decellularized lung scaffolds.,” *Cells. Tissues. Organs*, vol. 195, no. 3, pp. 222–31, Jan. 2012.

[226] H. Xu, B. Xu, Q. Yang, X. Li, X. Ma, Q. Xia, Y. Zhang, C. Zhang, Y. Wu, and Y. Zhang, “Comparison of decellularization protocols for preparing a decellularized porcine annulus fibrosus scaffold.,” *PLoS One*, vol. 9, no. 1, p. e86723, Jan. 2014.

[227] C. W. Cheng, L. D. Solorio, and E. Alsberg, “Decellularized tissue and cell-derived extracellular matrices as scaffolds for orthopaedic tissue engineering.,” *Biotechnol. Adv.*, vol. 32, no. 2, pp. 462–84, Jan. 2014.

[228] A. Roosens, P. Somers, F. De Somer, V. Carriel, G. Van Nooten, and R. Cornelissen, “Impact of detergent-based decellularization methods on porcine tissues for heart valve engineering.,” *Ann. Biomed. Eng.*, Feb. 2016.

[229] U. Böer, A. Lohrenz, M. Klingenberg, A. Pich, A. Haverich, and M. Wilhelmi, “The effect of detergent-based decellularization procedures on cellular proteins and immunogenicity in equine carotid artery grafts.,” *Biomaterials*, vol. 32, no. 36, pp. 9730–7, Dec. 2011.

[230] B. Zvarova, F. E. Uhl, J. J. Uriarte, Z. D. Borg, A. L. Coffey, N. R. Bonenfant, D. J. Weiss, and D. E. Wagner, “Residual detergent detection method for nondestructive cytocompatibility evaluation of decellularized whole lung scaffolds.,” *Tissue Eng. Part C. Methods*, vol. 22, no. 5, pp. 418–28, Mar. 2016.

[231] A. Mirzarafie, K. Grainger, B. Thomas, W. Bains, F.I. Ustok, and C.R. Lowe. “A fast and mild decellularization protocol for obtaining extracellular matrix,” *Rejuvenation Res.*, vol. 7, no. 2, pp. 159-60, Apr. 2014.

[232] S. Vasudevan, J. Huang, B. Botterman, H. S. Matloub, E. Keefer, and J. Cheng, “Detergent-free decellularized nerve grafts for long-gap peripheral nerve reconstruction.,” *Plast. Reconstr. surgery. Glob. open*, vol. 2, no. 8, p. e201, Aug. 2014.

[233] T. V Anilkumar, V. P. Vineetha, D. Revi, J. Muhamed, and A. Rajan, “Biomaterial properties of cholecyst-derived scaffold recovered by a non-detergent/enzymatic method.,” *J. Biomed. Mater. Res. B. Appl. Biomater.*, vol. 102, no. 7, pp. 1506–16, Oct. 2014.

[234] S. M. G. Arnold, S. Goldstein, and D. C. Gale, “Functional Performance and Biomechanics of Decellularized Human Aortic Valves,” *QScience Proc.*, vol. 2012, no. 4, p. 52, Jun. 2012.

[235] M. Tabuchi, J. Negishi, A. Yamashita, T. Higami, A. Kishida, and S. Funamoto, “Effect of decellularized tissue powders on a rat model of acute myocardial infarction.,” *Mater. Sci. Eng. C. Mater. Biol. Appl.*, vol. 56, pp. 494–500, Nov. 2015.

[236] C. F. C. Brown, J. Yan, T. T. Y. Han, D. M. Marecak, B. G. Amsden, and L. E. Flynn, “Effect of decellularized adipose tissue particle size and cell density on adipose-derived stem cell proliferation and adipogenic differentiation in composite methacrylated chondroitin

sulphate hydrogels.," *Biomed. Mater.*, vol. 10, no. 4, p. 045010, Jan. 2015.

[237] F. S. Steven, "The depolymerising action of pepsin on collagen molecular weights of the component polypeptide chains," *Biochim. Biophys. Acta - Gen. Subj.*, vol. 130, no. 1, pp. 190–5, Nov. 1966.

[238] J. M. Singelyn, J. A. DeQuach, S. B. Seif-Naraghi, R. B. Littlefield, P. J. Schup-Magoffin, and K. L. Christman, "Naturally derived myocardial matrix as an injectable scaffold for cardiac tissue engineering.," *Biomaterials*, vol. 30, no. 29, pp. 5409–16, Oct. 2009.

[239] F. Pati, J. Jang, D.-H. Ha, S. Won Kim, J.-W. Rhie, J.-H. Shim, D.-H. Kim, and D.-W. Cho, "Printing three-dimensional tissue analogues with decellularized extracellular matrix bioink.," *Nat. Commun.*, vol. 5, p. 3935, Jan. 2014.

[240] J. Visser, P. A. Levett, N. C. R. te Moller, J. Besems, K. W. M. Boere, M. H. P. van Rijen, J. C. de Grauw, W. J. A. Dhert, P. R. van Weeren, and J. Malda, "Crosslinkable hydrogels derived from cartilage, meniscus, and tendon tissue.," *Tissue Eng. Part A*, vol. 21, no. 7–8, pp. 1195–206, Apr. 2015.

[241] V. Russo, E. Omidi, A. Samani, A. Hamilton, and L. E. Flynn, "Porous, Ventricular Extracellular Matrix-Derived Foams as a Platform for Cardiac Cell Culture.," *Biores. Open Access*, vol. 4, no. 1, pp. 374–88, Jan. 2015.

[242] F. S. Steven, "The Nishihara techniques for the solubilization of collagen. Application to the preparation of soluble collagens from normal and rheumatoid connective tissue.," *Ann. Rheum. Dis.*, vol. 23, pp. 300–1, Jul. 1964.

[243] G. Quintarelli, M. C. Dellovo, C. Balduini, and A. A. Castellani, "The effects of alpha amylase on collagen-proteoglycans and collagen-glycoprotein complexes in connective tissue matrices.," *Histochemie.*, vol. 18, no. 4, pp. 373–5, Jan. 1969.

[244] B. S. Kim, J. S. Choi, J. D. Kim, Y. C. Choi, and Y. W. Cho, "Recellularization of decellularized human adipose-tissue-derived extracellular matrix sheets with other human cell types.," *Cell Tissue Res.*, vol. 348, no. 3, pp. 559–67, Jun. 2012.

[245] "2014 American Society of Plastic Surgeons Statistics." [Online]. Available: www.plasticsurgery.org.

[246] C. W. Patrick, "Breast tissue engineering.," *Annu. Rev. Biomed. Eng.*, vol. 6, pp. 109–30, Jan. 2004.

[247] C. W. Patrick, "Adipose tissue engineering: the future of breast and soft tissue reconstruction following tumor resection.," *Semin. Surg. Oncol.*, vol. 19, no. 3, pp. 302–11.

[248] J. P. Rubin and K. G. Marra, "Soft tissue reconstruction.," *Methods Mol. Biol.*, vol. 702, pp. 395–400, Jan. 2011.

[249] C. T. Gomillion and K. J. L. Burg, "Stem cells and adipose tissue engineering.," *Biomaterials*, vol. 27, no. 36, pp. 6052–63, Dec. 2006.

[250] D. L. Crandall, G. J. Hausman, and J. G. Kral, "A Review of the Microcirculation of Adipose Tissue: Anatomic, Metabolic, and Angiogenic Perspectives," *Microcirculation*, vol. 4, no. 2, pp. 211–232, Jan. 1997.

[251] D. von Heimburg, M. Kuberka, R. Rendchen, K. Hemmrich, G. Rau, and N. Pallua, "Preadipocyte-loaded collagen scaffolds with enlarged pore size for improved soft tissue engineering.," *Int. J. Artif. Organs*, vol. 26, no. 12, pp. 1064–76, Dec. 2003.

[252] A. E. Steiert, M. Boyce, and H. Sorg, “Capsular contracture by silicone breast implants: possible causes, biocompatibility, and prophylactic strategies.,” *Med. Devices (Auckl).*, vol. 6, pp. 211–8, Jan. 2013.

[253] J. S. Choi, B. S. Kim, J. Y. Kim, J. D. Kim, Y. C. Choi, H.-J. Yang, K. Park, H. Y. Lee, and Y. W. Cho, “Decellularized extracellular matrix derived from human adipose tissue as a potential scaffold for allograft tissue engineering.,” *J. Biomed. Mater. Res. A*, vol. 97, no. 3, pp. 292–9, Jun. 2011.

[254] D. E. Discher, D. J. Mooney, and P. W. Zandstra, “Growth factors, matrices, and forces combine and control stem cells.,” *Science*, vol. 324, no. 5935, pp. 1673–7, Jun. 2009.

[255] C. W. Patrick, B. Zheng, C. Johnston, and G. P. Reece, “Long-term implantation of preadipocyte-seeded PLGA scaffolds.,” *Tissue Eng.*, vol. 8, no. 2, pp. 283–93, Apr. 2002.

[256] J. O. Chung, D. H. Cho, D. J. Chung, and M. Y. Chung, “Associations among body mass index, insulin resistance, and pancreatic β-cell function in Korean patients with new-onset type 2 diabetes.,” *Korean J. Intern. Med.*, vol. 27, no. 1, pp. 66–71, Mar. 2012.

[257] T.-J. Lee, S. H. Bhang, W.-G. La, S.-H. Kwon, J.-Y. Shin, H. H. Yoon, H. Shin, D.-W. Cho, and B.-S. Kim, “Volume-stable adipose tissue formation by implantation of human adipose-derived stromal cells using solid free-form fabrication-based polymer scaffolds.,” *Ann. Plast. Surg.*, vol. 70, no. 1, pp. 98–102, Jan. 2013.

[258] J. R. Mauney, T. Nguyen, K. Gillen, C. Kirker-Head, J. M. Gimble, and D. L. Kaplan, “Engineering adipose-like tissue in vitro and in vivo utilizing human bone marrow and adipose-derived mesenchymal stem cells with silk fibroin 3D scaffolds.,” *Biomaterials*, vol. 28, no. 35, pp. 5280–90, Dec. 2007.

[259] C. W. Patrick, “Tissue engineering strategies for adipose tissue repair,” *Anat. Rec.*, vol. 263, no. 4, pp. 361–366, 2001.

[260] S.-W. Cho, K. W. Song, J. W. Rhie, M. H. Park, C. Y. Choi, and B.-S. Kim, “Engineered adipose tissue formation enhanced by basic fibroblast growth factor and a mechanically stable environment.,” *Cell Transplant.*, vol. 16, no. 4, pp. 421–34, Jan. 2007.

[261] S.-W. Kang, S.-W. Seo, C. Y. Choi, and B.-S. Kim, “Porous poly(lactic-co-glycolic acid) microsphere as cell culture substrate and cell transplantation vehicle for adipose tissue engineering.,” *Tissue Eng. Part C. Methods*, vol. 14, no. 1, pp. 25–34, Mar. 2008.

[262] S.-D. Lin, K.-H. Wang, and A.-P. Kao, “Engineered adipose tissue of predefined shape and dimensions from human adipose-derived mesenchymal stem cells.,” *Tissue Eng. Part A*, vol. 14, no. 5, pp. 571–81, May 2008.

[263] B. Weiser, L. Prantl, T. E. O. Schubert, J. Zellner, C. Fischbach-Teschl, T. Spruss, A. K. Seitz, J. Tessmar, A. Goepferich, and T. Blunk, “In vivo development and long-term survival of engineered adipose tissue depend on in vitro precultivation strategy.,” *Tissue Eng. Part A*, vol. 14, no. 2, pp. 275–84, Mar. 2008.

[264] A. Alhadlaq, M. Tang, and J. J. Mao, “Engineered adipose tissue from human mesenchymal stem cells maintains predefined shape and dimension: implications in soft tissue augmentation and reconstruction.,” *Tissue Eng.*, vol. 11, no. 3–4, pp. 556–66, Jan. .

[265] K. J. Cronin, A. Messina, K. R. Knight, J. J. Cooper-White, G. W. Stevens, A. J. Penington, and W. A. Morrison, “New murine model of spontaneous autologous tissue engineering, combining an arteriovenous pedicle with matrix materials.,” *Plast. Reconstr. Surg.*, vol. 113,

no. 1, pp. 260–9, Jan. 2004.

[266] D. von Heimburg, S. Zachariah, I. Heschel, H. Kühling, H. Schoof, B. Hafemann, and N. Pallua, “Human preadipocytes seeded on freeze-dried collagen scaffolds investigated in vitro and in vivo.,” *Biomaterials*, vol. 22, no. 5, pp. 429–38, Mar. 2001.

[267] N. Torio-Padron, N. Baerlecken, A. Momeni, G. B. Stark, and J. Borges, “Engineering of adipose tissue by injection of human preadipocytes in fibrin.,” *Aesthetic Plast. Surg.*, vol. 31, no. 3, pp. 285–93, 2007.

[268] W. Jing, Y. Lin, L. Wu, X. Li, X. Nie, L. Liu, W. Tang, X. Zheng, and W. Tian, “Ectopic adipogenesis of preconditioned adipose-derived stromal cells in an alginate system.,” *Cell Tissue Res.*, vol. 330, no. 3, pp. 567–72, Dec. 2007.

[269] Y. Itoi, M. Takatori, H. Hyakusoku, and H. Mizuno, “Comparison of readily available scaffolds for adipose tissue engineering using adipose-derived stem cells.,” *J. Plast. Reconstr. Aesthet. Surg.*, vol. 63, no. 5, pp. 858–64, May 2010.

[270] Y. Hiraoka, H. Yamashiro, K. Yasuda, Y. Kimura, T. Inamoto, and Y. Tabata, “In situ regeneration of adipose tissue in rat fat pad by combining a collagen scaffold with gelatin microspheres containing basic fibroblast growth factor.,” *Tissue Eng.*, vol. 12, no. 6, pp. 1475–87, Jun. 2006.

[271] Y. Kimura, M. Ozeki, T. Inamoto, and Y. Tabata, “Adipose tissue engineering based on human preadipocytes combined with gelatin microspheres containing basic fibroblast growth factor.,” *Biomaterials*, vol. 24, no. 14, pp. 2513–21, Jun. 2003.

[272] J. H. Kang, J. M. Gimble, and D. L. Kaplan, “In vitro 3D model for human vascularized adipose tissue.,” *Tissue Eng. Part A*, vol. 15, no. 8, pp. 2227–36, Aug. 2009.

[273] E. Bellas, B. J. B. Panilaitis, D. L. Glettig, C. A. Kirker-Head, J. J. Yoo, K. G. Marra, J. P. Rubin, and D. L. Kaplan, “Sustained volume retention in vivo with adipocyte and lipoaspirate seeded silk scaffolds.,” *Biomaterials*, vol. 34, no. 12, pp. 2960–8, Apr. 2013.

[274] D. Jaikumar, K. M. Sajesh, S. Soumya, T. R. Nimal, K. P. Chennazhi, S. V Nair, and R. Jayakumar, “Injectable alginate-O-carboxymethyl chitosan/nano fibrin composite hydrogels for adipose tissue engineering.,” *Int. J. Biol. Macromol.*, vol. 74, pp. 318–26, Mar. 2015.

[275] C. Halberstadt, C. Austin, J. Rowley, C. Culberson, A. Loebsack, S. Wyatt, S. Coleman, L. Blacksten, K. Burg, D. Mooney, and W. Holder, “A hydrogel material for plastic and reconstructive applications injected into the subcutaneous space of a sheep.,” *Tissue Eng.*, vol. 8, no. 2, pp. 309–19, Apr. 2002.

[276] I. Wu, Z. Nahas, K. A. Kimmerling, G. D. Rosson, and J. H. Elisseeff, “An injectable adipose matrix for soft-tissue reconstruction.,” *Plast. Reconstr. Surg.*, vol. 129, no. 6, pp. 1247–57, Jun. 2012.

[277] B. N. Brown, J. M. Freund, L. Han, J. P. Rubin, J. E. Reing, E. M. Jeffries, M. T. Wolf, S. Tottey, C. A. Barnes, B. D. Ratner, and S. F. Badylak, “Comparison of three methods for the derivation of a biologic scaffold composed of adipose tissue extracellular matrix.,” *Tissue Eng. Part C. Methods*, vol. 17, no. 4, pp. 411–21, Apr. 2011.

[278] D. A. Young, D. O. Ibrahim, D. Hu, and K. L. Christman, “Injectable hydrogel scaffold from decellularized human lipoaspirate.,” *Acta Biomater.*, vol. 7, no. 3, pp. 1040–9, Mar. 2011.

[279] F. A. Saleh, J. E. Frith, J. A. Lee, and P. G. Genever, “Three-dimensional in vitro culture techniques for mesenchymal stem cells.,” *Methods Mol. Biol.*, vol. 916, pp. 31–45, Jan. 2012.

[280] M. A. Baxter, R. F. Wynn, S. N. Jowitt, J. E. Wraith, L. J. Fairbairn, and I. Bellantuono, "Study of telomere length reveals rapid aging of human marrow stromal cells following in vitro expansion.," *Stem Cells*, vol. 22, no. 5, pp. 675–82, Jan. 2004.

[281] A. Banfi, A. Muraglia, B. Dozin, M. Mastrogiacomo, R. Cancedda, and R. Quarto, "Proliferation kinetics and differentiation potential of ex vivo expanded human bone marrow stromal cells: Implications for their use in cell therapy.," *Exp. Hematol.*, vol. 28, no. 6, pp. 707–15, Jun. 2000.

[282] C. P. Ng, A. R. M. Sharif, D. E. Heath, J. W. Chow, C. B. Y. Zhang, M. B. Chan-Park, P. T. Hammond, J. K. Y. Chan, and L. G. Griffith, "Enhanced ex vivo expansion of adult mesenchymal stem cells by fetal mesenchymal stem cell ECM.," *Biomaterials*, vol. 35, no. 13, pp. 4046–57, Apr. 2014.

[283] L. Gu and D. J. Mooney, "Biomaterials and emerging anticancer therapeutics: engineering the microenvironment.," *Nat. Rev. Cancer*, vol. 16, no. 1, pp. 56–66, Dec. 2015.

[284] P. Godara, C. D. McFarland, and R. E. Nordon, "Design of bioreactors for mesenchymal stem cell tissue engineering," *J. Chem. Technol. Biotechnol.*, vol. 83, no. 4, pp. 408–20, Apr. 2008.

[285] S. Hofmann, H. Hagenmüller, A. M. Koch, R. Müller, G. Vunjak-Novakovic, D. L. Kaplan, H. P. Merkle, and L. Meinel, "Control of in vitro tissue-engineered bone-like structures using human mesenchymal stem cells and porous silk scaffolds.," *Biomaterials*, vol. 28, no. 6, pp. 1152–62, Feb. 2007.

[286] L. F. Mellor, T. L. Baker, R. J. Brown, L. W. Catlin, and J. T. Oxford, "Optimal 3D culture of primary articular chondrocytes for use in the rotating wall vessel bioreactor.," *Aviat. Space. Environ. Med.*, vol. 85, no. 8, pp. 798–804, Aug. 2014.

[287] D. A. Gaspar, V. Gomide, and F. J. Monteiro, "The role of perfusion bioreactors in bone tissue engineering.," *Biomatter*, vol. 2, no. 4, pp. 167–75, Jan. 2012.

[288] L. De Bartolo, S. Salerno, E. Curcio, A. Piscioneri, M. Rende, S. Morelli, F. Tasselli, A. Bader, and E. Drioli, "Human hepatocyte functions in a crossed hollow fiber membrane bioreactor.," *Biomaterials*, vol. 30, no. 13, pp. 2531–43, May 2009.

[289] G. J. M. Cabrita, B. S. Ferreira, C. L. da Silva, R. Gonçalves, G. Almeida-Porada, and J. M. S. Cabral, "Hematopoietic stem cells: from the bone to the bioreactor.," *Trends Biotechnol.*, vol. 21, no. 5, pp. 233–40, May 2003.

[290] R. Gómez-Sjöberg, A. A. Leyrat, D. M. Pirone, C. S. Chen, and S. R. Quake, "Versatile, fully automated, microfluidic cell culture system.," *Anal. Chem.*, vol. 79, no. 22, pp. 8557–63, Nov. 2007.

[291] A. K.-L. Chen, S. Reuveny, and S. K. W. Oh, "Application of human mesenchymal and pluripotent stem cell microcarrier cultures in cellular therapy: achievements and future direction.," *Biotechnol. Adv.*, vol. 31, no. 7, pp. 1032–46, Nov. 2013.

[292] H.-C. Chen and Y.-C. Hu, "Bioreactors for tissue engineering.," *Biotechnol. Lett.*, vol. 28, no. 18, pp. 1415–23, Sep. 2006.

[293] F. Zhao, R. Chella, and T. Ma, "Effects of shear stress on 3-D human mesenchymal stem cell construct development in a perfusion bioreactor system: Experiments and hydrodynamic modeling.," *Biotechnol. Bioeng.*, vol. 96, no. 3, pp. 584–95, Feb. 2007.

[294] G. Yourek, S. M. McCormick, J. J. Mao, and G. C. Reilly, "Shear stress induces osteogenic

differentiation of human mesenchymal stem cells.," *Regen. Med.*, vol. 5, no. 5, pp. 713–24, Sep. 2010.

[295] G. D'Ippolito, S. Diabira, G. A. Howard, B. A. Roos, and P. C. Schiller, "Low oxygen tension inhibits osteogenic differentiation and enhances stemness of human MIAMI cells.," *Bone*, vol. 39, no. 3, pp. 513–22, Sep. 2006.

[296] A. L. van Wezel, "Growth of cell-strains and primary cells on micro-carriers in homogeneous culture.," *Nature*, vol. 216, no. 5110, pp. 64–5, Oct. 1967.

[297] Y. Wang and F. Ouyang, "Bead-to-bead transfer of Vero cells in microcarrier culture.," *Cytotechnology*, vol. 31, no. 3, pp. 221–4, Nov. 1999.

[298] B. Li, X. Wang, Y. Wang, W. Gou, X. Yuan, J. Peng, Q. Guo, and S. Lu, "Past, present, and future of microcarrier-based tissue engineering," *J. Orthop. Transl.*, vol. 3, no. 2, pp. 51–7, Apr. 2015.

[299] M. Hervy, J. L. Weber, M. Pecheul, P. Dolley-Sonneville, D. Henry, Y. Zhou, and Z. Melkoumian, "Long term expansion of bone marrow-derived hMSCs on novel synthetic microcarriers in xeno-free, defined conditions.," *PLoS One*, vol. 9, no. 3, p. e92120, Jan. 2014.

[300] B. Lei, K.-H. Shin, D.-Y. Noh, I.-H. Jo, Y.-H. Koh, H.-E. Kim, and S. E. Kim, "Sol-gel derived nanoscale bioactive glass (NBG) particles reinforced poly(ε-caprolactone) composites for bone tissue engineering.," *Mater. Sci. Eng. C. Mater. Biol. Appl.*, vol. 33, no. 3, pp. 1102–8, Apr. 2013.

[301] J. Varani, M. Dame, T. F. Beals, and J. A. Wass, "Growth of three established cell lines on glass microcarriers.," *Biotechnol. Bioeng.*, vol. 25, no. 5, pp. 1359–72, May 1983.

[302] M. H. Amer, L. J. White, and K. M. Shakesheff, "The effect of injection using narrow-bore needles on mammalian cells: administration and formulation considerations for cell therapies.," *J. Pharm. Pharmacol.*, vol. 67, no. 5, pp. 640–50, May 2015.

[303] M. Y. Kim and J. Lee, "Chitosan fibrous 3D networks prepared by freeze drying," *Carbohydr. Polym.*, vol. 84, no. 4, pp. 1329–36, Apr. 2011.

[304] Y. J. Kwon and C.-A. Peng, "Calcium-alginate gel bead cross-linked with gelatin as microcarrier for anchorage-dependent cell culture.," *Biotechniques*, vol. 33, no. 1, pp. 212–4, 216, 218, Jul. 2002.

[305] Y. Yang, F. M. V Rossi, and E. E. Putnins, "Ex vivo expansion of rat bone marrow mesenchymal stromal cells on microcarrier beads in spin culture.," *Biomaterials*, vol. 28, no. 20, pp. 3110–20, Jul. 2007.

[306] N. E. Timmins, M. Kiel, M. Günther, C. Heazlewood, M. R. Doran, G. Brooke, and K. Atkinson, "Closed system isolation and scalable expansion of human placental mesenchymal stem cells.," *Biotechnol. Bioeng.*, vol. 109, no. 7, pp. 1817–26, Jul. 2012.

[307] G. Eibes, F. dos Santos, P. Z. Andrade, J. S. Boura, M. M. A. Abecasis, C. L. da Silva, and J. M. S. Cabral, "Maximizing the ex vivo expansion of human mesenchymal stem cells using a microcarrier-based stirred culture system.," *J. Biotechnol.*, vol. 146, no. 4, pp. 194–7, Apr. 2010.

[308] J. P. Rubin, J. M. Bennett, J. S. Doctor, B. M. Tebbets, and K. G. Marra, "Collagenous microbeads as a scaffold for tissue engineering with adipose-derived stem cells.," *Plast. Reconstr. Surg.*, vol. 120, no. 2, pp. 414–24, Aug. 2007.

[309] T. K.-P. Goh, Z.-Y. Zhang, A. K.-L. Chen, S. Reuveny, M. Choolani, J. K. Y. Chan, and S. K.-W. Oh, "Microcarrier culture for efficient expansion and osteogenic differentiation of human fetal mesenchymal stem cells.," *Biores. Open Access*, vol. 2, no. 2, pp. 84–97, Apr. 2013.

[310] C. Ferrari, F. Balandras, E. Guedon, E. Olmos, I. Chevalot, and A. Marc, "Limiting cell aggregation during mesenchymal stem cell expansion on microcarriers.," *Biotechnol. Prog.*, vol. 28, no. 3, pp. 780–7, Jan. .

[311] P.-C. Tseng, T.-H. Young, T.-M. Wang, H.-W. Peng, S.-M. Hou, and M.-L. Yen, "Spontaneous osteogenesis of MSCs cultured on 3D microcarriers through alteration of cytoskeletal tension.," *Biomaterials*, vol. 33, no. 2, pp. 556–64, Jan. 2012.

[312] J. G. Carmelo, A. Fernandes-Platzgummer, J. M. S. Cabral, and C. L. da Silva, "Scalable ex vivo expansion of human mesenchymal stem/stromal cells in microcarrier-based stirred culture systems.," *Methods Mol. Biol.*, vol. 1283, pp. 147–59, Jan. 2015.

[313] Y. Zhou, Z. Yan, H. Zhang, W. Lu, S. Liu, X. Huang, H. Luo, and Y. Jin, "Expansion and delivery of adipose-derived mesenchymal stem cells on three microcarriers for soft tissue regeneration.," *Tissue Eng. Part A*, vol. 17, no. 23–24, pp. 2981–97, Dec. 2011.

[314] Y.-N. Wu, Z. Yang, J. H. P. Hui, H.-W. Ouyang, and E. H. Lee, "Cartilaginous ECM component-modification of the micro-bead culture system for chondrogenic differentiation of mesenchymal stem cells.," *Biomaterials*, vol. 28, no. 28, pp. 4056–67, Oct. 2007.

[315] A. Bertolo, S. Häfner, A. R. Taddei, M. Baur, T. Pötzel, F. Steffen, and J. Stoyanov, "Injectable microcarriers as human mesenchymal stem cell support and their application for cartilage and degenerated intervertebral disc repair.," *Eur. Cell. Mater.*, vol. 29, pp. 70–80, Jan. 2015.

[316] S.-W. Choi, Y. Zhang, Y.-C. Yeh, A. Lake Wooten, and Y. Xia, "Biodegradable porous beads and their potential applications in regenerative medicine," *J. Mater. Chem.*, vol. 22, no. 23, p. 11442, 2012.

[317] Y. C. Ng, J. M. Berry, and M. Butler, "Optimization of physical parameters for cell attachment and growth on macroporous microcarriers.," *Biotechnol. Bioeng.*, vol. 50, no. 6, pp. 627–35, Jun. 1996.

[318] K. Nilsson, F. Buzsaky, and K. Mosbach, "Growth of anchorage–dependent cells on macroporous microcarriers," *Bio/Technology*, vol. 4, no. 11, pp. 989–90, Nov. 1986.

[319] K. Y. Tan, S. Reuveny, and S. K. W. Oh, "Recent advances in serum-free microcarrier expansion of mesenchymal stromal cells: parameters to be optimized.," *Biochem. Biophys. Res. Commun.*, vol. 3, pp. 769-73, May 2016.

[320] F. Dos Santos, A. Campbell, A. Fernandes-Platzgummer, P. Z. Andrade, J. M. Gimble, Y. Wen, S. Boucher, M. C. Vemuri, C. L. da Silva, and J. M. S. Cabral, "A xenogeneic-free bioreactor system for the clinical-scale expansion of human mesenchymal stem/stromal cells.," *Biotechnol. Bioeng.*, vol. 111, no. 6, pp. 1116–27, Jun. 2014.

[321] M. S. Croughan, J. F. Hamel, and D. I. Wang, "Effects of microcarrier concentration in animal cell culture.," *Biotechnol. Bioeng.*, vol. 32, no. 8, pp. 975–82, Oct. 1988.

[322] M. S. Croughan, J. F. Hamel, and D. I. Wang, "Hydrodynamic effects on animal cells grown in microcarrier cultures.," *Biotechnol. Bioeng.*, vol. 29, no. 1, pp. 130–41, Jan. 1987.

[323] A. W. Nienow, C. J. Hewitt, T. R. J. Heathman, V. A. M. Glyn, G. N. Fonte, M. P. Hanga, K.

Coopman, and Q. A. Rafiq, “Agitation conditions for the culture and detachment of hMSCs from microcarriers in multiple bioreactor platforms,” *Biochem. Eng. J.*, vol. 108, pp. 24–29, Apr. 2016.

[324] A. W. Nienow, “Reactor engineering in large scale animal cell culture.,” *Cytotechnology*, vol. 50, no. 1–3, pp. 9–33, Mar. 2006.

[325] F. Guilak, D. M. Cohen, B. T. Estes, J. M. Gimble, W. Liedtke, and C. S. Chen, “Control of stem cell fate by physical interactions with the extracellular matrix.,” *Cell Stem Cell*, vol. 5, no. 1, pp. 17–26, Jul. 2009.

[326] F. dos Santos, P. Z. Andrade, M. M. Abecasis, J. M. Gimble, L. G. Chase, A. M. Campbell, S. Boucher, M. C. Vemuri, C. L. da Silva, and J. M. S. Cabral, “Toward a clinical-grade expansion of mesenchymal stem cells from human sources: a microcarrier-based culture system under xeno-free conditions.,” *Tissue Eng. Part C. Methods*, vol. 17, no. 12, pp. 1201–10, Dec. 2011.

[327] J. Chang, H. Lei, Q. Liu, S. Qin, K. Ma, S. Luo, X. Zhang, W. Huang, Z. Zuo, H. Fu, and Y. Xia, “Optimization of culture of mesenchymal stem cells: a comparison of conventional plate and microcarrier cultures.,” *Cell Prolif.*, vol. 45, no. 5, pp. 430–7, Oct. 2012.

[328] M. Dominici, K. Le Blanc, I. Mueller, I. Slaper-Cortenbach, F. Marini, D. Krause, R. Deans, A. Keating, D. Prockop, and E. Horwitz, “Minimal criteria for defining multipotent mesenchymal stromal cells. The International Society for Cellular Therapy position statement.,” *Cytotherapy*, vol. 8, no. 4, pp. 315–7, Jan. 2006.

[329] M. Théry, “Micropatterning as a tool to decipher cell morphogenesis and functions.,” *J. Cell Sci.*, vol. 123, no. Pt 24, pp. 4201–13, Dec. 2010.

[330] M. D. Treiser, E. H. Yang, S. Gordonov, D. M. Cohen, I. P. Androulakis, J. Kohn, C. S. Chen, and P. V Moghe, “Cytoskeleton-based forecasting of stem cell lineage fates.,” *Proc. Natl. Acad. Sci. U. S. A.*, vol. 107, no. 2, pp. 610–5, Jan. 2010.

[331] S. Sart, A. Errachid, Y.-J. Schneider, and S. N. Agathos, “Controlled expansion and differentiation of mesenchymal stem cells in a microcarrier based stirred bioreactor.,” *BMC Proc.*, vol. 5 Suppl 8, p. P55, Jan. 2011.

[332] A. Shekaran, E. Sim, K. Y. Tan, J. K. Y. Chan, M. Choolani, S. Reuveny, and S. Oh, “Enhanced in vitro osteogenic differentiation of human fetal MSCs attached to 3D microcarriers versus harvested from 2D monolayers.,” *BMC Biotechnol.*, vol. 15, no. 1, p. 102, Jan. 2015.

[333] N. V Ghone and W. L. Grayson, “Recapitulation of mesenchymal condensation enhances in vitro chondrogenesis of human mesenchymal stem cells.,” *J. Cell. Physiol.*, vol. 227, no. 11, pp. 3701–8, Nov. 2012.

[334] A. Bertolo, F. Arcolino, S. Capossela, A. R. Taddei, M. Baur, T. Pötzel, and J. Stoyanov, “Growth Factors Cross-Linked to Collagen Microcarriers Promote Expansion and Chondrogenic Differentiation of Human Mesenchymal Stem Cells.,” *Tissue Eng. Part A*, vol. 21, no. 19–20, pp. 2618–28, Oct. 2015.

[335] B. Lindroos, S. Boucher, L. Chase, H. Kuokkanen, H. Huhtala, R. Haataja, M. Vemuri, R. Suuronen, and S. Miettinen, “Serum-free, xeno-free culture media maintain the proliferation rate and multipotentiality of adipose stem cells in vitro.,” *Cytotherapy*, vol. 11, no. 7, pp. 958–72, Jan. 2009.

[336] L. G. Chase, U. Lakshmipathy, L. A. Solchaga, M. S. Rao, and M. C. Vemuri, “A novel serum-free medium for the expansion of human mesenchymal stem cells.,” *Stem Cell Res. Ther.*, vol. 1, no. 1, p. 8, Jan. 2010.

[337] G. Rajaraman, J. White, K. S. Tan, D. Ulrich, A. Rosamilia, J. Werkmeister, and C. E. Gargett, “Optimization and scale-up culture of human endometrial multipotent mesenchymal stromal cells: potential for clinical application.,” *Tissue Eng. Part C. Methods*, vol. 19, no. 1, pp. 80–92, Jan. 2013.

[338] K. T. Kunas and E. T. Papoutsakis, “The protective effect of serum against hydrodynamic damage of hybridoma cells in agitated and surface-aerated bioreactors,” *J. Biotechnol.*, vol. 15, no. 1–2, pp. 57–69, Jul. 1990.

[339] T. R. J. Heathman, V. A. M. Glyn, A. Picken, Q. A. Rafiq, K. Coopman, A. W. Nienow, B. Kara, and C. J. Hewitt, “Expansion, harvest and cryopreservation of human mesenchymal stem cells in a serum-free microcarrier process.,” *Biotechnol. Bioeng.*, vol. 112, no. 8, pp. 1696–707, Aug. 2015.

[340] J. G. Carmelo, A. Fernandes-Platzgummer, M. M. Diogo, C. L. da Silva, and J. M. S. Cabral, “A xeno-free microcarrier-based stirred culture system for the scalable expansion of human mesenchymal stem/stromal cells isolated from bone marrow and adipose tissue.,” *Biotechnol. J.*, vol. 10, no. 8, pp. 1235–47, Aug. 2015.

[341] C. Schirmaier, V. Jossen, S. C. Kaiser, F. Jüngerkes, S. Brill, A. Safavi-Nab, A. Siehoff, C. van den Bos, D. Eibl, and R. Eibl, “Scale-up of adipose tissue-derived mesenchymal stem cell production in stirred single-use bioreactors under low-serum conditions,” *Eng. Life Sci.*, vol. 14, no. 3, pp. 292–303, May 2014.

[342] J. A. King and W. M. Miller, “Bioreactor development for stem cell expansion and controlled differentiation.,” *Curr. Opin. Chem. Biol.*, vol. 11, no. 4, pp. 394–8, Aug. 2007.

[343] E. T. Papoutsakis, “Fluid-mechanical damage of animal cells in bioreactors.,” *Trends Biotechnol.*, vol. 9, no. 12, pp. 427–37, Dec. 1991.

[344] D. Schop, F. W. Janssen, E. Borgart, J. D. de Bruijn, and R. van Dijkhuizen-Radersma, “Expansion of mesenchymal stem cells using a microcarrier-based cultivation system: growth and metabolism,” *J. Tissue Eng. Regen. Med.*, vol. 2, no. 2–3, pp. 126–35, Mar. 2008.

[345] J. A. Gilbertson, A. Sen, L. A. Behie, and M. S. Kallos, “Scaled-up production of mammalian neural precursor cell aggregates in computer-controlled suspension bioreactors.,” *Biotechnol. Bioeng.*, vol. 94, no. 4, pp. 783–92, Jul. 2006.

[346] L. Flynn and K. A. Woodhouse, “Adipose tissue engineering with cells in engineered matrices.,” *Organogenesis*, vol. 4, no. 4, pp. 228–35, Oct. 2008.

[347] P. Bauer-Kreisel, A. Goepferich, and T. Blunk, “Cell-delivery therapeutics for adipose tissue regeneration.,” *Adv. Drug Deliv. Rev.*, vol. 62, no. 7–8, pp. 798–813, Jun. 2010.

[348] Y. Zhang, Y. He, S. Bharadwaj, N. Hammam, K. Carnagey, R. Myers, A. Atala, and M. Van Dyke, “Tissue-specific extracellular matrix coatings for the promotion of cell proliferation and maintenance of cell phenotype.,” *Biomaterials*, vol. 30, no. 23–24, pp. 4021–8, Aug. 2009.

[349] B. P. Chan and K. W. Leong, “Scaffolding in tissue engineering: general approaches and tissue-specific considerations.,” *Eur. Spine J.*, vol. 17 Suppl 4, pp. 467–79, Dec. 2008.

[350] S. Uriel, E. Labay, M. Francis-Sedlak, M. L. Moya, R. R. Weichselbaum, N. Ervin, Z.

Cankova, and E. M. Brey, “Extraction and assembly of tissue-derived gels for cell culture and tissue engineering.,” *Tissue Eng. Part C. Methods*, vol. 15, no. 3, pp. 309–21, Sep. 2009.

[351] F. B. J. L. Stillaert, P. Blondeel, M. Hamdi, K. Abberton, E. Thompson, and W. A. Morrison, “Adipose tissue induction in vivo.,” *Adv. Exp. Med. Biol.*, vol. 585, pp. 403–12, Jan. 2006.

[352] A. Chaubey and K. J. L. Burg, “Extracellular Matrix Components as Modulators of Adult Stem Cell Differentiation in an Adipose System,” *J. Bioact. Compat. Polym.*, vol. 23, no. 1, pp. 20–37, Jan. 2008.

[353] H. Hauner, T. Skurk, and M. Wabitsch, “Cultures of human adipose precursor cells.,” *Methods Mol. Biol.*, vol. 155, pp. 239–47, Jan. 2001.

[354] K. Gorzelniak, J. Janke, S. Engeli, and A. M. Sharma, “Validation of endogenous controls for gene expression studies in human adipocytes and preadipocytes.,” *Horm. Metab. Res.*, vol. 33, no. 10, pp. 625–7, Oct. 2001.

[355] L. Flynn, G. D. Prestwich, J. L. Semple, and K. A. Woodhouse, “Adipose tissue engineering with naturally derived scaffolds and adipose-derived stem cells.,” *Biomaterials*, vol. 28, no. 26, pp. 3834–42, Sep. 2007.

[356] M. A. Lazar, “Becoming fat.,” *Genes Dev.*, vol. 16, no. 1, pp. 1–5, Jan. 2002.

[357] J. Eyckmans, T. Boudou, X. Yu, and C. S. Chen, “A hitchhiker’s guide to mechanobiology.,” *Dev. Cell*, vol. 21, no. 1, pp. 35–47, Jul. 2011.

[358] D. T. Scadden, “The stem-cell niche as an entity of action.,” *Nature*, vol. 441, no. 7097, pp. 1075–9, Jun. 2006.

[359] C. J. Flaim, D. Teng, S. Chien, and S. N. Bhatia, “Combinatorial signaling microenvironments for studying stem cell fate.,” *Stem Cells Dev.*, vol. 17, no. 1, pp. 29–39, Feb. 2008.

[360] A. J. Engler, S. Sen, H. L. Sweeney, and D. E. Discher, “Matrix elasticity directs stem cell lineage specification.,” *Cell*, vol. 126, no. 4, pp. 677–89, Aug. 2006.

[361] J. Cortiella, J. Niles, A. Cantu, A. Brettler, A. Pham, G. Vargas, S. Winston, J. Wang, S. Walls, and J. E. Nichols, “Influence of acellular natural lung matrix on murine embryonic stem cell differentiation and tissue formation.,” *Tissue Eng. Part A*, vol. 16, no. 8, pp. 2565–80, Aug. 2010.

[362] S. L. J. Ng, K. Narayanan, S. Gao, and A. C. A. Wan, “Lineage restricted progenitors for the repopulation of decellularized heart.,” *Biomaterials*, vol. 32, no. 30, pp. 7571–80, Oct. 2011.

[363] R. McBeath, D. M. Pirone, C. M. Nelson, K. Bhadriraju, and C. S. Chen, “Cell shape, cytoskeletal tension, and RhoA regulate stem cell lineage commitment.,” *Dev. Cell*, vol. 6, no. 4, pp. 483–95, Apr. 2004.

[364] J.-T. Ayala-Sumuano, C. Velez-Del Valle, A. Beltrán-Langarica, J. M. Hernández, and W. Kuri-Harcuch, “Adipogenic genes on induction and stabilization of commitment to adipose conversion.,” *Biochem. Biophys. Res. Commun.*, vol. 374, no. 4, pp. 720–4, Oct. 2008.

[365] V. Large, O. Peroni, D. Letexier, H. Ray, and M. Beylot, “Metabolism of lipids in human white adipocyte.,” *Diabetes Metab.*, vol. 30, no. 4, pp. 294–309, Sep. 2004.

[366] W.-S. Kim, B.-S. Park, J.-H. Sung, J.-M. Yang, S.-B. Park, S.-J. Kwak, and J.-S. Park, “Wound healing effect of adipose-derived stem cells: a critical role of secretory factors on human dermal fibroblasts.,” *J. Dermatol. Sci.*, vol. 48, no. 1, pp. 15–24, Oct. 2007.

[367] J. J. Castellot, M. J. Karnovsky, and B. M. Spiegelman, “Potent stimulation of vascular endothelial cell growth by differentiated 3T3 adipocytes.,” *Proc. Natl. Acad. Sci. U. S. A.*, vol. 77, no. 10, pp. 6007–11, Oct. 1980.

[368] J. J. Castellot, M. J. Karnovsky, and B. M. Spiegelman, “Differentiation-dependent stimulation of neovascularization and endothelial cell chemotaxis by 3T3 adipocytes.,” *Proc. Natl. Acad. Sci. U. S. A.*, vol. 79, no. 18, pp. 5597–601, Sep. 1982.

[369] R. P. Keatch, A. M. Schor, J. B. Vorstius, and S. L. Schor, “Biomaterials in regenerative medicine: engineering to recapitulate the natural.,” *Curr. Opin. Biotechnol.*, vol. 23, no. 4, pp. 579–82, Aug. 2012.

[370] E. Sachlos, “Novel collagen scaffolds with predefined internal morphology made by solid freeform fabrication,” *Biomaterials*, vol. 24, no. 8, pp. 1487–97, Apr. 2003.

[371] T. M. Freyman, I. V. Yannas, and L. J. Gibson, “Cellular materials as porous scaffolds for tissue engineering,” *Prog. Mater. Sci.*, vol. 46, no. 3–4, pp. 273–282, Jan. 2001.

[372] C. S. Chen, I. V. Yannas, and M. Spector, “Pore strain behaviour of collagen-glycosaminoglycan analogues of extracellular matrix,” *Biomaterials*, vol. 16, no. 10, pp. 777–83, Jul. 1995.

[373] F. J. O’Brien, B. A. Harley, I. V Yannas, and L. J. Gibson, “The effect of pore size on cell adhesion in collagen-GAG scaffolds.,” *Biomaterials*, vol. 26, no. 4, pp. 433–41, Feb. 2005.

[374] E. Sachlos and J. T. Czernuszka, “Making tissue engineering scaffolds work. Review: the application of solid freeform fabrication technology to the production of tissue engineering scaffolds.,” *Eur. Cell. Mater.*, vol. 5, pp. 29–39, Jun. 2003.

[375] Q. Lv and Q. Feng, “Preparation of 3-D regenerated fibroin scaffolds with freeze drying method and freeze drying/foaming technique.,” *J. Mater. Sci. Mater. Med.*, vol. 17, no. 12, pp. 1349–56, Dec. 2006.

[376] H. Lu, Y.-G. Ko, N. Kawazoe, and G. Chen, “Cartilage tissue engineering using funnel-like collagen sponges prepared with embossing ice particulate templates.,” *Biomaterials*, vol. 31, no. 22, pp. 5825–35, Aug. 2010.

[377] H. H. Oh, H. Lu, N. Kawazoe, and G. Chen, “Differentiation of PC12 cells in three-dimensional collagen sponges with micropatterned nerve growth factor.,” *Biotechnol. Prog.*, vol. 28, no. 3, pp. 773–9, May 2012.

[378] C. Gupoing, D. Akahane, N. Kawazoe, K. Yamamoto, and T. Tateishi, “Chondrogenic differentiation of mesenchymal stem cells in a leakproof collagen sponge,” *Mater. Sci. Eng. C. Biomim. Supramol. Syst.*, vol. 28, no. 1, pp. 195–201, 2008.

[379] Y. C. P Cha, J. Gao, “Construction of scaffold with human extracellular matrix from adipose tissue,” *Chinese J Plast Surg*, vol. 28, no. 1, pp. 55–60, 2012.

[380] A. Samani, J. Bishop, C. Luginbuhl, and D. B. Plewes, “Measuring the elastic modulus of ex vivo small tissue samples.,” *Phys. Med. Biol.*, vol. 48, no. 14, pp. 2183–98, Jul. 2003.

[381] Y. C. Fung, *Biomechanics: Tissue Properties of Living Tissues*, 2nd ed. Springer-Verlag, 1993.

[382] A. Samani, J. Zubovits, and D. Plewes, “Elastic moduli of normal and pathological human breast tissues: an inversion-technique-based investigation of 169 samples.,” *Phys. Med. Biol.*, vol. 52, no. 6, pp. 1565–76, Mar. 2007.

[383] K. R. Legate, S. A. Wickström, and R. Fässler, “Genetic and cell biological analysis of integrin outside-in signaling.,” *Genes Dev.*, vol. 23, no. 4, pp. 397–418, Feb. 2009.

[384] S. Gobaa, S. Hoehnel, M. Roccio, A. Negro, S. Kobel, and M. P. Lutolf, “Artificial niche microarrays for probing single stem cell fate in high throughput.,” *Nat. Methods*, vol. 8, no. 11, pp. 949–55, Nov. 2011.

[385] K. H. Nakayama, C. A. Batchelder, C. I. Lee, and A. F. Tarantal, “Decellularized rhesus monkey kidney as a three-dimensional scaffold for renal tissue engineering.,” *Tissue Eng. Part A*, vol. 16, no. 7, pp. 2207–16, Jul. 2010.

[386] T. W. Bauer and G. F. Muschler, “Bone graft materials: An overview of the basic science,” *Clin. Orthop. Relat. Res.*, no. 371, pp. 10–27, Feb. 2000.

[387] L. Forrest, J. Dixon, and D. S. Jackson, “Comparative studies on the insoluble collagens of guinea-pig dermis and dermal scar tissue,” *Connect. Tissue Res.*, vol. 1, no. 4, pp. 243–50, Jan. 1972.

[388] F. S. Steven, M. E. Grant, S. Ayad, D. S. Jackson, J. B. Weiss, and S. J. Leibovitch, “The action of crude bacterial alpha-amylase on tropocollagen. A case of strictly limited proteolysis.,” *Biochim. Biophys. Acta*, vol. 236, no. 1, pp. 309–18, Apr. 1971.

[389] L. Flynn and C. Yu, “Collagenous foam materials,” WO2013173906 A1, 2012.

[390] C. S. Ranucci, A. Kumar, S. P. Batra, and P. V Moghe, “Control of hepatocyte function on collagen foams: sizing matrix pores toward selective induction of 2-D and 3-D cellular morphogenesis.,” *Biomaterials*, vol. 21, no. 8, pp. 783–93, Apr. 2000.

[391] T. Chun, “Peri-adipocyte ECM remodeling in obesity and adipose tissue fibrosis,” *Adipocyte*, vol. 1, no. 2, pp. 89-95, Apr. 2012.

[392] J. S. Park, J. S. Chu, A. D. Tsou, R. Diop, Z. Tang, A. Wang, and S. Li, “The effect of matrix stiffness on the differentiation of mesenchymal stem cells in response to TGF-β.,” *Biomaterials*, vol. 32, no. 16, pp. 3921–30, Jun. 2011.

[393] B. A. Harley, J. H. Leung, E. C. C. M. Silva, and L. J. Gibson, “Mechanical characterization of collagen-glycosaminoglycan scaffolds.,” *Acta Biomater.*, vol. 3, no. 4, pp. 463–74, Jul. 2007.

[394] J. Sottile, “Regulation of angiogenesis by extracellular matrix.,” *Biochim. Biophys. Acta*, vol. 1654, no. 1, pp. 13–22, Mar. 2004.

[395] N. E. Vrana, N. Builles, H. Kocak, P. Gulay, V. Justin, M. Malbouyres, F. Ruggiero, O. Damour, and V. Hasirci, “EDC/NHS cross-linked collagen foams as scaffolds for artificial corneal stroma,” *J. Biomater. Sci. Polym. Ed.*, vol. 18, no. 12, pp. 1527–45, Feb. 2007.

[396] Y. A. Romanov, V. A. Svintsitskaya, and V. N. Smirnov, “Searching for alternative sources of postnatal human mesenchymal stem cells: candidate MSC-like cells from umbilical cord.,” *Stem Cells*, vol. 21, no. 1, pp. 105–10, Jan. 2003.

[397] P. S. In ’t Anker, S. A. Scherjon, C. Kleijburg-van der Keur, G. M. J. S. de Groot-Swings, F. H. J. Claas, W. E. Fibbe, and H. H. H. Kanhai, “Isolation of mesenchymal stem cells of fetal or maternal origin from human placenta.,” *Stem Cells*, vol. 22, no. 7, pp. 1338–45, Jan. 2004.

[398] B. Cao, B. Zheng, R. J. Jankowski, S. Kimura, M. Ikezawa, B. Deasy, J. Cummins, M. Epperly, Z. Qu-Petersen, and J. Huard, “Muscle stem cells differentiate into haematopoietic lineages but retain myogenic potential.,” *Nat. Cell Biol.*, vol. 5, no. 7, pp. 640–6, Jul. 2003.

[399] C. De Bari, F. Dell'Accio, P. Tylzanowski, and F. P. Luyten, "Multipotent mesenchymal stem cells from adult human synovial membrane.," *Arthritis Rheum.*, vol. 44, no. 8, pp. 1928–42, Aug. 2001.

[400] O. Ringdén, M. Uzunel, I. Rasmusson, M. Remberger, B. Sundberg, H. Lönnies, H.-U. Marschall, A. Dlugosz, A. Szakos, Z. Hassan, B. Omazic, J. Aschan, L. Barkholt, and K. Le Blanc, "Mesenchymal stem cells for treatment of therapy-resistant graft-versus-host disease.," *Transplantation*, vol. 81, no. 10, pp. 1390–7, May 2006.

[401] M. Wolfe, R. Pochampally, W. Swaney, and R. L. Reger, "Isolation and culture of bone marrow-derived human multipotent stromal cells (hMSCs).," *Methods Mol. Biol.*, vol. 449, pp. 3–25, Jan. 2008.

[402] K. Bieback, A. Hecker, T. Schlechter, I. Hofmann, N. Brousos, T. Redmer, D. Besser, H. Klüter, A. M. Müller, and M. Becker, "Replicative aging and differentiation potential of human adipose tissue-derived mesenchymal stromal cells expanded in pooled human or fetal bovine serum," *Cytotherapy*, vol. 14, no. 5, pp. 570-83, Apr. 2012.

[403] J. E. Frith, B. Thomson, and P. G. Genever, "Dynamic three-dimensional culture methods enhance mesenchymal stem cell properties and increase therapeutic potential.," *Tissue Eng. Part C. Methods*, vol. 16, no. 4, pp. 735–49, Aug. 2010.

[404] P. Nold, C. Brendel, A. Neubauer, G. Bein, and H. Hackstein, "Good manufacturing practice-compliant animal-free expansion of human bone marrow derived mesenchymal stroma cells in a closed hollow-fiber-based bioreactor.," *Biochem. Biophys. Res. Commun.*, vol. 430, no. 1, pp. 325–30, Jan. 2013.

[405] M. Serra, C. Brito, M. F. Q. Sousa, J. Jensen, R. Tostões, J. Clemente, R. Strehl, J. Hyllner, M. J. T. Carrondo, and P. M. Alves, "Improving expansion of pluripotent human embryonic stem cells in perfused bioreactors through oxygen control.," *J. Biotechnol.*, vol. 148, no. 4, pp. 208–15, Aug. 2010.

[406] Y. Hong, Y. Gong, C. Gao, and J. Shen, "Collagen-coated polylactide microcarriers/chitosan hydrogel composite: injectable scaffold for cartilage regeneration.," *J. Biomed. Mater. Res. A*, vol. 85, no. 3, pp. 628–37, Jun. 2008.

[407] T. J. Keane and S. F. Badylak, "Biomaterials for tissue engineering applications.," *Semin. Pediatr. Surg.*, vol. 23, no. 3, pp. 112–8, Jun. 2014.

[408] I. T. Swinehart and S. F. Badylak, "Extracellular matrix bioscaffolds in tissue remodeling and morphogenesis.," *Dev. Dyn.*, vol. 245, no. 3, pp. 351–60, Mar. 2016.

[409] B. G. Ilagan and B. G. Amsden, "Macroporous photocrosslinked elastomer scaffolds containing microposity: preparation and in vitro degradation properties.," *J. Biomed. Mater. Res. A*, vol. 93, no. 1, pp. 211–8, Apr. 2010.

[410] I. G. Fels, "Hydration and density of collagen and gelatin," *J. Appl. Polym. Sci.*, vol. 8, no. 4, pp. 1813–24, Jul. 1964.

[411] J. L. Wilson, M. A. Najia, R. Saeed, and T. C. McDevitt, "Alginate encapsulation parameters influence the differentiation of microencapsulated embryonic stem cell aggregates.," *Biotechnol. Bioeng.*, vol. 111, no. 3, pp. 618–31, Mar. 2014.

[412] V. Popov, *Contact Mechanics and Friction: Physical Principles and Applications*. Springer Science & Business Media, 2010.

[413] V. Wang, G. Misra, and B. Amsden, "Immobilization of a bone and cartilage stimulating

peptide to a synthetic bone graft.," *J. Mater. Sci. Mater. Med.*, vol. 19, no. 5, pp. 2145–55, May 2008.

[414] B. O. Diekman, C. R. Rowland, D. P. Lennon, A. I. Caplan, and F. Guilak, "Chondrogenesis of adult stem cells from adipose tissue and bone marrow: induction by growth factors and cartilage-derived matrix.," *Tissue Eng. Part A*, vol. 16, no. 2, pp. 523–33, Feb. 2010.

[415] U. Hersel, C. Dahmen, and H. Kessler, "RGD modified polymers: biomaterials for stimulated cell adhesion and beyond.," *Biomaterials*, vol. 24, no. 24, pp. 4385–415, Nov. 2003.

[416] C. N. Grover, J. H. Gwynne, N. Pugh, S. Hamaia, R. W. Farndale, S. M. Best, and R. E. Cameron, "Crosslinking and composition influence the surface properties, mechanical stiffiness and cell reactivity of collagen-based films," *Acta Biomater.*, vol. 8, no. 8, pp. 3080–90, Aug. 2012.

[417] P. D. Yurchenco, "Basement membranes: cell scaffoldings and signaling platforms.," *Cold Spring Harb. Perspect. Biol.*, vol. 3, no. 2, p. a004911, Feb. 2011.

[418] B. Turco, "Characterization and cell-seeding of decellularized adipose tissue foams for wound healing," Queen's University, 2014.

[419] M. M. Stevens and J. H. George, "Exploring and engineering the cell surface interface.," *Science*, vol. 310, no. 5751, pp. 1135–8, Nov. 2005.

[420] M. G. Haugh, C. M. Murphy, R. C. McKiernan, C. Altenbuchner, and F. J. O'Brien, "Crosslinking and mechanical properties significantly influence cell attachment, proliferation, and migration within collagen glycosaminoglycan scaffolds.," *Tissue Eng. Part A*, vol. 17, no. 9–10, pp. 1201–8, May 2011.

[421] Y. Zhang, Y. He, S. Bharadwaj, N. Hammam, K. Carnagey, R. Myers, A. Atala, and M. Van Dyke, "Tissue-specific extracellular matrix coatings for the promotion of cell proliferation and maintenance of cell phenotype.," *Biomaterials*, vol. 30, no. 23–24, pp. 4021–8, Aug. 2009.

[422] A. Ode, A. Kurtz, K. Schmidt-Bleek, P. Schrade, P. Kolar, F. Buttgereit, K. Lehmann, D. W. Hutmacher, G. N. Duda, and G. Kasper, "CD73 and CD29 concurrently mediate the mechanically induced decrease of migratory capacity of mesenchymal stromal cells," *European Cells and Materials*. vol. 22, pp. 26-42, Jul. 2011.

[423] M.-N. Kang, H.-H. Yoon, Y.-K. Seo, and J.-K. Park, "Effect of mechanical stimulation on the differentiation of cord stem cells.," *Connect. Tissue Res.*, vol. 53, no. 2, pp. 149–59, Jan. 2012.

[424] L. Zimmerlin, V. S. Donnenberg, M. E. Pfeifer, E. M. Meyer, B. Péault, J. P. Rubin, and A. D. Donnenberg, "Stromal vascular progenitors in adult human adipose tissue.," *Cytometry. A*, vol. 77, no. 1, pp. 22–30, Jan. 2010.

[425] Kshitiz, J. Park, P. Kim, W. Helen, A. J. Engler, A. Levchenko, and D.-H. Kim, "Control of stem cell fate and function by engineering physical microenvironments.," *Integr. Biol. (Camb).*, vol. 4, no. 9, pp. 1008–18, Sep. 2012.

[426] P. Giannoni, M. Siegrist, E. B. Hunziker, and M. Wong, "The mechanosensitivity of cartilage oligomeric matrix protein (COMP)," *Biorheology*, vol. 40, no. 1,2,3. IOS Press, pp. 101–109, 01-Jan-2003.

[427] A. W. Nienow, Q. A. Rafiq, K. Coopman, and C. J. Hewitt, "A potentially scalable method

for the harvesting of hMSCs from microcarriers," *Biochem. Eng. J.*, vol. 85, pp. 79–88, 2014.

[428] W. Safwani, S. Makpol, S. Sathapan, and K. H. Chua, "The impact of long-term in vitro expansion on the senescence-associated markers of human adipose-derived stem cells.," *Appl. Biochem. Biotechnol.*, vol. 166, no. 8, pp. 2101–13, Apr. 2012.

[429] W. K. Z. Wan Safwani, S. Makpol, S. Sathapan, and K. H. Chua, "The changes of stemness biomarkers expression in human adipose-derived stem cells during long-term manipulation," *Biotechnol. Appl. Biochem.*, vol. 58, no. 4, pp. 261–70, Jul. 2011.

[430] F. Gattazzo, A. Urciuolo, and P. Bonaldo, "Extracellular matrix: a dynamic microenvironment for stem cell niche.," *Biochim. Biophys. Acta*, vol. 1840, no. 8, pp. 2506–19, Aug. 2014.

[431] J. Lee, A. A. Abdeen, A. S. Kim, and K. A. Kilian, "Influence of Biophysical Parameters on Maintaining the Mesenchymal Stem Cell Phenotype," *ACS Biomater. Sci. Eng.*, vol. 1, no. 4, pp. 218–26, Apr. 2015.

[432] J. P. Winer, P. A. Janmey, M. E. McCormick, and M. Funaki, "Bone marrow-derived human mesenchymal stem cells become quiescent on soft substrates but remain responsive to chemical or mechanical stimuli.," *Tissue Eng. Part A*, vol. 15, no. 1, pp. 147–54, Jan. 2009.

[433] J. K. Fraser, M. Zhu, I. Wulur, and Z. Alfonso, "Adipose-derived stem cells.," *Methods Mol. Biol.*, vol. 449, pp. 59–67, Jan. 2008.

[434] R. O. Hynes, "The extracellular matrix: not just pretty fibrils.," *Science*, vol. 326, no. 5957, pp. 1216–9, Nov. 2009.

[435] J. C. Bodle, A. D. Hanson, and E. G. Loboa, "Adipose-derived stem cells in functional bone tissue engineering: lessons from bone mechanobiology.," *Tissue Eng. Part B. Rev.*, vol. 17, no. 3, pp. 195–211, Jun. 2011.

[436] N. Kakudo, N. Morimoto, T. Ogawa, S. Taketani, and K. Kusumoto, "Hypoxia Enhances Proliferation of Human Adipose-Derived Stem Cells via HIF-1α Activation.," *PLoS One*, vol. 10, no. 10, p. e0139890, Jan. 2015.

Appendices

A.1 Supplemental figures

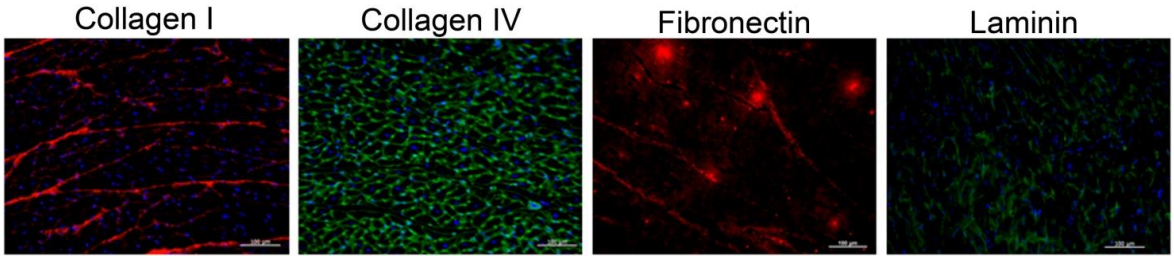

Figure A.1: Immunohistochemical stain of positive heart tissue controls for each ECM component. Scale bars = 100 µm.

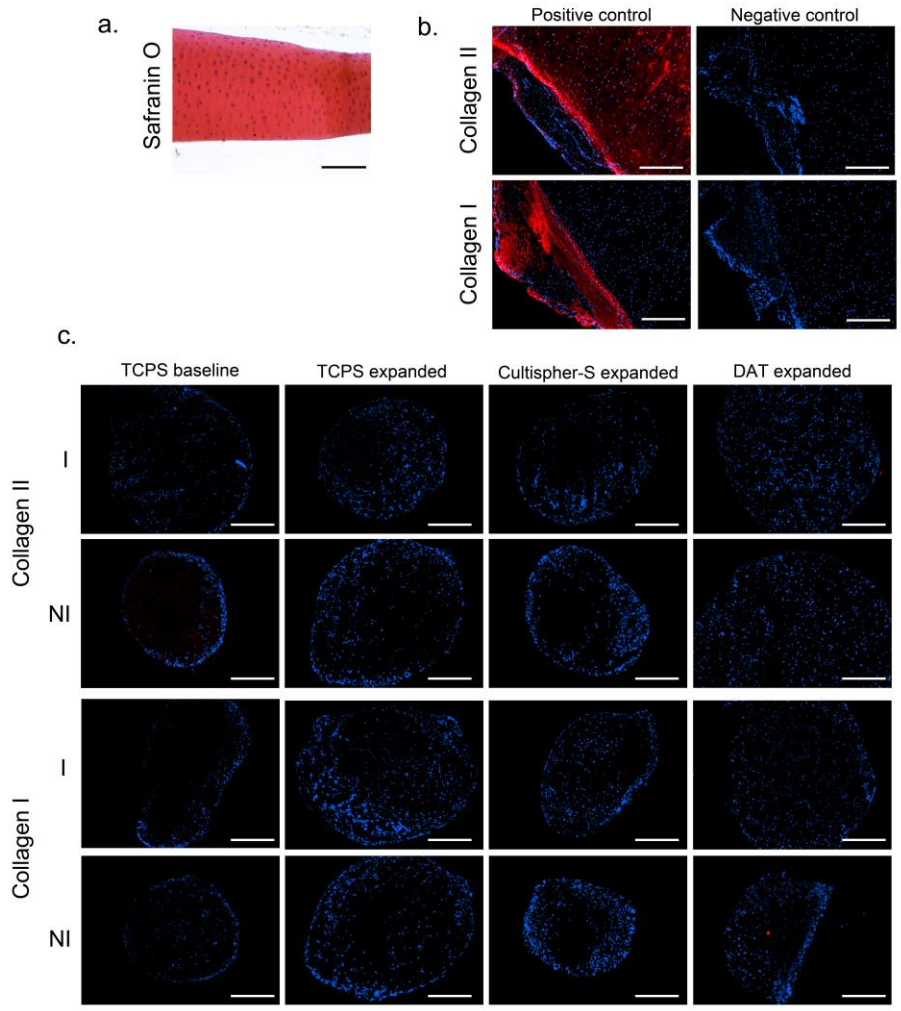

Figure A.2: Positive and negative controls for chondrogenic histological and IHC stains. a) Bovine articular cartilage served as a positive stain for safranin O. For collagen II and collagen I IHC, b) porcine ear cartilage was used as a positive control while sections with no primary antibodies served as negative controls. c) Representative no primary negative controls for ASC pellets. Scale bars = 100 µm.

A.2 Research ethics board approval

QUEEN'S UNIVERSITY HEALTH SCIENCES & AFFILIATED TEACHING HOSPITALS RESEARCH ETHICS BOARD (HSREB)

HSREB Renewal of Ethics Clearance

June 01, 2016

Dr. Lauren Flynn
Department of Chemical Engineering
Dupuis Hall, Queen's University

ROMEO/TRAQ #: 6004616
Department Code: CHEM-002-07
Study Title: Tissue Engineering with Adipose-Derived Stem Cells
Review Type: Delegated
Date Ethics Clearance Effective: June 24, 2016
Ethics Clearance Expiry Date: June 24, 2017

Dear Dr. Flynn,

The Queen's University Health Sciences & Affiliated Teaching Hospitals Research Ethics Board (HSREB) has reviewed the application. This study, including all currently approved documentation has been granted ethical clearance until the expiry date noted above.

Prior to the expiration of your ethics clearance, you will be reminded to submit your renewal report through ROMEO. Any lapses in ethical clearance will be documented below.

Yours sincerely,

Albert L. Clark.

Chair, Health Sciences Research Ethics Board

The HSREB operates in compliance with, and is constituted in accordance with, the requirements of the Tri-Council Policy Statement: Ethical Conduct for Research Involving Humans (TCPS 2); the International Conference on Harmonisation Good Clinical Practice Consolidated Guideline (ICH GCP); Part C, Division 5 of the Food and Drug Regulations; Part 4 of the Natural Health Products Regulations; Part 3 of the Medical Devices Regulations, Canadian General Standards Board, and the provisions of the Ontario Personal Health Information Protection Act (PHIPA 2004) and its applicable regulations. The HSREB is qualified through the CTO REB Qualification Program and is registered with the U.S. Department of Health and Human Services (DHHS) Office for Human Research Protection (OHRP). Federalwide Assurance Number: FWA#:00004184, IRB#:00001173

HSREB members involved in the research project do not participate in the review, discussion, or decision.

Western Research

Research Ethics

Western University Health Science Research Ethics Board
HSREB Delegated Initial Approval Notice

Principal Investigator: Dr. Lauren Flynn
Department & Institution: Schulich School of Medicine and Dentistry\Anatomy & Cell Biology,Western University

HSREB File Number: 105426
Study Title: Tissue Engineering with Adipose-derived Stem Cells
Sponsor: Canadian Institutes of Health Research

HSREB Initial Approval Date: August 13, 2014
HSREB Expiry Date: August 31, 2019

Documents Approved and/or Received for Information:

Document Name	Comments	Version Date
Other	Letter for OR and Clinic Staff to Introduce the Study (received June 2/14)	
Western University Protocol		2014/07/23
Letter of Information & Consent		2014/07/23

The Western University Health Science Research Ethics Board (HSREB) has reviewed and approved the above named study, as of the HSREB Initial Approval Datenoted above.

HSREB approval for this study remains valid until the HSREB Expiry Date noted above, conditional to timely submission and acceptance of HSREB ContinuingEthics Review. If an Updated Approval Notice is required prior to the HSREB Expiry Date, the Principal Investigator is responsible for completing andsubmitting an HSREB Updated Approval Form in a timely fashion.

The Western University HSREB operates in compliance with the Tri-Council Policy Statement Ethical Conduct for Research Involving Humans (TCPS2), theInternational Conference on Harmonization of Technical Requirements for Registration of Pharmaceuticals for Human Use Guideline for Good Clinical PracticePractices (ICH E6 R1), the Ontario Personal Health Information Protection Act (PHIPA, 2004), Part 4 of the Natural Health Product Regulations, Health CanadaMedical Device Regulations and Part C, Division 5, of the Food and Drug Regulations of Health Canada.

Members of the HSREB who are named as Investigators in research studies do not participate in discussions related to, nor vote on such studies when theyare presented to the REB.

The HSREB is registered with the U.S. Department of Health & Human Services under the IRB registration number IRB 00000940.

Ethics Officer, on behalf of Dr. Joseph Gilbert, HSREB Chair

Ethics Officer to Contact for Further Information

Erika Basile ebasile@uwo.ca	Grace Kelly grace.kelly@uwo.ca	Mina Mekhail mmekhail@uwo.ca	Vikki Tran vikki.tran@uwo.ca

This is an official document. Please retain the original in your files.